Hypoxia-Induced Radioresistance in Human Non-Small Cell Lung Carcinoma Cell Lines

Inaugural Dissertation

zur

Erlangung des Doktorgrades
Dr. nat. med.

der Medizinischen Fakultät
und
der Mathematisch-Naturwissenschaftlichen Fakultät
der Universität zu Köln

vorgelegt von

Hasan Nisar

Aus Pakistan

Print Express 24, Köln

2023

Hypoxia-Induced Radioresistance in Human Non-Small Cell Lung Carcinoma Cell Lines

Inaugural Dissertation

zur

Erlangung des Doktorgrades
Dr. nat. med.

der Medizinischen Fakultät
und
der Mathematisch-Naturwissenschaftlichen Fakultät
der Universität zu Köln

vorgelegt von

Hasan Nisar

Aus Pakistan

Print Express 24, Köln

2023

2

Betreuer: Prof. Dr. Jens Jordan

Referenten: Prof. Dr. Niels Gehring

                                   Prof. Dr. Christian Pallasch

                                   Prof. Dr. Priv. Doz. Dr. Lydia Meder

Datum der mündlichen Prüfung: 17.03.2022

Contents

7

Summary

Lung cancer accounts for 25 % of cancer-related deaths. Non-small cell lung carcinoma (NSCLC) constitutes 85 % of all lung cancers. Radiotherapy is used in treatment of over half of lung cancer patients. Tumor hypoxia is associated with treatment resistance particularly in the context of radiotherapy. Targeting tumor hypoxia to increase radiotherapy efficacy has met limited success clinically with no measurable mortality benefit. High linear energy transfer (LET) carbon ions are being used increasingly in cancer clinical trials and have the theoretical advantage of being less sensitive to the influence of oxygen. Studying DNA damage response (DDR) to low- (X-rays) and high-LET ionizing radiation under hypoxia may help identify molecular processes that can be potentially targeted therapeutically to overcome hypoxia-induced radioresistance. Additionally, tumor cells often experience reversible hypoxia due to tumor shrinkage secondary to treatment, neo-angiogenesis as well as intermittent vasospasm of feeding vessels. Thus, impact of reoxygenation on radioresistance also warrants greater understanding. The Nuclear Factor κB (NF-κB) pathway is associated with cellular inflammatory response to stressors like ionizing radiation and hypoxia and has been associated with enhanced cell survival. However, the role of NF-κB pathway in hypoxia-induced radioresistance remains elusive. Therefore, the radioresistance of NSCLC cells was evaluated under continuous hypoxia and following reoxygenation by performing clonogenic assays following irradiation with the objective of correlating hypoxia induced radioresistance in NSCLC cells to DDR in terms of DNA double strand break (DSB) induction, DSB repair, cell cycle progression as well as activation of pro-survival NF-κB pathway.

A549 (p53-wt) and H358 (p53-null) NSCLC cell lines were incubated after seeding for 48 h under hypoxia (0.1 % and 1 % O_2) and normoxia (20 % O_2) and irradiated using X-rays (200 KeV) and carbon ions (on target energy 25.7 MeV/nucleon). Following irradiation, hypoxic cells were either allowed to reoxygenate (transient hypoxia) or kept hypoxic (continuous hypoxia) till end of experiments. Radioresistance was evaluated in normoxic, continuously hypoxic and transiently hypoxic cells using Puck's colony forming ability (CFA) assay. DDR four hours following irradiation was assessed at transcriptional level in terms of cell cycle modulation, DNA DSB repair and activation of pro-survival NF-κB pathway by carrying out RNA sequencing and differential expression analysis of relevant genes in continuously and transiently hypoxic cells in comparison to normoxic controls. Cell cycle progression was determined by flow cytometry of cells after staining their nuclei with 4',6'-diamidino-2-phenylindole (DAPI). DSB induction and repair was assessed using γH2AX immunofluorescence microscopy and NF-κB pathway activation was evaluated by p65 (NF-κB subunit) nuclear translocation using p65 immunofluorescence microscopy, and by measuring production of NF-κB target proteins, interleukin (IL) 6 and IL-8.

CFA assays revealed that hypoxic cells were more radioresistant compared to normoxic controls when they were given 24 h to repair (late plating) following both X-rays and carbon ions exposure. Radioresistance was higher at 0.1 % O_2 compared 1 % O_2. Continuously hypoxic cells were more radiosensitive compared to normoxic controls when they were immediately re-seeded for growth of colonies following irradiation (immediate plating). This radiosensitivity was reversed if hypoxic cells were reoxygenated following irradiation (transient hypoxia). Carbon ions had a greater relative biological effectiveness (RBE) in killing hypoxic cells compared to X-rays. Cell cycle progression under hypoxia following both X-rays and carbon ions exposure in A549 and H358 cell lines was slowed as indicated by a greater proportion of cells in G1 phase and smaller population of cells in G2 phase compared to

normoxic controls. Phase redistribution was similar at 0.1 % and 1 % O_2. Differential expression analysis of cell cycle genes revealed weak transcriptional regulation in both cell lines indicating importance of post-translational cell cycle regulation in response to irradiation under hypoxia. Reoxygenation did not affect cell cycle phase distribution in first 24 h. DSB induction assessment based on γH2AX foci count 1 h after irradiation was lower under continuous and transient hypoxia in case of X-rays exposure but not in case of carbon ions exposure. No residual DSBs were observed at a dose of 2 Gy X-rays but DSBs induced by carbon ions took longer to resolve compared to those caused by X-rays. Differential expression analysis of DSB repair genes was unremarkable but that for NF-κB target genes showed overexpression of several pro-survival and pro-proliferation genes under hypoxia. The gene expression signature of both cell lines was unique with minimal overlap. Gene expression signature also varied following X-rays and carbon ions exposure. In case of H358 cells, reoxygenation resulted in transcriptional regulation of several genes not regulated under continuous hypoxia. IL-6 (following carbon ions exposure) and IL-8 (following both X-rays and carbon ions exposure) were upregulated in A549 cells while in H358 cells, only IL-8 was upregulated upon reoxygenation. Nuclear translocation of cytosolic p65 was found to occur earlier (at 2 h vs. 6 h) in A549 and H358 cells under continuous hypoxia (1 % O_2) following both X-rays and carbon ion exposure compared to normoxia. Reoxygenation had a minimal effect on p65 nuclear translocation in A549 cells. In H358 cells, p65 nuclear localization increased in response to reoxygenation but was not affected by irradiation. Both IL-6 and IL-8 secretion by A549 cells was amplified under hypoxia regardless of reoxygenation and irradiation resulted in its further increase. IL-8 secretion by H358 cells was increased under both continuous and transient hypoxia but irradiation further increased its production only under continuous hypoxia.

Hypoxia-induced radioresistance in continuously and transiently hypoxic A549 cells following X-rays and carbon ion exposure was found to be associated with cell cycle phase redistribution toward the radioresistant G1 phase, lesser DSB induction, earlier NF-κB activation, greater NF-κB target gene expression and higher NF-κB target protein synthesis and secretion. The same was true in case of continuously hypoxic H358 cells following X-rays exposure. However, transiently hypoxic H358 cells behaved differently: reoxygenation increased basal p65 nuclear translocation and IL-8 secretion but irradiation did not lead to further increase in p65 nuclear intensity and IL-8 secretion.

Hypoxia-induced radioresistance effects faster growing cells (A549) more than less rapidly dividing cells (H358). Reoxygenation does not alter effects of hypoxia on cell survival, DNA damage and cell cycle but it does affect both cell lines differently in terms of NF-κB pathway activation and transcription of its target genes. While this work does not establish a causal relationship between NF-κB activation and radioresistance seen in hypoxic NSCLC cells, the association does show promise for further investigation into NF-κB as a potential molecular target for therapy in NSCLC. Although NF-κB activation is seen following high LET radiation exposure as well, hypoxic cells are more radiosensitive to carbon ions compared to low LET X-rays. Moreover, IL-6 and IL-8 secretion may serve as potential prognostic indicators of radioresistance.

Zusammenfassung

Lungenkrebs macht 25 % der krebsbedingten Todesfälle aus. Bei 85 % aller Lungenkrebserkrankungen handelt es sich um das nicht-kleinzellige Lungenkarzinom (NSCLC). Zur Behandlung von mehr als der Hälfte der Patienten mit Lungenkrebs wird Strahlentherapie eingesetzt. Tumorhypoxie ist insbesondere im Rahmen einer Strahlentherapie mit Therapieresistenz assoziiert. Die Ausrichtung der Strahlentherapie auf Tumorhypoxie zur Steigerung ihrer Wirksamkeit hatte bisher klinisch nur begrenzten Erfolg ohne messbare Reduktion der Mortalität. Kohlenstoffionen mit hohem linearem Energietransfer (LET) werden zunehmend in klinischen Studien zur Krebstherapie verwendet und haben den theoretischen Vorteil, dass ihre Wirkung weniger empfindlich gegenüber dem Einfluss von Sauerstoff ist. Die Untersuchung der DNA-Schadensantwort (*DNA damage response*, DDR) in Reaktion auf ionisierende Strahlung mit niedrigem (Röntgenstrahlung) und hohem LET-Wert unter Hypoxie kann dazu beitragen, molekulare Prozesse zu identifizieren, in die möglicherweise gezielt therapeut eingegriffen werden kann, um die durch Hypoxie induzierte Strahlenresistenz zu überwinden. Zusätzlich erfahren Tumorzellen häufig eine reversible Hypoxie aufgrund einer Tumorschrumpfung infolge der Behandlung, von Neo-Angiogenese sowie von intermittierendem Vasospasmus der versorgenden Gefäße. Daher muss auch der Einfluss der Reoxygenierung auf die Strahlenresistenz besser verstanden werden. Der *Nuclear Factor κB* (NF-κB)-Signalweg ist mit einer zellulären Entzündungsreaktion auf Stressoren wie ionisierende Strahlung und Hypoxie verbunden und wurde mit einem verbesserten Zellüberleben in Verbindung gebracht. Die Rolle des NF-κB-Signalwegs bei der Hypoxie-induzierten Strahlenresistenz bleibt jedoch schwer fassbar. Daher wurde die Strahlenresistenz von NSCLC-Zellen unter kontinuierlicher Hypoxie und nach Reoxygenierung bewertet, indem klonogene Assays nach der Bestrahlung durchgeführt wurden, mit dem Ziel, die durch Hypoxie induzierte Strahlenresistenz in NSCLC-Zellen mit DDR zu korrelieren in Bezug auf DNA Doppelstrangbruch (DSB)-Induktion, DSB-Reparatur und Zellzyklus-Progression sowie Aktivierung des überlebensfördernden NF-κB-Signalwegs.

A549 (p53-wt) und H358 (p53-null) NSCLC-Zelllinien wurden nach der Aussaat für 48 h unter Hypoxie (0,1 % und 1 % O_2) und Normoxie (20 % O_2) inkubiert und mit Röntgenstrahlen (200 KeV) bestrahlt. und Kohlenstoffionen (Energie 25,7 MeV/Nukleon). Nach der Bestrahlung wurden hypoxische Zellen entweder reoxigeniert (vorübergehende Hypoxie) oder bis zum Ende der Experimente hypoxisch gehalten (kontinuierliche Hypoxie). Die Strahlenresistenz wurde in normoxischen, kontinuierlich hypoxischen und vorübergehend hypoxischen Zellen mit dem Puck-Assay der Koloniebildungsfähigkeit (*colony forming ability*, CFA) bewertet. Die DDR vier Stunden nach der Bestrahlung wurde auf Transkriptionsebene in Bezug auf Zellzyklusmodulation, DNA-DSB-Reparatur und Aktivierung des überlebensfördernden NF-κB-Signalwegs bewertet, indem RNA-Sequenzierung und differenzielle Expressionsanalyse relevanter Gene in kontinuierlich und vorübergehend hypoxischen Zellen im Vergleich mit normoxischen Kontrollen durchgeführt wurden. Die Zellzyklusprogression wurde durch Durchflusszytometrie von Zellen bestimmt, nachdem ihre Zellkerne mit 4',6'-Diamidino-2-Phenylindol (DAPI) gefärbt worden waren. DSB-Induktion und -Reparatur wurden mittels γH2AX-Immunfluoreszenzmikroskopie bewertet. Die Aktivierung des NF-κB-Signalwegs wurde durch Translokation von der NF-κB-Untereinheit p65 in den Zellkern mit Hilfe von p65-Immunfluoreszenzmikroskopie und durch Messung der Produktion von NF-κB-Zielproteinen, Interleukin (IL) 6 und IL-8, erfasst.

Die CFA-Assays zeigten, dass hypoxische Zellen im Vergleich zu normoxischen Kontrollen

strahlenresistenter waren, wenn sie 24 Stunden Reparaturzeit hatten (spätes Ausplattieren), nachdem sie Röntgenstrahlen bzw. Kohlenstoffionen ausgesetzt waren. Die Strahlenresistenz war bei 0,1 % O_2 höher als bei 1 % O_2. Kontinuierlich hypoxische Zellen waren im Vergleich zu normoxischen Kontrollen strahlenempfindlicher, wenn sie unmittelbar nach der Bestrahlung erneut für das Wachstum von Kolonien ausgesät wurden (sofortiges Ausplattieren). Diese Strahlenempfindlichkeit kehrte sich um, wenn hypoxische Zellen nach der Bestrahlung wieder mit Sauerstoff versorgt wurden (vorübergehende Hypoxie). Kohlenstoffionen hatten im Vergleich zu Röntgenstrahlen eine größere relative biologische Wirksamkeit (RBE) beim Abtöten hypoxischer Zellen. Die Zellzyklusprogression unter Hypoxie nach sowohl Röntgen- als auch Kohlenstoffionen-Exposition in A549- und H358-Zelllinien wurde verlangsamt, wie sich durch einen größeren Anteil von Zellen in der G1-Phase und eine kleinere Population von Zellen in der G2-Phase im Vergleich zu normoxischen Kontrollen zeigte. Die Phasenumverteilung war bei 0,1 % und 1 % O_2 ähnlich. Eine differentielle Expressionsanalyse von Zellzyklusgenen zeigte eine schwache Transkriptionsregulation in beiden Zelllinien, was auf die Bedeutung der posttranslationalen Zellzyklusregulation als Reaktion auf Bestrahlung unter Hypoxie hinweist. Die Reoxygenierung beeinflusste die Zellzyklusphasenverteilung in den ersten 24 h nicht. Die Bewertung der DSB-Induktion basierend auf der Anzahl der γH2AX-Herde 1 Stunde nach der Bestrahlung war unter kontinuierlicher und vorübergehender Hypoxie im Falle einer Röntgenstrahlen-Exposition niedriger, aber nicht im Falle einer Kohlenstoffionen-Exposition. Bei einer Dosis von 2 Gy Röntgenstrahlen wurden keine verbleibenden DSBs beobachtet, aber die Reparatur von durch Kohlenstoffionen induzierten DSBs dauerte länger als bei den durch Röntgenstrahlen verursachten. Die differenzielle Expressionsanalyse von DSB-Reparaturgenen war unauffällig, jedoch die der NF-κB-Zielgene zeigte eine Überexpression mehrerer überlebens- und proliferationsfördernder Gene unter Hypoxie. Die Genexpressionssignatur beider Zelllinien war einzigartig mit minimaler Überlappung. Die Signatur der Genexpression unterschied sich auch nach der Exposition gegenüber Röntgenstrahlen und Kohlenstoffionen. Im Falle von H358-Zellen führte die Reoxygenierung zu einer Regulation der Transkription mehrerer Gene, die unter kontinuierlicher Hypoxie nicht reguliert wurden. IL-6 (nach Kohlenstoffionen-Exposition) und IL-8 (sowohl nach Röntgen- als auch Kohlenstoffionen-Exposition) wurden in A549-Zellen hochreguliert, während in H358-Zellen nur IL-8 nach Reoxygenierung hochreguliert wurde. Es wurde festgestellt, dass die Kerntranslokation von zytosolischem p65 in A549- und H358-Zellen unter kontinuierlicher Hypoxie (1 % O_2) sowohl nach Röntgenbestrahlung als auch Kohlenstoffionen-Exposition im Vergleich zu Normoxie früher auftrat (nach 2 h gegenüber 6 h). Die Reoxygenierung hatte eine minimale Auswirkung auf die Kerntranslokation von p65 in A549-Zellen. In H358-Zellen nahm die p65-Kernlokalisierung als Reaktion auf die Reoxygenierung zu, wurde aber durch die Bestrahlung nicht beeinflusst. Sowohl die IL-6- als auch die IL-8-Sekretion durch A549-Zellen wurde unter Hypoxie unabhängig von der Reoxygenierung verstärkt, und die Bestrahlung führte zu ihrer weiteren Zunahme. Die IL-8-Sekretion durch H358-Zellen war sowohl unter kontinuierlicher als auch vorübergehender Hypoxie erhöht, aber die Bestrahlung steigerte seine Produktion nur unter kontinuierlicher Hypoxie weiter.

Es wurde festgestellt, dass die durch Hypoxie induzierte Strahlenresistenz in kontinuierlich und vorübergehend hypoxischen A549-Zellen nach Röntgenbestrahlung und nach Kohlenstoffionen-Exposition mit einer Umverteilung der Zellzyklusphase in Richtung der strahlenresistenten G1-Phase, einer geringeren DSB-Induktion, einer früheren NF-κB-Aktivierung und einer stärkeren Expression von NF-κB-Zielgenen inklusive ihrer Proteinsynthese und Sekretion assoziiert ist. Dasselbe galt für kontinuierlich hypoxische H358-

Zellen nach Röntgenbestrahlung. Vorübergehend hypoxische H358-Zellen verhielten sich jedoch anders: Reoxygenierung erhöhte die basale p65-Kerntranslokation und IL-8-Sekretion, aber die Bestrahlung führte nicht zu einer weiteren Erhöhung der p65-Kernintensität und IL-8-Sekretion.

Hypoxie-induzierte Strahlenresistenz beeinflusst schneller wachsende Zellen (A549) stärker als sich weniger schnell teilende Zellen (H358). Die Reoxygenierung verändert die Auswirkungen der Hypoxie auf das Zellüberleben, die DNA-Schädigung und den Zellzyklus nicht, beeinflusst jedoch beide Zelllinien unterschiedlich in Bezug auf die Aktivierung des NF-κB-Signalwegs und die Transkription seiner Zielgene. Während diese Arbeit keinen kausalen Zusammenhang zwischen der NF-κB-Aktivierung und der Strahlenresistenz in hypoxischen NSCLC-Zellen herstellt, ist die gefundene Assoziation vielversprechend für weitere Untersuchungen zu NF-κB als potenziellem molekularem Ziel für die Therapie von NSCLC. Obwohl die NF-κB-Aktivierung auch nach einer Exposition mit Hoch-LET-Strahlung zu beobachten ist, scheinen hypoxische Zellen im Vergleich zu Röntgenstrahlen mit niedrigem LET strahlenempfindlicher gegenüber Kohlenstoffionen zu sein. Außerdem könnten IL-6- und IL-8-Sekretion als potenzielle prognostische Indikatoren für Strahlenresistenz dienen.

1. Introduction

Lung cancer is the second most diagnosed solid malignancy in both men and women. Its incidence has been on the decline in the last two decades due to decrease in smoking, but 70 % of lung cancers are diagnosed in later stages making curative therapy highly challenging. Therefore, lung cancer continues to have a 5-year overall survival (OS) of about only 15 % and accounts for 25 % of all cancer deaths annually. 85 % of all lung cancers are classified as non-small cell lung cancer (NSCLC) (1).

Cellular stressors like hypoxia and ionizing radiation are known to influence the tumor cells and their microenvironment in solid malignancies. Radiation exposure is a double-edged sword acting as both a carcinogen as well as a potential cure to solid malignancies. Radiotherapy constitutes a key treatment modality in the standard therapy for non-metastatic lung cancer. Cellular hypoxia is a common cause for treatment resistance in solid malignancies. Hypoxia-induced radioresistance was associated with poor prognosis in NSCLC in at least 3 meta-analyses and several early phase clinical trials targeting tumor hypoxia over the years have reported only limited success (see subchapter 1.2.4) (2). This indicates a need for greater understanding of the biological processes pertaining to cellular hypoxia in lung cancer particularly in the context of radioresistance.

1.1. Non-small cell lung carcinoma (NSCLC)

Non-small cell lung cancer is a clinical classification of lung cancers including all lung cancer types that on microscopic evaluation and tissue histochemistry analysis do not show undifferentiated small cells. NSCLC encompasses at least three distinct histopathological variants, namely, squamous cell carcinoma (40 %), large cell carcinoma (10 %) and adenocarcinomas (50 %). The proportion and incidence of adenocarcinomas is increasing due to decline in smoking which is a risk factor for squamous cell carcinoma. Microscopic diagnosis of biopsy specimens is supported by tumor histochemistry where the most widely accepted tumor marker for NSCLC is thyroid transcription factor-1 (TTF-1) (3).

1.1.1. Hallmarks of NSCLC and their therapeutic targeting

In 2011, Hanahan and Weinberg suggested ten hallmarks of carcinogenesis indicating acquisition of certain biological capacities and characteristics leading to cancer development (4). In the following, these characteristics are explained in the context of lung cancer, particularly NSCLC, to reflect the current understanding of this disease and to describe potential molecular processes that can be targeted to improve therapeutic strategies.

1.1.1.1. *Genome instability and mutation*

Acquisition of various hallmark capabilities by malignant tumors depends to a large extent on genomic instability of cells on their way to becoming neoplastic. Genomic instability refers to an increased rate of mutations in the genome of cells secondary to carcinogen exposure or a decreased capacity of cells to repair these spontaneous mutations due to genetic defects in DNA repair pathways. These include base excision repair (BER), nucleotide excision repair (NER), mismatch repair (MMR), homologous repair (HR) and nonhomologous end joining (NHEJ) genes (see Box 1). Common heritable genetic syndromes resulting from repair gene defects include Li Fraumeni Syndrome affecting the tumor protein p53 (TP53), Xeroderma Pigmentosum and Ataxia Telangiectasia affecting NER genes and Hereditary Nonpolyposis Colorectal Carcinoma Syndrome (HNPCCS) affecting MMR genes. Another cause of genetic instability is aging which may lead to loss of telomeric function and consequent chromosomal

breakage-fusion-bridge cycles that lead to chromosomal deletions and amplifications which in turn increases genomic mutability. The mutant genotypes that thus appear, provide a selective advantage to these subclones, that may facilitate their eventual outgrowth in a local tissue environment (4).

Genomic instability within premalignant and malignant cells is determined by analysis of the resulting genomic heterogeneity of gene copy numbers, translocations, and mutations in these cells. Such intra-tumoral heterogeneity has been reported in NSCLC and has been associated with exogenous mutational processes such as smoking as well as endogenous processes linked to APOBEC (apolipoprotein B mRNA editing enzyme, catalytic polypeptide-like) cytidine deaminase activity (5).

> **Box 1 Therapeutic targeting of genomic instability**
>
> *Poly-(ADP-ribose) polymerase (PARP) plays a central role in BER and NER pathways. PARP inhibitors block these DNA repair pathways allowing for single strand breaks to be converted to double strand breaks. Recently, it was shown that the NSCLC cell line A549 with ATM or BRCA1/2 knockout is sensitive to PARP inhibitors (6).*

1.1.1.2.   Sustained proliferative signaling

Acquiring the ability to undergo sustained proliferation is arguably fundamental to multistep tumor progression in premalignant cells. Growth of normal cells is under tight homeostatic regulation mediated by growth factors that bind to cell-surface receptors and activate several intracellular signaling pathways. These pathways regulate cell cycle progression as well as cell growth and differentiation. Pre-cancer cells are known to deregulate proliferative signaling early during carcinogenesis. This occurs in a number of ways such as autocrine growth receptor stimulation through increased receptor ligand synthesis, paracrine growth stimulation through secretion of ligands which stimulate neighboring cells to produce growth signaling molecules, increased growth signaling through greater growth receptor expression, structural alterations in surface receptors or their downstream mediators resulting in ligand independent proliferation or negative-feedback disruption (4).

Several growth ligands and their corresponding receptors are expressed in NSCLC, stimulating growth by autocrine and paracrine mechanisms. The Erythroblastic leukemia viral oncogene homolog (ERBB) family is a group of transmembrane receptor tyrosine kinases which is often responsible for growth stimulation in NSCLC. The transmembrane tyrosine receptor kinases, ERBB-1 (epidermal growth factor receptor, EGFR) and ERBB-2 (human epidermal growth receptor 2, HER2) may be expressed in NSCLC independent of each other. Upon ligand binding, ERBB receptors dimerize and induce intrinsic kinase activity that initiates a cascade of secondary intracellular signal transduction which often includes mitogen activated protein (MAP) kinases. Furthermore, lung cancer cells can also express ligands for EGFR (see Box 2) such as epidermal growth factor (EGF) and transforming growth factor α (TGF-α) (7).
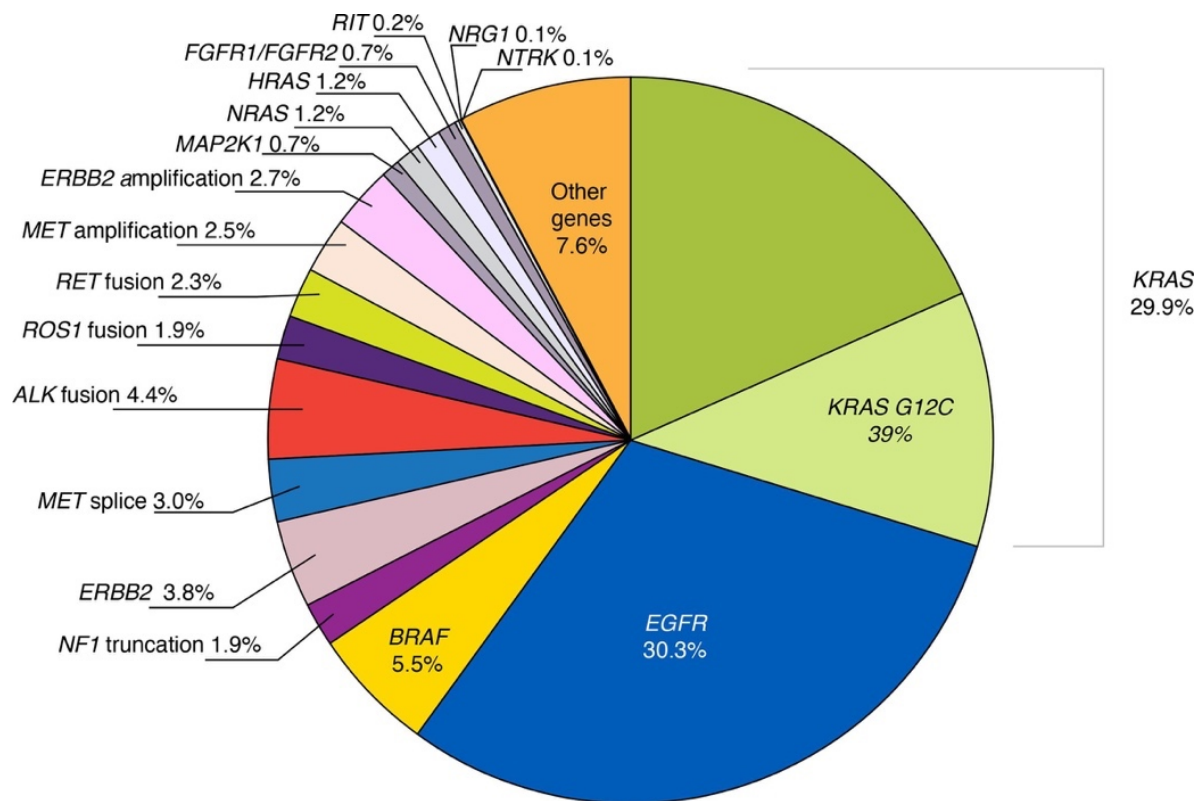
Figure 1.1   *Pie chart representing commonly occurring genetic mutations in human NSCLC (8).*

<div style="border:1px solid blue; background-color:#e6e6f5;">

Box 2 Therapeutic targeting of proliferative signaling pathways

Mutated EGFR is currently being targeted in early and late stages of NSCLC as a standard option. The most common mutations in EGFR associated with responsiveness to oral EGFR tyrosine kinase inhibitor (TKI) therapy are exon 19 deletions and L858R point mutation in exon 21. In addition, Her2 targeting using monoclonal antibodies is also taking place within Phase III NSCLC clinical trials (9).

Kirsten rat sarcoma virus oncogene homolog (KRAS) is a G-protein with intrinsic guanosine triphosphatase (GTPase) activity. Activating mutations result in unregulated signaling through the Extracellular signal-regulated MAP kinase (ERK) pathway. About 15-20 % of all NSCLCs show KRAS mutations, especially adenocarcinomas. KRAS mutations are associated with poor survival and reduced response to EGFR TKI therapy. Most common KRAS mutations are observed at codon 12. KRAS point mutation G12C is associated with responsiveness to an oral KRAS G12C inhibitor (9). The Ras protein is activated by farnesyltransferase which has led to the development of specific inhibitors of this enzyme that are currently in clinical trials. Ongoing vaccination trials with mutant KRAS peptides in NSCLC patients are also reported (7).

Anaplastic lymphoma kinase (ALK) is a receptor tyrosine kinase that may be rearranged in NSCLC (5 % of cases). This results in constitutional growth-related signaling through the ALK kinase domain. The presence of an ALK rearrangement is associated with response to oral ALK TKIs and is already part of standard treatment of NSCLC (9).

The proto-oncogene UR2 sarcoma virus oncogene homolog 1 (ROS1) is a receptor tyrosine kinase that can be rearranged in NSCLC, resulting in dysregulated growth-related signaling through the ROS1 kinase domain. ROS1 rearrangement is associated with clinical response

</div>

to oral ROS1 TKIs (9).

The B-Raf proto-oncogene (BRAF) is a serine/threonine kinase and is a part of the ERK signaling pathway. Activating mutations in BRAF have been reported in NSCLC and result in dysregulated signaling through the ERK pathway. One such mutation is the point mutation that results in a change in amino acid position 600 (V600E) that has been associated with clinical response to combined therapy with oral inhibitors of BRAF and ERK (9).

The Met proto-oncogene (MET) is a receptor tyrosine kinase. A mutation that results in loss of exon 14 has been identified in NSCLC which leads to dysregulated signaling and is associated with clinical response to oral MET TKIs (9).

The Ret proto-oncogene (RET) is a tyrosine kinase receptor. Its rearrangement has been reported to result in dysregulated signaling through the RET kinase domain in NSCLC. RET rearrangement is associated with clinical response to oral RET TKIs (9).

1.1.1.3. Deregulating cellular energetics

Sustained proliferative signaling should require corresponding upregulation of cellular energetics to support enhanced cell growth in the form of greater oxidative phosphorylation. However, cancer cells commonly exhibit a phenotype or behavior referred to as the Warburg effect, i.e: Even in the presence of oxygen, cancer cells can limit their energy metabolism largely to glycolysis (Figure 1.2). This "aerobic glycolysis" seems counterproductive because it has an 18-fold lower efficiency for adenosine triphosphate (ATP) production compared to mitochondrial oxidative phosphorylation. However, cancer cells compensate for this by upregulating glucose transporters, especially glucose transporter type 1 (GLUT1), as well as by upregulating multiple enzymes of the glycolysis pathway. On the other hand, Warburg effect allows for the diversion of glycolytic intermediates into various other biosynthetic pathways, particularly those generating nucleosides and amino acids, and in this way facilitating production of building blocks needed for cell division and new cell assembly (4).

NSCLC, being rapidly dividing, exhibits markedly increased glucose uptake upon ^{18}F-fluorodeoxyglucose (FDG) positron emission tomography (PET). GLUT1 expression is also found to be increased in excised tumor tissue upon immunofluorescence staining. Greater glucose uptake and GLUT1 expression has been observed in squamous cell carcinoma relative to adenocarcinoma (10).

Box 3 Therapeutic targeting of pathways of cellular energetics

The overexpression of the glycolytic enzyme, pyruvate kinase isozyme M2 (PKM2), in NSCLC has been reported to be associated with resistance to platinum-based chemotherapy. Its inhibition by metformin has been shown to partially reverse treatment resistance (11).
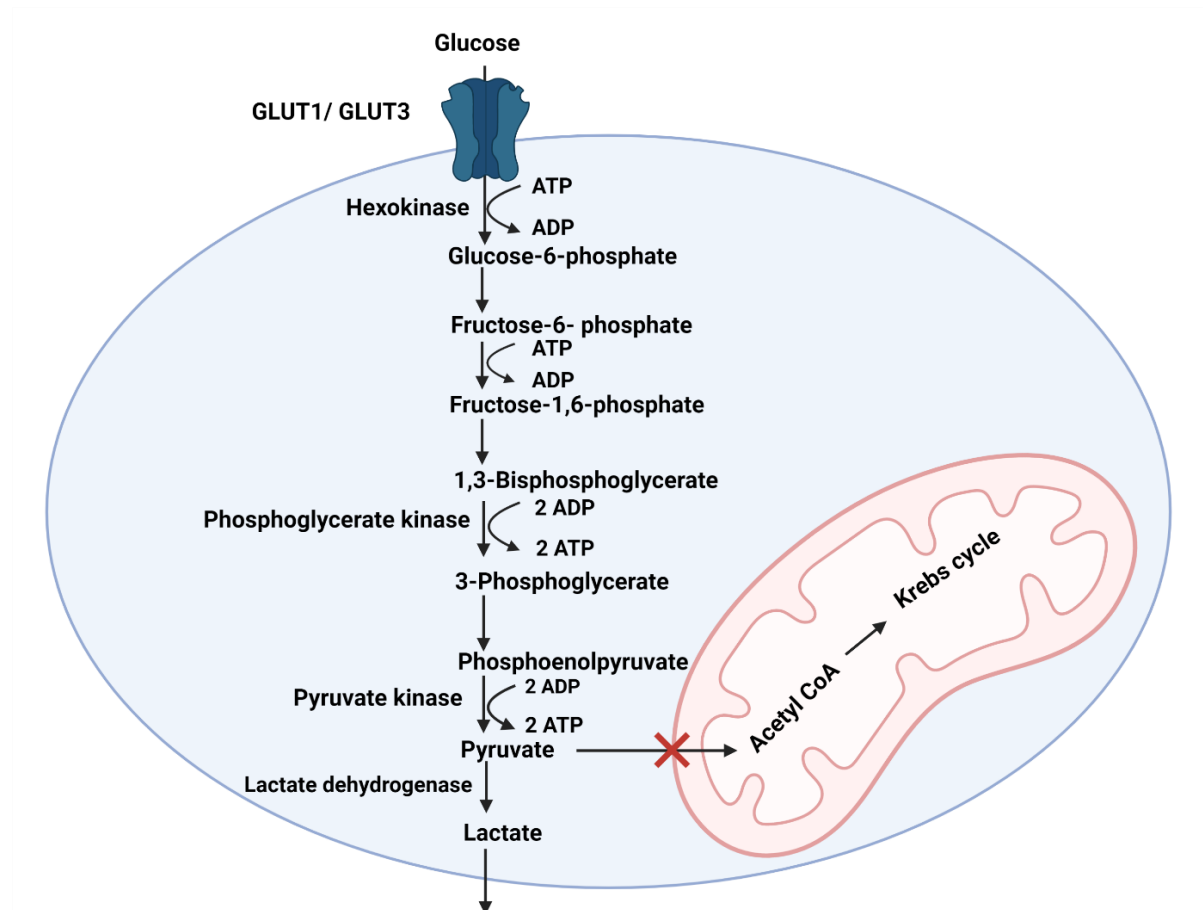
Figure 1.2   Cancer cells upregulate glucose transporters 1 & 3 (GLUT 1 & 3)) and all glycolytic enzymes converting pyruvate into lactate rather than into acetyl-coenzyme A (acetyl-CoA) even in the presence of oxygen, a phenomenon referred to as the Warburg Effect. Glycolysis results in net production of two ATP molecules per glucose molecule. ADP, adenosine diphosphate; ATP, adenosine triphosphate. Created with Biorender.com.

1.1.1.4.   Evading growth suppression

Besides sustained growth signaling and reprograming of glucose metabolism, a key hallmark capability of cancerous cells is bypassing of growth suppressing cellular programs which are regulated by tumor suppressor genes (TSGs). These genes negatively regulate cell proliferation by inhibiting the cell cycle progression and funneling cells toward apoptosis or senescence. Additionally, the expression of genes such as Moesin-ezrin-radixin like (MERLIN) tumor suppressor gene (NF2) inhibits growth of normal cells in response to cell-to-cell contact; This is called "contact inhibition" and is considered absent in malignant cells (4).

TSGs inactivation is a two-step process: chromosomal loss of one allele in a heritable fashion, and damage to the second allele by somatic mutation or hypermethylation of its promoter. Studies of loss of heterozygosity (LOH) can be used as a marker of TSG inactivation and have shown that several chromosomal regions may be damaged in NSCLC. The most common ones include the TP53 locus on 17p, the p16 locus on 9p and the retinoblastoma (RB) locus on 13q (12).

TP53 inactivation occurs in about 50% cases of NSCLC. In normal cells, the TP53 encoded protein p53 is upregulated in response to stressors like DNA damage or hypoxia, and acts as a transcription factor for genes including the cyclin dependent kinase inhibitor 1A (CDKN1A),

gene encoding p21, the mouse double minute 2 homolog (MDM2) proto-oncogene, growth arrest and DNA damage inducible (GADD45) genes, and the BCL2 associated X apoptosis regulator (BAX) gene. This results in regulation of the G1/S and G2/M check points, as well as apoptosis. Additionally, p53 also transcribes MDM2 which results in proteasomal degradation of p53 through negative feedback. MDM2 is overexpressed in 25 % of NSCLCs which represents another way of suppressing p53 function in NSCLC (12).

The cyclin dependent kinase inhibitor 2A (CDKN2A) gene encoding p16 is inactivated in 30-50 % NSCLC tumors. It is part of the p16-cyclin D1-CDK4-RB pathway which controls the G1/S transition of the cell cycle. Normally, in response to growth signals, cyclin D1 and cyclin dependent kinase 4 (CDK4) phosphorylate RB inactivating its inhibitory effect on G1/S transition. In response to extracellular stress signals, p16 activation occurs which inhibits CDK4 kinase activity resulting in RB stabilization and hence G1 cell cycle arrest. Therefore, p16 inactivation as well as cyclin D1 (25-47 % NSCLC) or CDK4 overexpression are potential mechanisms for abrogating the G1/S checkpoint (12).

> **Box 4 Therapeutic targeting of growth suppression pathways**
>
> In lung cancer, p53 serves as a prototypic model for gene replacement therapy with phase II studies reporting limited success. Flavopiridol which inhibits CDK4 and hence the p16-cyclin D1-CDK4 pathway is being tested in NSCLC clinical trials (12).

1.1.1.5.   Resisting cell death

Apoptosis is understood as a natural barrier to carcinogenesis. Apoptosis is often suppressed in malignant tumors which may cause treatment resistance. Intrinsic apoptosis is understood to be more relevant to cancer pathogenesis compared to extrinsic apoptosis. It can be activated by several intracellular signals which culminate in the activation of caspase 9, which in turn triggers a proteolytic cascade resulting in a coordinated disassembly of the cell. The overall balance between pro- and antiapoptotic proteins of the Bcl-2 family plays the decisive role in determining whether apoptosis is induced or not. BCL2 apoptosis regulator (Bcl-2), BCL2-like 1 (BCL2L1 or Bcl-x), BCL2 like 2 (BCL2L2 or Bcl-w), MCL1 apoptosis regulator BCL2 family member (MCL1 or Mcl-1) and B cell leukemia/lymphoma 2 related protein A1a (Bcl2a1a) are antiapoptotic while BAX and BCL2 antagonist/killer 1 (BAK1 or Bak) are proapoptotic (see Box 5). p53 induces apoptosis by upregulating the expression of proapoptotic proteins while the nuclear factor-κB (NF-κB, see subchapter 1.2.1.2) pathway inhibits apoptosis by upregulating antiapoptotic proteins. The most common way for cancer cells to evade apoptosis is the loss of TP53 tumor suppressor function. Alternatively, tumors may increase expression of antiapoptotic regulators (4).

Besides p53 inactivation (discussed in subchapter 1.1.1.4), BCL2 expression is found to be high in lung cancers although this has been reported more often in SCLC than NSCLC. Expression of the inhibitor of apoptosis protein 1 (IAP-1) has also been reported in NSCLC (7).

> **Box 5 Therapeutic targeting of cell death pathways**
>
> In preclinical NSCLC trials, BCL-xL antisense and bispecific BCL2-BCLxL antisense therapy are being evaluated as pro-apoptosis strategies (7,12).

1.1.1.6.   Inducing angiogenesis

Postnatally, the normal vasculature is largely quiescent except for angiogenesis activated during wound healing or in the reproductively viable uterine endometrium. However, continual

neovascularization develops relatively early on during multistage carcinogenesis to sustain metabolic needs of tumor cells. The tumor blood vessels thus formed are typically characterized by irregular blood flow predisposing tumor cells to develop cyclic and chronic hypoxia which in turn stimulates further neo-angiogenesis. The process of new blood vessel formation is stimulated mainly by vascular endothelial growth factor A (VEGFA or VEGF) secreted by tumor cells which binds to the VEGF receptors (VEGFR) 1-3 present on existing nearby vascular endothelial cells. VEGFA secretion by tumor cells may be stimulated by the action of oncogenes such as Ras and myc and also due to enhanced transcription following NF-κB pathway activation. VEGFA may also be released by inflammatory cells in the tumor microenvironment (TME) by the action of tumor promoting inflammatory cytokines. Additionally, VEGF ligands may be sequestered in the extracellular matrix that may be released by extracellular matrix-degrading proteases (e.g., matrix metallopeptidase 9, MMP-9) secreted by tumor cells (4).

NSCLC is generally highly vascular and the expression ratio of the VEGF189 mRNA isoform compared to other VEGF isoforms corelates with postoperative relapse rate and survival (13) (see Box 6).

> **Box 6 Therapeutic targeting of angiogenic signaling**
>
> Clinically, plasma VEGF levels can predict the extent of angiogenesis in NSCLC, but this is not standard clinical practice (12). As of 2022, Bevacizumab, a monoclonal antibody targeting VEGFA, has been become part of standard treatment options in conjunction with Erlotinib to treat EGFR mutated (Exon 19 deletion), non-squamous NSCLC (9).

1.1.1.7. Enabling replicative immortality

Chromosomal ends possess multiple tandem hexameric (TTAGGG) nucleotide repeats called telomeres which serve to maintain chromosomal integrity during cell division. Repeated cell divisions over time gradually shorten telomeric length to the point where the chromosomal ends are left exposed. Subsequent cell divisions eventually lead to end-to-end fusions generating unstable dicentrics which in turn lead to mitotic catastrophe and cell death. Therefore, normally cells can only undergo a finite number of divisions.

Cancer cells, on the other hand, develop replicative immortality by developing the ability to replenish their telomere sequences through the production of telomerase. This DNA polymerase can add TTAGGG repeats onto the telomeres. Telomerase protein subunit telomerase reverse transcriptase (TERT) has been shown to have additional functions pertaining to cell proliferation and inhibiting apoptosis (4).

Activation of telomerase is generally understood to be a late step in carcinogenesis. Nonetheless, it is a potential screening molecular marker that can be detected in preneoplastic cells derived from the bronchial epithelium (7,12). Telomere length has also been proposed as a prognostic factor in NSCLC (see Box 7), as a marker for chromosomal instability (14).

> **Box 7 Therapeutic targeting of Telomerase**
>
> Drugs targeting telomerase may have therapeutic potential and many such drugs involving anti-sense approaches have been reported in preclinical studies (7,12). More recently, development of specific ligands leading to G quadruplex telomeric structure stabilization are being developed which limit telomeric accessibility to telomerase (14).

1.1.1.8. Tumor promoting inflammation

All neoplastic lesions contain variable numbers of immune cells; this tumor-associated inflammation has been found to enhance tumorigenesis and cancer progression by secreting bioactive molecules in the TME resulting in sustained cell proliferation, reduced cell death, increased angiogenesis, and extracellular matrix (ECM) modification. Additionally, inflammatory cells can increase mutability in the developing tumor by release of reactive oxygen species (ROS). The cells responsible for tumor promoting inflammation comprise of immune cells like neutrophils, tumor-associated macrophages (TAMs, see Box 8) and myeloid-derived suppressor cells (MDSCs), as well as cancer-associated fibroblasts (CAFs). TAMs resemble M2 macrophages and additionally suppress cytotoxic T lymphocytes (CTLs) and natural killer (NK) cell activity besides promoting angiogenesis and tumor progression through mechanisms described earlier. CAFs secrete a variety of ECM components and are strongly implicated in causing desmoplasia which is reactive fibrosis around malignant tumors (4,15).

In NSCLC, there is marked infiltration of different types of immune cells which has been associated with angiogenesis Furthermore, tertiary lymphoid structures in lung parenchyma that are absent in the normal adult lung have been reported (16). In a study involving 104 NSCLC patients, infiltration of TAMs was identified using immunofluorescence staining of tumor tissue. TAM infiltration was associated with increased tumor cell survival particularly in case of hypoxic cells (17).

> **Box 8 Therapeutic targeting of tumor-promoting inflammation**
>
> Preclinical NSCLC trials in murine models targeting recruitment of TAMs are being increasingly reported where emphasis is on the blockade of C-C motif chemokine receptors type 2 (CCR2) and type 5 (CCR5) both of which upon activation promote chemotaxis and differentiation of TAMs at the tumor site (17).

1.1.1.9. Evading immune destruction

Besides having tumor promoting effects, the immune system also has tumor-antagonizing effects by eradicating neoplastic cells through constant immune surveillance. Cytotoxic CD8+ T cells recognize the tumor-specific antigens embedded on major histocompatibility complex (MHC) class I molecules presented by antigen-presenting cells (APCs) and thereby perform targeted tumor cell killing. Activation of the T cell receptor (TCR) by MHC I proteins requires co-stimulation of the CD28 surface receptor on CD8+ T cells (4).

Avoiding immune recognition is a hallmark capacity in malignant tumors that arises through "immunoediting" which is the selection of clones that can evade the immune system. Tumor cells may evade immune recognition in a number of ways; they may directly downregulate expression of tumor antigens or MHC class I molecules, secrete immunosuppressive cytokines (e.g.: IL-10 and tumor growth factor (TGF)-β), stimulate inhibitory cell types (e.g.: regulatory T cells (Tregs), regulatory B cells (Bregs), TAMs and MDSCs), or cause the expression of inhibitory surface receptors such as cytotoxic T-lymphocyte associated protein 4 (CTLA-4) and programmed cell death 1 (PD-1) receptors on T cells (18).

CTLA4 (CD152) when expressed by T cells competes with CD28 for its ligands expressed on APC surface, namely, CD80 and CD86, for which it has higher affinity. The subsequent binding of CTLA4 with these ligands inhibits the CD28 costimulatory signal required for TCR activation thereby inhibiting CD8+ T cells cytotoxicity against tumor cells (18,19).

PD-1 (CD279) when expressed by T cells binds to its ligand, programmed cell death ligand 1

(PD-L1, see Box 9) expressed by APCs or tumor cells at the time of TCR and CD28 activation. The newly activated TCR releases a src-kinase from its intracellular domain which phosphorylates TCR, CD28 and now additionally PD-1. This in turn causes PD-1 to recruit protein tyrosine phosphatase non-receptor type 11 (PTPN11) which dephosphorylates TCR, CD28 and PD1 resulting in inhibition of CD8+ T cells cytotoxicity (18,19).

CTLA4 and PDL-1 are collectively referred to as immune checkpoint ligands. Expression of immune checkpoint ligands can be an innate, constitutive ability developed by some of the tumor cells, or it may be induced in tumor cells secondary to inflammatory signals produced by the immune system.

Box 9 Therapeutic targeting of immune escaping mechanisms

PD-L1 expression has been described in approximately 50% of NSCLCs (19). Testing for PD-L1 expression through immunohistochemistry is standard clinical practice in metastatic NSCLC and immunotherapy with PD-1 and PDL-1 inhibitors is recommended if PD-L1 expression by tumor cells is 1% or higher (9).

1.1.1.10. Tissue invasion and metastases

Malignant tumors are distinct from benign tumors because of their hallmark capability to invade surrounding tissue and metastasize to distant sites via blood and lymph. The current understanding is that this capability is mainly regulated by the cell program called epithelial-mesenchymal transition (EMT). In this reversible program, polarized epithelial cells that interact by means of their basal surface with the basement membrane, lose their polarity and cellular junctions, and gain relative motility by transforming into cells with a mesenchymal phenotype (20).

EMT is induced by various stressors including hypoxia, ROS and radiation. It is mediated by transcription factors such as snail family transcriptional repressor 1, (SNAI1 or Snail), snail family transcriptional repressor 2, SNAI2 or Slug), Twist family basic helix loop helix transcription factor 1 and 2 (Twist 1 and Twist 2), as well as Zinc finger E-box binding homeobox 1 and 2 (Zeb1 and Zeb2). These EMT transcription factors are expressed in various amounts and combinations to evoke EMT. EMT can be activated transiently or stably, and to differing degrees resulting in variable potential for invasion and metastasis among different tumors and within the course of disease of a particular tumor. Furthermore, once micro-metastases are lodged at a distant site, EMT is understood to reverse so that a mesenchymal-epithelial transition (MET) occurs, and colonized cells become identical to those of the parent tumor before EMT. Lastly, stromal cells in the tumor microenvironment (TME) may also play a role in EMT-mediated invasion and metastasis of tumor cells through crosstalk. Cytokines such as IL-1, IL-6, IL-8, TNF-α and TGF-β as well as several proteinases and growth factors released by cells in the TME have been implicated in inducing EMT-like changes in tumors (4).

In NSCLC, TGF-β, IL-6, mutated Ras protein, mutated EGFR and ALK fusion proteins are known to activate the EMT program through secondary signaling pathways, ultimately leading to activation of EMT transcription factors. TGF-β can activate signaling cascades including phosphatidylinositol 3-kinase (PI3K)-Akt, and mitogen-activated protein kinase (MAPK) pathways; Interleukin-6 (IL-6) can activate the Janus kinase-signal transducer and activator of transcription 3 (JAK-STAT3) signaling pathway; Ras, mutant EGFR and ALK fusion proteins can activate the PI3K-Akt and MAPK pathways; These signaling pathways can upregulate the expression of EMT transcription factors either directly or indirectly by downstream activation of other pathways including NF-κB (12).

1.1.2.   Tumor progression and hypoxia

Tumor hypoxia has profound impact on tumor cells and the TME, influencing most hallmarks of carcinogenesis including tumor proliferation, cell death, angiogenesis, inflammatory response, tumor invasive and metastatic potential, and even genomic mutability. In this context, tumor hypoxia can lead to new cancer formation but also to tumor aggressiveness and treatment resistance in existing cancers, including NSCLC. This is discussed in detail in subchapter 1.2.

1.2.   Tumor hypoxia

Physiologists define tissue hypoxia as reduced availability of oxygen to cells restricting their normal functioning. The threshold of oxygen partial pressure at which this happens is harder to define. The oxygen concentration where a tissue functions normally is referred to as physoxia and varies across tissues. In case of lung tissue, physoxia is generally described as 40-45 mm of Hg (~6 % O_2) (21,22). In case of the lung, tissue hypoxia can be understood as oxygen partial pressure below this range.

However, in case of tumor tissue, the threshold of oxygen partial pressure for defining tumor hypoxia is the cut-off where tumor cell adaptation to reduced availability of oxygen may lead to treatment resistance. This is generally agreed upon as 10 mm of Hg (~1 %) in literature although cell type and environmental conditions play a role (23,24).

Direct measurement of tissue oxygen partial pressures using oxygen sensitive microsensors has shown that tumors cells and TME are characterized by much lower PO_2 values than their normal counterparts (25).

Tumor hypoxia arises due to rapid, uncontrolled proliferation of cancer cells without an efficient vascular supply. Neo-angiogenesis is, therefore, activated to keep up with metabolic demands of the tumor cells. The resulting vessel formation in tumors is architecturally chaotic and the new vessels are scantily lined with poorly differentiated pericytes leading to turbulent and non-laminar blood flow that makes the tumor vasculature leaky and prone to thrombosis (4).

The unstable and irregular perfusion of tumor cells results in hypoxia which was previously termed as "acute" and currently referred more commonly to as "cyclic" as it is generally reversible and repetitive (26). Such perfusion-limited hypoxia is additionally associated with reoxygenation of tumor cells.

It has long been established through direct oxygen partial pressure measurements that cells at 150 μm from a feeding vessel or more become anoxic and are liable to necrosis but cells at distances below this cutoff have a continuum of different oxygen concentrations ranging from normoxia and mild hypoxia to severe hypoxia and necrosis. Such diffusion-limited hypoxia due to chaotic vascular branching and rapid tumor growth is persistent and more commonly referred to as "chronic" or "continuous" hypoxia (27).

1.2.1. Key regulators of cellular adaptation to hypoxia

Many signaling pathways have a role in the hypoxia-mediated cell response. However, the single most important pathway is the hypoxia-inducible factor (HIF) pathway. Perhaps the second most important pathway in this regard is the NF-κB pathway which is responsible for the hypoxia-induced inflammatory response. Additionally, there is cross talk between the two pathways, and they also directly upregulate each other's transcription.

1.2.1.1. HIF signaling pathway

Hypoxia Inducible Factor-1 (HIF-1) was initially discovered by Greg Semenza (28) who in 2019 was awarded the Nobel Prize in Physiology or Medicine for his contributions to understanding cellular oxygen-sensing mechanisms. Today we know that there are in fact three HIF proteins (HIF-1-3) that constitute the master regulators of the cellular response to hypoxia.

The HIF family comprises of transcription factors composed of two subunits. The α subunits are present in the cytosol and are rapid degraded in under 10 min at normal oxygen concentration. This degradation is a consequence of hydroxylation of α subunits by Prolyl-hydroxylases (PHD1-4) (Figure 1.3). PHD2 and PHD3 are themselves transcriptional targets of HIF and thus form a negative feedback loop. Hydroxylation by PHDs leads to recruitment of the Von-Hippel-Landau (VHL) protein which forms an E3 ubiquitin ligase complex ubiquitinating HIF-α for subsequent proteasomal degradation. Under hypoxia, PHDs are inactivated resulting in stabilization of HIF-α subunits that then undergo nuclear translocation where they dimerize with HIF-β subunits. The HIF complex thus formed then binds to hypoxia response elements (HREs) in DNA along with coactivators p300 and Creb-binding protein (CBP), which initiates transcription of HIF target genes. HIF complex is antagonized by factor inhibiting HIF (FIH) which hydroxylates HIF subunits and blocks their interaction with p300 and CBP.

HIF-1 is the most common transcription factor in the HIF family. However, HIF-2 and HIF-3 also have a role in hypoxia related transcriptional response. It is generally understood that HIF-1 is more relevant in acute hypoxia while HIF-2 may be more relevant in chronic hypoxia. Relative expression of the type of HIF has also been shown to differ among cell types. (22,29).
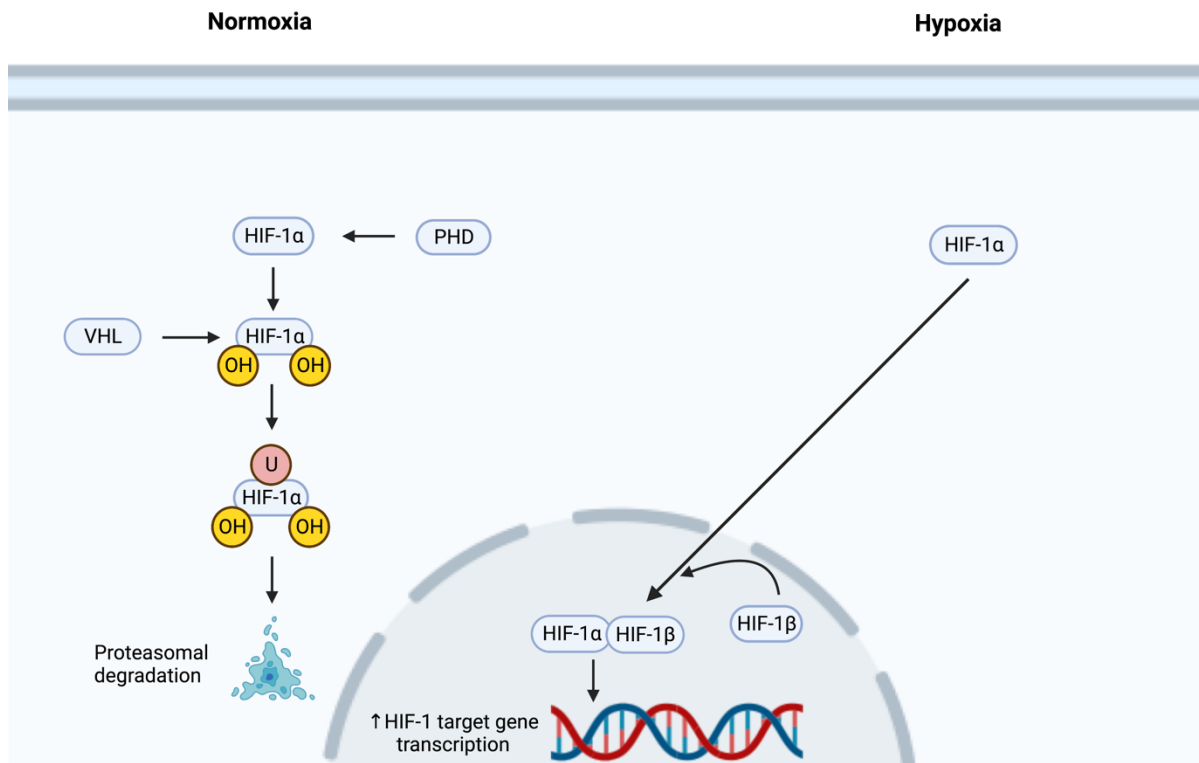
Figure 1.3   HIF-1α is degraded within 5-10 minutes under normal intracellular oxygen partial pressures (normoxia) as a result of hydroxylation by PHD which signals VHL to initiate ubiquitination of HIF-1α and subsequent proteasomal degradation. Under hypoxia, PHD is inactivated, stabilizing HIF-1α which undergoes nuclear translocation and dimerization with HIF-1β to act as a transcription factor for genes possessing an HRE. HIF, hypoxia-inducible factor; HRE, hypoxia response element; OH, hydroxyl group; PHD, Prolyl-hydroxylase; U, ubiquitin; VHL, Von-Hippel-Landau protein; Created with Biorender.com.

1.2.1.2.   NF-κB signaling pathway

NF-κB was discovered by Baltimore and Sen in 1986 (30) and is an inducible dimeric transcription factor which transcribes hundreds of target genes involved in immune response and inflammation. Additionally, it Is involved in regulating cell survival by promoting cell proliferation and inhibiting apoptosis. However, there are few cases and cell types where NF-κB has been reported to contribute to cell death.

The mammalian NF-κB family comprises of five different monomers: RelA (p65), c-Rel, RelB, NF-κB1 (p105, precursor of p50), and NF-κB2 (p100, precursor of p52). These monomers form homodimers and heterodimers. Different NF-κB dimeric complexes are formed based on cell type and stimulus.

Normally, NF-κB dimers are bound to Inhibitor of kappa B (IκB) proteins in the cytoplasm. Several stimuli such as cytokines, DNA damage and hypoxia can recruit signaling proteins that converge onto the IκB kinase (IKK) complex (IKKα, IKKβ, IKKγ) which degrades IκBs releasing NF-κB dimers. After release from the protein complex with IκB, the dimers translocate into the nucleus and bind to kappa B sites in promoter regions of their target genes. p65 contains a transcriptional activation domain and can activate gene transcription, while p50 is lacking such a domain and its homodimers cannot activate gene expression. NF-κB is pushed out from the

nucleus by IκB.

NF-κB signaling can be activated in several different ways (Figure 1.4):

The **canonical pathway** is triggered by stimuli such as Tumor necrosis factor-α (TNF-α) and Interleukin-1 (IL-1) released in response to, for example radiation exposure. They bind to their specific receptors which brings about activation of TGF-β activated kinase 1 (TAK1) that causes phosphorylation of IKKβ in the IKK heterotrimer complex. The phosphorylated IKK complex in turn causes phosphorylation of IκBα or IκBβ. Phosphorylation of IκB proteins leads to their ubiquitination which brings about degradation of IκB proteins by 26S proteasome. The freed NF-κB is then phosphorylated. In case of the canonical pathway, p65 within the p65/p50 dimer is phosphorylated following which the dimer translocates into the nucleus and binds to specific DNA sites as transcribing various target genes. With some delay, newly synthesized IκBα enters the nucleus and prevents the NF-κB dimer from DNA binding by transporting the dimers back into the cytoplasm and thereby terminating the activation. The canonical pathway can get activated within minutes (31).

The **alternative pathway** is triggered by stimuli such as CD40 ligand (CD40LG), TNF superfamily member 13b (TNFSF13B or BAFF) or TNF superfamily member 11 (TNFSF11 or RANKL) binding to their specific receptors (CD40, BAFF-R, RANK). This stimulates NF-κB inducing kinase (NIK) that phosphorylates the IKKα homodimer complex that in turn processes NF-κB2 (p100) to p52 and activates the p52/RelB dimer to translocate into the nucleus initiating target gene transcription. The alternative pathway gets activated over several hours (31).

The **genotoxic stress-induced pathway** is activated by DNA double strand breaks (DSBs) rather than by external stress stimuli. DSBs are sensed and responded to by ataxia telangiectasia mutated (ATM) protein resulting in phosphorylation of NF-κB essential modulator (NEMO or IκBγ) which triggers its SUMOylation by small ubiquitin like modifier 1 (SUMO-1). NEMO SUMOylation may be promoted by p53 induced death domain containing protein (PIDD) through receptor interacting protein 1 (RIP1). The SUMOylated NEMO undergoes mono-ubiquitination by E3 ubiquitin ligase. The ubiquitinated NEMO is then exported into the cytoplasm where it activates TAK1 to phosphorylate the IKK complex. In this way, the genotoxic pathway ultimately converges with the canonical pathway of NF-κB activation. The phosphorylated IKK complex in turn phosphorylates IκBα resulting in its degradation and release of cytosolic NF-κB which can then enter the nucleus to act as an activated transcription factor. The genotoxic pathway gets activated within 1-2 h after DSB induction (32).
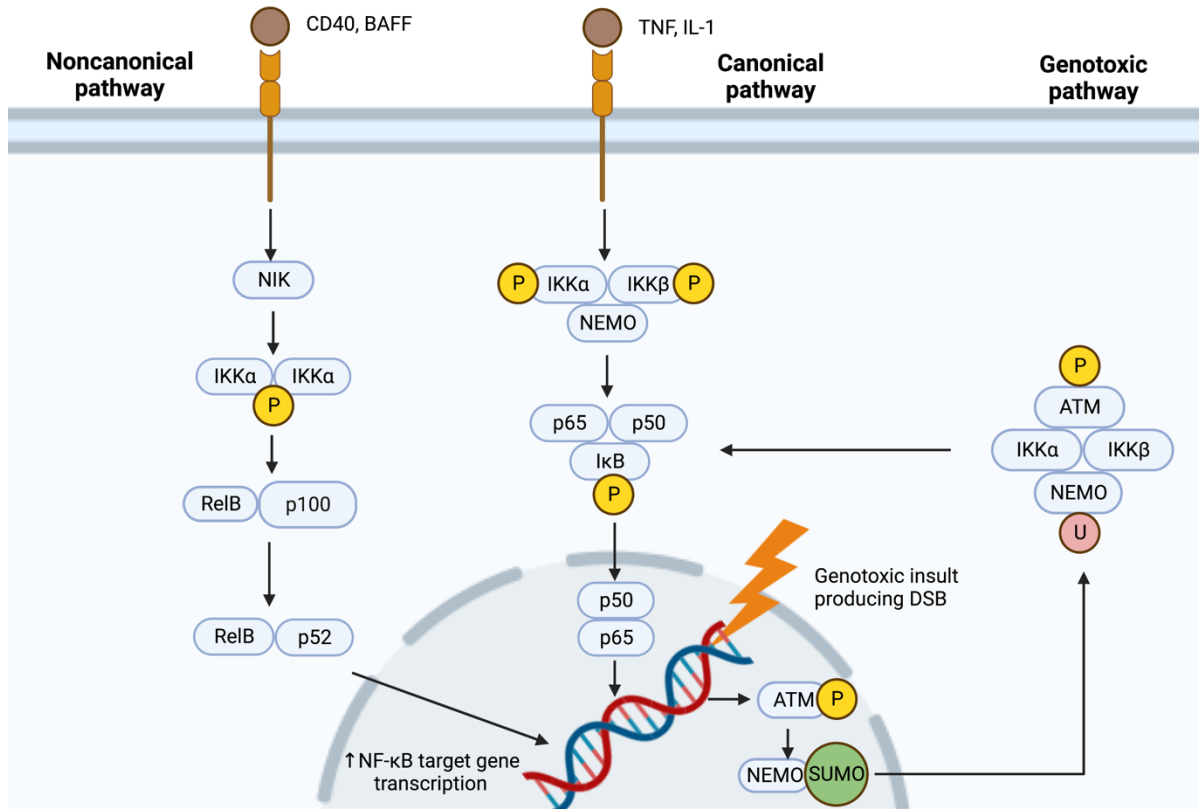
Figure 1.4   Both the canonical pathway and non-canonical (alternative) pathway of NF-κB activation are induced by external ligands as opposed to the ligand-independent genotoxic (atypical) pathway.

In both pathways, IKK complex initiates degradation of IκB. The IKK complex comprises IKKα, β and γ (NEMO) subunits in case of canonical pathway and only two IKKα subunits in case of the alternative pathway.

In the genotoxic pathway, a signalosome containing, amongst others, ATM and NEMO transports the activation signal from the cell nucleus to the cytoplasm and IκB is degraded after phosphorylation via IKK and ubiquitination.

Degradation of IκB frees NF-κB (RelB/p52 or p50/p65) to translocate into the nucleus where they act as transcription factors.

CD40, cluster of differentiation 40 protein; BAFF, B cell activating factor; TNF, tumor necrosis factor; IL-1, interleukin 1; NIK, NF-κB inducing enzyme; IKK, IκB kinase; NEMO, NF-κB essential modulator; IκB, inhibitor of κB; P, phosphate; ATM, ataxia telangiectasia mutant protein; U, ubiquitination; SUMO, SUMOylation; DSB, double strand break; Created with Biorender.com.

27

1.2.2. Cellular adaptations to hypoxia in tumor cells

The focus of this section is to highlight the effects of hypoxia on tumor cells and TME, and how these effects may contribute toward tumor aggressiveness and treatment resistance. The effects will vary according to hypoxia severity and duration along with the type of cancer.

1.2.2.1. Regulation of cell proliferation

Hypoxia has been demonstrated to inhibit cell proliferation in several cell types and a wide variety of cancer cell lines. This is brought about by cell cycle arrest at the G1/S junction (Box 1Box 11). A variety of mechanisms are mentioned in literature to explain how this happens (25,33).

Hypoxia is known to indirectly increase expression of cyclin dependent kinase (CDK) inhibitors (CDKIs) p21 and p27 because of p53 stabilization. Hypoxia, through HIF-1, can also decrease MYC Proto-Oncogene (c-Myc) expression counteracting its downregulating effect on p21 and p27 (33). HIF-1 can further inhibit c-Myc by interfering with its complex formation with Myc-associated protein X (Max) (25). Lastly, HIF-1 can physically displace c-Myc from its binding sites on the DNA helix resulting in de-repression of p21 and p27 synthesis. Overexpression of these CDKIs due to c-Myc suppression inhibits CDK4, CDK6 and cyclin D inhibiting cell cycle progression in G1 phase (33).

Hypoxia also inhibits DNA replication by inhibiting the mini-chromosome maintenance (MCM) protein complex crucial for initiating DNA replication. This is understood to happen through inhibition of the MCM complex after binding with HIF-1 and HIF-2 protein dimers following their activation under hypoxia (25).

However, even under hypoxia, many cancers seem to maintain proliferation which is due to counteracting effects of oncogenic growth signals (33). Additionally, hypoxia can in some cases also activate HIF-2 which can upregulate c-Myc activity by stabilizing the myc-Max complex, facilitating its inhibition of CDKIs and thus promoting cell cycle progression (25).

While the **NF-κB pathway** has been reported to promote cell proliferation and regulate the cell cycle in normal and tumor cells, its role in doing so in case of hypoxia remains unclear.

> *Box 11   Clinical implication of reduced cell proliferation*
>
> While cell cycle inhibition does not contribute toward tumor aggressiveness, decreased cellular proliferation does impact treatment efficacy of radiotherapy and classical chemotherapy which are relatively more cytotoxic in case of rapidly dividing cells.

1.2.2.2. Regulation of energy metabolism

Hypoxia shifts cells to glycolysis. However, glycolysis produces 18 times less ATP per glucose molecule. Additionally, in proliferating tumor cells glucose is also needed as a source for synthesis of DNA building blocks like ribose penta-phosphate and nucleotides. This puts tremendous pressure on glucose supply. To make up for this increased demand, glucose transporters like GLUT-1 (SLC2A1- solute carrier family 2 member 1) and GLUT-3 (SLC2A3- solute carrier family 2 member 3) are also upregulated. Increased glycolysis along with diminished oxidative phosphorylation under hypoxia results in greater lactate production (Box 12). To prevent cytosolic acidification, lactate is excreted from the cell through monocarboxylate transporters, thereby decreasing extracellular pH. This acidification of the TME may be worsened by upregulation of carbonic anhydrase IX (CA-IX) under hypoxia which is expressed in many tumors (Box 12) (29).

The metabolic reprogramming of glycolysis under hypoxia is mediated mainly through the HIF-1 pathway. HIF-1 has been shown to upregulate hexokinase 1 and 3, aldolase A and C, glyceraldehyde 3-phosphate dehydrogenase (GPDH) and lactate dehydrogenase (LDH) as well as GLUT-1 and 3. Besides regulating expression of glycolytic enzymes, HIF-1 also modulates the function of the electron transport chain in hypoxia. It causes replacement of cytochrome C oxidase (COX) subunit COX4-1 with COX4-2 and this reduces mitochondrial consumption of oxygen (29).

> **Box 12   Clinical implication of altered energy metabolism**
>
> The acidification of TME resulting from hypoxia-induced metabolic adaptations promotes cell migration and invasion; hence increases tumor aggressiveness. Clinically, CA-IX expression is a poor prognostic feature in tumors (29).

1.2.2.3.   Hypoxia and cell death

Hypoxia can initially induce apoptosis in tumor cells. This is understood to be due to stabilization of p53 through HIF-1 directly as well as through inhibition of mouse double minute 2 homolog (MDM2) by HIF-1. The p53 then activates the intrinsic pathway of apoptosis. However, this also creates a selection pressure against cells with wild-type TP53. Therefore, chronic hypoxia results in survival of inactivated TP53 cell clones that are resistant to apoptosis (Box 13) (23,25).

On the other hand, hypoxia has also been shown to upregulate synthesis of antiapoptotic proteins through activation of **NF-κB** and Krüppel-like factors 5 (KLF5)-mediated transcription (34,35).

Besides apoptosis, chronic hypoxia has also been shown to induce autophagy. This can be beneficial for tumor cell survival in many cases because it digests unfolded proteins and damaged organelles, especially mitochondria, that can lead to an increase of ROS. It can also provide tumor cells with recycled metabolites and cell products. Hypoxia is understood to regulate autophagy through HIF-1 by inducing expression of Bcl2 interacting protein 3 (BNIP3) and BNIP3 ligand (BNIP3L) which in turn promote release of Beclin-1 that is the main regulator of autophagy. Additionally, since mechanistic target of Rapamycin (mTOR) protein normally inhibits autophagy, its inhibition under hypoxia can induce autophagy (23,25).

> **Box 13   Clinical implication of selection of p53 mutants**
>
> Selection of TP53-mutated tumor cells by hypoxia along with other mechanisms of inhibiting apoptosis, as well as removal of damaged cell organelle through autophagy can lead to treatment resistance.

1.2.2.4.   Angiogenesis

Tumor cells exhibit neo-angiogenesis and the main driver for this is hypoxia (see Box 14), mainly by the upregulation VEGF, both through HIF-dependent and independent mechanisms (35,36).

Both HIF-1 and HIF-2 are known to promote tumor vascularization through VEGF expression, the former being more important in acute setting while the latter being more relevant in chronic hypoxia (25). VEGF expression may also be induced by the NF-κB pathway through an inflammatory response to hypoxia mediated by the tumor cells and their microenvironment (35).

Hypoxia may induce other pro-angiogenic factors in tumor cells including platelet-derived growth factor-β (PDGF-β), angiopoietin-2 (ANGPT2) and stromal-derived factor 1α (SDF-1α). Hypoxia has also been shown to diminish expression of the anti-angiogenic factor thrombospondin-1 (TSP-1) (36).

> **Box 14   Clinical implication of angiogenic switch**
>
> The response of tumor cells to hypoxia in the form of boosting neo-angiogenesis contributes to their growth and invasion and hence is a cause of tumor aggressiveness.

1.2.2.5.   Stemness, invasion and metastasis

The presence of "cancer stem cells" (CSCs) in solid tumors is not definitively proven (25). However, hypoxia is understood to regulate stem cell-like features in some cancer cells which include pluripotency, apoptotic resistance as well as relative motility to initiate tumor invasion and metastasis (Box 15). These characteristics are generally acquired because of the EMT cell program following hypoxia which is mainly initiated by the HIF-1 pathway (25,37).

Hypoxia contributes to EMT by upregulating EMT transcriptional factors such as SNAI1, SNAI2, TWIST, TCF3 (transcription factor 3), ZEB1 and ZEB2 (see subchapter 1.1.1.10). Hypoxia has been shown to regulate many other proteins that promote cancer cell migration such as right open reading frame kinase 3 (RIOK3) which induces actin cytoskeleton re-organization, collagen prolyl hydroxylases which induce collagen deposition and breast cancer cell migration, and lysyl oxidase (LOX) which increases focal adhesion kinase activity. This induction of migration results in increased tumor invasiveness and metastasis. Additionally, hypoxia has also been shown to be involved in "homing" disseminated tumor cells to distant sites and establishing premetastatic niches in these distant sites for overt metastases (25).

Besides HIF signaling, the **NF-κB pathway** has also been reported as a driver of EMT secondary to hypoxia in tumors like pancreatic and colorectal cancers. There is a two-way crosstalk between HIF and NF-κB pathways. The latter is known to be induced following HIF-1 accumulation and HIF-1α is a direct target gene of NF-κB pathway (36). Hypoxia can also activate NF-κB by a Ras/Raf mediated signaling pathway. NF-κB can upregulate SNAI1 and TWIST transcription inducing EMT (38).

> **Box 15   Clinical implication of enhanced aggressiveness**
>
> Tumor invasiveness and metastases are the most pivotal indices for tumor aggressiveness and causes of treatment resistance. Most prognostic markers used in oncology are indicators of either tumor invasiveness or metastatic potential.

1.2.2.6.   Tumor immune response to hypoxia

Tumor hypoxia generates an immune response in tumors in many ways, contributing to an overall tumor promoting and immunosuppressive effect through stimulation of regulatory T-cells and TAMs and inhibition of dendritic cells and CTLs. In addition, hypoxia can induce PD-L1 expression which contributes to evasion from immune surveillance (25).

The tumor immune response to hypoxia is primarily mediated by **NF-κB pathway** activation in tumor cells as well as inflammatory cells within the TME. The pathway is activated via release of damage associated molecular patterns (DAMPs) by necrotic cells. DAMPS include ATP/ADP, membrane debris, high mobility group box 1 (HMGB1) protein, nucleic acids, etc. by necrotic cells. NF-κB pathway activation leads to the expression of NF-κB target genes

leading to the inflammatory reparative response (IRR) which contributes to tumor cell survival (Box 16) (35).

> *Box 16* *Clinical implication of inflammatory reparative response (IRR)*
>
> The overall effect of hypoxia induced IRR depends on cell type and can positively influence cell survival, immune invasion, EMT and angiogenesis all of which contribute to tumor aggressiveness and treatment resistance.

1.2.2.7. Increased mutability

Severe intra-tumor hypoxia ($\leq 0.1\%$ O_2) promotes genomic instability (Box 17) (22) through an increase in number of mutations and the inhibition of DNA repair. HIF-1 is reported to cause genetic instability in cancer cells through inhibition of DNA mismatch repair genes mutS homolog 2 and 6 (MSH2 and MSH6). HIF-2 has not been reported to increase genomic instability like HIF-1 and instead is known to regulate DNA repair in response to ROS damage (25).

> *Box 17* *Clinical implication of enhanced mutability*
>
> Genetic instability in pre-existing tumors results in tumor heterogeneity which can lead to treatment resistance and more aggressive phenotype development.

1.2.3. Hypoxia and reoxygenation in tumor cells

Reoxygenation of previously hypoxic cells occurs in case of acute (intermittent or cyclic) hypoxia where a collapsed or spasmodic vessel becomes patent again allowing reperfusion. Neo-angiogenesis stimulated by hypoxia can also perfuse previously hypoxic cells. Additionally, it can also be observed following chemotherapy or radiotherapy resulting in shrinkage of the tumor mass and more effective diffusion of oxygen to previously hypoxic cells (26,39).

1.2.3.1. ROS production and effects on NF-κB signaling

Reoxygenation results in generation of ROS contributing to oxidative stress and subsequent cell damage. In this case, ROS generation depends on nicotinamide adenine dinucleotide phosphate hydrogen (NADPH) oxidases and the electron transport chain in the mitochondrial membrane. Tumor cells capable of autophagy are better equipped to survive ROS-induced oxidative stress.

ROS-mediated NF-κB activation is cell type-dependent. ROS-induced alternative phosphorylation of IκBα on Tyr42 leads to IκBα ubiquitination and degradation. This alternative phosphorylation has also been shown to happen through PI3K-Akt pathway. Degradation of IκBα through its usual phosphorylation at Ser32 or 36 by IκBα-Kinase (IKK) is less common in case of reoxygenation. Degradation of IκBα frees the cytosolic NF-κB which then activates target gene transcription after nuclear translocation (26).

1.2.3.2. Protein synthesis and effects on HIF signaling

Reoxygenation is supposed to trigger protein synthesis which had previously been stalled due to relative depletion of ATP. By the same argument, reoxygenation can stimulate translation of HIF-1-regulated transcripts sequestered in stress vacuoles during hypoxia by promoting their release (26).

Repeated cycles of hypoxia and reoxygenation have also been shown to result in relative

abundance of cytosolic HIF-1α due to increased stabilization which amplifies the HIF-1-mediated response during a subsequent period of hypoxia. This is understood to be mediated through the PI3K-Akt pathway activation during reoxygenation (26,36).

1.2.4.   Hypoxia in NSCLC

Interestingly, the first tumor where hypoxia was observed was lung cancer. Thomlinson and Gray reported in 1955 that hypoxic lung carcinoma cell columns were surrounded by a necrotic mass caused by an oxygen gradient (26,40). Since then, multiple PET studies utilizing hypoxia-specific radiotracers have shown that hypoxia is detectable in up to 80 % of NSCLC patients comprising of all clinical stages (2,41).

HIF-1α expression is associated with treatment resistance to radiotherapy, chemotherapy, and targeted therapy with EGFR TKIs and three separate meta-analyses have confirmed that HIF-1α expression is associated with decrease in overall survival (OS) in NSCLC patients (42–44). Similarly, carbonic anhydrase-IX, another common hypoxia marker, has also been found to be expressed in NSCLC patients and is of prognostic importance (2).

Therefore, because hypoxia-induced therapy resistance is well-characterized in NSCLC, therapies targeting hypoxia should, in theory, improve clinical outcomes. One such approach is the use of hypoxic cell radiation sensitizers (e.g.: misonidazole and nimorazole). Misonidazole has been tested in Phase III trials but showed increased peripheral neuropathy (45). Nimorazole is understood to have better toxicity profile but is currently not part of any clinical trials.

Another approach is to increase oxygen delivery to tumors (e.g., carbogen and nicotinamide). However, radiotherapy with carbogen and nicotinamide was not found to improve loco-regional control while treatment toxicity was increased (46).

Cytotoxic prodrugs activated by hypoxia (e.g., tirapazamine and evofosfamide) have also been developed and used but favorable results were reported only with tirapazamine but at the cost of increased adverse effects (47).

Drugs like metformin have been used to decrease tumor cell oxygen consumption. A randomized phase II trial is currently in progress to assess if metformin administered concurrently with chemoradiation can improve survival in locally advanced NSCLC patients (NCT02186847).

To conclude, targeting of hypoxia in NSCLC, in the context of improving radiotherapy outcomes, is yet to show any distinctly favorable outcome.

1.3. Physical and biological fundamentals of radiotherapy

Radiotherapy involves the use of ionizing radiation for treating human cancers. It has been around for over 100 years starting almost immediately after the discovery of X-rays and radioactivity in 1895 and 1896, respectively. It offers locoregional control against malignant tumors as an alternative or as an adjunct to surgery and is used in treatment of about half of all cancer patients (48).

Ionizing radiation is a double-edged sword in the sense that it is toxic to both normal and malignant tissues. This limits the maximum radiation dose that may be delivered to a tumor without exceeding normal tissue tolerance of neighboring structures delineating the importance of the therapeutic window between tumor control and normal tissue toxicity.

Widening of the therapeutic window can theoretically be achieved by two strategies: either radio-sensitization of tumor cells or radioprotection of normal tissue cells. In this context, efforts are underway to overcome factors such as tumor hypoxia which make tumor cells resistant to treatment.

1.3.1. Quality of ionizing radiation

In radiation biology, the quality of ionizing radiation is described by the ionization density along its tracks through matter. This is quantified by linear energy transfer (LET) which is the mean energy (KeV) deposited in matter by ionizing radiation per unit length (μm) of its track. Based on LET, ionizing radiation can be divided into low- and high-LET radiation (48).

1.3.1.1. Low-LET radiation

X-rays, γ rays and electrons are low-LET ionizing radiation with their LET in water ranging between 0.2 to 5 KeV/μm, losing energy gradually along radiation tracks leading to diffuse ionizing damage.

1.3.1.2. High-LET radiation

Carbon ions are an example of high-LET ionizing radiation with their LET in water being in the range of 50-200 KeV/μm dependent on the energy of the ion beam. High-LET radiation forms broader ionization tracks through biological tissue as its interaction with matter is more intense due to high charge and atomic number (Z); however, most of this energy is deposited at the end of the track in a small volume; such energy deposition is referred to as the Bragg peak (Figure 2.5). It results in dense ionization in biomolecules such as DNA and thereby induces complex DNA damage.

1.3.2. Ionizing radiation-induced DNA damage

The main cellular target of ionizing radiation is nuclear DNA. It may pass through the cell and nucleus to ionize DNA directly which is referred to as "direct action"; or it may ionize intracellular water molecules producing highly reactive hydroxyl (OH$^\bullet$) radicals, which being relatively long-lived, can diffuse to DNA to ionize it, referred to as "indirect action" of ionizing radiation (Figure 1.5). Super oxide anions ($O_2^{\bullet-1}$) and hydrogen peroxide (H_2O_2) molecules also contribute to indirect action of radiation and their formation depends on the presence of molecular oxygen.

Ionization of DNA manifests as damage to a nitrogenous base or interruption of its sugar-phosphate backbone, resulting in single or double-strand breaks (SSBs or DSBs) in the DNA helix. SSBs are of minor relevance for cell survival owing to effective repair but DSBs pose a greater challenge to survival and virtually a single unrepaired DSB in a cell can lead it down the path of cell death (48).
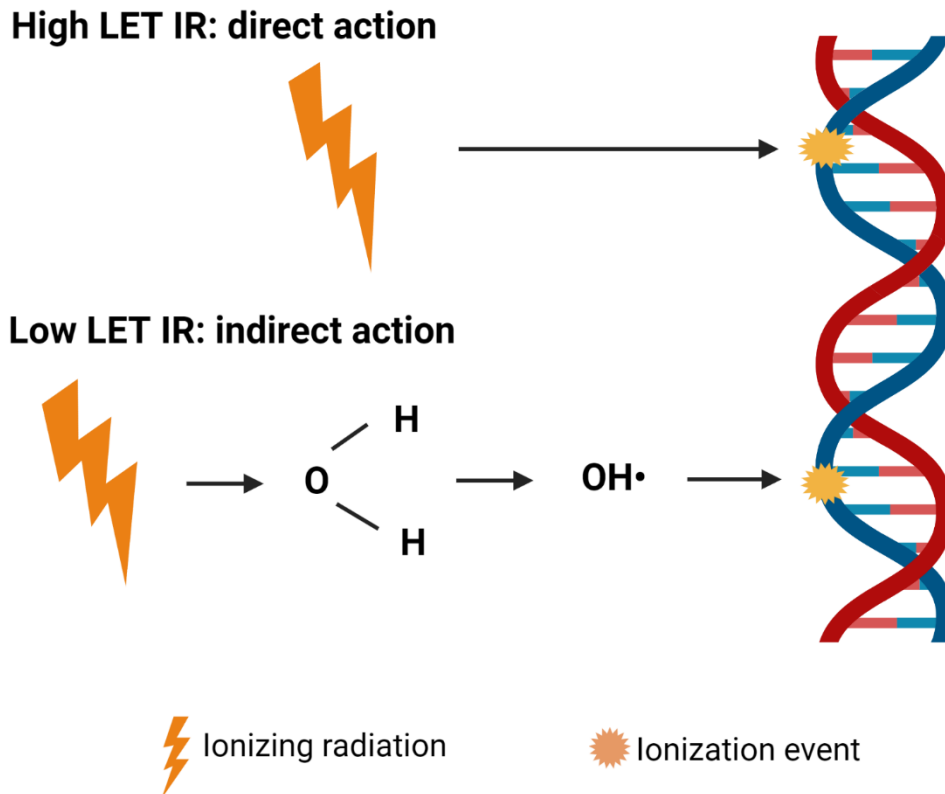
Figure 1.5   Indirect effect of ionizing radiation on DNA through radiolysis of water forming OH• radicals may diffuse to the DNA resulting in its damage; and direct effect of ionizing radiation through direct interaction of photon or charged particle with the DNA helix resulting in its damage.

IR, ionizing radiation; LET, linear energy transfer; OH•, hydroxyl radical; O, oxygen atom; H, hydrogen atom. Created with Biorender.com.

Direct action of ionizing radiation dominates for high-LET radiation qualities. On the other hand, the ratio between indirect and direct action is around 3:1 for low-LET radiation. A direct implication of this is greater dependence of low-LET radiation on oxygen as a source for ROS-induced DNA damage (49).

A second difference between low- and high-LET radiation-induced toxicity is the type of DNA lesions. High-LET radiation tends to produce a higher number of complex lesions also referred to as cluster lesions or "locally multiply damaged sites", that may be defined as two or more lesions within 10-20 DNA base pairs. Such lesions, particularly, clustered DSBs, are much harder to repair in comparison to the damage produced by low-LET radiation (49).

An index which considers the severity of biological damage induced by high-LET radiation compared to low-LET radiation is called Relative Biological Effectiveness (RBE). The RBE of 250 KeV X-rays is defined as 1. The RBE of carbon ions in comparison is in the range of 2.5 to 3 depending upon cell type and actual energy of the carbon ions (49).

1.3.3.   Radiation-induced cytotoxicity and hypoxia

Besides all the cellular adaptations mentioned in the subchapter on Tumor Hypoxia (subchapter 1.2) that result in treatment resistance in general, hypoxia also has a more direct physicochemical basis for producing radioresistance. This is often referred to as the "oxygen enhancement effect". DNA strand breaks in tumor cells induced by exposure to ionizing

radiation are peroxidized in the presence of oxygen and the peroxidized DNA radicals are harder to repair for available DNA repair pathways (50). Furthermore, presence of oxygen directly augments indirect damage to DNA by producing more ROS because of ionization by radiation. Mammalian cells with normal oxygen concentration have been shown to be 2.5- to 3-times more radiosensitive than anoxic cells. In other words, as cells become progressively hypoxic radiation toxicity begins to decrease (48).

Thus hypoxia-induced radioresistance is based on the oxygen enhancement effect in addition to the biological effects of hypoxia on tumor cells. It varies with the duration of hypoxia (acute vs. chronic) and tends to persist even after the cells are reoxygenated (50).

1.3.4. DNA Damage Response to ionizing radiation exposure

The DNA Damage Response (DDR) in tumor cells determines the cellular outcome following DNA damage caused by radiation (Figure 1.6). The DDR is constituted by interrelated cell signaling pathways that sense DNA damage (sensors) and initiate an appropriate response to the DNA damage primarily by "effectors" that are focused on cell cycle arrest, DNA damage repair, and cell death and survival pathways. Coordination of pathways between the sensors and effectors is carried out by "transducers" (22,51).

1.3.4.1. DNA damage sensors

DNA damage sensor s are proteins that recognize specific DNA lesions and initiate the DDR. The nature of the lesion dictates the presence of the initial damage-sensing protein. Since DNA DSBs constitute the most important lesion for radiation-induced cytotoxicity, the focus of the following description is on this lesion. DSBs are recognized by the MRN complex, consisting of three proteins: meiotic recombination 11 homolog 1 protein (MRE11), Rad50 homolog double strand break repair protein (RAD50), and Nijmegen breakage syndrome 1 protein (NBS1). The Ku proteins (Ku70 and 80) can also recognize and bind to the ends of DSBs (22,51).

1.3.4.2. DNA damage signal transducers

Upon DNA damage recognition, transduction of the signal from the sensors to the effectors is carried out mostly through post-translational modification of signaling proteins. Such modifications typically affect the chromatin in the vicinity of DNA damage to facilitate recruitment of effector proteins at the damaged site. Modifications can also alter protein activity to initiate downstream signaling to effector pathways. Some common transducer proteins include Ataxia telangiectasia Mutated (ATM), ATR serine/threonine kinase (ATR), DNA-dependent protein kinase catalytic subunit (DNA-PKcs) and the histone H2AX (22,51):

- ATM is a protein kinase which is recruited to DSBs with the help of the MRN complex and phosphorylates cell cycle checkpoint kinase 2 (CHK2), p53 and H2AX variant histone (H2AX).

- DNA- PKcs is a kinase that is recruited by the Ku70/Ku80 complex at the site of DSBs. DNA-PKcs in turn phosphorylates H2AX as well as effector proteins involved in DNA repair and cell cycle regulation.

- ATR is primarily a transducer for SSBs. With regards to its role in DSBs, ATR responds a little later than ATM and DNA-PKcs but once complexed with MRN, it is capable of phosphorylating H2AX and activates cell cycle checkpoint kinase 1 (CHK1).

- H2AX is a histone protein and a component of the nucleosome around which DNA is wound. H2AX becomes phosphorylated by ATM, ATR and DNA-PKcs at the DSB site. The phosphorylated form of H2AX is termed γH2AX. After phosphorylation, H2AX

activates effector DSB repair pathways.
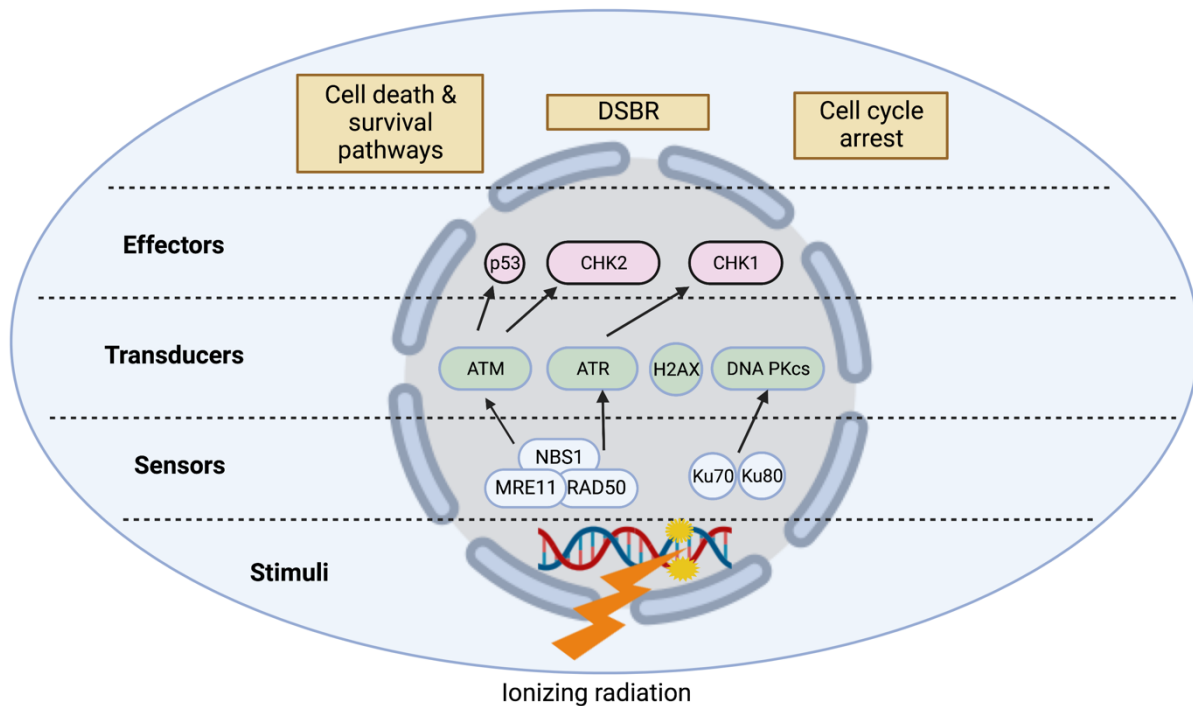
Figure 1.6   DNA damage response (DDR) to stimuli such as ionizing radiation-induced DSBs through sensors like MRN complex (NBSI, MRE11, RAD50) and Ku proteins (Ku70 & Ku80) that signal to transducers like ATM, ATR, DNA-PKcs and H2AX to activate effector pathways of cell cycle arrest, DNA repair and cell death mainly via p53, CHK1 and CHK2. NBS1, Nijmegen breakage syndrome 1 protein; MRE11, meiotic recombination 11 homolog 1 protein; RAD50, RAD50 homolog double strand repair protein; Ku, Ku antigen; ATM, Ataxia telangiectasia mutated; ATR, ATR serine/threonine kinase; H2AX, H2A histone family member X; DNA PKcs, DNA-dependent protein kinase catalytic subunit; CHK1 & CHK2, checkpoint kinase 1 & 2; DSBR, double strand break repair; Created with Biorender.com.

1.3.4.3.   DNA damage response effectors

Cell cycle arrest pathways

A major effector pathway of the DDR is cell cycle checkpoint activation through inhibition of the cyclin/CDK complexes which drive the cell cycle through its various phases (Figure 1.7). Key effectors in this regard are p53, CHK1 and CHK2 (22,51).

p53 phosphorylation by ATM results in its dissociation from MDM2 and accumulation in the nucleus upregulating its role in transcription. This results in induction of the cyclin-dependent kinase inhibitor 1A (CDKN1A) gene encoding the p21 protein. Activated p21 inhibits CDK4 and CDK6 activity causing cell cycle arrest at the G1/S checkpoint. Additionally, p21 causes arrest at the G2/M checkpoint by binding to and inactivating the CDK1-cyclin B complex.

CHK1 and CHK2 also cause cell cycle arrest by phosphorylating the phosphatase cell division cycle 25A (CDC25) isoforms which leads to inhibition of CDK2-cyclin E and of CDK1-cyclin B complexes, which results in G1 and G2 cell cycle arrest respectively (51,52).
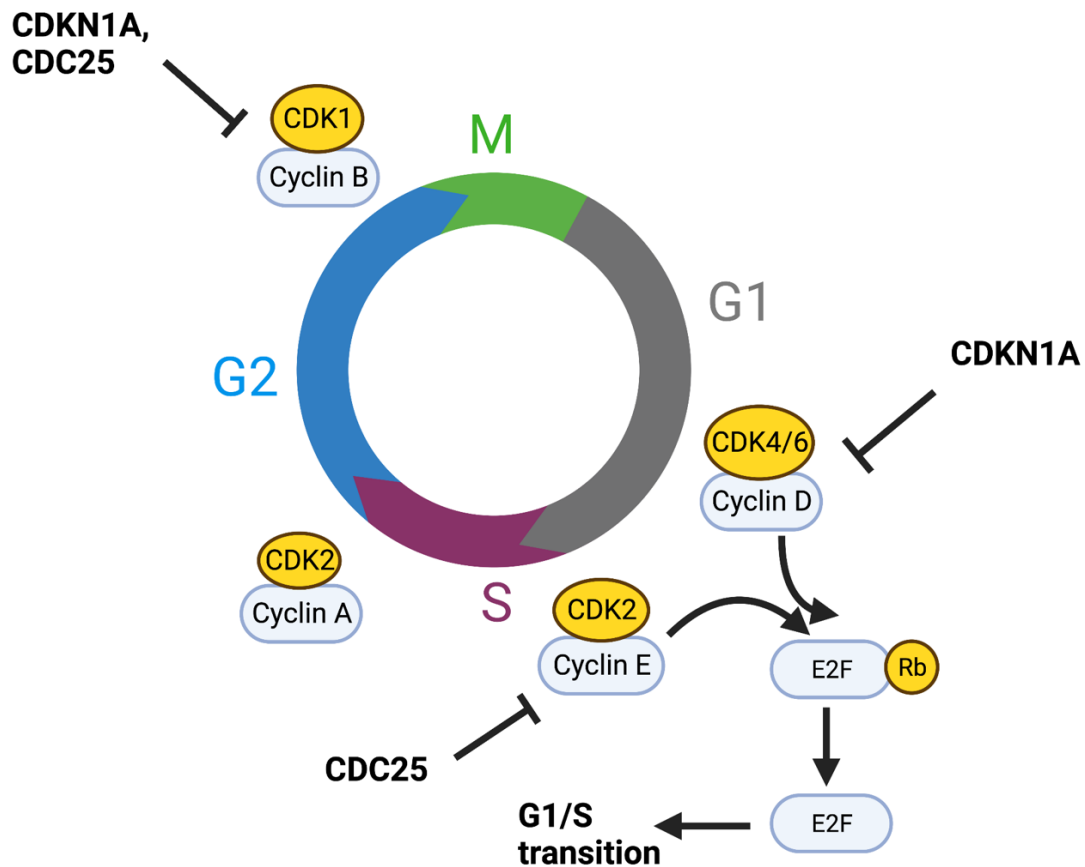
Figure 1.7   The cell cycle is under tight regulation of specific CDKs which complex with specific cyclins to control transitioning of cells from one cell cycle phase to the next. With regards to cell cycle inhibition in response to DNA damage, the transition of cells from G1 to S phase and also from G2 to M phase is particularly important and is inhibited through the action of CDKN1A (p21) and CDC25 in response to p53 nuclear accumulation. CDKN1A, cyclin dependent enzyme inhibitor 1A; CDC25, cell division cycle 25A; CDK, cyclin dependent kinase; E2F, E2F transcription factor; Rb, retinoblastoma protein; Created with Biorender.com.

G1/S checkpoints are often disabled in many tumor cells either due to genetic changes that occur during carcinogenesis or due to oncogenic signaling pathways propagating proliferation. Therefore, inhibition at the G2/M checkpoint is more prominent after radiation exposure and more important for cell survival (51,52).

DNA repair pathways

Cell cycle inhibition provides DNA repair pathways time to repair DNA damage. Radiation induces a large burden of oxidized base lesions and SSBs, as well as more cytotoxic DSBs. The main repair pathways that tackle these lesions are base excision repair (BER), nucleotide excision repair (NER), single strand break repair (SSBR) and double strand break repair (DSBR) pathways, of which DSBR is the most crucial to resist radiation-induced cytotoxicity so that the focus of this chapter is mainly on DSBR.

BER detects and removes damaged bases in the DNA, resulting in SSBs that are repaired by DNA polymerases in the presence of X-ray repair cross complementing 1 (XRCC1) (short patch pathway) or proliferating cell nuclear antigen (PCNA) (long patch pathway) followed by

ligation (51,52).

NER can repair more "bulky" lesions compared to BER and is activated by either the DNA damage sensor Xeroderma pigmentosa complementation group C (XPC) or by Cockayne syndrome proteins A and B (CSA and CSB).

SSBR applies many of the same enzymes as BER. If DNA ends are oxidized due to ample availability of molecular oxygen, they cannot be recognized by ligases or polymerases without additional end processing which theoretically would not be needed as much in case of hypoxia. Unrepaired closely spaced SSBs can ultimately result in DSBs, which would then require DSBR machinery (51,52).

DSBR comprises of two different repair pathways: homologous recombination (HR) which makes use of the replicated homologous sister chromatid as a repair template and non-homologous end joining (NHEJ) that does not rely on such a repair template. As a result, HR is a high-fidelity repair mechanism with a very high likelihood of restoring the original DNA sequence while NHEJ is relatively error prone. Owing to its dependence on the sister chromatid in mammalian cells, HR can only take place when DNA has already replicated and is thus possible only during late S and G2 phases of the cell cycle while NHEJ can, in principle, occur in any phase of the cell cycle. The cellular decision to utilize NHEJ or HR repair pathway depends on several proteins including the transducer H2AX. Phosphorylation of H2AX promotes ubiquitination of H2A proteins by ring finger protein 8 and ring finger protein 168 (RNF8 & RNF168) in the surrounding chromatin. Mono-ubiquitinated H2A attracts the tumor protein p53 binding protein 1 (TP53BP1) which in turn initiates NHEJ while poly- ubiquitinated H2A attracts ubiquitin interaction motif containing protein 1 (UIMC1) protein which recruits the HR pathway (51,52).

In case of **non-homologous end joining (NHEJ)**, the DNA ends at the site of the DSB are stabilized by the Ku70-Ku80 heterodimer (Ku), DNA-PKcs, H2AX and 53BP1. This enables DNA-PKcs and Artemis to repair the DSB following which the DNA ends are ligated by DNA ligase 4 (LIG4), X-ray repair, complementing defective, in Chinese hamster, 4 (XRCC4) and XRCC4-like factor (XLF). NHEJ is the only DSBR mechanism active in G1 phase and is responsible for repairing 90 % of DSBs in G2 phase (51,52).

In case of **homologous recombination (HR)**, the MRN complex binds to the DNA ends at the site of the DSB, stabilized by H2AX. MRE11 homolog (MRE11) in the MRN complex initiates DNA end processing by resection of the double-stranded ends which is aided by C-terminal binding protein interacting protein (CtIP) and BRCA1 (breast cancer 1). This is followed by annealing of the newly generated single-stranded DNA (ssDNA) to the unwound sister chromatid by the action of RAD51 recombinase (RAD51), forming a crossover structure (holiday junction). This binding to ssDNA is aided by BRCA2 (breast cancer 2). DNA polymerases are then able to repair the damaged site using the unwound sister chromatid as a template. The holiday junction is then reversed to reset the chromatin to its original configuration with the help of specialized nucleases, finally followed by ligation of adjacent ends. Hypoxia leads to lower levels of HR proteins and mildly compromised repair capacity (51,52).

Cell death pathways

Failure of DNA repair after irradiation leads to the initiation of cell death via different pathways: mitotic catastrophe, apoptosis, and senescence. The specific pathway the cell will be committed to depends on the cell type, oxygenation status, radiation dose and quality (LET), as well as cell cycle phase at the time of irradiation. In principle, the most common pathway of

cell death following irradiation in solid tumors is mitotic catastrophe followed by apoptosis while senescence is relatively uncommon.

Mitotic catastrophe is understood as cell death due to aberrant mitosis and results from induction of mitosis prematurely before completion of DNA synthesis and repair. This tends to result in atypical chromosome segregation forming giant cells with multiple nuclei. Sometimes, cells may take up to 5-7 cell divisions until they die during mitosis or during the following interphase. Mitotic catastrophe occurs if G2/M checkpoint is not functioning properly due to inhibition or loss of this checkpoint regulators in tumor cells such as ATM, ATR, CHK1, CHK2, p53 and p21. Additionally, deregulation of different kinases governing mitotic checkpoints such as aurora kinases, polo kinases as well as BUB1 Mitotic Checkpoint Serine/Threonine Kinase (BUB1), can also contribute to mitotic catastrophe (51,52).

Apoptosis is the second most common cell death pathway employed by tumor cells following irradiation. Unrepaired or extensive DNA damage results in increased and prolonged activation of p53. This leads to additional phosphorylation of p53 at Ser 46 besides Ser 15 and in such cases p53 mediates apoptosis via intrinsic pathway rather than cell cycle arrest. Due to its crucial role in the choice between cell survival and death, p53 has been given the title of "guardian of the genome". Apoptosis results in chromatin condensation (pyknosis) followed by cell membrane blebbing and nuclear fragmentation (karyorrhexis) ultimately leading to the cell breaking down into apoptotic bodies removed by macrophages (53).

Stress-induced premature senescence (SIPS) can be triggered by ionizing radiation in TP53 wild type tumor cells because of accumulation of radiation-induced chromosomal aberrations in such cells. Senescent cells are arrested in G1 phase and are metabolically active, capable of secreting cytokines. It has also been proposed that senescence in tumor cells may, in fact, be reversible and thus a means to escape further radiation-induced cytotoxicity. Senescence is understood to be mediated through p53-induced activation of p21 that causes G1 arrest. After induction of the G1 arrest in senescent cells, p21 levels have been found to decrease followed by an upregulation of p16 which also causes G1 arrest through stabilization of the Rb-E2F complex (53).

1.3.5.   Signaling pathways implicated in radioresistance

Based on our understanding of DDR, radioresistance in tumor cells can either result from factors that directly inhibit the physicochemical cytotoxic effect of ionizing radiation as is the case with hypoxia, or through mechanisms which may help tumor cells evade cell cycle inhibition and cell death thereby enhancing tumor cell proliferation and cell survival. In recent times, evidence has been put forth for many such cell signaling pathways.

The **EGFR signaling pathway** can be activated in response to ionizing radiation in a ligand independent manner. It can cause dimerization of EGFR receptors and their nuclear translocation where EGFR target gene transcription is activated. This includes expression of cyclin D1 that facilitates G1/S cell cycle progression and hence increased proliferation in tumor cells. EGFR also acts as transcription factor for anti-apoptotic BCL-X thereby opposing cell death by apoptosis. Lastly, EGFR is also known to activate NHEJ, and its nuclear translocation is associated with an increase in Ku70 and Ku80 inside the nucleus (54).

The **PI3K-AKT signaling pathway** can be activated indirectly following irradiation through the action of EGFR-HER-2 and is known to suppress nuclear translocation of newly formed cell cycle inhibitors p21 and p27 contributing toward cell cycle progression and cellular proliferation. Additionally, it can lead to inactivation of pro-apoptotic protein BAD as well as caspase-9 thereby inhibiting apoptotic cell death (54).

The **NF-κB signaling pathway,** as explained in subchapter 1.2.1.2, can be activated by ionizing radiation in several ways including its activation by DSBs, DAMPS, ROS, and through the PI3K-AKT pathway (32,54).

The **ERK1/2 pathway** is one of three MAPK pathways with Ras/Raf being its upstream regulators. It can be induced because of radiation exposure and hypoxia and by EGFR signaling. Therefore, it is prone to overstimulation following activation of EGFR and Ras/Raf mutations which is a common occurrence in NSCLC. Upon activation it has an important role in cell proliferation and differentiation. It may have a protective role against mitotic catastrophe through activation of the G2/M checkpoint allowing cells time for DNA repair. It is also understood to promote both NHEJ and HR in cells although precise mechanisms are unclear. Additionally, it has been shown to regulate the production of VEGF-A promoting tumor neo-angiogenesis (54).

EMT-inducing signaling pathways have been shown to be activated in response to ionizing radiation. Accordingly, ROS play a key role in radiation-induced EMT. While ROS generated from radiolysis of water have very short life spans (10^{-9} s), ROS production because of radiation-induced mitochondrial damage can persist for days. Those pathways that have been reported commonly in literature to regulate the EMT program in response to ROS include TGF-β, EGFR, Wnt, Notch, Hedgehog, NF-κB, Ras/Raf/ERK and PI3K-Akt (54).

1.3.6. Linking together NSCLC, hypoxia, and radiotherapy

Radiotherapy is part of standard management for nonmetastatic NSCLC and provides locoregional disease control as an adjunct to surgery (in Stage I-III) or as an alternative to surgery in surgically unfit patients. Presence of hypoxia in NSCLC lesions and its contribution to radioresistance is well-documented making hypoxia a potential target for improving efficacy of radiotherapy. However, targeting hypoxia in NSCLC to improve radiotherapy outcomes has not translated into a survival advantage (2,41–44). This along with other clinical trials targeting tumors elsewhere in the body giving disappointing results, has led to a realization in the scientific community for a need to better understand the biology of hypoxia-induced radioresistance.

Tumor hypoxia is not just responsible for negatively influencing the physicochemical aspect of ionizing radiation-induced cytotoxicity but is also understood to promote radioresistance and enhanced survival of tumor cells following irradiation, through activation of a wide variety of signaling pathways that promote angiogenesis, modulate cell stemness, inhibit apoptosis, trigger inflammatory reparative response (IRR) and increase tumor cell heterogeneity (25,35,36). Additionally, reoxygenation of previously hypoxic cells is a common clinical occurrence in tumor cells and leads to cellular responses variable from continuous hypoxia (26,39).

Ionizing radiation activates, through ROS production, many of the same pathways as tumor hypoxia, leading to the possibility of developing a pro-survival phenotype over the course of irradiation that is radioresistant (50,54). NF-κB pathway is of particular interest in the context of hypoxia-induced radioresistance because it has a pro-survival footprint in most mammalian cells and in tumor cells. It constitutes the second arm of ATM-modulated DDR to ionizing radiation, in the context of cell survival, the first arm being p53 (32). It has also been reported to be a major pathway activated by hypoxia second only to HIF pathways (35,55).

1.4. Aims of the study

1.4.1. Knowledge gaps

Current literature appears mostly silent with regards to basic questions such as determining and quantifying the effects of severity of hypoxia, with and without subsequent reoxygenation, on radioresistance in NSCLC. Comprehensive studies comparing the effect of radiation quality on hypoxia-induced radioresistance in NSCLC are also lacking. Similarly, the combined influence of hypoxia and irradiation on the NF-κB pathway activation has also not been reported in literature to the best of my knowledge. Additionally, reoxygenation is known to activate NF-κB (26) and this has even been shown in lung tissue (56) but how this modulates DDR to irradiation is also currently unknown.

While the radiation response is classically a DDR comprising cell cycle arrest, DSB repair, and activation of cell death and survival pathways, not much is documented in literature on evaluating these three components of DDR following irradiation under hypoxia in NSCLC or even other malignant cells.

Molecular and histological tissue and tumor characteristics affect radiosensitivity (57), oxygen consumption (24) and NF-κB activation (32). While the general effect of hypoxia severity in the context of radioresistance is well documented (50,58), the relationship between progressive decline in oxygen partial pressures and NF-κB activation is not reported in literature with or without irradiation. Finally, cell survival is lower (59–61) and NF-κB activation is higher (62) in case of high-LET radiation compared to low-LET radiation (X-rays) but the impact of high-LET radiation (carbon ions) on NF-κB activation in hypoxic tumor cells, especially NSCLC cells is currently unknown.

1.4.2. Hypothesis

Hypoxia-induced radioresistance in NSCLC is:

- Influenced by radiation quality (X-rays vs. carbon ions), severity of hypoxia (1 % O_2 vs. 0.1 % O_2) and reoxygenation.

- Characterized by changes in cell cycle progression, DSB induction and repair, as well as activation of pro-survival cell signaling pathways in a manner that is influenced by radiation quality, severity of hypoxia and subsequent reoxygenation.

- Associated with NF-κB pathway activation and this activation can be influenced by radiation quality, severity of hypoxia and reoxygenation.

1.4.3. Specific Aims

To characterize hypoxia-induced radioresistance in two NSCLC cell lines, A549 and H358 cells, and to determine their radiation response under hypoxia, including activation of the NF-κB pathway and other relevant signaling pathways, following X-rays and carbon ions exposure, by undertaking the following steps:

- Understanding **growth** and **energy metabolism** of the NSCLC cell lines under moderate (1 % O_2) and severe (0.1 % O_2) hypoxia

- Determining **radioresistance** of the NSCLC cell lines and **possible underlying mechanisms**
  under the following varying conditions

  - Radiation quality (X-rays and carbon ions),

- Severity of hypoxia (1 % O_2 and 0.1 % O_2) and
- Reoxygenation vs. continuous hypoxia

by focusing on

- **Cell survival** in terms of changes in clonogenic potential following irradiation under hypoxia as a key indicator of radioresistance
- **Radiation response (DDR)** under hypoxia in terms of:
  - Changes in **cell cycle** phase distribution and cell cycle progression
  - **DNA DSB** induction and repair kinetics
  - **Global transcription** profiling to identify signaling pathways related to cell survival with focus on the NF-κB pathway
- **NF-κB pathway activation** and secretion of selected **target cytokines** of NF-κB following exposure to ionizing radiation under hypoxia

2. Materials and methods

2.1.　　Cell lines

Two human non-small cell lung adenocarcinoma (NSCLC) cell lines were selected for the purpose of this research work, namely, A549 and H358.

Both cell lines were procured from LGC Genomics (Berlin, Germany) which is the European Partner of American Tissue Culture Collection (ATCC Manassas, Virginia, USA).

Cell line details are provided in Table 2.1.

Table 2.1.　　Characteristics of the human non-small cell lung carcinoma (NSCLC) cell lines

Cell Line Parameter	A549	H358
Morphology	Epithelial	Epithelial
Growth Properties	Adherent	Adherent
Doubling time	22 h	38 h
TP53*	Wild type	Homozygous deletion
KRAS*	Missense mutation G12S	Missense mutation G12C

* TP53, tumor protein p53 gene; KRAS, Kirsten rat sarcoma virus gene

2.2.　　Equipment and software

The various equipment used during the PhD work is listed in Table 2.2 along with the respective model names and suppliers.

Table 2.2　　Equipment, model names and suppliers

Item	Model name / Designation	Supplier
Autoclave	Varioklav 155 S	HP Labortechnik, Oberschleißheim, Germany
Automated cell counter	LUNA	Logos Biosystems, South Korea
Centrifuge	Multifuge 3 S-R	Thermo Scientific, Schwerte, Germany
CO_2 incubator	Heraeus HERAcell 150	Thermo Fisher Scientific, Germany
Dissolved oxygen meter	Seven2go DO meter S9	Mettler Toledo, Giessen, Germany
Flow cytometer	Cytoflex S	Beckman Coulter, Indianapolis, USA
Fluorescence microscope	Axio Imager M2	Zeiss, Jena, Germany
Fuchs-Rosenthal counting chamber	Brand	Wertheim, Germany
Hypoxia workstation (at DLR and at GANIL)	InvivO$_2$ 400	Baker Ruskinn, South Wales, United Kingdom
Inverse microscope	Axiovert 35	Carl Zeiss AG, Oberkochen, Germany

Item	Model name / Designation	Supplier
Laminar flow hood type 2	Herasafe	Thermo Fisher Scientific, Schwerte, Germany
Manual colony counter	Schuett count (with a magnifying glass.)	Schuett-biotec, Göttingen, Germany
Microelectrophoresis unit	Bioanalyzer 2100r	Agilent Technologies, Karlsbrunn, Germany
Microplate reader	Infinite M200Pro Multiskan FC	Tecan, Groeding, Austria Thermo Fischer Scientific, Waltham, MA, USA
Pipette devices (10, 100, 1000 µl)	Eppendorf Research® plus, Eppendorf Reference® 2, Multipette	Eppendorf Ltd, Hamburg, Germany
Shaking incubator	Multitron	Infors GmbH, Einsbach, Germany
Ultrasonic water bath	Sonorex Digiplus	Bandelin, Berlin, Germany
Vortex mixer	IKA MS3	IKA-Werke GmbH, Staufen, Germany
X-ray cabinet irradiator	X-strahl RS225	Gulmey, Surrey, United Kingdom
X-ray dosimeter with ionizing chamber	UNIDOS^{webline} with chamber TM30013	PTW, Freiburg, Germany

A list of software used for analyzing data collected through the course of this PhD work is provided in Table 2.3.

Table 2.3   Software with purpose of use and supplier

Software	Purpose of Use	Supplier
2100 Expert Software for Bioanalyzer	Assessment of quantity and integrity of RNA	Agilent Technologies, Karlsbrunn, Germany
CFA_DOSE v1.04 and CFA_AllData v1.04	Radiation dose response curve analysis	Excel macrosheets developed by Dr Christa Baumstark
Energy vs. LET vs. Range calculator version 1.24	Calculation of range and LET in water of carbon ions	Free software built by Vladimir Zajic using Visual C++ 5.0 MFC
FloJo version 10	Assigning cells to different cell cycle phases based on cellular DNA content	BD Biosciences, USA
GraphPad Prism 9	Data analysis and graphing software	GraphPad, CA, USA
Image Processing and Analysis in Java (ImageJ)	Image analysis	Free online software, http://rsbweb.nih.gov/ij/download.html
Sigma Plot 16.0	Data analysis and graphing software	SPSS, Munich, Germany
SkanIt Software (ver. 6.1.1.7)	Microplate reader control panel and basic analysis	Thermo Fisher Scientific, Schwerte, Germany
Zen Blue version 3.3	Fluorescence imaging control panel	Zeiss, Jena, Germany

2.3.　Consumables, chemicals, kits and solutions

A list of consumables along with suppliers, used during the PhD work, is given in Table 2.4.

Table 2.4　　Consumables with supplier names

Material	Supplier
Cell culture dishes: ∅ 3 cm with 4 indentations for microscope coverslips	Greiner Bio-One GmbH, Frickenhausen, Germany
Cell culture dishes: ∅ 3 and 6 cm	LABsolute, Th. Geyer GmbH, Germany
Cell scrapers (24 cm × 1.3 cm)	TPP, Trasadingen, Switzerland
Centrifuge tubes: 15 ml and 50 ml (Falcon)	Nunc, Wiesbaden, Germany
Cryotubes 1.8 ml	Nunc, Wiesbaden, Germany
Dispenser Tips: 50 ml	STARLAB International GmbH, Hamburg, Germany
Microscope coverslips: ∅ 10 mm	Paul Marienfeld GmbH & Co. KG (Lauda-Koenigshofen), Germany
Mr Frosty freezing container	ThermoFisher Scientific, Waltham, MA, USA
Polyethersulfone (PES)- membrane: 0.2 µm	Millipore Corp., Bedford, USA
Powder-free Latex Exam Gloves	Kimberly Clark, Neenah, WI, USA
qPCR adhesive seal sheets	4titude Ltd, Berlin, Germany
Safe-Lock tubes: 0.5 ml, 1.5 ml and 2.0 ml	Eppendorf Ltd., Hamburg, Germany
Slide Flasks 9 cm^2	ThermoFisher Scientific, Waltham, MA, USA
Syringes: 2 ml	Terumo Syringe, Leuven, Belgium
Tissue culture flasks: 80 cm^2 and 25 cm^2 (with and without filter in cap)	LABsolute, Th. Geyer GmbH, Germany STARLAB International GmbH, Hamburg, Germany

The chemicals along with suppliers, that were used in this PhD work, are listed in Table 2.5.

Table 2.5   Chemicals with suppliers

Chemical	Supplier
4',6-Diamidino-2-phenylindole (DAPI)	Sigma Aldrich, Steinheim, Germany
α-MEM medium	PAN Biotech, Aidenbach, Germany
β-D-Glucose-Monohydrate	Merck, Darmstadt, Germany
β-Mercaptoethanol	Sigma Aldrich, Steinheim, Germany
Amphotericin B (250 µg/ml)	PAN Biotech, Aidenbach, Germany
Crystal violet	Merck, Darmstadt, Germany
Ethanol 99.8 % vol	Merck, Darmstadt, Germany
Fetal Bovine Serum (FBS)	Biochrom AG, Berlin, Germany
Formaldehyde 37 %	Merck, Darmstadt, Germany
Isopropanol	VWR, Darmstadt, Germany
L-Glutamine	PAN Biotech, Aidenbach, Germany
Mounting medium	Invitrogen, California, USA
Neomycin / Bacitracin	Biochrom AG, Berlin, Germany
Penicillin / Streptomycin	PAN Biotech, Aidenbach, Germany
Polyethylene glycol sorbitan monolaurate (TWEEN^{TM} 20)	Sigma Aldrich, Steinheim, Germany
Potassium chloride	Merck Darmstadt, Germany
Propidium iodide	Invitrogen, Carlsbad, USA
Ribonuclease (RNAse)	Calbiochem, La Jolla, USA
Sodium chloride	Merck Darmstadt, Germany
Triton X-100	Sigma Aldrich, Steinheim, Germany
Trypan blue 0.4 %	ThermoFisher Scientific, Waltham, MA, USA
Trypsin/EDTA	PAN Biotech, Aidenbach, Germany

A list of reagent kits or assays along with their suppliers, used during the PhD work, is provided in Table 2.6.

Table 2.6   Reagent kits with supplier names

Reagent Mixture	Supplier
Glucose-Glo™ Assay	Promega GmbH, Walldorf, Germany
Invitrogen Human IL-6 Uncoated ELISA Kit	Thermo Fischer Scientific, Waltham, USA
Invitrogen Human IL-8 Uncoated ELISA Kit	Thermo Fischer Scientific, Waltham, USA
Lactate-Glo™ Assay	Promega GmbH, Walldorf, Germany
RNA 6000 Nano Assay	Agilent Technologies, Böblingen, Germany
RNA ladder	Agilent Technologies, Böblingen, Germany
RNeasy Plus Mini Kit	QIAGEN, Hilden, Germany

A list of different types of media and solutions prepared for use during this PhD work, is given in Table 2.7.

Table 2.7   Cell culture media and other prepared solutions

Solution	Constituents with stock solution concentration
Culture Medium α-MEM	500 mL α-MEM 1 % (v/v) Penicillin (10000 U/mL) / Streptomycin (10 mg/mL) 1 % (v/v) Neomycin/Bacitracin (1 mL Bacitracin (2500 U/mL) mixed in 50 mL Neomycin sulfate (10 mg/mL)) 1 % (v/v) Amphotericin (250 µg/mL) 1 % (v/v) L-Glutamine (200 mmol/L) 2 % (v/v) Glucose (0.94 mol/L / 17 %) stored at 4 °C 10 % (v/v) FBS Stored at 4 °C
Conditioned Medium α-MEM	500 mL freshly prepared Culture Medium α-MEM 500 mL Culture Medium α-MEM filtered (PES-membrane: 0.2 µm) after growing of H358 cells (with a starting cell number of 20,000 cells/cm^2) in it for 5 days, stored at 4 °C
Freezing Medium	70 % (v/v) Culture Medium α-MEM 20 % (v/v) FBS 10 % (v/v) Dimethyl sulfoxide (DMSO) (10 mmol/L stock) Freshly prepared for use
100 % Ethanol	100 mL Ethanol (100%) stored at -20 °C
Chlorine dioxide solution	50 % Citric acid solution (50 mL)

Solution	Constituents with stock solution concentration
	28 % Sodium chlorite solution (50 mL)
	Diluted further in 2 L deionized water
Crystal violet staining solution	0.5 g Crystal violet
	50 mL Formaldehyde 37 % stock solution
	Ad 500 mL Tap water
	Stored at room temperature
DAPI staining solution	0.1 µg/mL DAPI in PBS stored at -20 °C
Formaldehyde fixation solution	10 mL Formaldehyde 37 % stock solution
	90 mL PBS
	Stored at 4 °C
Phosphate buffered saline (PBS) 5x	80 g NaCl
	2 g KCl
	14.4 g $Na_2HPO_4 \times 2H_2O$
	2 g KH_2PO_4
	2000 mL *A. dest.*
	pH 7.2 (Adjusted with sodium hydroxide (NaOH) – 6 mol/L, and hydrochloric acid (HCl) - 6 mol/L)
	Stored at -20 °C
Poly-D-lysine (0.01 mg/ml)	100 µL Poly-D-lysine (1 mg/mL)
	10 mL *Aqua dest.*
	Stored at 4 °C
Propidium iodide (PI) staining solution	50 µg/mL RNAse A
	0.1 % (v/v) Triton X-100
	20 µg/mL PI
	in PBS
	Stored at 4 °C
TNF-α stock solution (10 µg/ml)	Dissolved in 1 % BSA
	Aliquots of 50 µL, stored at -80 °C
Tris/Borate/EDTA (TBE) buffer 10x	1 mol/L TRIS (hydroxymethyl) amino ethane
	0.97 mol/L Boric acid
	0.02 mol/L EDTA pH 8.3
	Stored at room temperature
Trypsin/EDTA (0.5% trypsin, 0.2% EDTA) 10x	10 mL Trypsin/EDTA (0.5 % trypsin, 0.2 % EDTA)
	90 mL PBS
	Stored at 4 °C

2.4. Cell culture methods

2.4.1. Cell culture conditions

Cell culture work was conducted under sterile conditions in biosafety level 1 (BSL-1) laboratories. The cell lines were periodically screened for Mycoplasma contamination: Therefore, 500 µL supernatant from each cell line were collected, 48 h after seeding, and dispatched to the Deutsche Sammlung von Mikroorganismen und Zellkulturen (DSMZ), Braunschweig, Germany, for Mycoplasma testing by PCR.

Cell culturing was carried out either in normoxic or hypoxic conditions (Table 2.8).

Table 2.8   Cell culture conditions used in this work

Cell culture condition	Incubation	Handling of cells during cell culture	Warming of media and solutions
Normoxia	37 °C, saturated humidity, 5 % CO_2 and ~20 % O_2	Laminar flow hood type 2 (Table 2.2) Cleaned before and after use with isopropanol (70 %)	Water bath
Hypoxia	37 °C, saturated humidity, 5 % CO_2 and 1 % or 0.1 % O_2	Hypoxia workstation (Table 2.2, Figure 2.1) Cleaned before and after use with 5 % chlorine dioxide (Table 2.7)	Ultrasonic bath (30 min) followed by shifting to hypoxia workstation 30 min prior to use, to allow for gas removal and equilibration.
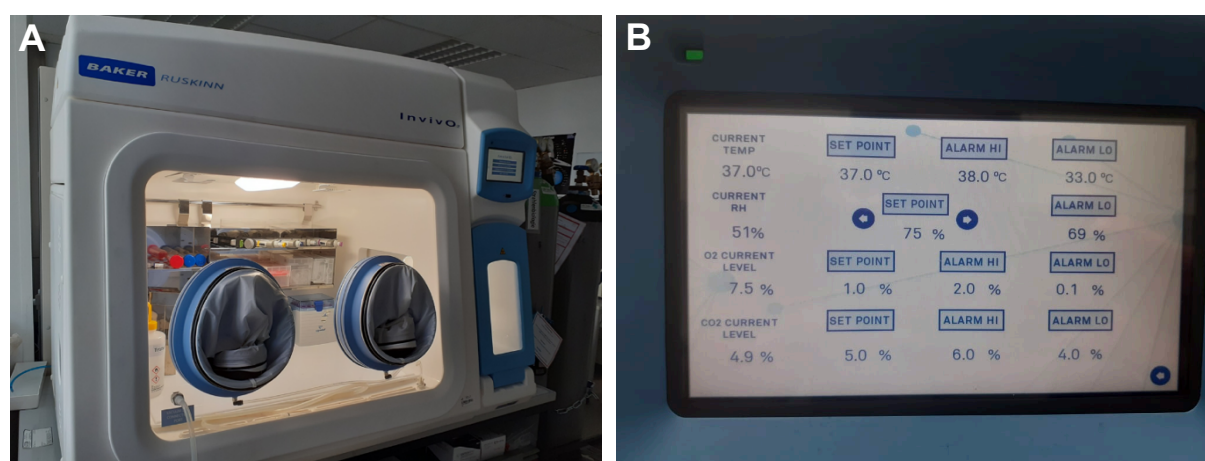
Figure 2.1   InvivO$_2$ 400 hypoxia workstation with interlock chamber for bringing material in and out of main hypoxia chamber acting as both work bench and incubator (A) and its control panel for setting oxygen levels, temperature and humidity (B).

2.4.2. Cell culture propagation

Both cell lines were seeded in 25 cm^2 or 80 cm^2 tissue culture flasks in Culture Medium α-MEM (Table 2.7) according to the parameters described in Table 2.9. They were subsequently passaged by washing them with PBS (Table 2.7) and then detaching with 0.05% trypsin in 0.02% EDTA solution for up to 5 min in the CO$_2$ incubator. After detachment, the cells were suspended in culture medium to stop the action of trypsin. For determining the cell number, they were diluted 1:1 with trypan blue and then counted using LUNA Automated Cell Counter.

Table 2.9   Seeding parameters for cell lines

Cell Line	Seeding Density	Frequency of Passage
A549	5,000 / cm^2	Every fourth day
H358	20,000 / cm^2	Every week

2.4.3. Cryopreservation

Cell lines were stored in liquid nitrogen at -196 °C after trypsinizing them, centrifuging them for 10 min at room temperature and 300$\times$g, and then re-suspending the resulting cell pellet in freshly prepared freezing medium (Table 2.7) at a concentration of 1×10^6 cells/mL. 1 mL aliquot of cell suspension was transferred in each cryotube. Cells were first cooled down to -80 °C at a rate of -1 °C/min in a precooled Mr. Frosty freezing container to minimize cell damage by formation of ice needles secondary to rapid cooling, and then shifted to liquid nitrogen.

2.4.4. Cell thawing

To thaw cells, cryotubes were brought out from liquid nitrogen following standard safety procedures and then thawed at room temperature. Once ice in the cryotubes melted, the contents transferred into 75 cm^2 flasks filled with 20 ml pre-warmed culture medium. Medium was exchanged not later than after 24 h to remove DMSO which can otherwise damage cells.

2.5. Oxygen incubation protocols

All experiments performed with either A549 or H358 cell lines followed three oxygen incubation protocols.

2.5.1. Protocol 1: Normoxia

The first group comprised cells grown under normoxic cell culture conditions for 48 h followed by irradiation (see 2.6) in ambient air and then shifted back to the standard incubator (~20 % O$_2$) till the specific time point for final handling when they were handled in a normal laminar flow hood.

2.5.2. Protocol 2: Continuous Hypoxia

The second experimental group comprised cells grown under hypoxic cell culture conditions for 48 h followed by irradiation in airtight containers and then shifted back to the hypoxia workstation till the specific time point for final handling which was also carried out in the hypoxia workstation.

2.5.3. Protocol 3: Transient Hypoxia

The third experimental group comprised cells grown under hypoxic conditions for 48 h followed by irradiation in air-tight containers and then shifted to a standard incubator (~20 % O$_2$) till the specific time point for final handling when they were handled in a normal laminar flow hood.

So, cells in group 3 were allowed to reoxygenate once their irradiation was completed.

	Incubation (48 h)	Irradiation	Subsequent handling (1 h to 3 weeks)
Normoxia	20 % O_2	20 % O_2	20 % O_2
Continuous hypoxia	0.1 % or 1 % O_2	0.1 % or 1 % O_2	0.1 % or 1 % O_2
Transient hypoxia	0.1 % or 1 % O_2	0.1 % or 1 % O_2	20 % O_2

Figure 2.2   Oxygen incubation protocols: Cells were seeded in suitable culture dishes for the experiments under the laminar flow hood and then transferred to the incubator (normoxia) or in the hypoxia workstation. Transiently hypoxic samples were shifted to the standard CO_2 incubator after irradiation to allow reoxygenation. Created with Biorender.com.

2.6.   Irradiation

2.6.1.   X-rays

X-rays exposure (LET: 0.3-3.0 KeV/µm) was performed at Aerospace Institute of Medicine, DLR, using the X-rays facility X-strahl RS 225. It was operated at a voltage of 200 KV and a current of 15 mA. A stable dose rate of 1.0 Gy/min was ensured by keeping the distance of the sample from the X-ray source to 450 mm. Low energy X-rays were eliminated using a copper (Cu) filter with a thickness of 0.5 mm.

Cells in exponential growth phase (after 48 h incubation following seeding) were irradiated either in cell culture flasks (25 or 80 cm^2) or in cell culture dishes ($\varnothing$ 3 cm or 6 cm). The cell layer was perpendicular to the direction of X-rays. Dose and dose rate were monitored using the UNIDOS[webline] dosimeter with the ionization chamber TM30013. Airtight containers were used at the time of transporting and irradiating hypoxic samples. Preliminary testing was done by measuring dissolved oxygen in medium to verify stable oxygen levels in samples during transport between hypoxia chamber and X-rays machine. Furthermore, preliminary dosimetry was also carried out to verify radiation dose precision during irradiation of samples in airtight chambers. After X-irradiation, cells underwent a medium change and were then incubated further till specific experiments mandated specific handling.
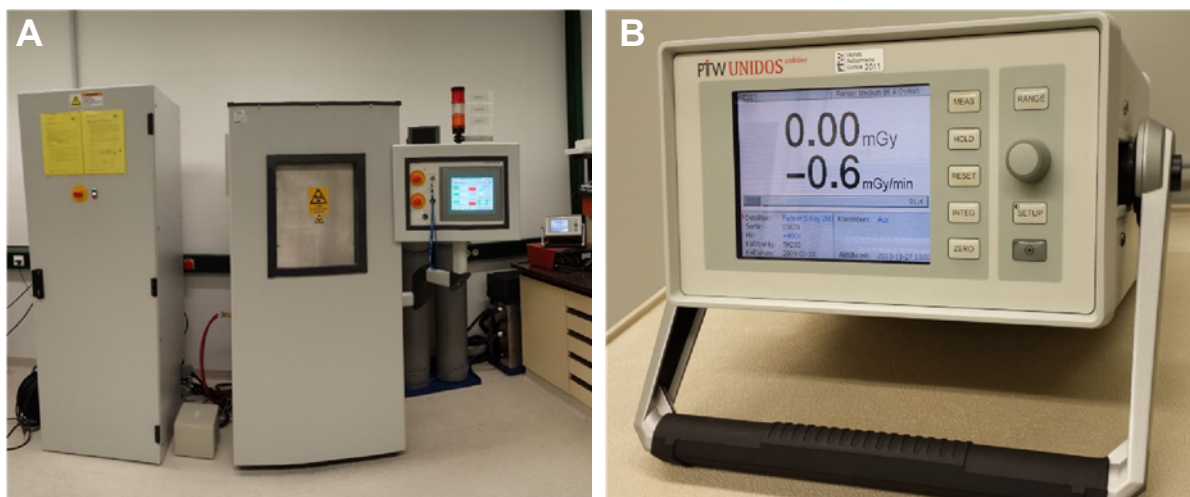
Figure 2.3   X-ray facility and dosimeter: (A) X-Strahl RS 225 X-Ray Facility at DLR comprising of a generator, an exposure cabinet (lead door closed) and a control panel (from left to right) and (B) Front side of the UNIDOS^{webline} dosimeter showing the operation panel. The ionization chamber of the dosimeter is placed within the exposure cabinet of the X-ray irradiator.

2.6.2.   Carbon ions

The exposures to carbon (C-12) ions were carried out at the heavy ion accelerator "Grand Accélérateur National de Ions Lourds" (GANIL) in Caen, France. The carbon beam specifications are listed in Table 2.10. Dosimetry was performed by Ganil staff (63,64). The fluence for heavy ions (P/cm^2) was used to make radiation dose (Gy) calculations using Equation 2.1 (65):

Dose (Gy) $= 1.6 \times 10 \times$ LET (keV/µm) $\times$ F (P/cm^2)   Equation 2.1

Table 2.10   Carbon ions (C-12) beam and particle specifications

Parameters	Details
Energy	95 MeV per nucleon (MeV/n) On target: 25.7 MeV/n
Energy degrader used	16.9 mm Poly methyl methacrylate (PMMA)
Range in water	2231 µm
LET in H_2O	74.3 ± 1.2 keV/µm (measured), 76.3 keV/µm (calculated)
Dose rate	1 Gy/min

Cells in exponential growth phase (after 48 h incubation following seeding) were directly exposed either in 25 cm^2 flasks with a quadratic growth area or in slide flasks (9 cm^2), by placing the samples in upright position in multiple sample holders in front of the beam line (Figure 2.4 A&B) so that the cell layer was perpendicular to the radiation beam. For cell survival experiments (chapter 2.9), 12.5 cm^2 flasks were used to ensure that the necks of the flasks were well within radiation field ensuring dose uniformity. The flasks were completely filled with

culture medium to prevent desiccation of the cells during exposure. During carbon ion exposure, cells were in the plateau region of the Bragg curve resulting in constant LET over the thickness of the cells (Figure 2.5). Up two 23 samples were placed in the sample holders (up to 6 per row). They were sequentially exposed to carbon ions by remote control of the sample holder via the biology sample holder software (Figure 2.4 C).

Samples were brought back to the laboratory in a prewarmed container following irradiation. The medium was removed and replaced with 5 mL α-MEM culture medium in a laminar flow hood or in the hypoxia workstation. Cells were then incubated in a CO_2 incubator of in the hypoxia workstation according to the oxygen incubation protocol (chapter 2.5) further till specific experiments mandated specific handling (chapter 2.9 to 2.13).
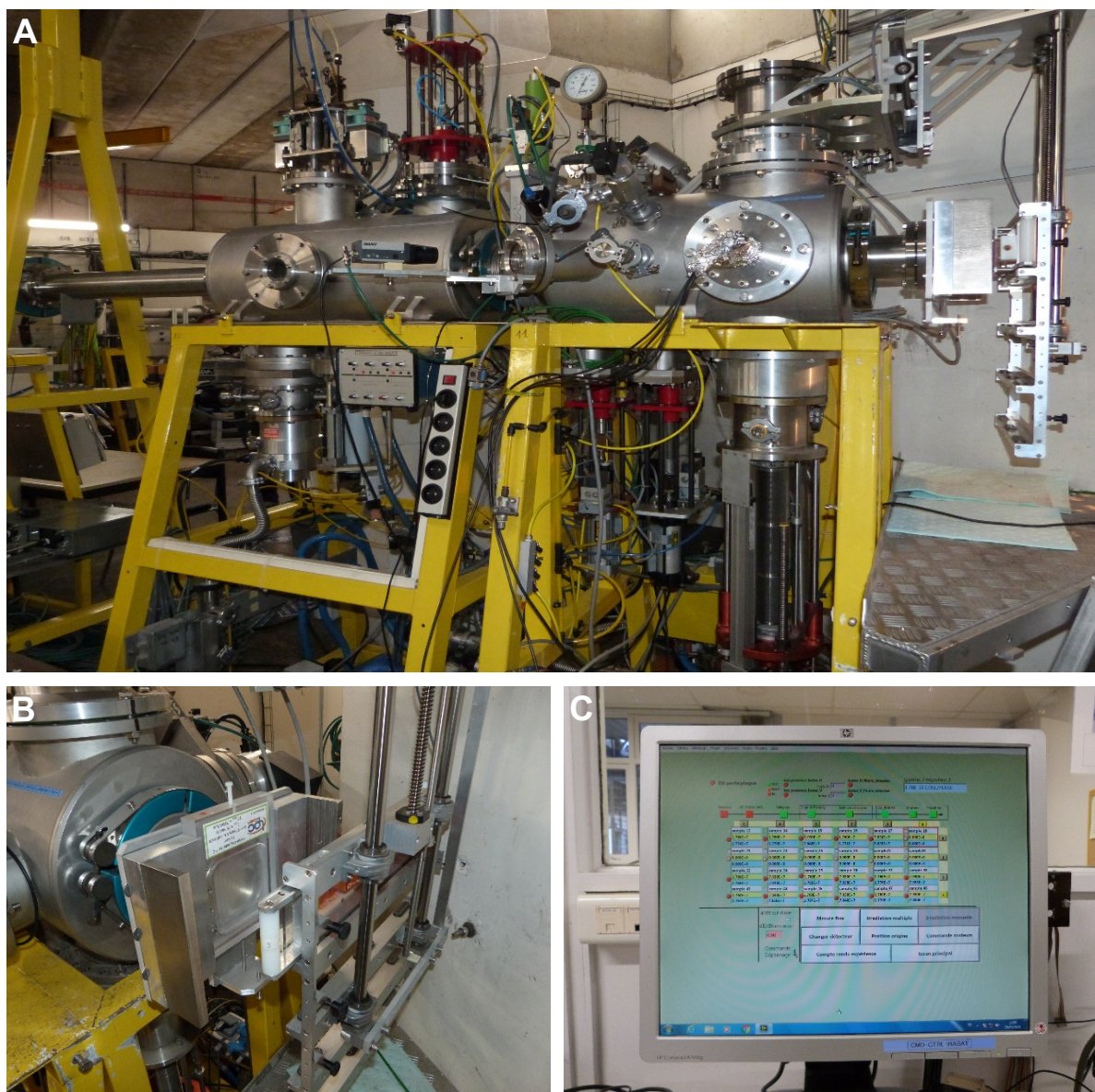
Figure 2.4   (A) Heavy ion beam room D1 at GANIL housing the beam line with the exit window and the biology sample holder in front of the exit window (B). The multi row biology sample holder facing the beam exit window with the PMMA degrader in front (C) The display of the computer in the Beam Control Room showing the software for operating the biology sample holder and the irradiation of the samples within the holder with defined fluences.

C-12 (GANIL)
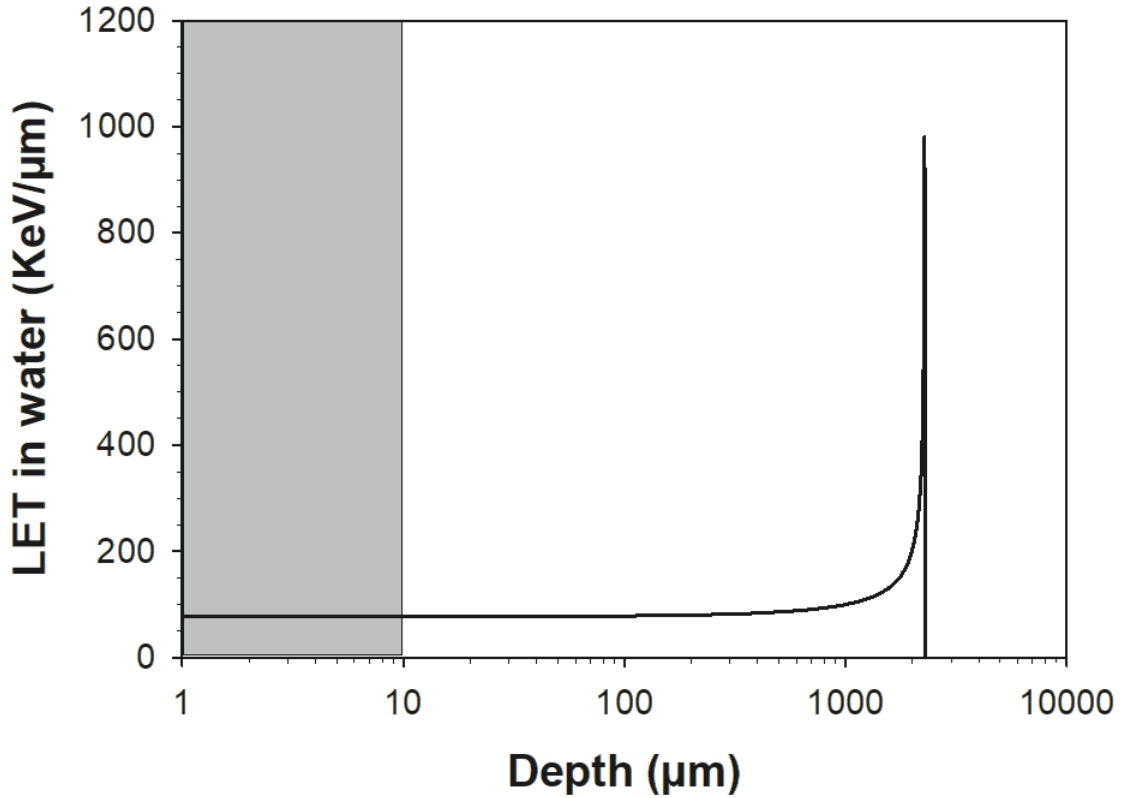
Figure 2.5   *Bragg curve of carbon ions beam (25.7 MeV/n) at GANIL showing the linear energy transfer (LET) by carbon ions as they traverse through a water phantom. The LET in water at different depths was calculated using the "Energy vs. LET vs. Range calculator version 1.24". The LET remained constant at ~75 KeV/μm to a depth of ~1000 μm beyond which there is sharp surge to over 1000 KeV/μm, the Bragg peak, followed by a sharp drop to zero indicating the stopping of the ions. The cells (their estimated maximal thickness is represented in grey) were irradiated in the plateau phase of the curve at a constant LET of ~75 KeV/μm.*

2.6.2.1.   Calculation of average carbon ions hits per cell nucleus

To calculate the average hits per cell nucleus of A549 cells, cell nucleus area was determined after staining with the nuclear stain, DAPI (Table 2.7). The stained nuclei were photographed using Zeiss Axio Imager M2 fluorescence microscope. The nucleus area (A) of 200 cells was measured using the software Image J and an average area of 118.8 ± 52.5 μm^2 was calculated.

For each fluence (F) the cells were exposed to, the expected fluence (F_e) in particles (P) per cell nucleus was calculated using Equation 2.2:

F_e (P/cell nucleus) $= 10^{-8} \times A$ (μm^2) $\times F$ (P/cm^2)   *Equation 2.2*

The Poisson distribution of the carbon ions hits in the cell nuclei was calculated according to Equation 2.3.

$$F_x(x) = \frac{F_e^x}{x!}, \ x = 0,1,2,3\dots \hspace{3cm} \textit{Equation 2.3}$$

Finally, the average number of carbon ions hits was calculated and the fractions of unhit and hit cell nuclei were summed up (Table 2.11).

Table 2.11   Hit calculation for carbon ions (C-12, 25.7 MeV/n) exposure of A549 cells

Fluence (P/cm^2)	Dose (Gy)	Unhit fraction	Hit fraction	Average hits
4.40E+06	0.50	0.01	1.00	5.2
8.79E+06	1.00	0.00	1.00	10.4
1.76E+07	2.00	0.00	1.00	20.9
3.52E+07	4.00	0.00	1.00	41.8
5.28E+07	6.00	0.00	1.00	62.7
7.03E+07	8.00	0.00	1.00	83.6

2.7.   Growth kinetics

To evaluate the growth behavior of A549 and H358 cells in hypoxia, growth curve experiments were performed keeping cells of the same passage growing in normoxia as control (Table 2.12).

Therefore, a total of three biological replicates with two technical replicates each were seeded in $\varnothing$ 3 cm cell culture dishes (A=7 cm^2). Cell growth was followed for up to seven days. After every 24 h, cells were trypsinized and the cell number was counted using the LUNA automated cell counting chamber.

Table 2.12   Experiment parameters used in cell growth curves experiments

Cell Line	Seeding Density	Volume of α-MEM Medium	Volume of trypsin	Medium change on
A549	5,000 / cm^2	3 mL	1 mL	Day 4
H358	20,000 / cm^2	3 mL	1 mL	Day 4

The cell doubling time (T2) was calculated using the following formula (66):

$$T2 = \frac{\Delta t}{log_2(\frac{\Delta N}{N_0}+1)} \hspace{3cm} \textit{Equation 2.4}$$

with

N_0 = number of cells at the beginning of exponential growth phase

ΔN = increase of cell number during exponential growth phase

Δt = length of exponential growth phase in hours

2.8.   Metabolic assays

The effect of hypoxia on metabolism was assessed in A549 and H358 cells using cells of the same passage grown in normoxia as control. Metabolism was assessed in terms glucose consumption and lactate production using the Promega Glucose-Glo™ and the Lactate-Glo™ Assay, respectively (Table 2.6) on supernatants collected from cells growing under different cell culture conditions.

2.8.1.   Working principle

Both kits contain a dehydrogenase that uses the respective substrate (glucose or lactate) and nicotinamide adenine dinucleotide (NAD+) to generate the reduced form nicotinamide adenine dinucleotide hydride (NADH) which then acts as cofactor for a reductase that transforms pro-luciferin into luciferin (Figure 2.6). A recombinant luciferase then acts on the luciferin to produce luminescence that can be detected using a luminescence reader. The luminescence signal is directly proportional to the amount of the respective substrate in the sample at any given time.
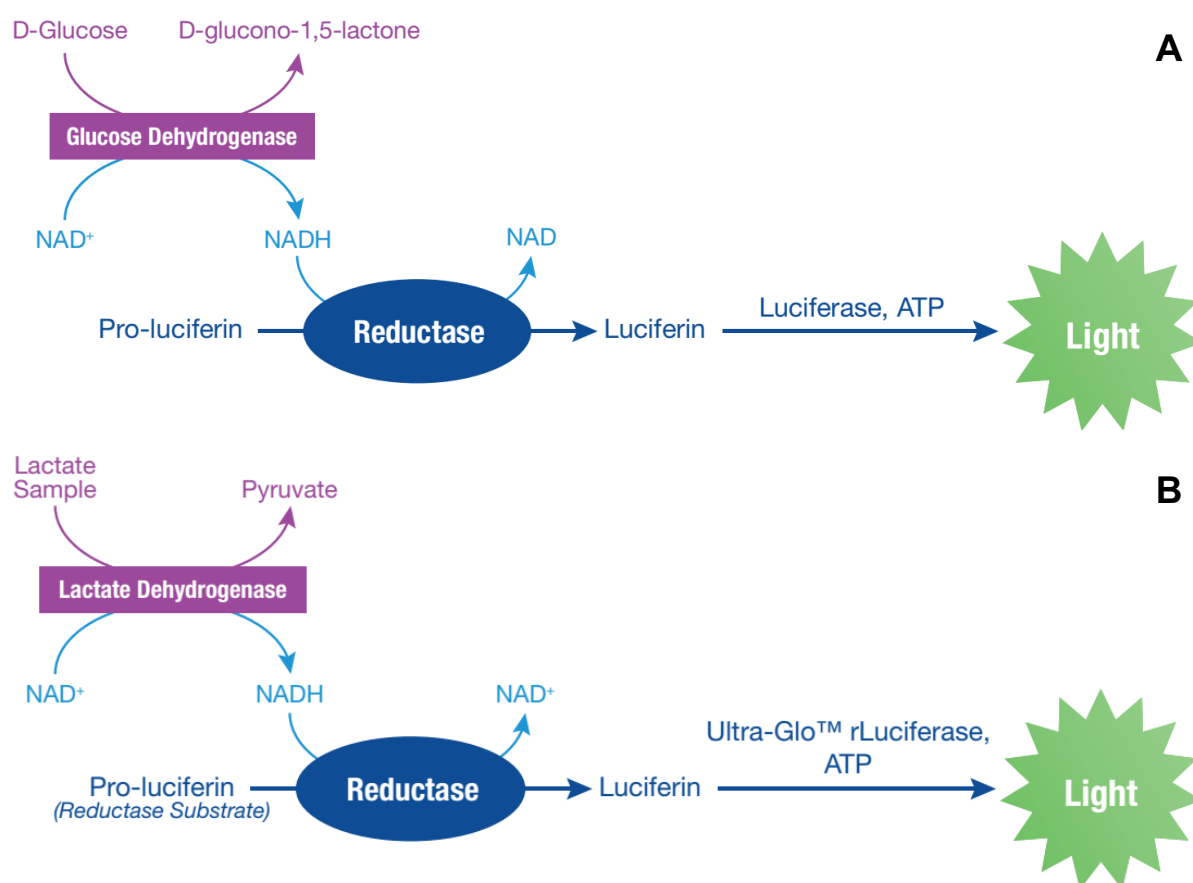
Figure 2.6   Working principle of the Glucose Glo™ (A) and the Lactate Glo™ Assay (B). ATP, adenosine triphosphate; NAD+, nicotinamide adenine dinucleotide; NADH, nicotinamide adenine dinucleotide hydride (67,68).

2.8.2.   Experimental design

Glucose and lactate levels were measured in supernatants collected at 24 h time intervals for up to 3 days of incubation in either hypoxia (0.1 % O_2 and 1 % O_2) or normoxia (20 % O_2) following initial seeding in petri dishes ($\varnothing$ 6 cm) at a density of 5,000 cells/cm^2 and 20,000

cells/cm^2 for A549 and H358, respectively. Three biological replicates were performed with two technical replicates each.

2.8.3. Sample and reagent preparation

Supernatants collected for each condition and timepoint were initially diluted to 1:20 with PBS and stored at -80 °C. At the time of performing the assays, supernatants were diluted further with PBS to a final dilution of 1:500 for the glucose assay and 1:100 for the lactate assay.

The assay kits stored at -80 °C were allowed to thaw on ice and then mixed according to standard protocols provided in their respective manuals (Table 2.13). The prepared reagent thus obtained was then mixed with the diluted sample supernatants in a ratio of 1:1 (50 μL each) in a 96-well plate. Additionally, known concentrations of glucose (10 to 50 μmol/L) and lactate (10 to 200 μmol/L) were also loaded into the 96-well plate to obtain a standard curve. PBS was used as a glucose-free negative control.

Furthermore, to normalize glucose and lactate values to the cell number, the cells in each sample were counted by detaching the cells with trypsin and then using the LUNA cell counter.

Table 2.13   Chemical components of the Promega Glucose Glo^{TM} (left) and Lactate Glo^{TM} (right) kits and the required volumes of the detection reagent in μL per well of a 96-well plate.

Component	Volume (μL) per reaction	
	Glucose Glo^{TM}	Lactate Glo^{TM}
Luciferin Detection Solution	50	50
Reductase	0.25	0.25
Reductase substrate	0.25	0.25
Glucose Dehydrogenase	2	NA
Lactate Dehydrogenase	NA	0.25
NAD	0.25	0.25
Sample (cell culture supernatant)	50 (diluted 1:500)	50 (diluted 1:100)

2.8.4. Luminescence measurement

To measure respective luminescence from each sample in a 96-well plate, the multimode microplate reader Infinite M200Pro (Tecan, Groeding, Austria) was used. The well plate was first shaken for 60 seconds to mix samples thoroughly with the reagent and then incubated for 1 h at 25 °C before luminescence was measured. The photon counting detector in the specific plate reader used required no gain calibration. The integration time per well and signal attenuation were modulated to ensure a reasonably high photon count in sample wells while keeping background counts in blank wells as low as possible.

2.9.   Colony forming ability (CFA) assay

Puck's colony forming ability (CFA) assay (69) is the gold standard method for determining cell survival through assessing colony forming ability of irradiated cells. This gives quantitative information regarding loss of reproductive capability of cells and relative cellular radiosensitivity at different radiation doses and also with respect to different types or qualities of radiation.

2.9.1. Experimental design

The CFA experiments were designed to compare surviving cell fractions for both A549 and H358 cell lines cultured under normoxia (20 % O_2) and hypoxia (1 % O_2 and also 0.1 % O_2 in some cases) following irradiation. The hypoxic experimental groups were further divided into continuously and transiently hypoxic groups based on their oxygen environment after irradiation as explained previously in chapter 2.5. Both Immediate and Late Plating experiments were carried out for each experimental group.

Experimental design and its parameters are described in Table 2.14.

Table 2.14   Experimental design parameters for colony forming ability (CFA) assays

Parameter	A549		H358
Radiation quality	X-rays	Carbon Ions	X-rays only
Radiation doses	0, 0.5, 1, 2, 4, 6 & 8 Gy	0, 0.5, 1, 2, 4 & 6 Gy	0, 0.5, 1, 2, 4, 6 & 8 Gy
Experimental groups	Normoxia *Immediate & Late Plating*		Normoxia *Immediate & Late Plating*
	Transient Hypoxia (1 % O_2) *Immediate & Late Plating*		Transient Hypoxia (1 % O_2) *Immediate & Late Plating*
	Continuous Hypoxia (1 % O_2) *Immediate & Late Plating*		Continuous Hypoxia (1 % O_2) *Immediate & Late Plating*
	Transient Hypoxia (0.1% O_2) *Immediate & Late Plating*		
Incubation time for colony growth	2 weeks		3 weeks
Plating efficiency	Normoxia: 30 % Hypoxia: 20 %		Normoxia: 15 % Hypoxia: 15 %
Technical replicates per radiation dose	6		6
Biological replicates per experimental condition	3		3

2.9.2. Cell preparation and irradiation

Cells were seeded in 25 cm^2 tissue culture flasks for X-rays exposure and 12.5 cm^2 flasks for carbon ion exposure at a seeding density of 5,000 cells/cm^2 and 20,000 cells/cm^2 for A549 and H358, respectively, and allowed to grow for 48 h either in a standard incubator at 20 % O_2 (normoxia) or in the hypoxia workstation at 1 % O_2 (hypoxia). For some experiments, A549 cells were also grown at 0.1% O_2. After 48 h, the cells were irradiated with different doses of X-rays (chapter 2.6.1). A549 cells were also irradiated with different doses of carbon ions in some experiments (chapter 2.6.2). The irradiation of hypoxic cells was carried out by shifting them into airtight boxes during irradiation.

Following irradiation, cells were plated in petri dishes ($\varnothing$ 6 cm) either immediately after radiation exposure (immediate plating) or after a 24 h recovery period (late plating). For this, cells for each dose were trypsinized, counted and a specific number of cells was transferred into 50 mL centrifuge tubes containing 35 mL culture medium based on the PE and anticipated killing effect of the applied radiation dose. For this purpose, a CFA excel macrosheet developed by Prof. Dr. Christa Baumstark-Khan, Version 1.04, was used. This volume of cell suspension was then transferred into six petri dishes ($\varnothing$ 6 cm, 5 mL per dish) per dose. In case of H358 cells, the medium used for plating the petri dishes was conditioned (fresh culture medium mixed with filtered culture medium used previously; 1:1 by volume, according to Table 2.7).

Normoxic cells and transiently hypoxic cells were plated in a standard laminar hood (type 2) while continuously hypoxic cells were plated in the hypoxia workstation. Cells used for delayed plating were incubated in a standard incubator in case of normoxic and transiently hypoxic cells while the continuously hypoxic cells were incubated in the hypoxia workstation.

2.9.3. Staining and counting of colonies

After an incubation of 14 days (in case of A549 cells) and 21 days (in case of H358 cells), medium was aspirated, petri dishes were gently washed with tap water, and grown colonies were fixed and stained with 5 mL of crystal violet staining solution (Table 2.7) per petri dish for 20 min following which the staining solution was removed and the colonies were once again gently washed with tap water. The petri dishes were then air-dried overnight, and the grown colonies (accumulation of ≥50 cells) were then counted using a schuett-biotec.de counter with a magnifying glass.

2.9.4. Calculation of survival

Excel macro sheets developed by Prof. Dr. Christa Baumstark-Khan were used for analyzing CFA data (CFA excel sheet, version 1.07), calculating dose-effect curves and comparing survival data from different cell lines and conditions (CFA-AllData_V1.04). In the CFA excel sheet, plating efficiency (PE), relative cellular survival (S) and its natural log (ln S) were calculated based on the equations listed below.

PE is the ratio of the colonies counted to the number of cells seeded and was calculated using Equation 2.5.

$$PE = \frac{Number\ of\ colonies\ counted}{Number\ of\ cells\ seeded} \cdot 100 \qquad \text{Equation 2.5}$$

The fraction of cells that survive a certain radiation dose (surviving fraction, S) was calculated according to equation 2.6:

$$S = \frac{PE\ after\ irradiation}{PE\ without\ irradiation} \qquad \text{Equation 2.6}$$

2.9.5. Generation of dose response curves

A radiation dose response curve is generated by plotting the cell surviving fraction on a logarithmic scale as a function of dose plotted on a linear scale (Figure 2.7).

The surviving fraction (S) and its natural logarithm (ln S) were modeled by both the multi-hit multi-target model, also referred to as the Linear Quadratic Model, using Equation 2.7 and the single-hit multi-target model (70) using Equation 2.9 to evaluate which model fits best to the experimental data.

$$S(D) = e^{-\alpha D - \beta D^2}$$
Equation 2.7

This can also be expressed as:

$$-lnS = \alpha D + \beta D^2$$
Equation 2.8

with

$\qquad$ S(D) = surviving fraction of cells at the given dose D

$\qquad$ α $\quad$ = constant that describes the initial slope

β $\quad$ = constant that describes the bending of the curve

and

$$S(D) = 1 - (1 - e^{-\frac{D}{D_0}})^n$$
Equation 2.9

with

$\qquad$ S(D) = surviving fraction of cells at a given dose D

$\qquad$ D_0 = dose that reduces cell survival to 37 %

n = extrapolation number (point, where the final slope would cut the y-axis when extrapolated)

For higher doses, Equation 2.9 can be simplified to:

$$ln(S) = \frac{-D}{D_0} + ln(n)$$
Equation 2.10
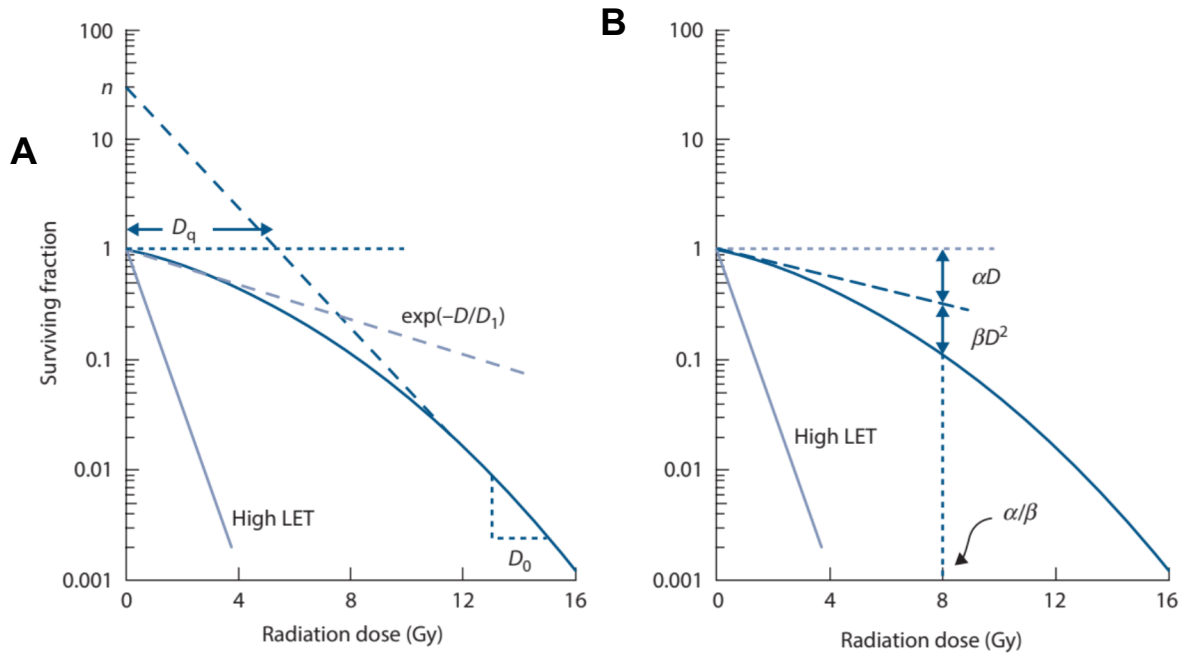
Figure 2.7   Dose-effect curves calculated according to the single-hit multi-target model (A) and multi-hit multi-target (Linear Quadratic) model (B). Dose-effect curves for low-LET radiation (e.g., X-rays) show a "shoulder" while the dose-effect curves for high-LET radiation (e.g., carbon ions) show a plain exponential decrease with increasing dose (71). The quasi-threshold dose "D_q" represents the "shoulder width" of the curve. The extrapolation number "n" is obtained by extending the linear part of the curve to the 100 % survival line. D_0 is the slope of the linear part of the curve. The constants α and β represent the initial slope and the bending of the curve respectively.

2.9.6.   Calculation of relative biological effectiveness

The Relative Biological Effectiveness (RBE) of carbon ions is calculated by dividing the doses assumed to cause the same biological effect of the reference radiation (X-rays) and the test radiation (carbon ions). This was carried out by dividing the D_0 value for X-rays with the D_0 value for the carbon ions (Equation 2.11).

$$RBE_{Survival\ reduction} = \frac{D_{0\ (X\text{-}rays)}}{D_{0\ (test\ radiation)}}$$ *Equation 2.11*

2.9.7.   Calculation of oxygen enhancement ratio

The Oxygen enhancement ratio (OER) of hypoxia is calculated by dividing the doses assumed to cause the same biological effect under normoxia and hypoxia. This was carried out by dividing the D_0 value for normoxia with the D_0 value for hypoxia (Equation 2.12).

$$OER = \frac{D_{0\ (Normoxia)}}{D_{0\ (Hypoxia)}}$$ *Equation 2.12*

2.10. γH2AX and p65 immunofluorescence microscopy

Following irradiation, the cellular response to DNA Double Strand Breaks (DSBs) and NF-κB activation were assessed by visualising γH2AX foci and p65 intensity changes, respectively, at various time intervals through immunofluorescence microscopy in all experimental groups.

2.10.1. Working principle

Primary antibodies specific for γH2AX and p65 were used to stain the samples followed by staining with fluorescent secondary antibodies and a fluorescent nuclear stain. The light source of the microscope was then used to excite the specific fluorophores in the samples and the light emitted by the fluorescent dye was focused on the detector by the objective.

1. Light source
2. Excitation filter
3. Microscope stage
4. Objective
5. Dichroic mirror
6. Emission filter
7. Detector
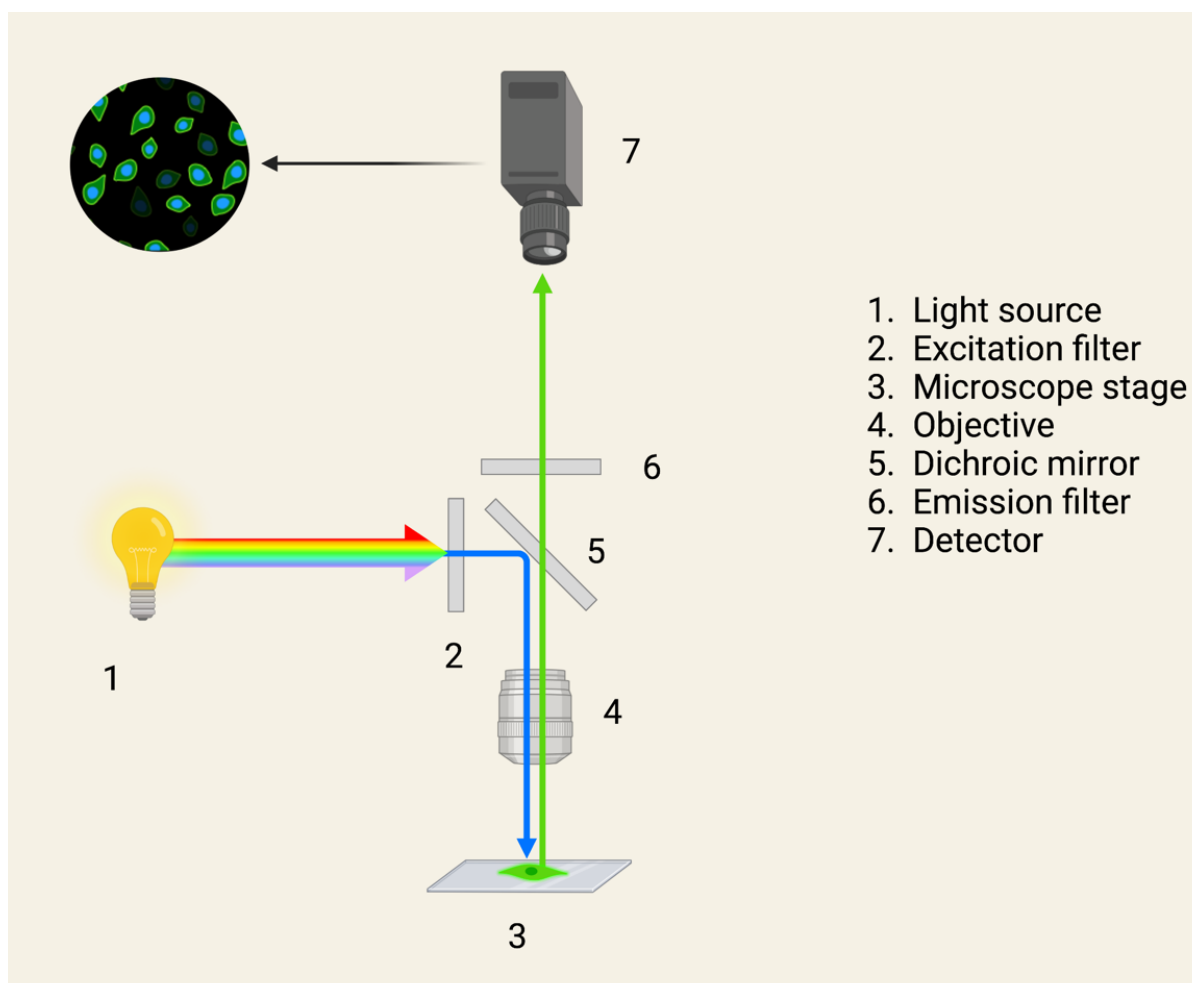
Figure 2.8   Fluorescence microscopy working principle: Excitation wavelengths are incident on the cell preparation placed on the microscopic stage after being filtered by an excitation filter. Emission wavelengths of interest coming from the fluorophores within the cell preparation reach the detector after being filtered through an emission filter. The fluorescent image becomes visible in the eye piece and the workstation user interface display. Created with Biorender.com.

The type of DNA damage accounting for cell death after irradiation are mainly DSBs that can be quantified by visualising γH2AX foci. Since most of the initial DSBs are expected to be repaired in the first 24 hours after irradiation, following up irradiated cells in this time period can give information on DSB repair kinetics in a particular cell line following irradiation with a particular dose and quality of radiation.

The translocation of p65 (Rel A) from the cytoplasm to the nucleus as a part of the cellular response following irradiation as well as stressors like hypoxia was assessed over time through serial fluorescence microscopy imaging resulting in an intensity gradient of p65 immunofluorescence in the nucleus and the cytoplasm, indicating translocation of p65 from the cytoplasm to the nucleus and thereby NF-κB activation.

2.10.2. Experimental design

The γH2AX immunofluorescence microscopy experiments were designed to compare basal DSBs and DSBs following irradiation for both A549 and H358 cells cultured under normoxia (20 % O_2) and hypoxia (1 % O_2 and 0.1 % O_2 in some cases) (Table 2.15).

Similarly, the p65 immunofluorescence microscopy experiments were designed to compare the nuclear intensity gradient for both A549 and H358 cells cultured under normoxia (20 % O_2) and hypoxia (1% O_2 and also 0.1% O_2 in some cases) following irradiation.

The hypoxic experimental groups were further divided into continuously and transiently hypoxic groups based on their oxygen environment after irradiation as explained previously (subchapter 0).

Table 2.15   Experimental parameters for immunofluorescence microscopy

Experimental Parameter	A549	H358
Radiation quality	X-rays and carbon ions	X-rays
Experimental groups	Normoxia Transient Hypoxia (1 % O_2) Continuous Hypoxia (1 % O_2) Transient Hypoxia (0.1% O_2) Continuous Hypoxia (0.1% O_2)	Normoxia Transient Hypoxia (1 % O_2) Continuous Hypoxia (1 % O_2)
Radiation doses	γH2AX: 0, 2 Gy p65: 0, 8 Gy	γH2AX: 0, 2 Gy p65: 0, 8 Gy
Fixation time points for DSB measurement	γH2AX: 1, 2, 6, 12, 18 & 24 h p65: 2, 6 & 24 h	γH2AX: 1, 2, 6, 12, 18 & 24 h p65: 2, 6 & 24 h
Positive control (for p65 only)	TNF-α (20 ng/ml) fixed at 6 h	TNF-α (20 ng/ml) fixed at 6 h
Technical replicates per radiation dose	2	2
Biological replicates per experimental condition	3	3

2.10.3. Coverslip preparation, irradiation and fixation

Four microscope cover slips (∅ 10 mm) were placed within the coverslip indentations of ∅ 3 cm cell culture dishes and then coated with 100 µL of Poly D-Lysine (PDL; 0.01 mg/mL) for 1 h after which they were washed with sterile deionised water. Once dry, cells were seeded onto

the cover slips at a seeding density of 5,000 cells per cm^2 for A549 and 12,500 cells per cm^2 for H358 cells in standard culture medium.

Cell culture dishes housing the coverslips were then incubated for 48 h either in a standard incubator at 20 % O$_2$ (normoxia) or in the hypoxia workstation at 1 % O$_2$ (Hypoxia). After 48 h, the cells were irradiated at the defined doses (Table 2.15). A549 cells were also irradiated with carbon ions. The irradiation of hypoxic cells was carried out by shifting them into airtight containers at the time of irradiation. For carbon ion experiments at GANIL, cells were seeded in slide flasks instead of coverslips in order to avoid leakage during upright positioning for irradiation.

Following irradiation, the cells were shifted to a standard incubator in case of normoxic and transiently hypoxic experimental groups while the cells in the continuously hypoxic group were shifted back to the hypoxia workstation. Fixation of cells was carried out at defined timepoints (Table 2.15) by keeping coverslips or slide flasks immersed in 3.5 % formaldehyde for 30 minutes at 4 °C after which the formaldehyde was replaced with PBS and the cell culture dishes were stored at 4 °C till subsequent immunostaining.

2.10.4. Immunofluorescence staining

For immunostaining, fixed cells were permeabilized with a solution containing 5 % normal goat serum (NGS), 1 % DMSO and 0.3 % Triton X in PBS for 1 h at room temperature. In the following, they were stained with the primary antibody (Table 2.16) diluted in a staining solution comprised of PBS with 1 % DMSO and 0.3 % Triton X and then incubated overnight at 4 °C. The next day the cells were stained with the secondary antibody (Table 2.16) and the nuclear stain DAPI diluted using the same staining solution following which they were incubated for 45 minutes in the dark at room temperature. After 45 minutes, the coverslips were mounted on to microscope slides using mounting medium (DAKO, Agilent Technologies, Santa Clara, USA). The microscope slides were stored for next 24 h in the dark at room temperature after which they were shifted to 4 °C for longer term storage.

Table 2.16   Immunostaining parameters used for A549 and H358 cells

Parameter	γH2AX	p65
Primary antibody	Alexa Fluor 488 Mouse anti-γH2AX clone 2F3 (Biolegend)	Rabbit anti-NF-κB p65 mAb E379 (Abcam)
Reactivity	Human, mouse	Human, mouse
Final dilution	1:250 (for A549) 1:300 (for H358)	1:100 (for A549) 1:200 (for H358)
Secondary antibody	Goat anti mouse IgG-Atto488 (Sigma Aldrich)	Goat anti mouse IgG-Atto550 (Sigma Aldrich)
Final dilution	1:1000	1:1000
DAPI (5µg/ml)	1:400	1:400

2.10.5. Fluorescence microscopy and image analysis

Microscopy of the slides was conducted on the Zeiss Axio Imager M2 using a 40x/1.4 Oil objective. Images were taken using the DAPI and Atto488 channels (Figure 2.9) or the Atto550

channel (Figure 2.10). The exposure time and threshold for each channel were kept constant across three experimental groups for 1 biological replicate to ensure comparability of the images. For each cover slip, three 9x tile pictures were acquired.

Further analysis using the Image J software was carried out where single nuclei were identified in the DAPI channel (Fig 2.9A) and then γH2AX foci were counted within each nucleus in the Atto488 channel (Fig 2.9B).

A
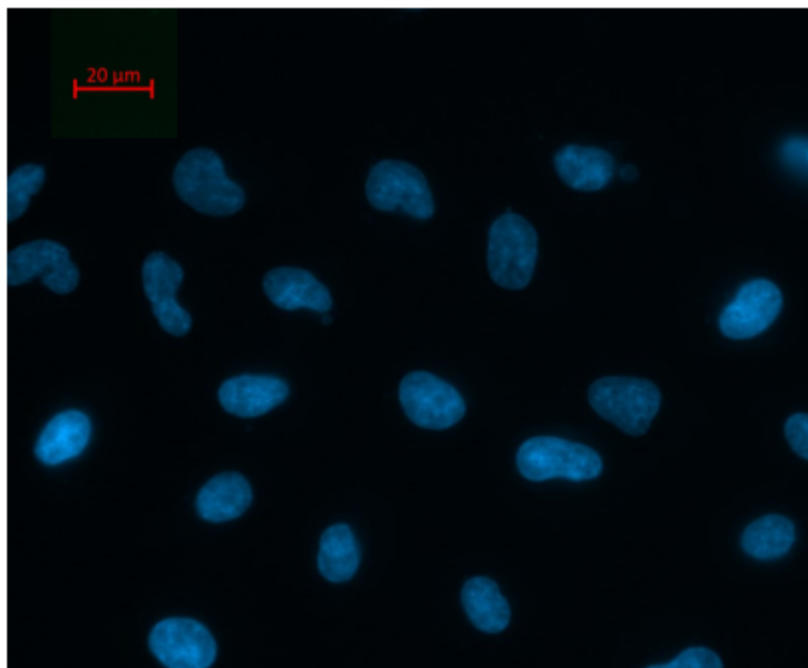
B
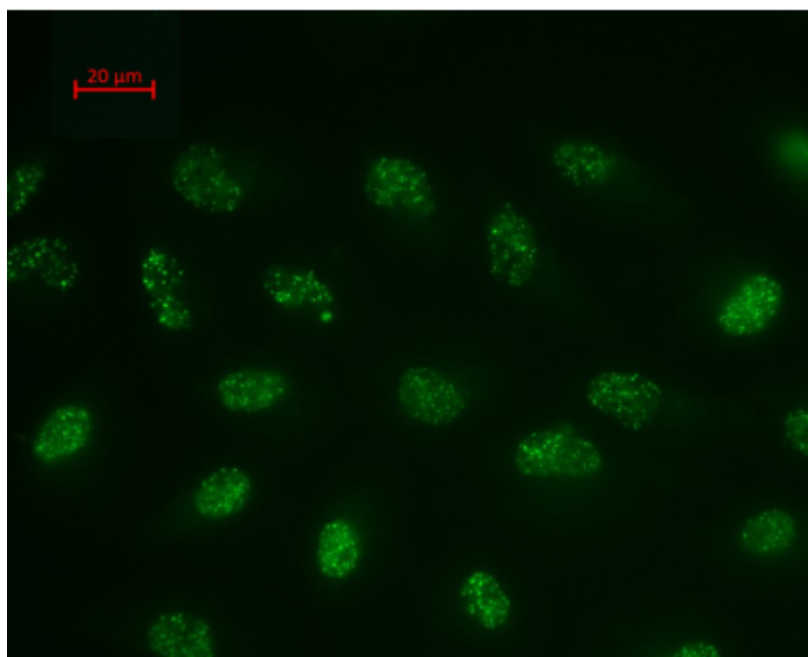
Figure 2.9 Fluorescence microscopy images of γH2AX-immunostained A549 cells exposed to 2 Gy dose of X-rays under normoxia. DAPI channel image (400x) of A549 cell nuclei stained with DAPI (A), Atto488 channel image (400x) showing γH2AX foci within the same nuclei (B) which were then counted using ImageJ software.

For analysis of p65 images on Image J, the cell nuclei were identified in the DAPI channel (Fig 2.10A) and then p65 staining intensity within each nucleus was measured in the Atto550 channel (Fig 2.10B).

A

B
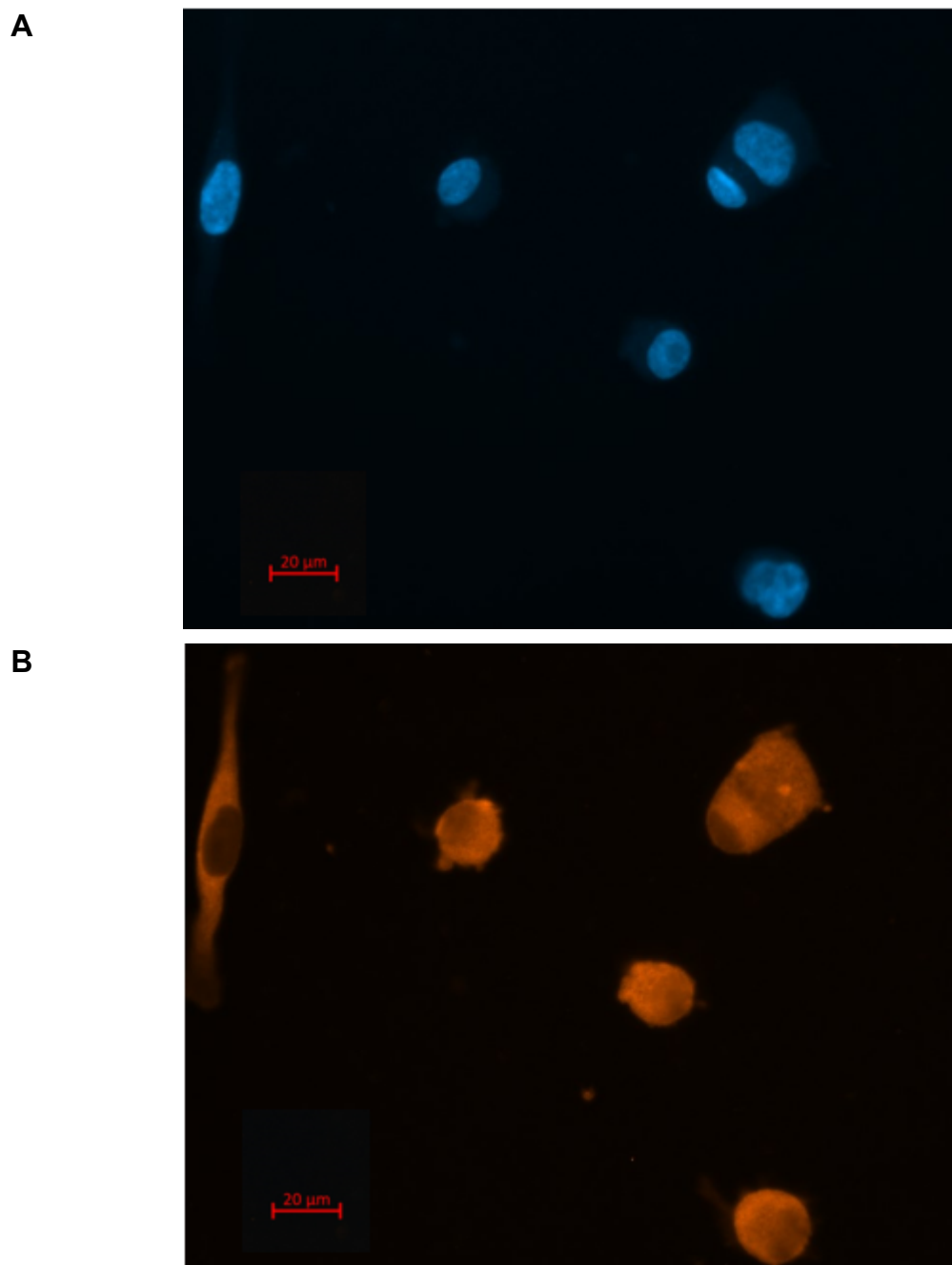
Figure 2.10   Fluorescence microscopy images of p65-immunostained A549 cells exposed to 8 Gy dose of X-rays under normoxia. DAPI channel image (400x) of nuclei of A549 cells stained with DAPI (A), Atto550 channel image (400x) showing variable nuclear and cytoplasmic fluorescence intensity indication localization of p65 (B). The nuclear intensity of each cell was recorded, the average for all cells in the image was calculated and then normalized against the unirradiated normoxic control.

2.11. Flow cytometric study of cell cycle

Cell cycle progression was analyzed to detect possible correlations of cell survival, DNA DSB repair and G2 arrest as the G2 and late S phases provide the main platform where DNA DSB are most effectively repaired through the HR pathway and exposure to ionizing radiation tends to arrest tumor cells in the G2 phase of the cell cycle.

2.11.1. Working principle

When cell nuclei are stained with a nuclear stain like DAPI, it stoichiometrically binds to DNA. Since cells in late S, G2 and M phases have twice the amount of DNA than those in G1 and early S phase, they will also have twice the amount of DAPI. This is used to distinguish between cell populations in G1 and G2 phases by means such as flow cytometry quantifying the fluorescence intensity of each single cell stained with the fluorophore DAPI (excitation wavelength = 358 nm and emission wavelength = 461 nm).

2.11.2. Experimental design

In these experiments, cell cycle progression following irradiation of A549 and H358 cells cultured under normoxia (20 % O_2) and hypoxia (1 % O_2 and 0.1 % O_2 in some cases) was compared. The hypoxic experimental groups were further divided into continuously and transiently hypoxic groups (Table 2.17) based on their oxygen environment after irradiation as explained in subchapter 2.5.

Table 2.17   Experimental parameters for flow cytometric analysis of cell cycle distribution

Experimental Parameter	A549	H358
Radiation quality	X-rays and carbon ions	X-rays
Experimental groups	Normoxia Transient Hypoxia (1 % O_2) Continuous Hypoxia (1 % O_2) Transient Hypoxia (0.1% O_2) Continuous Hypoxia (0.1% O_2)	Normoxia Transient Hypoxia (1 % O_2) Continuous Hypoxia (1 % O_2)
Radiation doses	8 Gy	8 Gy
Fixation time points	2, 6, 12, 18 and 24 h	2, 6, 12, 18, 24 and 48 h
Technical replicates per time point	2	2
Biological replicates per experimental condition	3	3

2.11.3. Sample preparation, irradiation and fixation

Cells were seeded at a density of 5,000 cells/cm^2 and 20,000 cells/cm^2 for A549 and H358 cell lines, respectively, using standard culture medium in cell culture dishes ($\varnothing$ 6 cm). The cell culture dishes were then incubated for 48 h either in a standard incubator at 20 % O_2 (normoxia) or in the hypoxia workstation at 1 % O_2 (hypoxia).

After 48 h, the cells were irradiated with an X-ray dose of 8 Gy. The irradiation of hypoxic cells was carried out by shifting them into airtight boxes at the time of irradiation. A549 cells were also irradiated with a carbon ion dose of 8 Gy in some experiments, in this case in 25 cm^2 tissue culture flasks. Following irradiation, the cells were shifted to a standard incubator in case of normoxic and transiently hypoxic experimental groups while the cells in the continuously hypoxic group were shifted back to the hypoxia workstation.

At defined time points, the cells were detached with 1 mL trypsin/EDTA solution and resuspended in 1.5 mL Eppendorf tubes containing 105 µL of 37 % formaldehyde so that the final formaldehyde concentration in the fixed cell solution became 3.5 %. The cells were then refrigerated (4 °C) for 30 minutes after which they were centrifuged for 10 minutes at 500×g, and the cell pellet was resuspended in PBS. Following this, the cells were stored at 4 °C.

2.11.4. Staining, flow cytometry and cell cycle analysis

On the day of flow cytometry, fixed cells were pipetted into a Nunc 96-well Polystyrene Round Bottom Microwell Plate. The 96-well plate was centrifuged at 500×g for 10 minutes and the supernatant was removed following which the cell pellets were resuspended in 150 µL per well of staining solution comprising of DAPI (500 ng/mL) and Triton X (3 µg/mL) in PBS. The plate was incubated for 30 minutes in the dark at room temperature before being loaded into the Cytoflex S flow cytometer.

$2×10^4$ cells were analyzed at a rate of 180 cells per second. Fluorescence of the samples were measured with a violet laser (405 nm) as excitation source. Blue fluorescence was measured in the fluorescence channel PB450 of the Cytoflex S and analyzed using FloJo software (V 10). A dot plot of areas for forward scatter (FSC) and side scatter (SSC) was created and the region of intact cells was gated by eliminating cell debris (Figure 2.11A). A second dot plot displayed the area of the fluorescence signal in PB450 channel on the y-axis versus the width of the fluorescence signal in PB450 channel on the x-axis (Figure 2.11B). Cells with twice the fluorescence width were regarded as doublets and omitted from the gate applied around the remaining cell population. Only single cells were then displayed in a histogram showing the height of the fluorescence signal in the PB450 channel.

This histogram plot was used for automated cell cycle analysis using Dean-Jett-Fox Cell Cycle Mathematical Model (Figure 2.11C) under the Module "Cell Cycle" of the FloJo software. The module provides cell percentages in G1, S, and G2 phases in an exportable table for further statistical analyses.
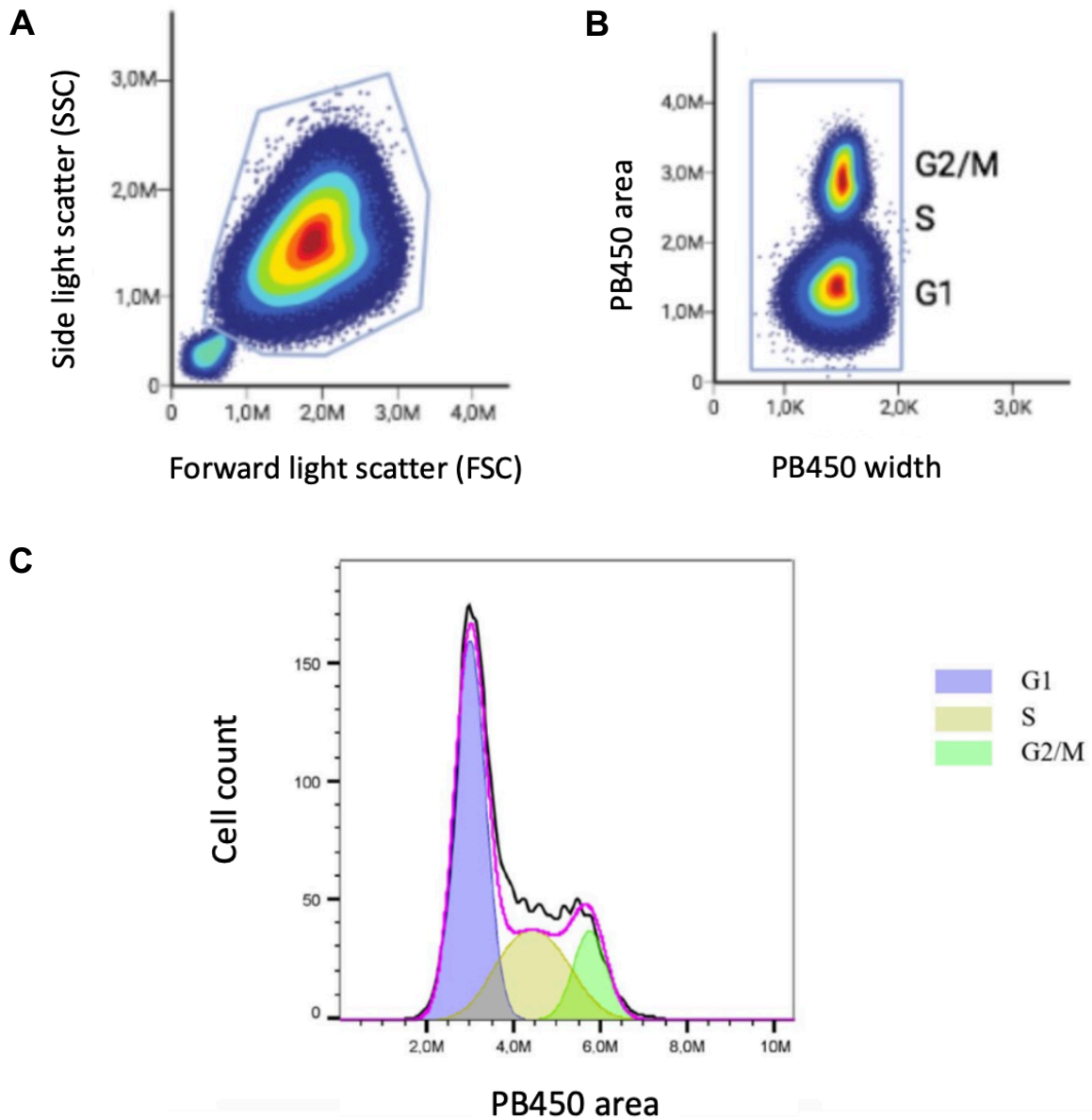
Figure 2.11   Gating strategy and histogram of DAPI fluorescence for cell cycle analysis: (A) Dot plot of FSC area and SSC area to separate the population of intact cells from cell debris; created with Biorender.com. (B) Dot plot of PB450 area against its width to separate duplets from singlets; created with Biorender.com (C). Histogram of PB450 area of single cells analyzed using Dean-Jett-Fox model to give cell populations in G1, G2 and S phases. Image adapted from FloJo data.

2.12. NF-κB target cytokines assessment using ELISA

Following irradiation, the production of two common NF-κB target cytokines, IL-6 and IL-8, was assessed in all experimental groups at different time intervals by means of Sandwich ELISAs.

2.12.1. Working principle

Invitrogen Human IL-6 and IL-8 Uncoated ELISA Kits (Table 2.6) were used for IL-6 and IL-8 detection in sample supernatants. Each kit makes use of a target-specific capture antibody and a biotin-conjugated detection antibody. The enzyme-antibody-target complex is formed by addition of Streptavidin-horseradish peroxidase (HRP) (for IL-6) or Avidin-HRP (for IL-8) which produce then a measurable signal after addition of 3,3´,5,5´´-tetramethylbenzidine (TMB) as the HRP substrate (Table 2.19). The intensity of this signal is directly proportional to the concentration of target (IL-6 or IL-8) present in the supernatant.

Table 2.18   Specific parameters of Sandwich ELISA kits used for cytokine quantification

Kit Parameters	Invitrogen IL-6 Kit	Invitrogen IL-8 Kit
Antibodies	Capture Antibody	Capture Antibody
	Biotin-conjugated Detection Antibody	Biotin-conjugated Detection Antibody
	Species: human	Species: human
	Specificity: endogenous and recombinant human IL-6	Specificity: endogenous human IL-8
Enzyme	Streptavidin-horseradish peroxidase	Avidin-horseradish peroxidase
Substrate	3,3´,5,5´´-tetramethylbenzidine (TMB)	3,3´,5,5´´-tetramethylbenzidine (TMB)
Analytical sensitivity for quantification	2 pg/mL	2 pg/mL
Assay range	2-200 pg/mL	2-250 pg/mL
Sample type	Supernatant (100 µL/well)	Supernatant (100 µL/well)

2.12.2. Experimental design

In the ELISA experiments to detect IL-6 and IL-8 in sample supernatants, production of these cytokines was compared in A549 and H358 cells, cultured under normoxia (20 % O_2) and hypoxia (1% O_2 and 0.1% O_2 in some cases) following irradiation. The hypoxic experimental groups were further divided into continuously and transiently hypoxic groups based on their oxygen environment after irradiation as explained in subchapter 2.5.

Table 2.19   Parameters of IL-6 and IL-8 ELISA experiments

Experimental Parameters	A549	H358
Radiation quality	X-rays and carbon ions	X-rays
Experimental groups	Normoxia Transient Hypoxia (1 % O_2) Continuous Hypoxia (1 % O_2) Transient Hypoxia (0.1% O_2) Continuous Hypoxia (0.1% O_2)	Normoxia Transient Hypoxia (1 % O_2) Continuous Hypoxia (1 % O_2)
Radiation doses	8 Gy	8 Gy
Fixation time points for DSB measurement	2, 6 and 24 h	2, 6 and 24 h
Technical replicates per time point	2	2
Biological replicates per experimental condition	3	3

2.12.3.   Cell seeding, irradiation and supernatant collection

Cells were seeded in $\varnothing$ 3 cm cell culture dishes at a seeding density of 5,000 cells per cm^2 (A549) or 25,000 cells per cm^2 (H358) in 3 mL standard culture medium. The dishes were then incubated for 48 h either in a standard incubator at 20 % O_2 (normoxia) or in the hypoxia workstation at 1 % O_2 (Hypoxia). After 48 h, the cells were irradiated with an X-ray dose of 8 Gy (see 2.6.1). The irradiation of hypoxic cells was carried out by shifting them into air tight boxes at the time of irradiation. A549 cells were also irradiated with 8 Gy carbon ions in some experiments (see 2.6.2).

Following irradiation, the cells were shifted to a standard incubator in case of normoxic and transiently hypoxic experimental groups while the cells in the continuously hypoxic group were shifted back to the hypoxia workstation. At the defined timepoints (2 h, 6 h, 24 h; TNF control at 6 h), the supernatant (3 mL) was collected in Eppendorf tubes and stored at -80 °C till subsequent handling. The cells on the other hand were trypsinized and counted with the LUNA automated cell counter for normalization of cytokine production to the cell number.

2.12.4.   ELISA workflow

For coating the wells of 96-well plates (Corning™ Costar™ 9018 ELISA plate) with the primary capture antibody (100 µL) diluted 1:250 in PBS, the plate was incubated at 4 °C overnight. Afterwards, the wells were blocked for nonspecific antibody binding using ELISA/ELISPOT diluent (200 µL) diluted (1:5) in deionized water. The plate was again incubated at 4°C overnight after loading the wells with the samples (100 µL), serial dilutions of the standard and negative controls (ELISA/ELISPOT diluent only) (Table 2.20). On the next day, the detection antibody (100 µL per well) diluted (1:250) in PBS was added and the plate was incubated for 1 h at room temperature. This was followed by incubation at room temperature for 30 minutes after addition of Streptavidin-HRP (100 µL) diluted (1:100) in ELISA/ELISPOT diluent for IL-6

or by addition of Avidin-HRP (100 µL) diluted (1:250) in ELISA/ELISPOT diluent for IL-8 in the wells. Finally, the plate was incubated for 15 minutes at room temperature after addition of TMB substrate (100 µL) to the wells at the completion of which the enzyme reaction was stopped by adding 2 N H_2SO_4 (100 µL) to the wells. All incubation steps were carried out on a shaker with 3 to 5 washings in between with wash buffer (PBS with 0.05 % Tween).

Table 2.20   Standard curve and negative control in ELISAs

Parameters	Invitrogen IL-6 Kit	Invitrogen IL-8 Kit
Standard Curve (Top standards provided with the kit)	200.0 pg/mL	250.0 pg/mL
	100.0 pg/mL	125.0 pg/mL
	50.0 pg/mL	62.5 pg/mL
	25.0 pg/mL	31.2 pg/mL
	12.5 pg/mL	15.6 pg/mL
	6.2 pg/mL	7.8 pg/mL
	3.1 pg/mL	3.9 pg/mL
	1.6 pg/mL	1.9 pg/mL
Negative Control	Blocking Solution provided with the kit (ELISA/ELISPOT diluent)	Blocking Solution provided with the kit (ELISA/ELISPOT diluent)

2.12.5.   Plate reading

Plates were read in a Multiskan FC microplate reader at 450 and 570 nm at 21 °C. Wavelength subtraction (Absorbance A (450 nm) – B (570 nm)) was done via the SkanIt Software (ver. 6.1.1.7) and displayed in an exportable table for further statistical analyses using Microsoft Excel to plot the standard curves and use them to derive actual cytokine concentrations from the absorbance values.

2.13. mRNA sequencing to assess activation of NF-κB and other pathways

Following irradiation, differential gene expression with an emphasis on NF-κB target genes was carried out for both A549 and H358 cell lines including all experimental groups using mRNA sequencing.

2.13.1. Working principle

mRNA sequencing uses total mRNA to construct cDNA through reverse transcription. The sequencer reads and quantifies the cDNA complementary to the mRNA based on the number of reads. Since transcription of mRNA from coding sequences from a gene (and not noncoding DNA) is the first step in gene expression, quantification of mRNA levels provides a measure of expression of the respective gene. However, since mRNA levels are influenced not only by promoter activity, but also by mRNA stability, mRNA levels do not always correlate with protein levels.

2.13.2. Experimental design

The mRNA sequencing experiments were performed to compare gene expression of A549 and H358 cells, cultured under normoxia (20 % O_2) and hypoxia (1 % O_2), following irradiation. The hypoxic experimental groups were further divided into continuously and transiently hypoxic groups based on their oxygen environment after irradiation as explained previously in subchapter 0.

Experimental design and its parameters are described in Table 2.21.

Table 2.21   Parameters of mRNA sequencing experiments

Experimental Parameter	A549	H358
Radiation quality	X-rays and carbon ions	X-rays
Experimental groups	Normoxia Transient Hypoxia (1 % O_2) Continuous Hypoxia (1 % O_2)	Normoxia Transient Hypoxia (1 % O_2) Continuous Hypoxia (1 % O_2)
Radiation doses	8 Gy	8 Gy
Lysis time point for RNA extraction	4 h	4 h
Biological replicates per experimental condition	4	4

2.13.3. Cell seeding, irradiation and RNA extraction

A549 and H358 cells were seeded at a seeding density of 5,000 and 25,000 cells per cm^2, respectively, in 25 cm^2 culture flasks containing 5 mL standard culture medium each. The dishes were then incubated for 48 h either in a standard incubator at 20 % O_2 (normoxia) or in the hypoxia workstation at 1 % O_2 (hypoxia). After 48 h, the cells were irradiated with an X-ray dose of 8 Gy (see 2.6.1). The irradiation of hypoxic cells was carried out by shifting them into airtight boxes at the time of irradiation. A549 cells were also irradiated with 8 Gy carbon ions in some experiments (see 2.6.2). Following irradiation, the cells were shifted to a standard

incubator in case of normoxic and transiently hypoxic experimental groups while the cells in the continuously hypoxic group were shifted back to the hypoxia workstation.

4 h after irradiation, flasks with cells were placed on ice, the culture medium was fully removed, and cells were lysed using RLT-lysis buffer (600 µL per flask) to which 14.3 mol/L β-mercaptoethanol was added (1:100). The lysed cells were collected using cell scrapers and transferred to Eppendorf tubes (1.5 mL) using 2 mL syringes with 21G canulas. The cell lysate was homogenized by pipetting up and down 5 times. Cell lysis was carried out for normoxic and transiently hypoxic cells under a standard bilaminar hood while lysis of continuously hypoxic cells was carried out in the hypoxia workstation. Samples were then frozen and stored at -80 °C until further use.

2.13.4. RNA isolation and quality control

Total RNA isolation was performed using RNeasy Plus Mini Kit by following the manufacturer's instructions. Equal volumes of ethanol (70 %) were added to the lysed cell samples to provide ideal binding conditions. The lysate from each sample was then transferred to RNeasy spin columns provided with the kit. Each spin column houses a silica membrane to which the RNA from the sample binds. All contaminants were then washed away through washing steps using RW1 (700 µL; 8000 × g for 15 sec) once and RPE (500 µL) wash buffer twice (first wash at 8000 × g for 15 seconds and second wash at 8000 × g for 2 minutes). Pure, concentrated RNA was then eluted in nuclease free water (50 µL) by centrifuging at 8000 × g for 1 minute.

RNA integrity and concentration was measured by micro-electrophoresis using the RNA 6000 Nano Assay in the Bioanalyzer after rinsing its electrodes using washing chips filled with surfactant (350 µL) and nuclease free water (350 µL) for 1 min each. 65 µL of the filtered RNA gel matrix (1500 × g for 10 minutes) was mixed with 1 µL of fluorescent dye in an RNAase-free Eppendorf tube, vortexed and then centrifuged at 13000 × g for 10 min. 9 µL each of the gel-dye mixture thus obtained was loaded in the well of a "Nanochip" marked "G" surrounded by a black circle, by means of a chip priming station and also in two more wells marked just "G" without the priming station. The gel-dye mixture serves as a sieving polymer and helps in creating integrated electrical circuits. 5 µL of the RNA 6000 Nano Marker was dispensed in the sample wells as well as the one marked for the ladder. 1 µL each of heat denatured (70 °C for 1 min) RNA samples and RNA ladder were added in the sample and ladder wells. The chip was then vortexed using the IKA MS3 vortex mixer for 1 minute at 30 × g before placing it in the Agilent 2100 Bioanalyzer which was operated according to its manual. The RNA 6000 Nano Assay ladder contains six RNA fragments having a total concentration of 150 ng/µL. Therefore, six peaks of different sizes (0.2, 0.5, 1.0, 2.0, 4.0 and 6.0 kb) are observed as shown in Figure 2.12 A.

The RNA quality was assessed by the 28S/18S rRNA ratio and the RNA integrity number (RIN). The samples with a 28S/18S ratio of around 2 and high RNA integrity (RIN) number above 9 were selected for outsourcing to GENEWIZ for mRNA sequencing (example electropherogram shown in Figure 2.12 B).
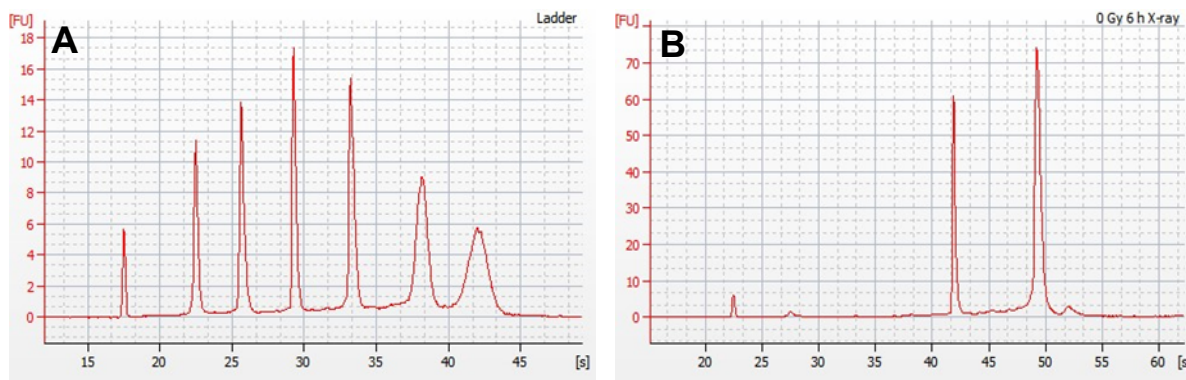
Figure 2.12   Electropherograms generated using Agilent 2100 Bioanalyzer; (A) RNA ladder electropherogram showing 6 characteristic peaks; (B) RNA sample electropherogram showing 5S, 18S and 28S peaks. RIN for this sample was 9.9.

2.13.5.   mRNA sequencing workflow

Actual mRNA sequencing and bioinformatics was outsourced to GENEWIZ Europe, Leipzig, Germany, as no sequencer was available at DLR.

2.13.5.1. Library preparation, sequencing, and sequencing quality control

mRNA enrichment was carried out via Poly A selection. Following mRNA enrichment, mRNA was fragmented out prior to reverse transcription for cDNA synthesis. Ends of cDNA first and second strands were polished by 5' phosphorylation and dA-tailing. This was followed by adaptor ligation of DNA fragments to generate complete library molecules allowing for the sequences to attach to the flow cell and thus enable sequencing. The sequencer used was Novaseq6000 with read lengths of 2×150 bp. Raw sequencing data quality was evaluated with the quality control analysis tool FastQC (72,73) (written by Simon Andrews of Babraham Bioinformatics) for each sample. Per base Quality and Reads Quality Score Distribution as well as GC Content Distribution were evaluated. The library preparation workflow is described in Figure 2.13.

2.13.5.2. Trimming and mapping sequence reads, and extracting gene hit counts

Possible adapter sequences and nucleotides with poor quality were removed by trimming sequence reads using Trimmomatic v.0.36 (written by Anthony Bolger, Björn Usadel Lab, Institute for Biology I, RWTH Aachen, Germany) (74).

The trimmed reads were aligned and mapped onto the *Homo sapiens* GRCh38 reference genome available on ENSEMBL, using the STAR (Spliced Transcripts Alignment to a Reference) aligner v.2.5.2b (75).

For calculating unique gene hit counts, Subread package v.1.5.2 was used (76). Only those unique reads were counted that fell within exon regions.
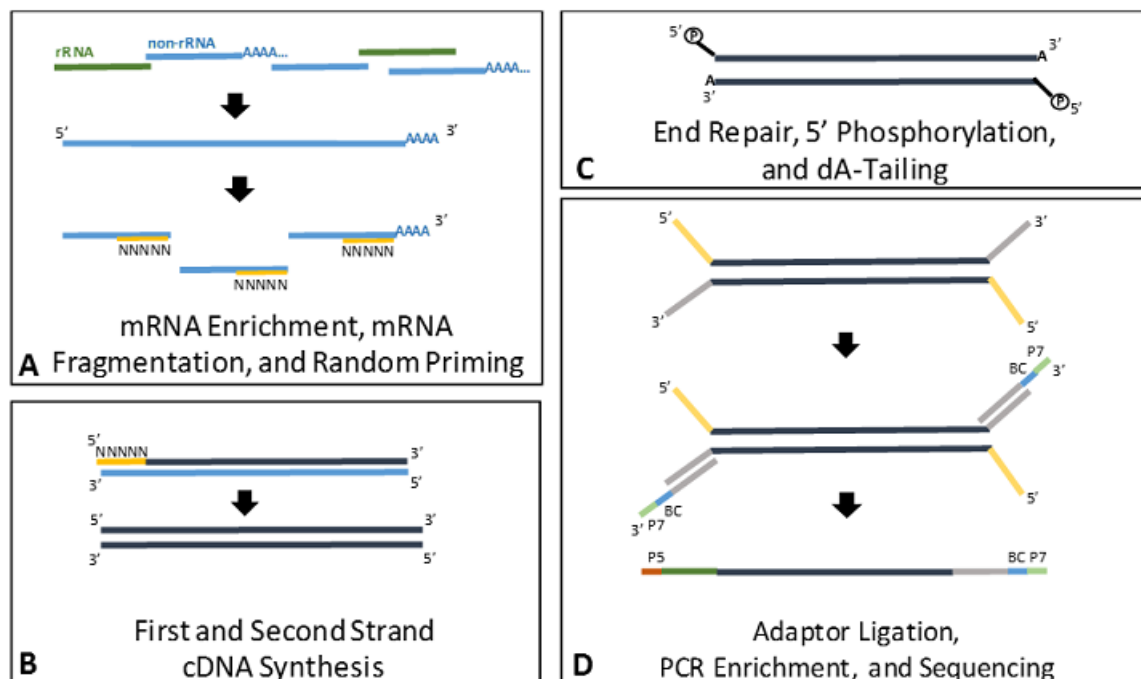
Figure 2.13 mRNA library preparation workflow. Schematic prepared by GENEWIZ Europe, Leipzig, Germany.

2.13.5.3. Analyses of differential gene expression

The gene hit counts were used for differential gene expression analysis by employing DSeq2 that is based on negative binomial distribution to model read counts. Gene expression in defined sample groups was compared (Table 2.22). The same comparison groups were used for A549 and H358 cells irradiated with X-rays and for A549 cells irradiated with carbon ions.

Prior to analysis, the original read counts were normalized to adjust for factors such as variations of sequencing yield between samples. The similarity among samples was assessed by measuring the Euclidean distance between them as well as by performing principal component analysis.

Hypothesis testing was performed using Wald test. Adjusted p-values were calculated using the Benjamini-Hochberg method. Genes with an adjusted p-value < 0.05 and absolute $\log_2$ fold change > 1 were considered as differentially expressed genes for each group comparison.

Table 2.22   Control and treatment groups defined for differential gene expression analysis

No.	Control Group	Treatment Group	Relevance
1	Normoxia Unirradiated	Transient Hypoxia (1% O_2) Unirradiated	Effect of reoxygenation in unirradiated cells
2	Normoxia Unirradiated	Continuous Hypoxia (1% O_2) Unirradiated	Effect of hypoxia in unirradiated cells
3	Normoxia Irradiated (8 Gy)	Transient Hypoxia (1% O_2) Irradiated (8 Gy)	Effect of reoxygenation in irradiated cells
4	Normoxia Irradiated (8 Gy)	Continuous Hypoxia (1% O_2) Irradiated (8 Gy)	Effect of hypoxia in irradiated cells

2.14.   Statistics

In principle, two to six technical replicates were performed for each biological repeat and at least three biological replicates were performed for each experimental condition. Following analysis using specific software for different methods (please refer to Table 2.3 for details), the arithmetical means, standard deviations and standard errors of mean for each condition were calculated using Excel. Then graphs were plotted, and tests of significance were performed using GraphPad Prism 9. CFAs dose response curves were plotted using Sigma Plot 16 software and data was analyzed using CFA-DOSE v1.04 and CFA_AllData v1.04 excel macrosheets developed by Prof. Dr. Christa Baumstark.

3. Results

As an initial step, the growth kinetics and energy metabolism of A549 and H358 cells were assessed at 0.1 % and 1 % oxygen concentration. This was followed by characterization of radioresistance in these cell lines under hypoxia compared to normoxia in terms of surviving cell fraction following exposure to low- and high-LET radiation using colony forming ability assays. Since results indicated that hypoxic cells showed better survival than normoxic controls regardless of LET, the central aspects of the DNA damage response (DDR) to irradiation were evaluated, namely cell cycle progression, DSB induction and resolution as well as the transcription profile of these NSCLC cell lines to seek possible explanations for better survival under hypoxia.

Since several NF-κB target genes were upregulated in both cell lines under hypoxia, NF-κB pathway activation along with synthesis of its target cytokines (IL-6 and IL-8) was quantified. Hypoxic cells showed a trend for earlier activation of NF-κB following irradiation which is associated with higher secretion of its target cytokines.

Additionally, the effect of reoxygenation was also evaluated by differentiating between continuous and transient hypoxia while studying cell survival, cell cycle progression, DSB induction and resolution, transcription profile, NF-κB activation and its target cytokine secretion.

3.1.   Cell growth kinetics

The growth kinetics of the human NSCLC cell lines A549 and H358 were characterized by keeping them in culture for 7 days in presence of 20 %, 1 % and 0.1 % O_2 concentrations.

3.1.1.   A549 cells at 0.1 % and 1 % oxygen

A549 cells (Figure 3.1) had a lag phase of 24 h (1 day) under all three O_2 concentrations followed by an exponential growth phase lasting till 120 h (5 days) after which they progressed into the stationary phase.

The normoxic cells (20 % O_2) divided faster from 24 h onward in comparison to hypoxic cells (1 % and 0.1 % O_2) and this difference was statistically significant at 48 h and onward. From 48 h onward, the growth rate of cells growing at 0.1 % O_2 was slower compared not just to normoxic cells but also to those growing at 1 % O_2 and these differences were statistically significant at 72 h and onward.
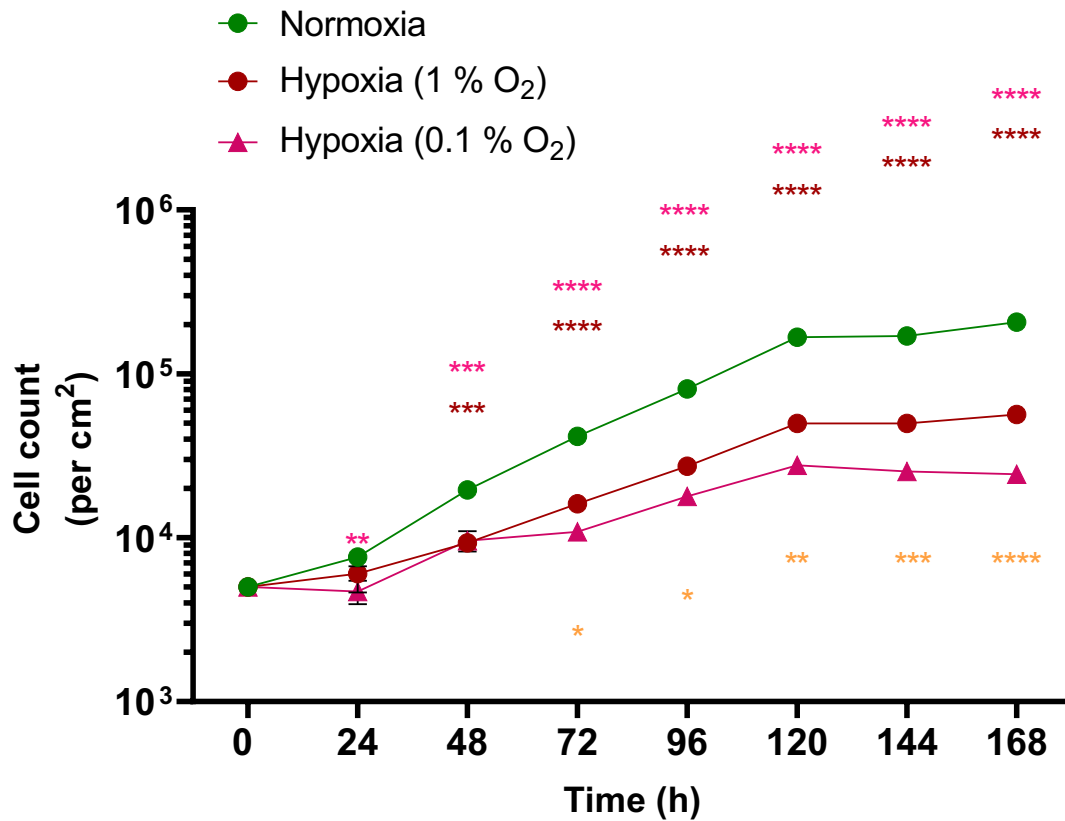
Figure 3.1   *Growth kinetics of A549 cells growing under 20 %, 1 % and 0.1 % O_2 over 168 h (7 days). Cells were seeded in petri dishes ($\varnothing$ 3 cm) and counted with an automated cell counter after staining them with trypan blue to identify living cells.*

*Significant differences in means are represented with pink asterisk for normoxia versus (vs.) 0.1 % O_2, with red asterisk for normoxia vs. 1 % O_2, and with orange asterisk for 1 % vs. 0.1 % O_2. *: $p<0.05$; **: $p<0.01$; ***: $p<0.001$; ****: $p<0.0001$; n = 3. Error bars represent SE.*

3.1.2. H358 cells at 0.1 % and 1 % oxygen

H358 cells had a lag phase of 24 h (1 day) while growing at 20 % and 1 % O_2 but this lag phase was prolonged to 72 h (3 days) for cells growing at 0.1 % O_2, interestingly without any initial population decline in first 24 h (Figure 3.2).

The exponential growth phase varied in length among the three O_2 concentrations. Normoxic cells (20 % O_2) were still in the exponential phase at completion of 168 h (7 days) while hypoxic cells (1 % and 0.1 % O_2) cells reached the stationary phase by 144 h (6 days) at a lower maximal cell density.

H358 cell growth slowed down progressively as O_2 concentration was decreased with the normoxic cells dividing faster from 48 h onward in comparison to hypoxic cells (1 % and 0.1 % O_2), a difference which became statistically significant at and beyond 72 h.

Interestingly, while cells growing at 0.1 % O_2 were late to enter the exponential growth phase compared to those growing at 1 % O_2, their growth caught up by 96 h after which there was no significant difference in growth rate of hypoxic cells growing at 1 % or 0.1 % O_2.
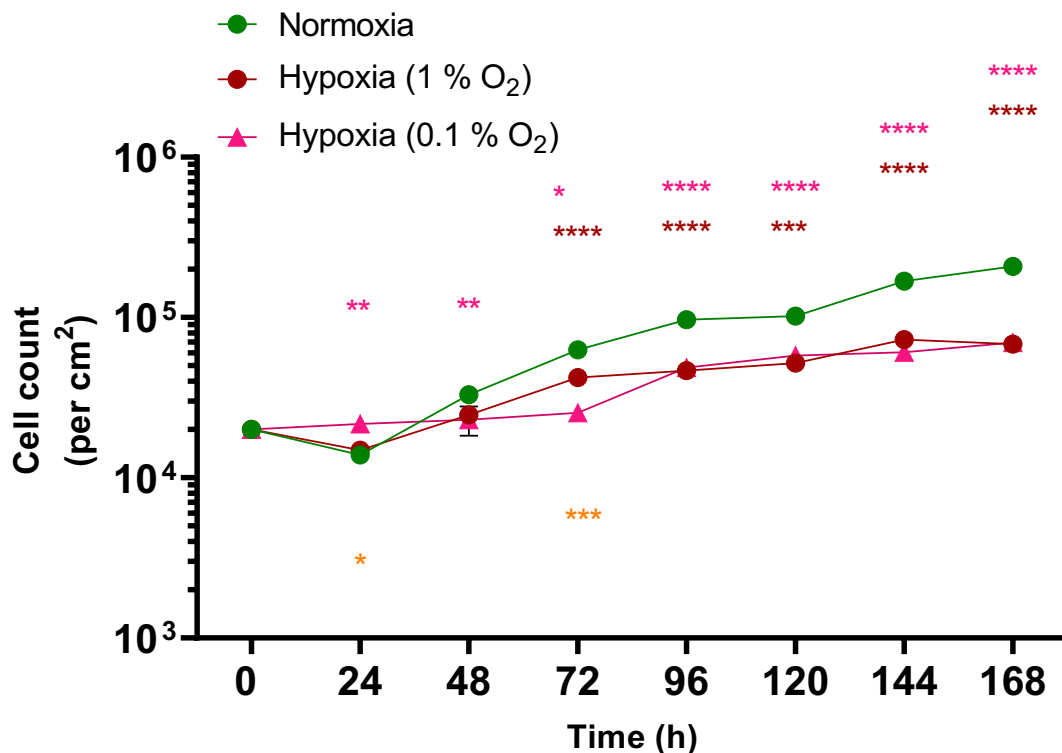
Figure 3.2   Growth kinetics of H358 cells growing under 20 %, 1 % and 0.1 % O_2 over 168 h (7 days). Cells were seeded in petri dishes (⌀ 3 cm) and counted with an automated cell counter after staining them with trypan blue to identify living cells.

Significant differences in means are represented with pink asterisk for normoxia vs. 0.1% O_2, with red asterisk for normoxia vs. 1 % O_2, and with orange asterisk for 1 % vs. 0.1 % O_2. ns: not significant; *: p<0.05; **: p<0.01; ***: p<0.001; ****: p<0.0001 n = 3. Error bars represent SE.

3.1.3. Doubling times under different oxygen concentrations

The doubling times of the two cell lines were calculated from their growth kinetics data during the exponential phase as an objective index for their growth rate (Table 3.1). The doubling times of A549 cells were smaller compared to those of H358 cells at all three O_2 concentrations.

The doubling times of A549 cells under O_2 concentrations of 1 % and 0.1 % in comparison to normoxia increased by about 32 % and 128 %, respectively.

The doubling times of H358 cells under O_2 concentrations of 1 % and 0.1 % in comparison to normoxia increased by about 57 % and 106 %, respectively.

Lowering the O_2 concentration from 1 % to 0.1 % increased the A549 doubling time by 73 % and the H358 doubling time by 31 %.

Table 3.1   Doubling times of A549 and H358 cells under various oxygen concentrations calculated from growth curves data using Korzynska & Zychowicz formula (Eq 2.4)

Cell line	Oxygen Protocol	Doubling time (h)	Significance level of the difference between cell lines
A549	Normoxia	23.45 ± 0.42	***
	Hypoxia - 1 % O_2	30.90 ± 2.31	****
	Hypoxia - 0.1 % O_2	53.46 ± 12.71	****
H358	Normoxia	33.28 ± 1.54	
	Hypoxia - 1 % O_2	52.34 ± 5.46	
	Hypoxia - 0.1 % O_2	68.59 ± 5.62	

***: $p<0.001$; ****: $p<0.0001$; n = 3

3.2. Energy metabolism under normoxia and hypoxia

Basic metabolic profiling of A549 and H358 cells at normal O_2 levels (20 %) compared to clinically relevant hypoxia (1 % and 0.1 % O_2) was carried out by following glucose and lactate levels in cell culture supernatants periodically over 72 h.

3.2.1. In A549 cells at 20 %, 0.1 % and 1 % oxygen

In case of A549 cells (Figure 3.3), glucose consumption per one million cells is higher when they grow at 0.1 % O_2 in comparison to 20 % O_2 (normoxia) after 24, 48 and 72 h of incubation. This corresponded with lactate production per one million cells which is also higher at 0.1 % O_2 compared to normoxia at all three time points. A similar trend for cells growing at 1 % O_2 was observed: glucose consumption and lactate production were greater compared to normoxic cells 48 and 72 h after incubation.

Additionally, lactate production per one million cells under normoxia was constant over the time period of three days whereas it increased with time in case of hypoxic cells (1 % and 0.1 % O_2).

3.2.2. In H358 cells at 20 %, 0.1 % and 1 % oxygen

Glucose consumption per one million cells was slightly higher in H358 cells when they grow at 0.1 % O_2 in comparison to 20 % O_2 (normoxia) after 48 and 72 h of incubation. However, this difference was not observed when comparing cells grown under 1 % O_2 to normoxic cells.

Lactate production of hypoxic cells is higher compared to normoxic cells at all time points in case of 0.1 % O_2 and at 72 h in case of 1 % O_2.

3.2.3. Comparison between A549 and H358 cells

While A549 cells showed a trend of greater glucose consumption and lactate secretion with time at 1 % and 0.1 % O_2 compared to at normoxia, H358 cells showed the same trend at 0.1 % O_2 but not at 1 % O_2 (Figure 3.3 & Figure 3.4).

Additionally, compared to A549 cells, H358 cells had a significantly lower rate of glucose consumption and lactate production which corresponds with their growth kinetics (Figure 3.4).
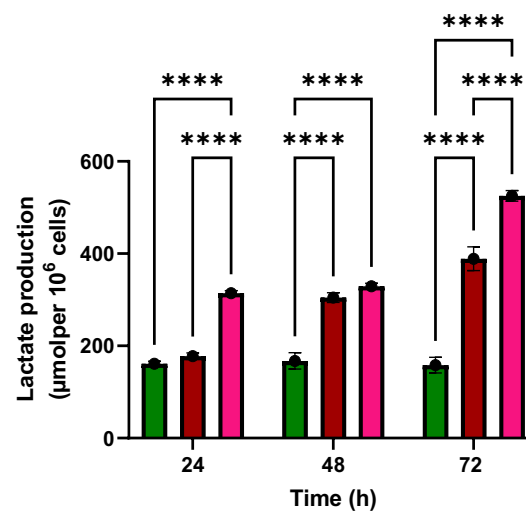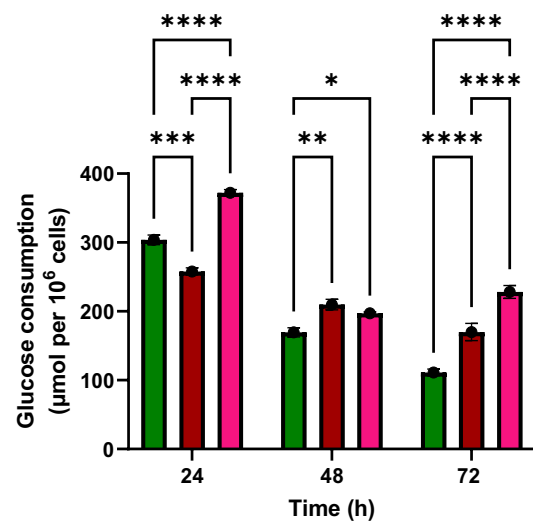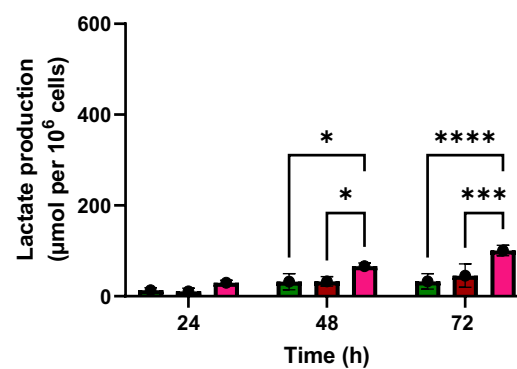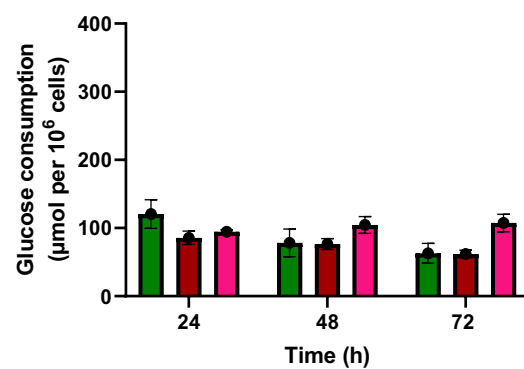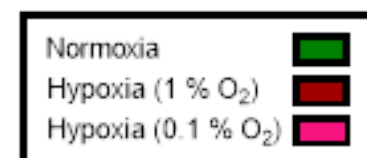
Figure 3.3   Glucose consumption (left) and lactate production (right) of A549 cells (top) and H358 cells (bottom), grown under 20 %, 1 % and 0.1 % oxygen. *: p<0.05; **: p<0.01; ***: p<0.001; ****: p<0.0001; n = 3. Error bars represent SE.
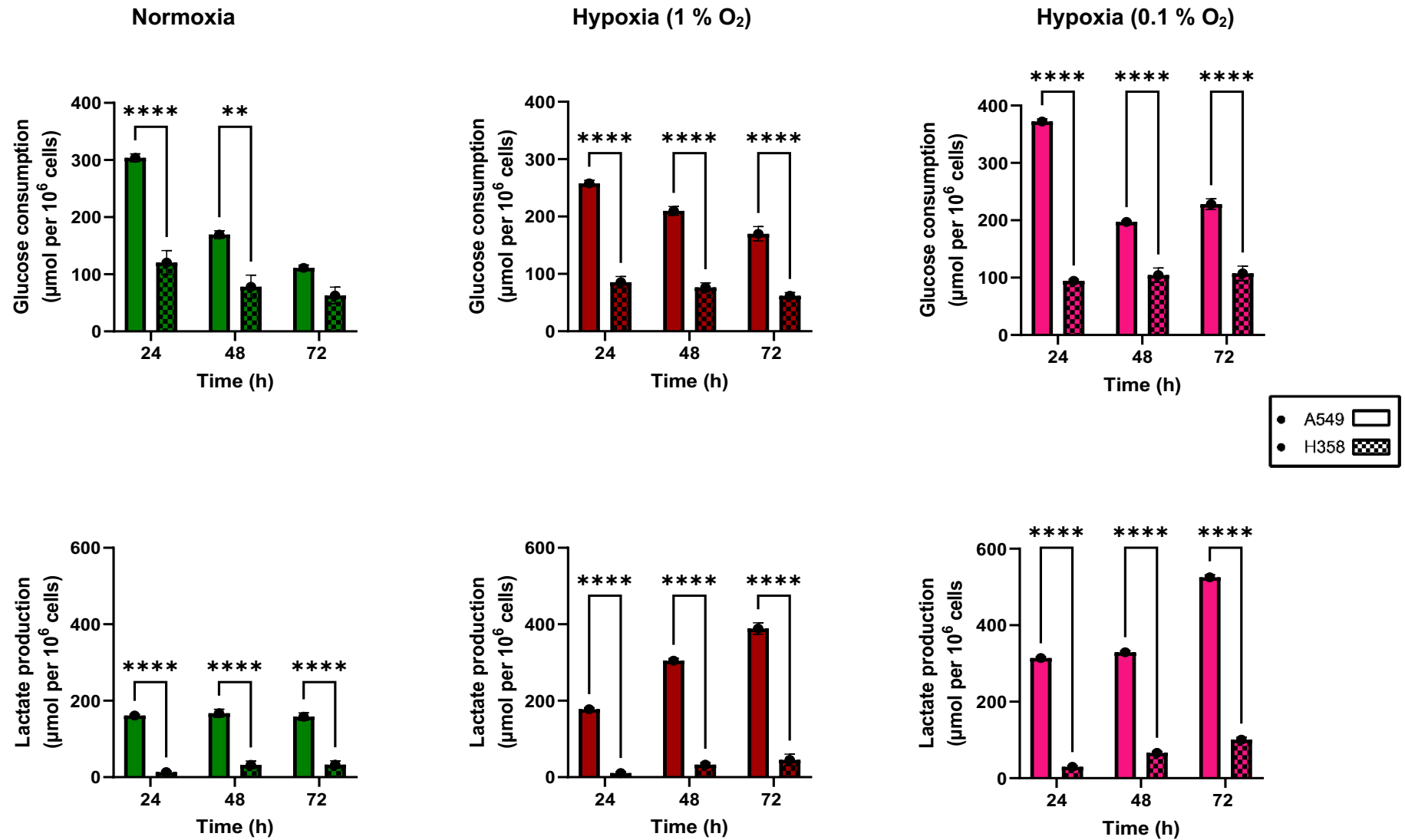
Figure 3.4   Glucose consumption (top) and lactate production (bottom) per million A549 and H358 cells, grown at 20 %, 1 % and 0.1 % oxygen concentration.   *: p<0.05; **: p<0.01; ***: p<0.001; ****: p<0.0001; n = 3. Error bars represent SE.

3.3.   Cell survival after radiation exposure in normoxia and hypoxia

Survival of A549 and H358 cells after exposure to ionizing radiation under cellular hypoxia (0.1 % and 1 % O_2) in comparison to normoxia was quantified using the Puck's Colony Forming Ability (CFA) assay. After irradiation, cells were plated immediately (Immediate Plating) or with a 24 h delay (Late Plating). The resulting dose response curves were calculated using the single-hit multi-target model and evaluated for significant differences in the curve parameters D_0 (radiation dose needed to kill 67 % of cells), OER and RBE.

3.3.1.   A549 cells after X-rays exposure at 20 %, 1 % and 0.1 % oxygen

A549 cells were incubated at 20 %, 1 % and 0.1 % O_2 for 48 h, irradiated, plated (Immediate plating, Figure 3.5A) and then grown in normal oxygen levels. The survival decreased in a dose-dependent manner. This decrease depended on plating time point and oxygen concentration. To quantify and compare these differences, D0 and OER were calculated and listed in Table 3.2 and Table 3.3Table 3.2.

In immediate plating experiments, the D_0 for A549 cells under 20 % O_2 (Table 3.2) was 1.98 Gy which was smaller than that for 1 % O_2 (2.23 Gy) and 0.1 % O_2 (2.09 Gy). Higher D_0 values for hypoxic cells indicate higher radioresistance compared to normoxic cells.

In dose response curves generated from late plating CFA assays (Figure 3.6B), the radioresistance of hypoxic cells compared to normoxic controls became even more apparent where the calculated D_0 (Table 3.2) for normoxia (1.75 Gy) was smaller than that for 1 % O_2 (2.32 Gy) and 0.1 % O_2 (2.87 Gy).

Furthermore, the oxygen enhancement ratios (OERs) were 1.13 and 1.32 after immediate and late plating, respectively, under 1 % O_2 (Table 3.3) when compared to normoxic controls. The OERs of 0.1 % O_2 were 1.05 in case of immediate CFA plating and 1.64 after late plating CFAs. In other words, the greatest effect of hypoxia was detected in late plating CFAs performed at 0.1 % O_2 where radioresistance was increased by 64 %.

Table 3.2   Parameters of the survival curves for A549 cells following X-ray exposure under various oxygen protocols.

Assay Type	Oxygen Protocol	D_0 *	
		μ ± SD	Significance level
Immediate Plating	Normoxia	1.98 ± 0.06	
	Transient Hypoxia - 1 % O_2	2.23 ± 0.05	****
	Transient Hypoxia - 0.1 % O_2	2.09 ± 0.03	****
	Continuous Hypoxia - 1 % O_2	1.41 ± 0.03	****
Late Plating	Normoxia	1.75 ± 0.07	
	Transient Hypoxia - 1 % O_2	2.32 ± 0.07	****
	Transient Hypoxia - 0.1 % O_2	2.87 ± 0.09	****
	Continuous Hypoxia - 1 % O_2	2.16 ± 0.06	****

* D_0 represents the radiation dose needed to reduce the surviving cell fraction to 37 % of its initial value calculated from the X-ray dose response curves from 0 Gy to 8 Gy. The difference in mean D_0 values for normoxic and hypoxic cells was tested for significance. Adj p value (α=0.05): ****: p<0.0001; n = 3

A

Immediate Plating

B

Late Plating
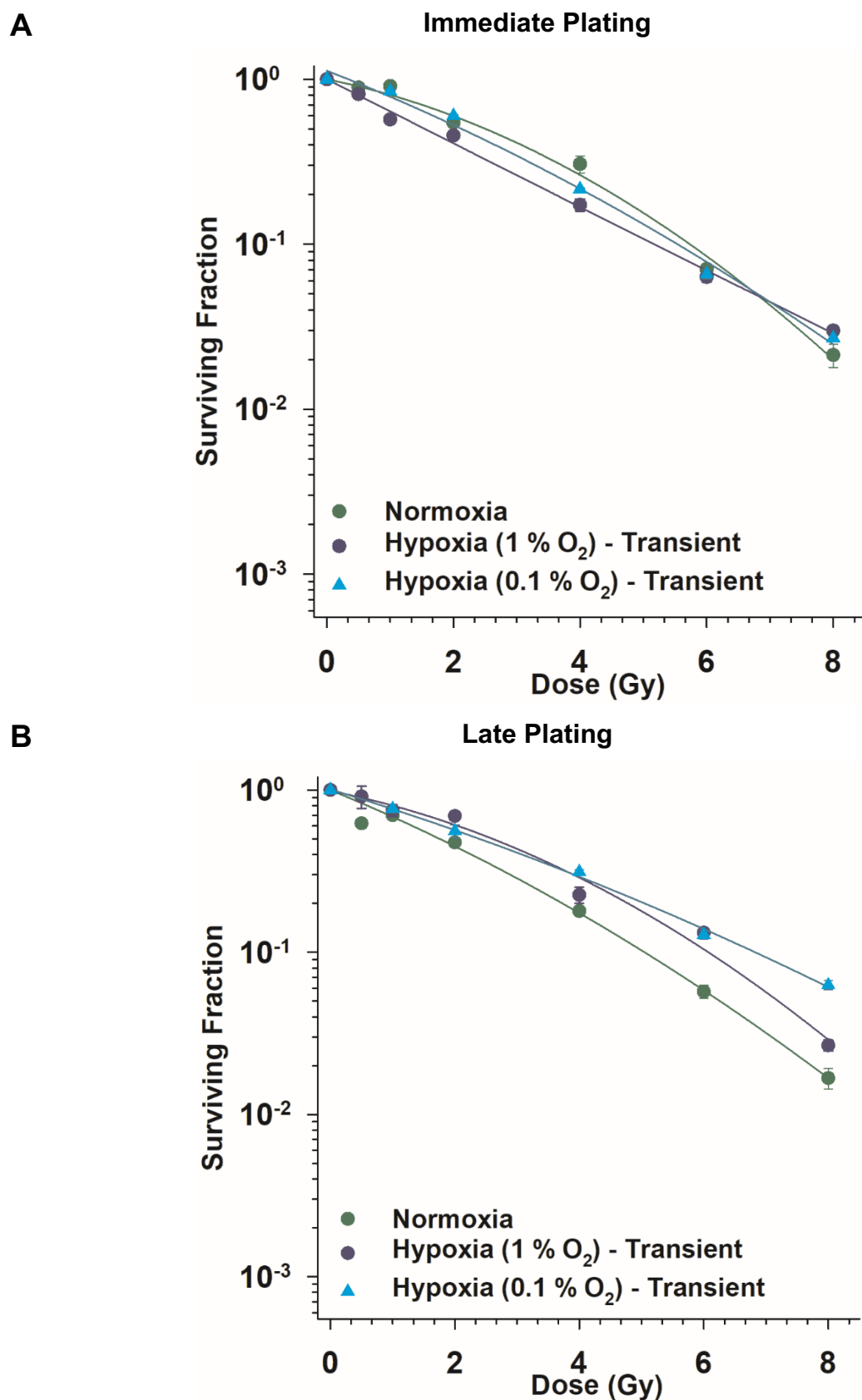
Figure 3.5   Survival of A549 cells after X-rays exposure under 20 %, 1 % and 0.1 % oxygen. Cells were grown for 48 h under these oxygen concentrations and transferred to 20 % oxygen after irradiation (transient hypoxia) for both immediate (A) and late (B) plating Colony Forming Ability (CFA) assays. n = 3. Error bars represent SD.

3.3.2. A549 cells after X-rays exposure in normoxia, continuous hypoxia and transient hypoxia

To further investigate the role of O_2 presence in cell survival following irradiation, CFA assays were performed in which the growing colonies were continuously incubated under hypoxia (1 % O_2) even after irradiation, till the time of colony fixation (continuous hypoxia) and compared to colonies that were allowed to grow in normal oxygen levels (transient hypoxia).

Surprisingly, the immediate plating survival curves of the continuously hypoxic cells were steeper compared to those of the transiently hypoxic and the normoxic cells (Figure 3.6A), indicating an increase in radiosensitivity in comparison to normoxia. This higher radiosensitivity of hypoxic A549 cells was quantifiable by a lower D_0 (1.41 Gy vs. 1.98 Gy for normoxic cells) (Table 3.2) and an OER (Table 3.3) less than 1 (0.71).

On the other hand, in late plating CFA assays, the continuously hypoxic cells were found to be more radioresistant than both normoxic cells as indicated by the less steep survival curve (Figure 3.6B) and the highest D_0 (2.16 Gy vs. 1.75 Gy, Table 3.2) and an OER of 1.23 (Table 3.3).

In other words, hypoxia-induced radioresistance towards X-rays is observable either if the hypoxic cells are allowed to grow post-irradiation in the presence of oxygen, or if they are allowed 24 h of repair time after irradiation before they are reseeded for colonies.

Table 3.3   OER of A549 survival following X-rays exposure under various oxygen protocols.

O_2 Protocol	Assay Type	OER: $\mu \pm$ SD
Transient Hypoxia – 1 % O_2	Immediate Plating	1.13 ± 0.03
	Late Plating	1.32 ± 0.06
Continuous Hypoxia – 1 % O_2	Immediate Plating	0.71 ± 0.04
	Late Plating	1.23 ± 0.05
Transient Hypoxia – 0.1 % O_2	Immediate Plating	1.05 ± 0.03
	Late Plating	1.64 ± 0.07

OER was calculated based on D_0 with normoxia as reference condition (Table 3.2)

A Immediate Plating

B Late Plating

Figure 3.6   Survival of A549 cells after X-rays exposure under normoxia and transient or continuous hypoxia. Hypoxia: Cells were grown for 48 h under 1 % oxygen and transferred to 20 % oxygen after irradiation (transient hypoxia) or kept at 1 % O_2 (continuous hypoxia) for both immediate (A) and late (B) plating Colony Forming Ability (CFA) assays. n = 3. Error bars represent SD.

3.3.3. A549 cells after carbon ions exposure in normoxia, continuous hypoxia and transient hypoxia

CFA experiments were performed after carbon ion exposure to determine the effect of hypoxia on cell killing by high-LET radiation. The effect was quantified in terms of D_0 and OER. Additionally, cell killing by high-LET radiation was compared to that to low-LET radiation (X-rays), resulting in the RBE for this effect. After irradiation, hypoxic cells (1 % O_2) were allowed to grow into colonies either in a normal incubator (transient hypoxia) or in a hypoxic incubator workbench (continuous hypoxia).

Up to a dose of 4 Gy, the survival decreased exponentially without a shoulder region under all conditions (Figure 3.7). Increasing the dose above 6 Gy did not further decrease the survival.

After exposure to carbon ions and immediate plating for CFA, the normoxic cells (D_0= 1.93 Gy) survived better compared to transiently (D_0= 1.59 Gy) and continuously hypoxic cells (D_0= 1.61 Gy). Reoxygenation in case of transiently hypoxic cells did not offset the increased radiosensitivity of hypoxic cells as it was observed for immediate plating after X-rays exposure. Consequently, the OER values (Table 3.5) for both continuous and transient hypoxia were below 1 (0.83 for transient hypoxia compared to 0.84 for continuous hypoxia).

However, late plating after carbon ions irradiation resulted in a better survival outcome for both transiently and continuously hypoxic cells. This radioresistance of hypoxic cells after late plating is reflected by the higher D_0 values for both transiently (D_0= 1.62 Gy) and continuously hypoxic cells (D_0= 2.27 Gy) in comparison to the normoxic cells (D_0= 1.49 Gy). This also reflects in OER greater than 1 for continuous hypoxia (OER= 1.52) and transient hypoxia (OER= 1.09).

Lastly, carbon ions were found to be more effective in killing A549 cells compared to X-rays regardless of the oxygenation status as indicated by RBE values in excess of 1 (Table 3.5).

Table 3.4   Parameters of the survival curves for A549 cells following carbon ions exposure under various oxygen protocols.

Assay Type	Oxygen Protocol	D_0*	
		μ ± SD	Significance level
Immediate Plating	Normoxia	1.93 ± 0.12	
	Transient Hypoxia - 1 % O_2	1.59 ± 0.10	****
	Continuous Hypoxia - 1 % O_2	1.61± 0.14	****
Late Plating	Normoxia	1.49 ± 0.07	
	Transient Hypoxia - 1 % O_2	1.62 ± 0.10	****
	Continuous Hypoxia - 1 % O_2	2.27 ± 0.23	****

* D_0 represents the radiation dose needed to reduce the surviving cell fraction to 37 % of its initial value calculated from the dose response curve from 0 Gy to 8 Gy.
The difference in mean D_0 values for normoxic and hypoxic cells was tested for significance. Adj p value (α=0.05); ****: p<0.0001; n = 3.

A Immediate Plating

B Late Plating
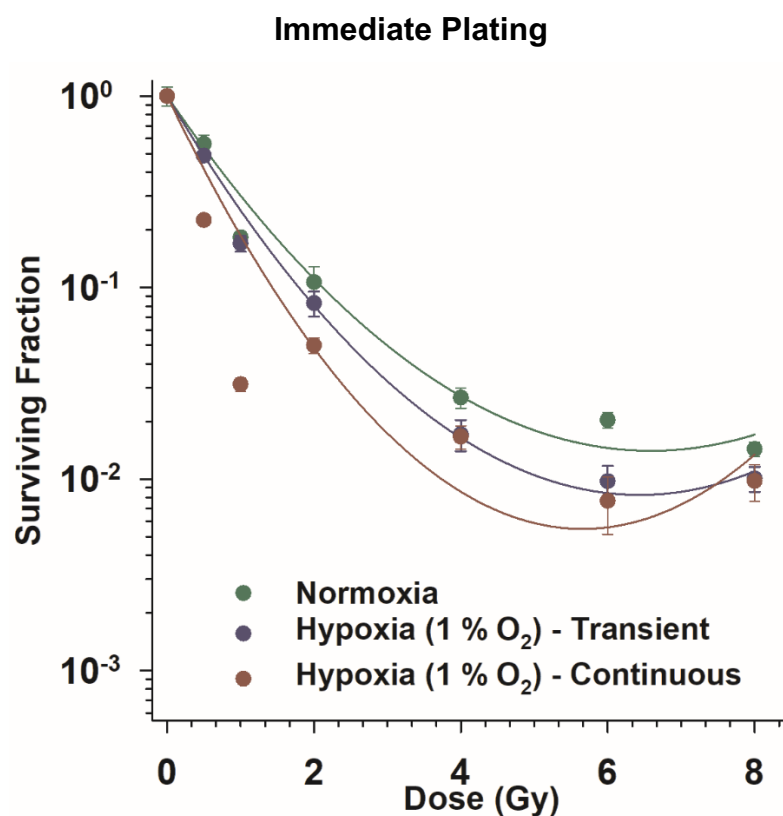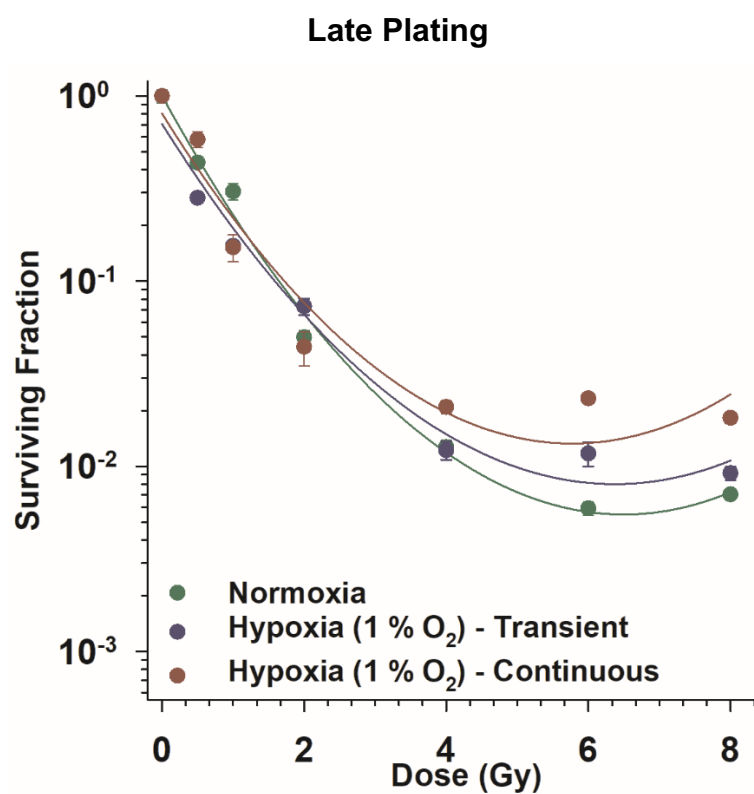
Figure 3.7   Survival of A549 cells after carbon ions exposure under normoxia and transient or continuous hypoxia. Hypoxia: Cells were grown for 48 h under 1 % oxygen and transferred to 20 % oxygen after irradiation (transient hypoxia) or kept at 1 % O_2 (continuous hypoxia) for both immediate (A) and late (B) plating Colony Forming Ability (CFA) assays. n = 3. Error bars represent SD.

Table 3.5   RBE for cell killing by carbon ions in A549 cells and OER under various oxygen protocols following immediate and late plating CFA assays.

O$_2$ Protocol	Assay Type	RBE *: μ ± SD	OER **: μ ± SD
Normoxia	Immediate Plating	2.69 ± 0.21	
	Late Plating	2.54 ± 0.15	
Transient Hypoxia - 1 % O$_2$	Immediate Plating	2.27 ± 0.14	0.83 ± 0.06
	Late Plating	2.95 ± 0.25	1.09 ± 0.07
Continuous Hypoxia - 1 % O$_2$	Immediate Plating	1.53 ± 0.14	0.84 ± 0.08
	Late Plating	2.34 ± 0.23	1.52 ± 0.15

* RBE: The calculation was based on the D_0 considering the linear range of the carbon ion survival curves (doses up to 4 Gy) relative to D_0 derived from the corresponding X-rays survival curves.

** OER was calculated based on D_0 with normoxia as reference condition. n= 3

3.3.4.   H358 cells after X-rays exposure in normoxia, continuous hypoxia and transient hypoxia

The effect of continuous and transient hypoxia (1 % O$_2$) on cell survival following X-rays exposure was also studied using the second NSCLC cell line, the H358 (Figure 3.8).

It could be argued that immediate plating CFA assays (Figure 3.8A) revealed the same trend as in A549 cells that transiently hypoxic cells are having a greater D_0 than normoxic cells while continuously hypoxic cells are having lower D_0 values than normoxic cells. However, the difference though statistically significant is clinically irrelevant (D_0= 2.36 Gy for normoxia vs. 2.40 Gy for transient hypoxia vs. 2.30 Gy for continuous hypoxia). For the same reason the OER differences are also very small (OER= 1.02 for transient hypoxia vs. normoxia; and 0.97 for continuous hypoxia vs. normoxia). In other words, survival in H358 cells appears more robust towards the effects of hypoxia in immediate plating experiments as compared to A549 cells.

After late plating CFA assays (Figure 3.8B), the surviving fraction of both continuously and transiently hypoxic cells was higher compared to normoxic cells as was the case for A549 cells, indicating more effective cell repair in case of hypoxic cells. This is also reflected in D_0 (Table 3.6) and OER values (Table 3.7) where continuously hypoxic cells have the highest D_0 and OER (D_0= 3.05 Gy and OER= 1.20) followed by transient hypoxia (D_0= 2.73 Gy and OER= 1.08) and then normoxia (D_0= 2.54 Gy).

Lastly, the relatively higher D_0 values of H358 cells compared to A549 cells regardless of the oxygen protocol used for growth and irradiation suggest that H358 cells are intrinsically more radioresistant than A549 cells.
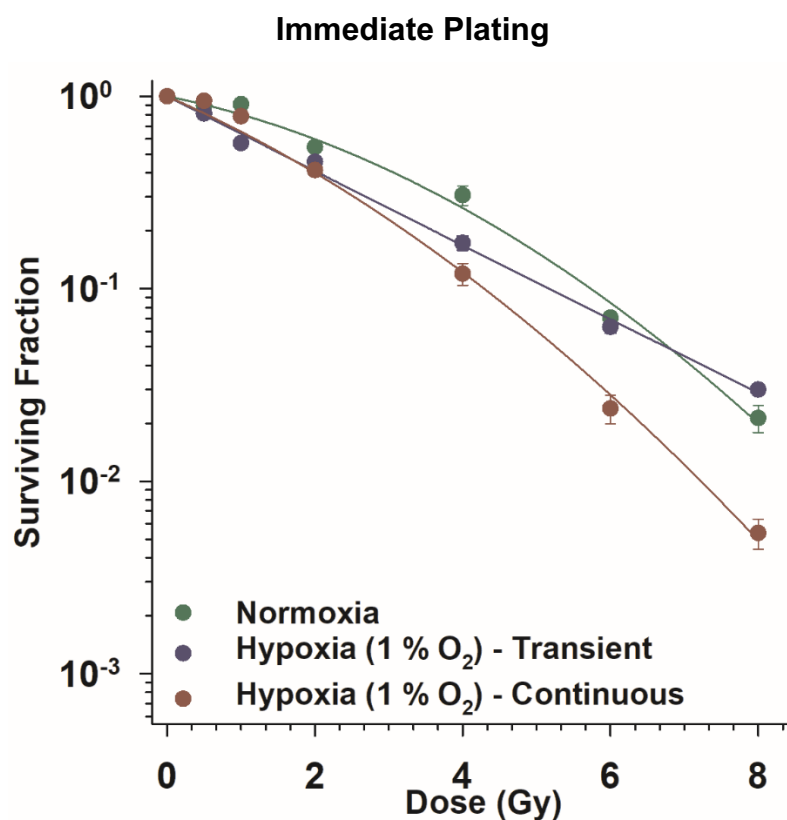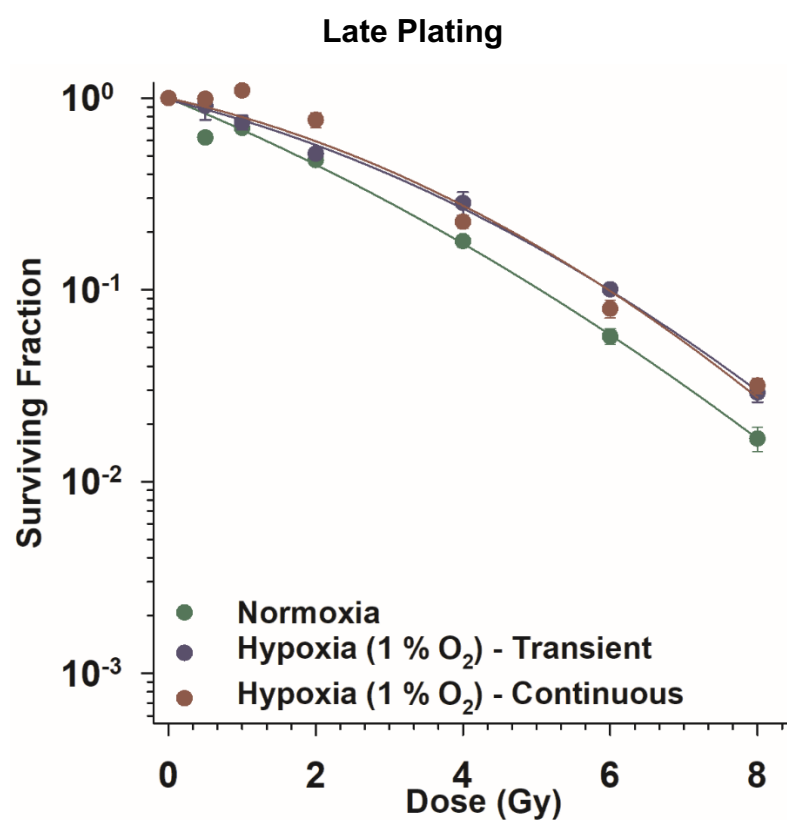
A

Immediate Plating

B
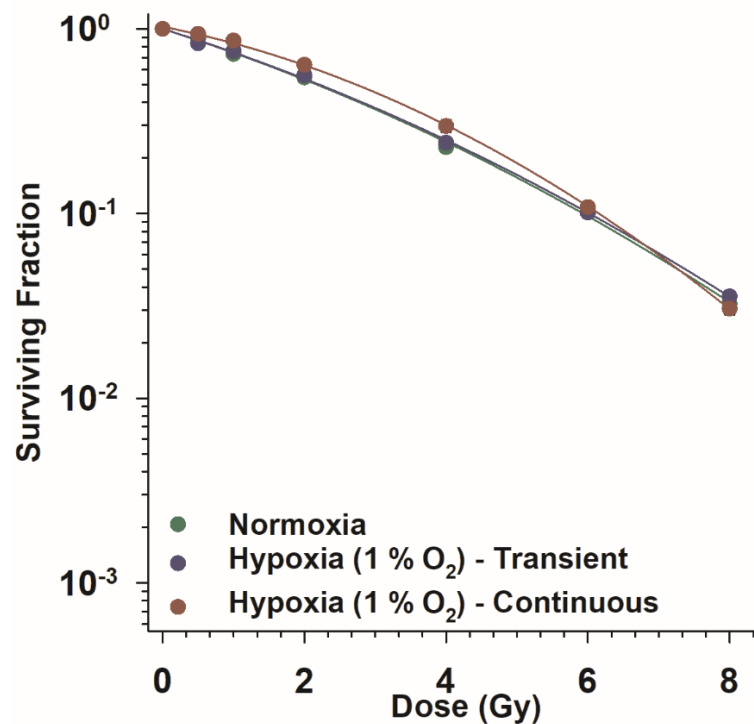
Late Plating
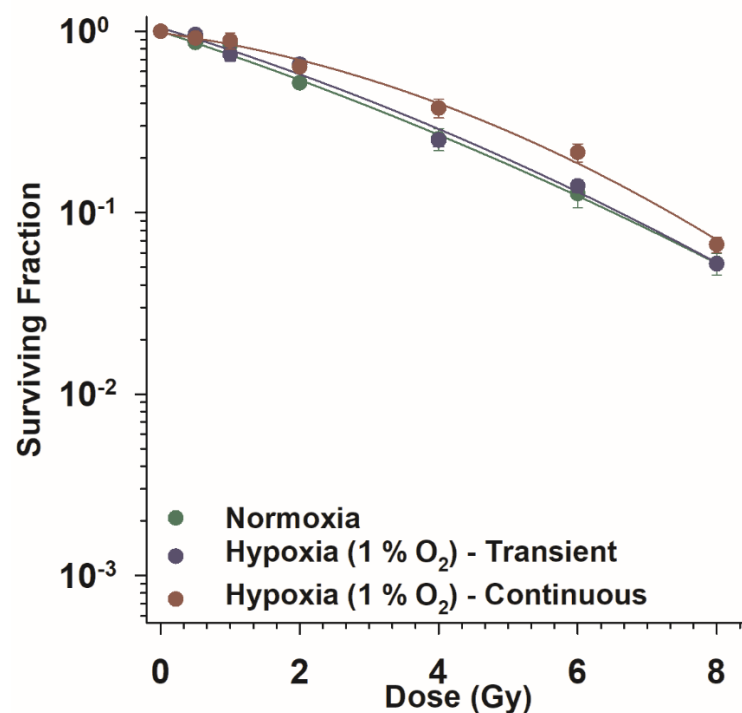
Figure 3.8   Survival of H358 cells after X-rays exposure under normoxia and transient or continuous hypoxia. Hypoxia: Cells were grown for 48 h under 1 % oxygen and transferred to 20 % oxygen after irradiation (transient hypoxia) or kept at 1 % O_2 till the time of colony fixation and staining (continuous hypoxia) for both immediate (A) and late (B) plating Colony Forming Ability (CFA) assays. If standard errors are not visible, they are smaller than the symbol. n = 3. Error bars represent SD.

Table 3.6   Parameters of the survival curves for H358 cells following X-ray exposure under various oxygen protocols.

Assay Type	Oxygen Protocol	D_0 *	
		µ ± SD	Significance level
Immediate Plating	Normoxia	2.36 ± 0.03	
Immediate Plating	Transient Hypoxia - 1 % O_2	2.40 ± 0.04	***
Immediate Plating	Continuous Hypoxia - 1 % O_2	2.30 ± 0.05	***
Late Plating	Normoxia	2.54 ± 0.09	
Late Plating	Transient Hypoxia - 1 % O_2	2.73 ± 0.07	****
Late Plating	Continuous Hypoxia - 1 % O_2	3.05 ± 0.13	****

* D_0 represents the radiation dose needed to reduce the surviving cell fraction to 37 % of its initial value calculated from the dose response curve from 0 Gy to 8 Gy.

The difference in mean D_0 values for normoxic and hypoxic cells was tested for significance. Adj p value (α=0.05): ***: $p < 0.001$; ****: $p < 0.0001$; n = 3

Table 3.7   OER of H358 survival following X-rays exposure under various oxygen protocols.

O_2 Protocol	Assay Type	OER *: µ ± SD
Transient Hypoxia- 1 % O_2	Immediate Plating	1.02 ± 0.02
Transient Hypoxia- 1 % O_2	Late Plating	1.08 ± 0.04
Continuous Hypoxia- 1 % O_2	Immediate Plating	0.97 ± 0.02
Continuous Hypoxia- 1 % O_2	Late Plating	1.20 ± 0.06

* OER was calculated based on D_0 with normoxia as reference condition (Table 3.6)

3.4. Cell cycle progression

In order to correlate hypoxia-induced radioresistance that was observed in CFA experiments with the important outcomes of the DDR, cell cycle progression after irradiation was studied in A549 and H358 cells grown under the oxygen protocols that were already used for the cell survival determination. The proportion of cells in G1, G2 and S phases in the presence or absence of radiation (8 Gy) were quantified after flow cytometric analysis of cellular DNA content.

3.4.1. A549 cells after X-rays exposure at 20 %, 1 % and 0.1 % oxygen

When A549 cells were grown under 0.1 % or 1 % O_2 in the absence of X ray exposure, a higher proportion of cells were in G1 phase along with a lower proportion of cells in G2 phase in comparison to cells growing at normal oxygen concentration (20 % O_2) (Figure 3.9) which corresponds to growth kinetics and energy metabolism under hypoxia discussed in sections 3.1 and 3.2.

Following X ray exposure (Figure 3.9 and Figure 3.10, Table 3.8), the percentage of normoxic cells in G1 phase sharply declined (lowest G1 population of 30.2 %) while minimal changes were observed for hypoxic cells (lowest G1 population of 52.6 % at 1% O_2 and 51.0 % at 0.1 % O_2). This difference was statistically significant at 10, 12 and 14 h after X-rays exposure.

This G1 population depletion under normoxia coincided with a sharp increase in G2 population after X-rays exposure. The onset of G2 population rise was as early as 6 h, peaked between 10 to 14 h, and then began to drop toward baseline by 18 h. These changes are characteristic of a radiation-induced G2/M block in normoxic A549 cells. Interestingly, under hypoxia, the rise in G2 population following X-rays exposure was minimal so much so that the maximum G2 population under normoxia was 62.2 % while that at 1 % O_2 was 33.2 % and at 0.1 % O_2 was 37.3 % (Table 3.8).

Furthermore, the difference of O_2 concentrations of 1 % and 0.1 % did not impact the cell cycle phase distribution of A549 cells with or without X-rays exposure in a statistically discernable way.

3.4.2. A549 cells after X-rays exposure in normoxia, continuous hypoxia and transient hypoxia

Cell cycle experiments were designed to additionally evaluate the impact of reoxygenation following X-ray exposure thereby dividing the hypoxic cells into two separate groups: the continuously hypoxic cells which remained under hypoxia till the specific fixation time point vs. the transiently hypoxic cells which were placed in a normal incubator at 20 % O_2 following irradiation.

Interestingly, Figure 3.9 and Figure 3.10 and Table 3.8 show that reoxygenation had no discernable impact on cell cycle kinetics in the first 24 h both without or with X-rays exposure. In comparison to normoxic cells, the transiently hypoxic cells continued to show a trend of higher G1 populations along with lower G2 populations as did the continuously hypoxic cells.

Furthermore, following X-rays exposure, transiently hypoxic cells did not exhibit a sharp G2/M block like normoxic cells. Instead, their post-exposure G1 and G2 populations followed essentially similar trajectories over time as did the continuously hypoxic cells.
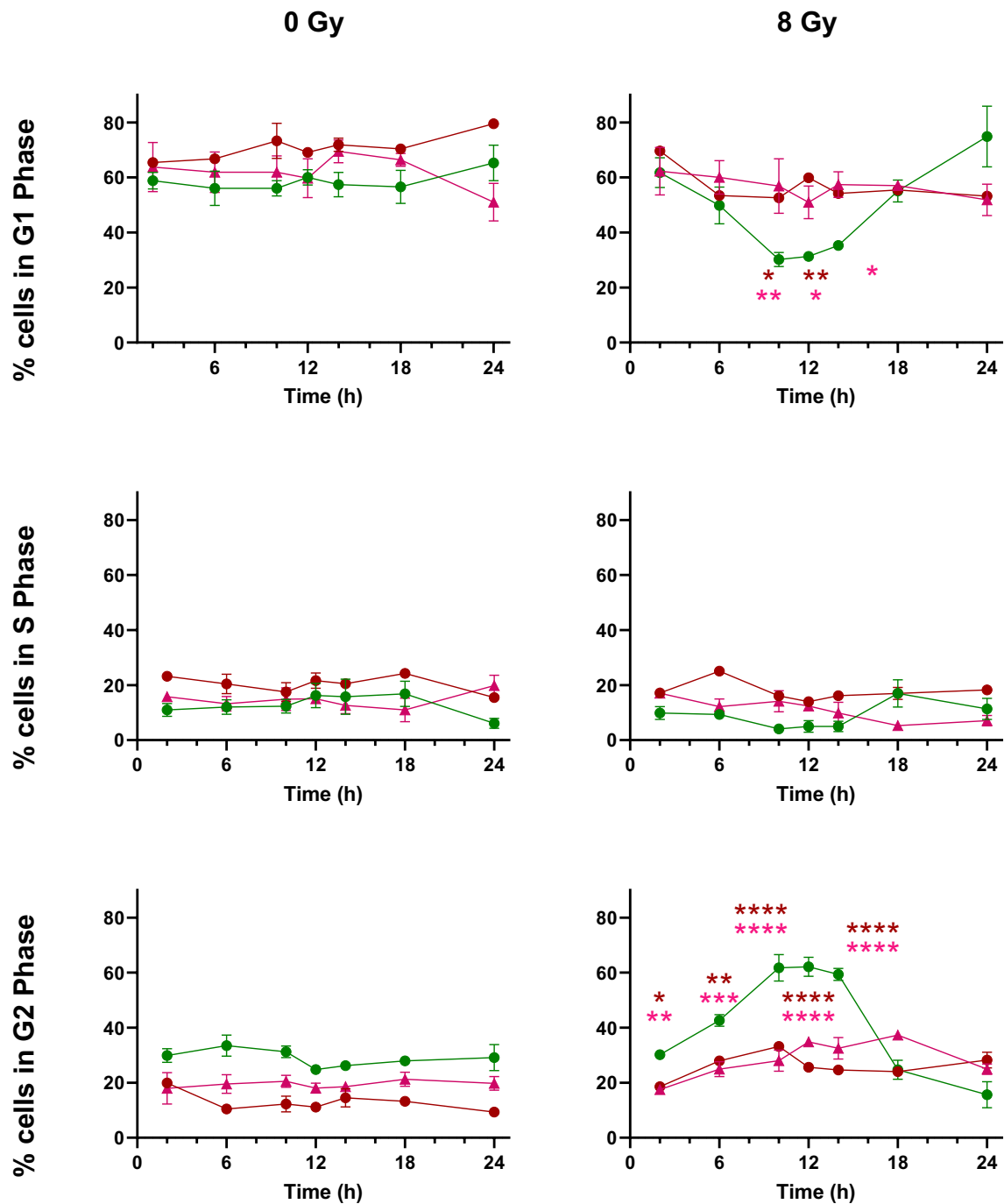
Figure 3.9   Distribution of A549 cells in different cell cycle phases at different time points following irradiation (8 Gy X-rays). Before, during and after irradiation, cells were incubated with 20 %, 1 % and 0.1 % O_2. Hypoxia was maintained until fixation of samples at due timepoints (continuous hypoxia).

Significant differences in mean cell populations are represented with dark red asterisk for normoxia vs. 1 % O_2- (continuous) and with light red asterisk for normoxia vs. 0.1 % O_2-(continuous); *: p<0.05; **: p<0.01; ***: p<0.001; ****: p<0.0001; n = 3. Error bars represent SE.
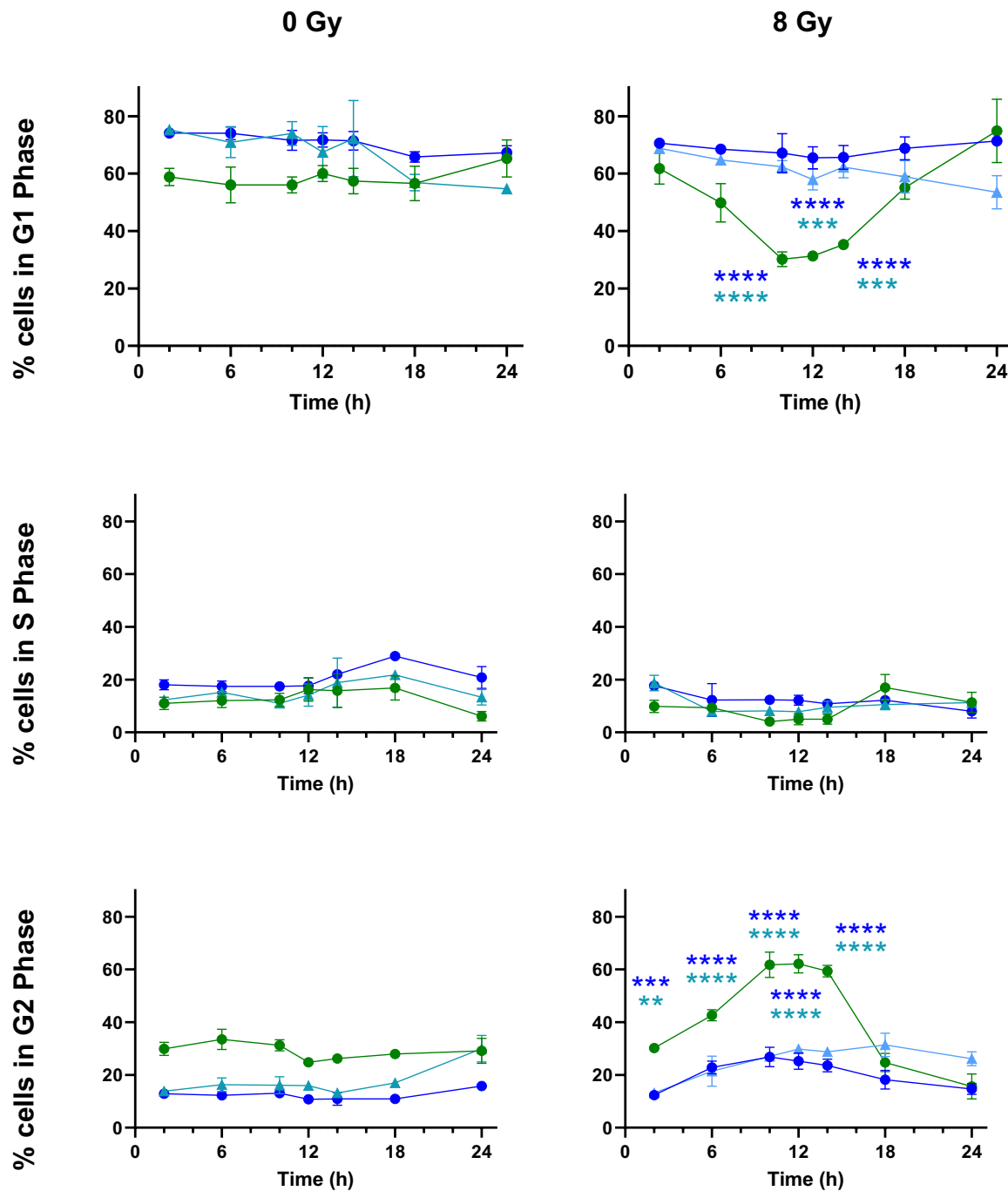
Figure 3.10   Distribution of A549 cells in different cell cycle phases at different time points following irradiation (8 Gy X-rays). Before and during irradiations, cells were incubated with 20 %, 1 % and 0.1 % O_2. Hypoxic cells were returned to the normal incubator following X-ray exposure (transient hypoxia).

Significant differences in mean cell population are represented with dark blue asterisk for normoxia vs. 1 % O_2-(transient) and with light blue asterisk for normoxia vs. 0.1 % O_2-(transient); **: p<0.01; ***: p<0.001; ****: p<0.0001; n = 3. Error bars represent SE.
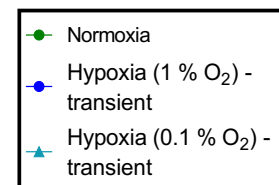
3.4.3. A549 cells after carbon ion exposure in normoxia, continuous hypoxia and transient hypoxia

Experiments with normoxic, continuously hypoxic and transiently hypoxic cells were repeated with carbon ion exposure, in order to determine cell cycle kinetics in hypoxic cells compared to normoxic controls in response to clinically relevant high-LET radiation (Figure 3.11).

Following carbon ion exposure, G1 populations of cells growing under all three oxygen protocols dropped. However, as with X-rays, the G1 population decline under normoxia was much greater than under hypoxia (Table 3.8). This difference was statistically significant 6 h after irradiation and later. Furthermore, unlike to the kinetics after X-rays irradiation, the percentage of cells in G1 did not return to baseline even 24 h after irradiation.

Correspondingly, the percentage of cells in G2 increased after carbon ion exposure of normoxic or hypoxic cells. As with X-rays, the G2 population increase was stronger for normoxic cells than for hypoxic cells (Table 3.8). This difference was statistically significant from 12 h onward. Unlike after X-rays exposure, the G2 populations did not return to baseline even after 24 h.

Table 3.8   Minimum percentage of A549 cells in the G1 and maximum percentage of cells in the G2 cell cycle phases following X-rays and carbon ion exposure along with time after radiation.

| Radiation quality | O$_2$ Protocol | G1 | | G2 | |
		Minimum % of cells in this phase after irradiation: $\mu \pm SE$	Time after radiation (h)	Maximum % of cells in this phase after irradiation: $\mu \pm SE$	Time after radiation (h)
X-rays	Normoxia	30.2 ± 2.6	12 h	62.2 ± 3.5	12 h
	Transient Hypoxia - 1 % O$_2$	67.2 ± 7.6	12 h	26.8 ± 4.3	10 h
	Continuous Hypoxia - 1 % O$_2$	52.6 ± 0.1	12 h	33.2 ± 1.8	10 h
	Transient Hypoxia - 0.1 % O$_2$	57.9 ± 3.2	12 h	31.3 ± 3.8	18 h
	Continuous Hypoxia - 0.1 % O$_2$	51.0 ± 3.4	12 h	37.3 ± 1.0	18 h
Carbon ions	Normoxia	32.2 ± 1.8	18 h	59.1 ± 8.8	18 h
	Transient Hypoxia - 1 % O$_2$	52.2 ± 5.7	18 h	35.5 ± 7.3	18 h
	Continuous Hypoxia - 1 % O$_2$	51.7 ± 7.3	12 h	37.7 ± 6.5	12 h

Cells were exposed to 8 Gy X-rays and carbon ions, respectively.
$\mu \pm SE$: arithmetical mean and standard error of the percentage in G1 or G2 phase of the cell cycle (n = 3)
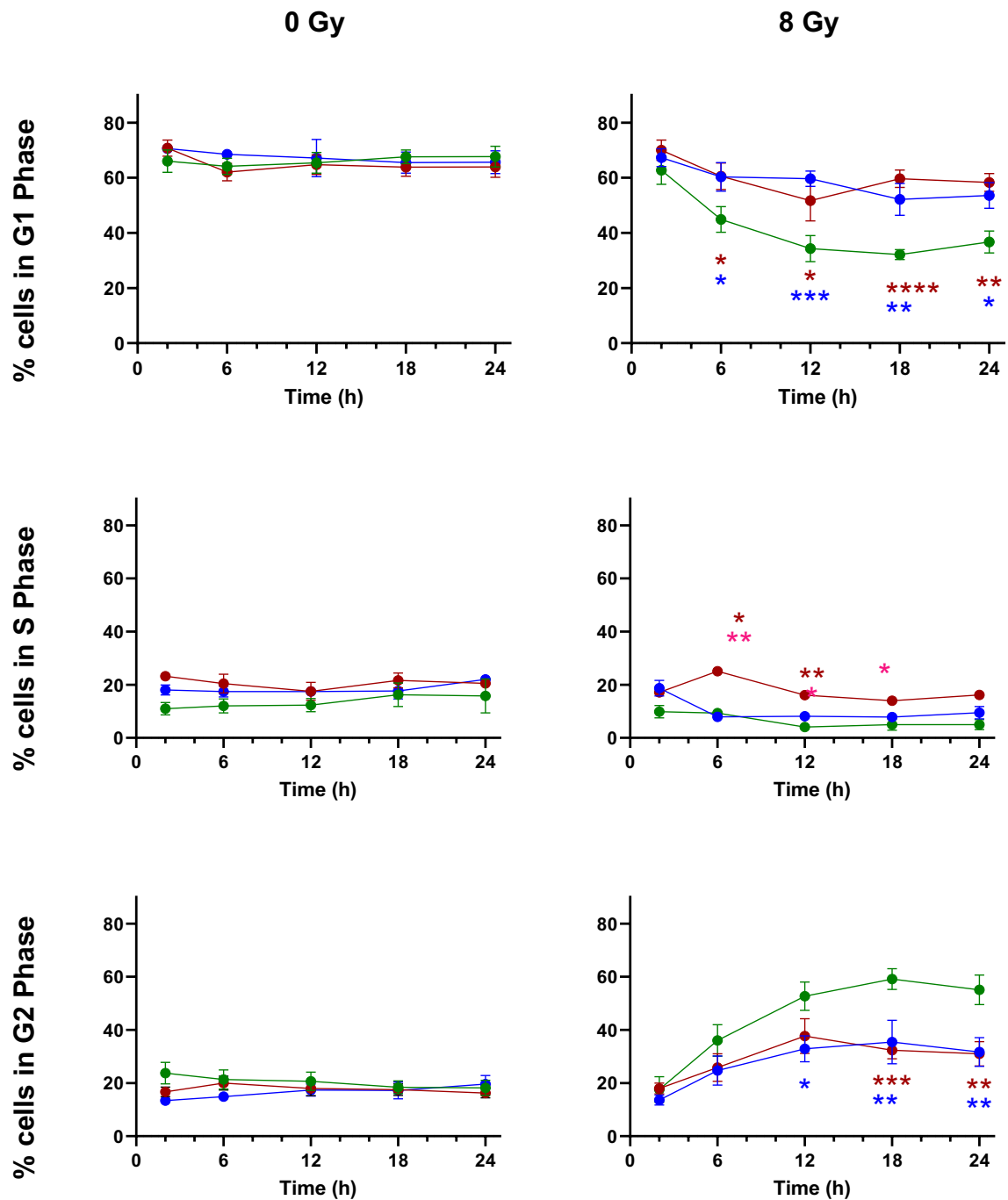
Figure 3.11   Distribution of A549 cells in different cell cycle phases at different time points following irradiation (8 Gy carbon ions). Cells were incubated under normoxia, continuous hypoxia (1 % O₂) and transient hypoxia (1 % O₂)

Significant differences in mean cell population are represented with red asterisk for normoxia vs. continuous hypoxia (1 % O₂) and with blue asterisk for normoxia vs. transient hypoxia (0.1 % O₂); *: p<0.05; **: p<0.01; ***: p<0.001; ****: p<0.0001; n = 3. Error bars represent SE.
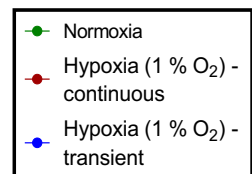
3.4.4. H358 cells after X-rays exposure in normoxia, continuous hypoxia and transient hypoxia

Experiments with normoxic, continuously hypoxic and transiently hypoxic cells were repeated using the H358 cell line to determine if the findings were consistent over the two cell lines (Figure 3.12).

In the absence of irradiation, a higher proportion of hypoxic cells was in G1 compared to normoxic controls. Similarly, a higher proportion of normoxic cells was in G2 compared to hypoxic counterparts. However, in case of transiently hypoxic cells, 48 h of reoxygenation resulted in a cell cycle phase distribution that was more similar to that of normoxic cells than of continuously hypoxic cells.

Following X-rays exposure, the percentage of cells in G1 decreased and that in G2 increased more sharply under normoxia compared to continuous and transient hypoxia (Table 3.9).

Table 3.9   Minimum percentage of A549 and H358 cells in the G1 and maximum percentage of cells in the G2 phase of the cell cycle following X-ray exposure along with time after radiation.

Cell Type	O$_2$ Protocol	G1		G2	
		Minimum % of cells in this phase after irradiation: μ ± SE	Time after radiation (h)	Maximum % of cells in this phase after irradiation: μ ± SE	Time after radiation (h)
A549	Normoxia	30.2 ± 2.6	12 h	62.2 ± 3.5	12 h
	Transient Hypoxia - 1 % O$_2$	67.2 ± 7.6	12 h	26.8 ± 4.3	10 h
	Continuous Hypoxia - 1 % O$_2$	52.6 ± 0.1	12 h	33.2 ± 1.8	10 h
H358	Normoxia	15.6 ± 5.2	18 h	69.2 ± 5.2	18 h
	Transient Hypoxia - 1 % O$_2$	26.9 ± 6.9	18 h	55.0 ± 3.6	18 h
	Continuous Hypoxia - 1 % O$_2$	28.7 ± 3.0	24 h	51.5 ± 4.5	24 h

Cells were exposed to 8 Gy X-rays.
μ ± SE: arithmetical mean and standard error of the percentage in G1 or G2 phase of the cell cycle (n = 3)
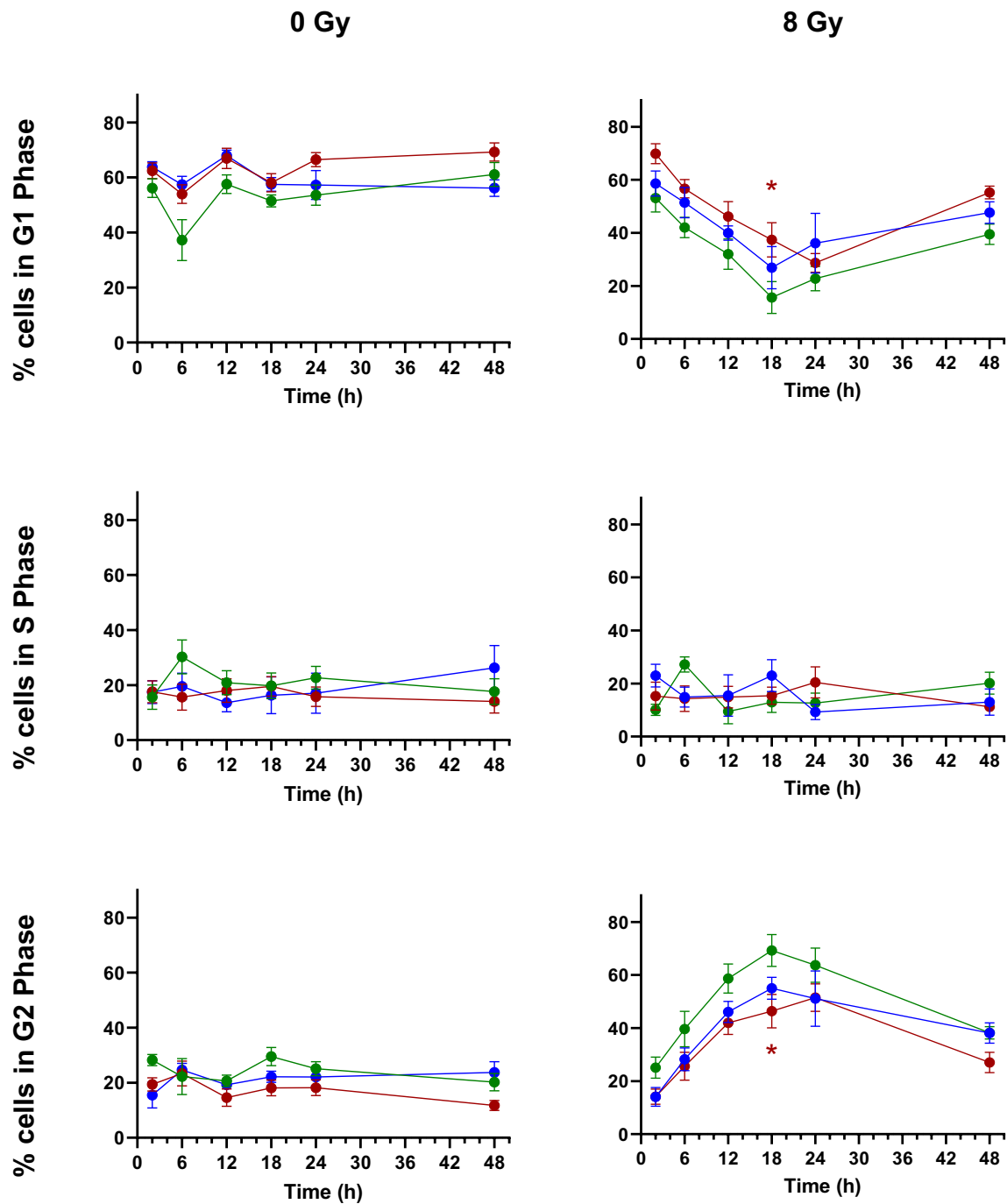
Figure 3.12 Distribution of H358 cells in different cell cycle phases at different time points following irradiation (8 Gy X-rays). Cells were incubated under normoxia, continuous hypoxia (1 % O$_2$) and transient hypoxia (1 % O$_2$).

*Significant differences in mean cell population are represented with red asterisk for normoxia vs. continuous hypoxia (1 % O$_2$) and with blue asterisk for normoxia vs. transient hypoxia (0.1 % O$_2$); *: $p<0.05$; **: $p<0.01$; ***: $p<0.001$; ****: $p<0.0001$; n = 3. Error bars represent SE.*

3.5. DNA double strand break (DSB) induction and repair

DSBs are the most important type of DNA damage following irradiation in terms of radiation lethality and induction of mutations and chromosomal aberrations. To evaluate the effect of hypoxia on DNA damage induction by ionizing radiation exposure and its repair in lung cancer cells, DNA DSBs within cell nuclei were followed over 24 h from the time of irradiation in normoxic and hypoxic cells, by counting γH2AX foci.

3.5.1. A549 cells after X-rays exposure at 20 %, 1 % and 0.1 % oxygen

In the absence of irradiation, the mean γH2AX foci number in A549 cells was not significantly different among the three oxygen concentrations at any of the time points (Figure 3.13, 0 Gy).

A trend of higher DSB induction (Table 3.10) was observed in normoxic A549 cells in comparison to those maintained at 1 % and 0.1 % O_2 (Figure 3.13, 2 Gy). This is obvious by the greater number of γH2AX foci per cell nucleus 1 h after X-rays exposure under normoxia compared to 1 % and 0.1 % continuous hypoxia (30.0 compared to 24.9 and 19.2 respectively).

However, from 2 h onward, there is no statistically significant difference among the cells growing in the three oxygen concentrations even though a statistically nonsignificant trend of greater number of foci in case of normoxia continues up to 12 h.

3.5.2. A549 cells after X-rays exposure in normoxia, continuous hypoxia and transient hypoxia

To evaluate the effect of reoxygenation, a direct comparison of the two different oxygen protocols, namely, transient and continuous hypoxia at 1 % O_2, was carried out in relation to normoxic cells, following X-rays exposure (Figure 3.13 & Figure 3.14).

While there was no statistically significant difference in γH2AX foci repair trajectories and residual damage in the presence (transient hypoxia) or absence (continuous hypoxia) of normal oxygen concentration after X-rays exposure, there was a trend of lower DSB induction under transient hypoxia. However, in case of 0.1 % O_2 (Table 3.10), transiently hypoxic cells showed significantly greater damage compared to continuously hypoxic cells.

Table 3.10   Average number of γH2AX foci per cell nucleus 1 h after irradiation being used as a surrogate for initial DSB induction in A549 cells, following X-rays and carbon ions exposure at various oxygen concentrations and protocols

Cell type	Radiation Quality	O$_2$ Protocol	γH2AX foci per cell nucleus 1 h after irradiation, $\mu \pm$ SE
A549	X-rays	Normoxia	30.0 ± 2.9
		Transient Hypoxia - 1 % O$_2$	21.8 ± 3.2
		Continuous Hypoxia - 1 % O$_2$	24.9 ± 2.2
		Transient Hypoxia - 0.1 % O$_2$	26.2 ± 1.3
		Continuous Hypoxia - 0.1 % O$_2$	19.2 ± 1.3
	Carbon ions	Normoxia	15.1 ± 1.0
		Transient Hypoxia - 1 % O$_2$	12.1 ± 3.2
		Continuous Hypoxia - 1 % O$_2$	15.2 ± 3.2

Cells were exposed to 2 Gy X-rays and carbon ions, respectively.

$\mu \pm$ SE: arithmetical mean and standard error of the γH2AX foci per cell nucleus (n = 3)
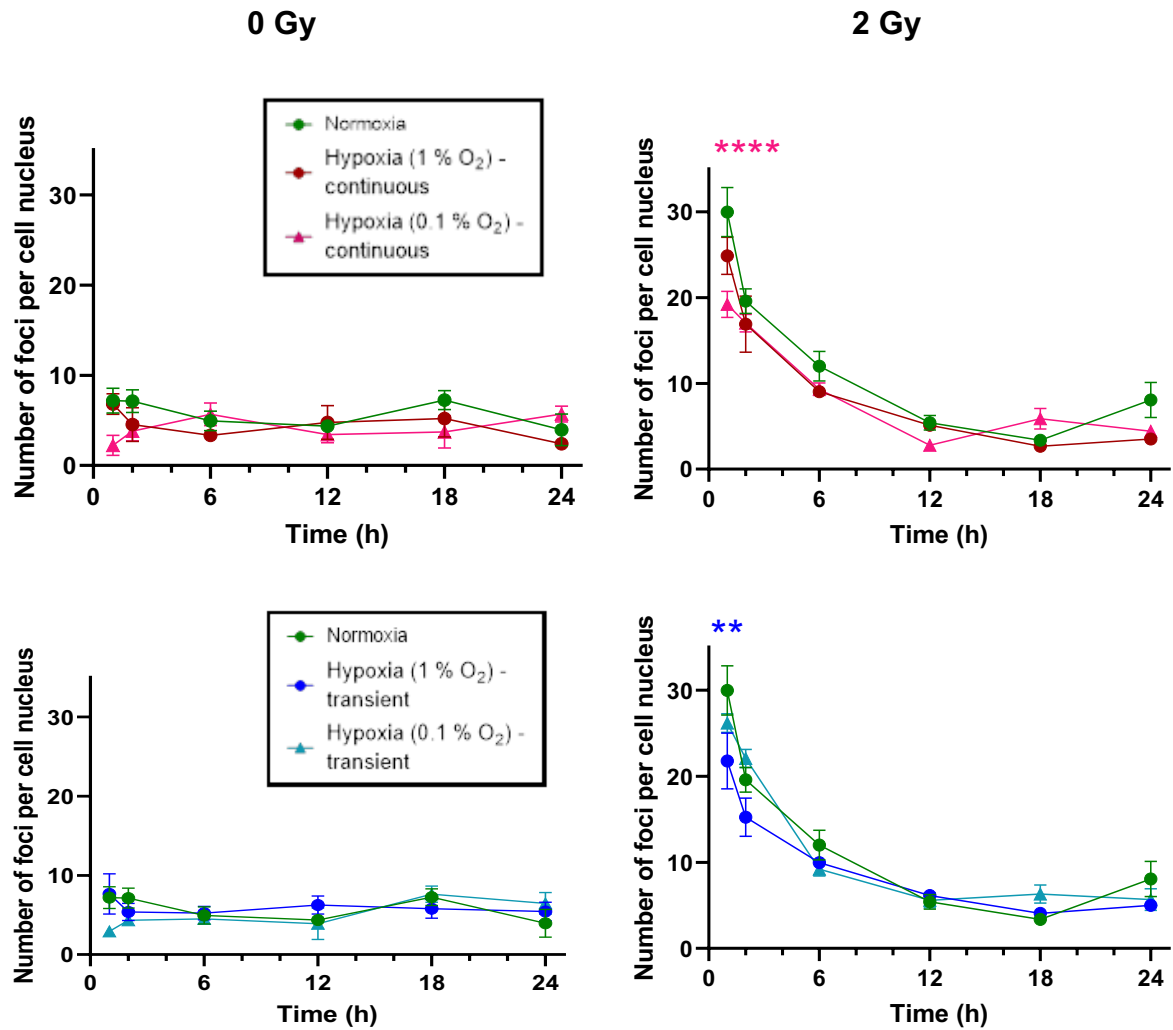
Figure 3.13   γH2AX foci induction and repair over time in A549 cells under normoxia, 1 % O₂ and 0.1 % O₂ following X-rays exposure. Transiently hypoxic cells (top) were re-oxygenated in a normal incubator after irradiation while continuously hypoxic cells (bottom) were kept under hypoxia until fixation.

*Significant differences in the mean number of γH2AX foci are represented with dark blue asterisk for normoxia vs. continuous hypoxia (1 % O₂) and with pink asterisk for normoxia vs. transient hypoxia (0.1 % O₂); *: p<0.05; **: p<0.01; ***: p<0.001; ****: p<0.0001; n = 3. Error bars represent SE.*

0 Gy   **2 Gy**
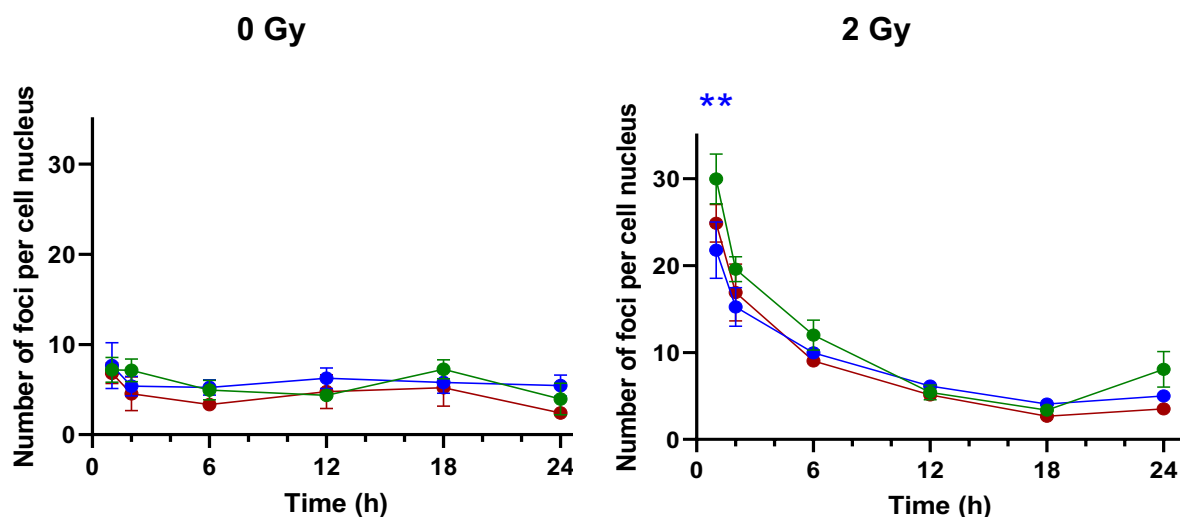
Figure 3.14   γH2AX foci induction and repair over time in A549 cells under normoxia, continuous and transient hypoxia (1 % O₂) following X-rays exposure. Transiently hypoxic cells were re-oxygenated in a normal incubator after irradiation while continuously hypoxic cells were kept under hypoxia until fixation.

Significant differences in mean no. of γH2AX are represented with dark blue asterisk for normoxia vs. transient hypoxia (1 % O₂); **: p<0.01; n = 3. Error bars represent SE.

3.5.3.   A549 cells after carbon ion exposure in normoxia, continuous hypoxia and transient hypoxia

DSB induction and repair were also evaluated following carbon ion exposure in A549 cells kept under normoxia and hypoxia (1 % O₂) (Figure 3.15).

No significant differences in DSB induction by carbon ions under normoxia and continuous hypoxia were observed based on the number of γH2AX foci 1 h after irradiation (15.1 ± 1.0 vs. 15.2 ± 3.2, respectively). A lower number of foci was induced in transiently hypoxic cells (12.1 ± 3.2) but this difference was not statistically significant.

No significant differences in the γH2AX foci counts at timepoints between 2 and 24 h were observed in continuously and transiently hypoxic cells in comparison to normoxia, thereby giving no indication for different repair velocities and differences in the residual damage level after 24 h.
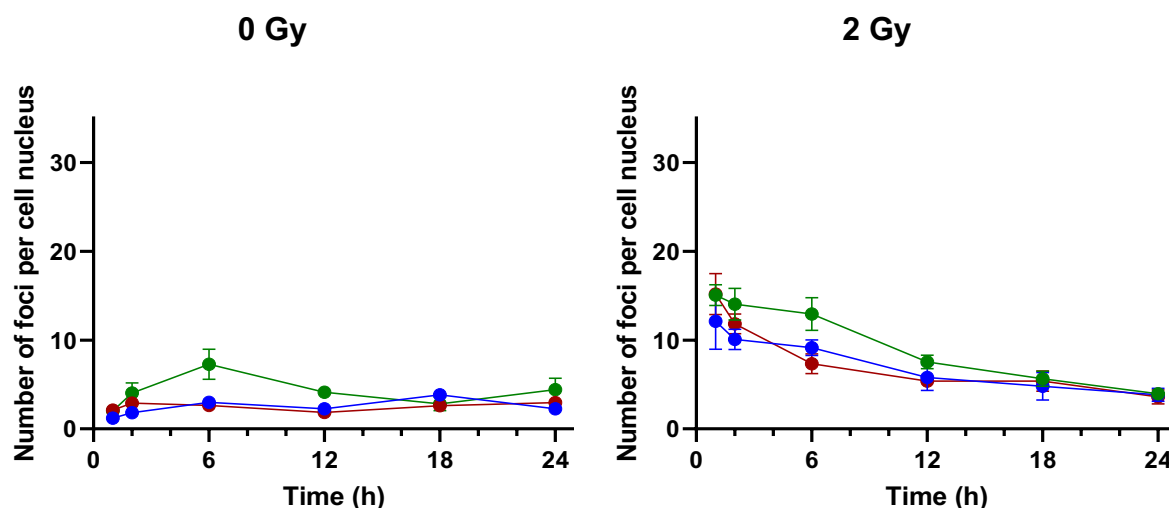
0 Gy

2 Gy

Figure 3.15   γH2AX foci induction and repair over time in A549 cells under normoxia, continuous hypoxia (1 % O₂) and transient hypoxia (0.1 % O₂) following carbon ion exposure. Transiently hypoxic cells were re-oxygenated in a normal incubator after irradiation while continuously hypoxic cells were kept under hypoxia until fixation.
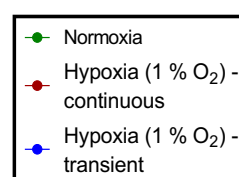
No significant differences in mean no. of γH2AX were found in the following comparisons: normoxia vs. continuous hypoxia (1 % O₂) and normoxia vs. transient hypoxia (1 % O₂); n = 3. Error bars represent SE.

3.5.4.   H358 cells after X-rays exposure in normoxia, continuous hypoxia and transient hypoxia

Experiments with normoxic, continuously hypoxic and transiently hypoxic cells were repeated using the H358 cell line (Figure 3.16) to determine if the findings were consistent for both cell lines.

Following X-rays exposure, much less DNA DSB were induced in H358 cells compared to A549 cells (Table 3.11). A trend of lower DNA DSB induction was observed in hypoxic cells in comparison to normoxic cells although the differences did not reach statistical significance. DSBs repair kinetics over time also followed similar trajectories among them.

Table 3.11   γH2AX foci induction by X-rays in A549 and H358 cells at different O_2 protocols

O_2 Protocol	Number of γH2AX foci at 1 h: μ ± SE	
	A549	H358
Normoxia	30.0 ± 2.9	7.9 ± 0.5
Transient Hypoxia – 1 % O_2	21.8 ± 3.2	4.9 ± 0.4
Continuous Hypoxia – 1 % O_2	24.9 ± 2.2	6.0 ± 1.3
μ ± SE: arithmetical mean ± standard error; n = 3		

0 Gy

2 Gy
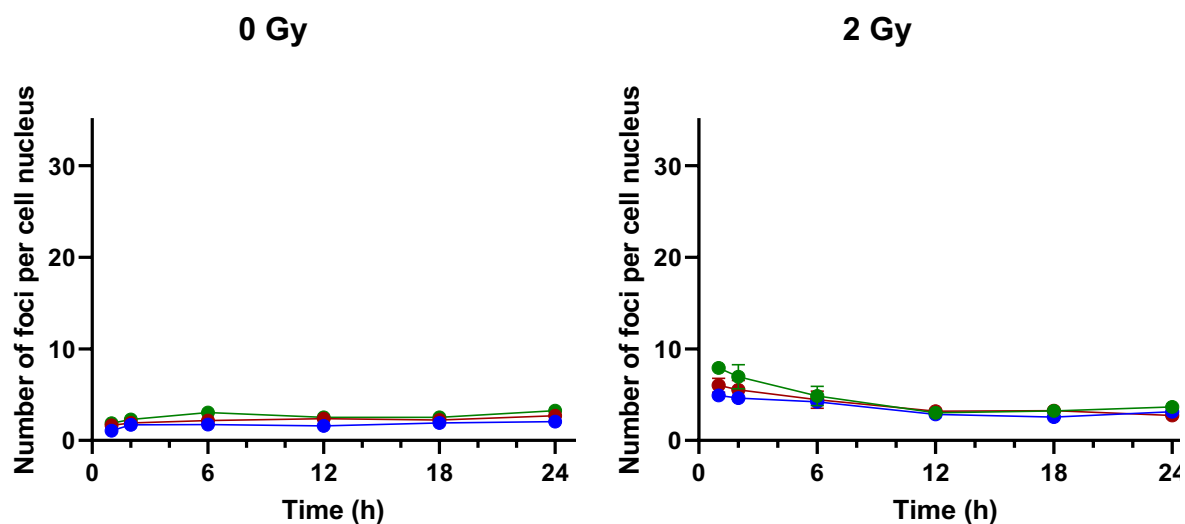
Figure 3.16   γH2AX foci induction and repair over time in H358 cells under normoxia, continuous hypoxia (1 % O₂) and transient hypoxia (1 % O₂) following X-rays exposure. Transiently hypoxic cells were re-oxygenated in a normal incubator after irradiation while continuously hypoxic cells were kept under hypoxia until fixation. n = 3. Error bars represent SE.

- Normoxia
- Hypoxia (1 % O₂) - continuous
- Hypoxia (1 % O₂) - transient
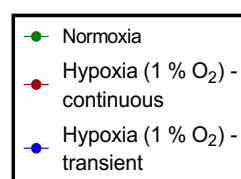
3.6.   Global gene expression analysis

To detect differences in gene expression of A549 and H358 cells growing under normoxia and hypoxia (1 % O_2) in the absence and presence of irradiation, mRNA sequencing was performed. Pathway enrichment analysis was carried out to find relevant pro-survival pathways that may be differentially upregulated under hypoxia but emphasis was restricted to cell cycle and DSBR regulating genes as well as target genes of the pro-survival NF-κB pathway.

3.6.1.   A549 cells after hypoxia in comparison to normoxia

Differential gene expression was evaluated between hypoxic (1 % O_2) A549 cells in comparison to normoxic controls with emphasis on genes regulating cell cycle as well as target gene expression of the pro-survival NF-κB pathway.

Only two genes were found to be upregulated in the case of continuously hypoxic cells compared to normoxic controls (Table 3.12) namely ANXA13 and CP. These cells were incubated after seeding for 52 h in hypoxia (1 % O_2). Transiently hypoxic cells showed regulation of nine genes but the ones showing the highest $\log_2$ fold change were the three upregulated genes, ANXA13, CP and KCNJ16 (Table 3.12). Transiently hypoxic cells were incubated in hypoxia (1 % O_2) and then reoxygenated in a standard incubator (~20 % O_2) for 4 h.

None of the differentially regulated genes under continuous or transient hypoxia were related to the cell cycle and they were not NF-κB target genes.

DSBR-related genes were not evaluated while analyzing gene expression after hypoxia only since there was no irradiation.

Table 3.12   Number of significant differentially expressed genes (DEGs) in A549 and H358 cells 52 h following hypoxic incubation (continuous hypoxia) or 4 h after reoxygenation of 48 h of hypoxic incubation (transient hypoxia), compared to normoxic incubation

Compared groups	Number of significant DEGs			
	A549 cells		H358 cells	
	Up-regulated	Down-regulated	Up-regulated	Down-regulated
Continuous Hypoxia 0 Gy vs. Normoxia 0 Gy	2	0	93	32
Transient Hypoxia 0 Gy vs. Normoxia 0 Gy	8	1	0	0

3.6.2.   H358 cells after hypoxia in comparison to normoxia

Continuously hypoxic (1 % O_2) H358 cells showed regulation of 125 different genes when compared to normoxic controls while no gene was found to be differentially regulated in transiently hypoxic cells in comparison to normoxic controls (Table 3.12). The incubation protocol was same as for A549 cells (subchapter 3.6.1).

The differentially regulated genes included CDKN1C ($\log_2$ fold change: -1.42, p_{adj}-value: 1.77×10^{-9}) as the only cell cycle-related gene when compared against a list of candidates from the KEGGS Pathways database.

DSBR-related genes were not evaluated while analyzing gene expression after hypoxia only since there was no irradiation.

Seven NF-κB target genes were upregulated in continuously hypoxic cells compared to normoxic cells and are shown in Table 3.13.

Table 3.13   Expression of NF-κB target genes that were differentially regulated under continuous hypoxia in comparison to normoxia

DEGs (gene name abbreviation)	Continuous Hypoxia vs. Normoxia	
	Log$_2$ fold change	Significance level
ENO2	1.87	*
PDGFB	1.49	*
TREM	1.47	*
PTAFR	1.41	***
PTGS2	1.14	****
BLNK	1.01	*
MYLK	1.01	**

*: $p_{adj}<0.05$; **: $p_{adj}<0.01$; ***: $p_{adj}<0.001$; ****: $p_{adj}<0.0001$

ENO2, enolase 2; PDGFB, platelet derived growth factor β; TREM, triggering receptor expressed on myeloid cells; PTAFR, platelet activating factor receptor; PTGS2, prostaglandin endoperoxide synthase 2; BLNK, B cell linker protein; MYLK, myosin light chain kinase.

3.6.3.   A549 cells after X-rays exposure in normoxia and hypoxia

To detect differences in gene expression of A549 cells growing under normoxia and hypoxia (1 % O$_2$) following irradiation, mRNA sequencing was performed using RNA that was extracted from samples lysed 4 h after irradiation. Emphasis was on the expression of cell cycle and DSBR regulating genes as well as NF-κB target genes.

Following X-ray exposure, gene expression in normoxic A549 cells was compared to that in continuously hypoxic and transiently hypoxic A549 cells. A summary of significant differential gene expression is shared in Table 3.14.

Table 3.14   Number of significant DEGs in A549 cells following X-rays exposure under hypoxia (8 Gy) compared to normoxia (8 Gy)

Compared groups	Number of Significant DEGs	
	Upregulated	Downregulated
Continuous Hypoxia 8 Gy vs. Normoxia 8 Gy	349	103
Transient Hypoxia 8 Gy vs. Normoxia 8 Gy	91	15

In A549 cells, 364 (270+94, Figure 3.17) genes were exclusively regulated under continuous hypoxia in comparison to normoxia following exposure to X-rays in both oxygen conditions. In total, 349 genes were upregulated (Figure 3.17A) and 103 genes were downregulated (Figure 3.17B) in irradiated continuously hypoxic cells compared to irradiated normoxic cells. This number was much lower for transiently hypoxic cells (91 up- and 15 downregulated genes), indicating that, over 4 h of reoxygenation, gene expression began to return to that observed under normoxia (Figure 3.17).

A   **Upregulated DEGs**   **B**   **Downregulated DEGs**

Figure 3.17   Number of differentially expressed genes 4 h after X-rays exposure (8 Gy) in A549 cells incubated under continuous hypoxia (red) and transient hypoxia (blue), compared to that in cells maintained in normoxia (control); Venn diagrams showing overlapping and exclusive DEGs among them.

The enrichment of DEGs commonly regulated following X-rays exposure of A549 cells, maintained under continuous and transient hypoxia in comparison to normoxia, in specific cellular pathways was analyzed using the KEGGs pathways database by means of the DAVID (2021) online tool. Both continuous and transient hypoxia differentially upregulated glycolysis/gluconeogenesis in comparison to normoxia as well chemokines that inhibited growth, activated inflammation and promoted and remodeled the actin cytoskeleton. However, the differential pathway regulation predominantly took place under continuous hypoxia including the HIF-1 pathway and several other cellular pathways modulating cell growth and metabolism. Additionally, continuous hypoxia induced pathways associated with ECM interaction and focal cellular adhesion may contribute toward epithelial mesenchymal transformation (EMT). The list of enriched pathways is attached in appendix (Table 9.1). Here, the emphasis is restricted to differentially expressed genes regulating cell cycle and DSBR as well NF-κB target genes.

3.6.3.1.   *Expression of cell cycle genes*

Differentially expressed genes under both continuous and transient hypoxia were screened for those related to the cell cycle, against a list of 129 cell cycle genes based on KEGGS pathways data base. In comparison to normoxia, only one cell cycle gene was found to be differentially regulated under continuous hypoxia and none in case of transient hypoxia (Table 3.15).

Table 3.15   Expression of cell cycle genes that were differentially regulated in both continuous and transient hypoxia in comparison to normoxia 4 h after X-rays exposure of A549 cells.

DEGs (gene name abbreviation)	Continuous Hypoxia vs. Normoxia	
	Log$_2$ fold change	Significance level
GADD45B	1.20	****

**** : $p_{adj}<0.0001$

GADD45B, growth arrest and DNA damage inducible protein B

3.6.3.2.   Expression of DSBR genes

Differentially expressed genes under both continuous and transient hypoxia were screened for those related to DSBR, against a list of 13 NHEJ genes and 28 HR genes based on KEGGS pathways data base. No DSBR gene was found to be differentially regulated under continuous or transient hypoxia when compared with normoxia.

3.6.3.3.   Expression of NF-κB target genes

Since the emphasis of this work was on the NF-κB pathway's role in hypoxic response to irradiation, it was examined which of the DEGs are targets of the transcription factors of the NF-κB family; the NF-κB target genes that were regulated as a result of X-rays exposure to A549 cells kept under 1 % O_2 compared to those kept at normal O_2 levels are enlisted in Table 3.16.

Table 3.16   Expression of NF-κB target genes that were differentially regulated in both continuous and transient hypoxia in comparison to normoxia 4 h after X-rays exposure of A549 cells.

DEGs (gene name abbreviation)	Continuous Hypoxia vs. Normoxia		Transient Hypoxia vs. Normoxia	
	Log$_2$ fold change	Significance level	Log$_2$ fold change	Significance level
ADAM19	1.62	**		
BNIP3	1.10	****		
IL-1A	3.52	****	2.32	***
PDGFB	1.78	****		
ENO2	1.11	****		
CCL2	1.22	****	1.09	****
ANGPT1	-1.09	*		
BCL2A1	1.15	*	1.33	****
GADD45B	1.20	****		
INHBA	1.55	**		
JUNB	1.40	****		
CCL28	2.09	**		
FABP6	1.22	*	1.23	*
F3	2.71	****	1.41	****
MMP9	1.62	****	1.53	**

DEGs (gene name abbreviation)	Continuous Hypoxia vs. Normoxia		Transient Hypoxia vs. Normoxia	
	Log$_2$ fold change	Significance level	Log$_2$ fold change	Significance level
PGK1	1.51	****	1.17	****
IL-8	1.38	****		

*: $p_{adj}<0.05$; **: $p_{adj}<0.01$; ***: $p_{adj}<0.001$; ****: $p_{adj}<0.0001$

ADAM19, a disintegrin and metalloprotease 19; BNIP3, Bcl-2 interacting protein 3; IL-1A, interleukin 1A; PDGFB, platelet derived growth factor β; ENO2, enolase 2; CCL2 & CCL28, C-C motif chemokine ligand 2 & 28; ANGPT1, angiopoietin 1; BCL2A1, B cell leukemia 2 related protein A1a; GADD45B, growth and DNA repair inducible protein B; INHBA, inhibin A; JUNB, Jun-B transcription factor; FABP6, fatty acid binding protein 6; F3, factor 3; MMP9, matrix metallopeptidase 9; PGK1, phosphoglycerate kinase 1, IL-8, interleukin 8.

3.6.4.   A549 cells after carbon ion exposure in normoxia and hypoxia

mRNA sequencing was carried out to determine possible differences in gene expression in A549 cells growing under normoxia and hypoxia following irradiation with carbon ions to evaluate gene expression differences in the same cell line as after X-rays exposure shared in previous section. Emphasis was on expression of cell cycle and DSBR regulating genes as well as NF-κB target genes.

Following carbon ion exposure, gene expression in normoxic A549 cells was compared to that in continuously hypoxic and transiently hypoxic A549 cells. A summary of significant differential gene expression is shared in Table 3.17.

Table 3.17   Number of significant DEGs in A549 cells growing under hypoxic oxygen protocols 4 h after carbon ion exposure (8 Gy) in comparison to corresponding normoxic controls

Compared groups	Number of Significant DEGs	
	Upregulated	Downregulated
Continuous Hypoxia 8 Gy vs. Normoxia 8 Gy	255	321
Transient Hypoxia 8 Gy vs. Normoxia 8 Gy	0	0

Following carbon ion exposure, no differences in gene regulation were observed between irradiated normoxic and transiently A549 hypoxic cells indicating that differential gene expression of transiently hypoxic cells exposed to carbon ions was very similar to that of normoxic cells exposed to carbon ions 4 h after irradiation. On the other hand, continuously hypoxic cells show exclusive regulation of 576 genes (Figure 3.18).

A **Upregulated DEGs**   **B** **Downregulated DEGs**
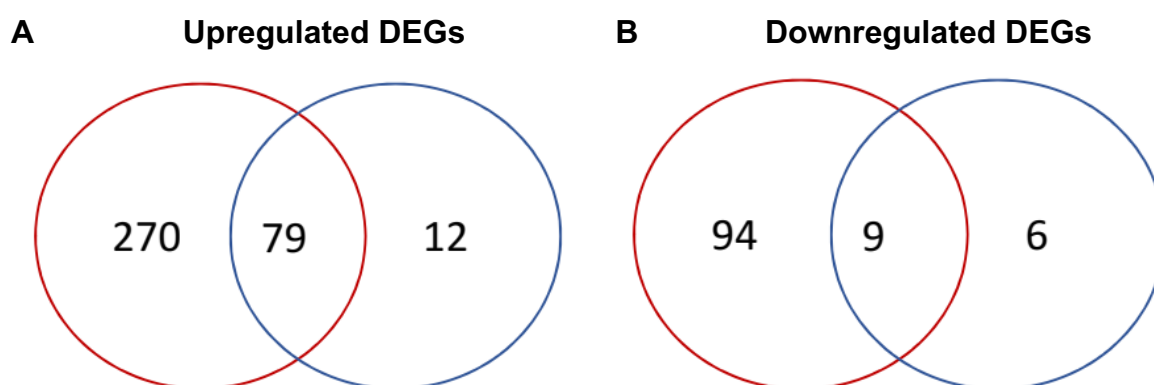

Figure 3.18   Number of differentially expressed genes 4 h after carbon ion exposure (8 Gy) in A549 cells incubated under continuous hypoxia (red) and transient hypoxia (blue), compared to that in irradiated A549 cells maintained in normoxia (control); Venn diagrams showing overlapping and exclusive DEGs among them.

DEGs commonly regulated following carbon ion exposure in A549 cells maintained under continuous and transient hypoxia in comparison to normoxia, were analyzed to determine if they enrich in specific cellular pathways using the KEGGs pathways database by means of the DAVID (2021) online tool. Pathways whose gene constituents were differentially regulated in case of continuous hypoxia in comparison to normoxia after carbon ion exposure were concerned with growth, proliferation, senescence and apoptosis along with changes in cytoskeleton and stem cell pluripotency. However, the number of genes enriching these pathways is greater in number. The list of enriched pathways is attached in appendix (Table 9.2). Here the emphasis is restricted to differentially expressed genes regulating cell cycle and DSBR as well NF-κB target genes.

3.6.4.1.   Expression of cell cycle genes

Differentially expressed genes under both continuous and transient hypoxia were screened for those related to the cell cycle, against a list of 129 cell cycle genes based on KEGGS pathways data base. In comparison to normoxia, only one cell cycle gene was found to be differentially regulated under continuous hypoxia and none in case of transient hypoxia (Table 3.18).

Table 3.18   Expression of differentially regulated cell cycle genes in continuous hypoxia in comparison to normoxia 4 h after carbon ion exposure of A549 cells.

DEGs (gene name abbre-viation	Continuous Hypoxia vs. Normoxia	
	Log$_2$ fold change	Significance level
E2F2	1.09	****

****: $p_{adj} < 0.0001$

E2F2, E2F2 transcription factor

3.6.4.2.   Expression of DSBR genes

Differentially expressed genes under both continuous and transient hypoxia were screened for those related to DSBR, against a list of 13 NHEJ genes and 28 HR genes based on KEGGS pathways data base. No DSBR gene was found to be differentially regulated under continuous or transient hypoxia when compared with normoxia.

3.6.4.3. Expression of NF-κB Target genes

NF-κB target genes regulated as a result of carbon ion exposure to A549 cells kept under continuous hypoxia (1 % O_2) compared to those kept at normal O_2 levels are enlisted in Table 3.19.

Transiently hypoxic cells irradiated with carbon ions showed no differential expression of NF-κB target genes compared to carbon ion exposed normoxic controls.

Table 3.19   Expression of NF-κB target genes that were differentially regulated in A549 cells under continuous hypoxia in comparison to normoxia 4 h after carbon ion exposure (8 Gy).

DEGs (gene name abbreviation)	Continuous Hypoxia vs. Normoxia	
	Log$_2$ Fold change	Significance level
ELF3	-1.48	****
ADAM19	1.56	****
SNAI1	1.22	****
SOX9	1.47	****
IL-1A	2.75	****
PDGFB	1.91	****
IL-6	1.13	****
IL-8	1.49	****
BCL2A1	1.52	**
ALOX12	-1.24	****
INHBA	1.52	**
JUNB	1.34	****
LIPG	1.43	***
TRAF1	1.28	****
F3	2.06	****
CD274	1.09	****
MMP9	2.41	****
GNRH2	-1.50	*

*: $p_{adj}<0.05$; **: $p_{adj}<0.01$; ***: $p_{adj}<0.001$; ****: $p_{adj}<0.0001$

ELF3, E74-like factor 2; ADAM19, a disintegrin and metalloprotease 19; SNAI1, snail family transcriptional repressor 1; SOX9, SRY-box transcription factor 9; IL-1A, 6 & 8, interleukin 1A, 6 and 8; PDGFB, platelet derived growth factor β; BCL2A1, B cell leukemia 2 related protein A1a ALOX12, Arachidonate 12-Lipoxygenase, 12S Type; INHBA, inhibin A; JUNB, Jun-B transcription factor; LIPG, Lipase G; TRAF1, F3, factor 3; CD274, CD274 molecule (PDL-1); MMP9, matrix metallopeptidase 9; GNRH2, gonadotropin releasing hormone 2.

3.6.5. H358 cells after X-rays exposure in normoxia and hypoxia

mRNA sequencing was carried out to determine differences in gene expression in H358 cells growing under normoxia and hypoxia (1 % O_2) following irradiation with X-rays. These data were compared to the gene expression data of the A549 cell line after exposure to X-rays (see subchapter 3.6.3) to evaluate possible differences between the two cell lines.

Following X-rays exposure, gene expression in normoxic H358 cells was compared to that in continuously hypoxic and transiently hypoxic H358 cells. A summary of significant differential gene expression is shared in Table 3.20.

Table 3.20   Number of significant DEGs in H358 cells growing under hypoxic oxygen protocols after X-rays exposure (8 Gy) in comparison to corresponding normoxic controls

Compared groups	Number of Significant DEGs	
	Upregulated	Downregulated
Normoxia 8 Gy vs. Continuous Hypoxia 8 Gy	392	476
Normoxia 8 Gy vs. Transient Hypoxia 8 Gy	525	374

Four hours after X-rays exposure, 597 genes were exclusively differentially regulated in irradiated cells maintained under continuous hypoxia compared to normoxia (Figure 3.19).

Group comparison between transiently hypoxic and normoxic cells showing more DEGs as opposed to group comparison between continuously hypoxic and normoxic cells indicated an effect of reoxygenation post-irradiation on gene expression which was not observed in the same intensity in A549 cells.

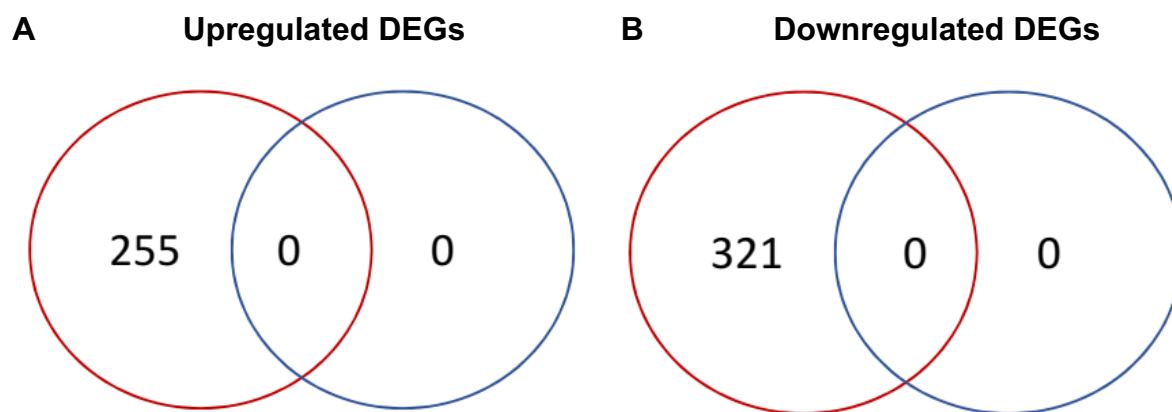**A   Upregulated DEGs**   **B   Downregulated DEGs**
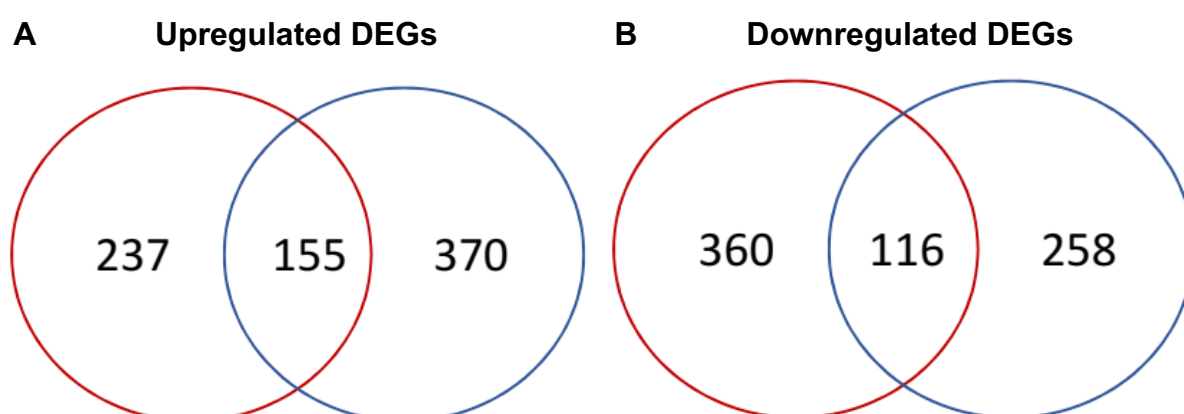
Figure 3.19   Number of differentially expressed genes after X-rays exposure (8 Gy) in H358 cells incubated under continuous hypoxia (red) and transient hypoxia (blue), compared to H358 cells maintained in normoxia (control); Venn diagrams show overlapping and exclusive DEGs among them.

Statistically significant DEGs following X-rays exposure of H358 cells maintained under continuous and transient hypoxia in comparison to normoxia were analyzed to determine their enrichment to specific cellular pathways using the KEGGs pathways database by means of the DAVID (2021) online tool. The cellular pathways enriched by either continuous or transient hypoxia in comparison to normoxia in cells exposed to X-rays were pertaining to actin cytoskeleton and cellular adherence junctions and therefore may contribute toward epithelial mesenchymal transformation. Under both, continuous and transient hypoxia, X-rays exposure resulted in activation of Ras and Hippo signaling pathways of cell growth and proliferation but the DEGs were different for the two oxygen protocols. Additionally, under continuous hypoxia, X-rays exposure activated ErbB and MAPK signaling pathways of growth and proliferation besides several genes in the HIF-1 pathway (appendix tables 9.3, 9.4 and 9.5). Furthermore, it differentially regulated many genes associated with tyrosine kinase inhibitor therapy resistance in NSCLC patients which may have clinical relevance. On the other hand, under transient hypoxia, X-rays exposure activated the PI3K-AKT pathway influencing cellular growth as well as the NF-κB and TNF signaling pathways influencing inflammation and cell survival (appendix). Here the emphasis is restricted to differentially expressed genes regulating cell cycle and DSBR as well NF-κB target genes.

3.6.6. Expression of cell cycle genes

Differentially expressed genes under both continuous and transient hypoxia were screened for those related to the cell cycle, and results are shown in Table 3.21.

Table 3.21   Expression of cell cycle genes that were differentially regulated in both continuous and transient hypoxia in comparison to normoxia 4 h after X-rays exposure of H358 cells.

DEGs (gene name abbreviation)	Continuous Hypoxia vs. Normoxia		Transient Hypoxia vs. Normoxia	
	Log$_2$ fold change	Significance level	Log$_2$ fold change	Significance level
TGFB2	1.08	*	1.71	****
MYC			1.67	****
RBL2	1.18	*		
STAG1	1.16	**		
EP300	1.15	**		
CDK6			1.12	***
PRKDC	1.08	*		
E2F2			-1.97	**
CDKN1C	-1.92	*		
GADD45G	-1.52	*	-1.31	*
E2F1			-1.47	*

*: $p_{adj}<0.05$; **: $p_{adj}<0.01$; ***: $p_{adj}<0.001$; ****: $p_{adj}<0.0001$

TGFB2, transforming growth factor β; MYC, Myc proto-oncogene; RBL2, Rb transcriptional corepressor like 2; STAG1, stromal antigen 1; EP300, E1A-associated protein p300; CDK6, cyclin dependent kinase 6; PRKDC, Protein Kinase, DNA-Activated, Catalytic Subunit; E2F1 & 2, E2F transcription factors 1 & 2; CDKN1C, cyclin dependent kinase inhibitor 1C; GADD45G, growth and DNA damage repair inducible gene G.

3.6.7. Expression of DSBR genes

Differentially expressed genes under both continuous and transient hypoxia were screened for those related to DSBR. No DSBR related gene was found to be differentially regulated following irradiation in transiently hypoxic H358 cells. However, continuously hypoxic H358 cells differentially expressed two DSBR genes compared to normoxic controls following X-rays exposure. Details are shown in Table 3.22.

Table 3.22   Expression of DSBR genes that were differentially regulated in continuous hypoxia in comparison to normoxia 4 h after X-rays exposure of H358 cells.

DEGs (gene name abbreviation)	Continuous Hypoxia vs. Normoxia	
	Log$_2$ fold change	Significance level
PRKDC	1.08	*
POLD2	-1.27	*

*: $p_{adj}<0.05$

PRKDC, Protein Kinase, DNA-Activated, Catalytic Subunit; POLD2, DNA Polymerase Delta 2, Accessory Subunit.

3.6.8. NF-κB target genes expression analysis

NF-κB target genes regulated as a result of X-rays exposure of H358 cells kept under continuous and transient hypoxia (1 % O_2) compared to those kept at normal O_2 levels are enlisted in Table 3.23. Transiently hypoxic cells irradiated with X-rays showed higher differential expression of NF-κB target genes compared to continuously hypoxic cells irradiated with X-rays.

Table 3.23   Expression of NF-κB target genes that were differentially regulated under both, continuous and transient hypoxia, in comparison to normoxia 4 h after X ray exposure (8 Gy) of H358 cells.

DEGs (gene name abbreviation)	Continuous Hypoxia, 8 Gy vs. Normoxia, 8 Gy		Transient Hypoxia, 8 Gy vs. Normoxia, 8 Gy	
	Log$_2$ fold change	Significance level	Log$_2$ fold change	Significance level
EDN1			2.29	****
IL-8			1.49	****
BDNF			1.02	*
ABCA1	1.63	****	1.08	*
TNFSF10			-1.97	****
PTHLH			1.22	****
SLC6A6	1.11	**		
ELF3			-1.68	****
OXTR			1.50	****
PTGES			-2.73	****

DEGs (gene name abbreviation)	Continuous Hypoxia, 8 Gy vs. Normoxia, 8 Gy		Transient Hypoxia, 8 Gy vs. Normoxia, 8 Gy	
	Log$_2$ fold change	Significance level	Log$_2$ fold change	Significance level
MAP4K1	-2.02	*	-2.18	**
CDK6			1.12	**
VEGFC			1.06	**
VIM			1.57	****
IRF7	-1.03	*	-1.08	*
REV3L	1.00	*		
PTGS2	1.59	*	1.77	**
BMP2	1.02	*		****
AHCTF1	1.18	*		
MYC			1.67	****
TNFAIP3			1.86	****
UCP2			-1.03	****
BLNK			1.29	***
IDO1			-1.11	****
EGFR	1.53	**	1.29	*
MYLK	1.50	**	1.66	****
MDK	-1.01	*	-1.08	**
APOD			1.39	*
THBS1			2.25	***
CAV1			1.08	****
CXCL1			1.12	***
TERT			-1.02	****
FABP6			-1.71	*
REL	1.11	**		
CR2			-1.33	**
MX1			-1.54	****
UPP1	-1.22	*	-1.41	*
KITLG			1.44	**
F3			1.53	**
TREM1			1.27	**
KCNK5			-1.12	****
KLF10			1.27	**
PSME2	-1.16	*	-1.15	*
NRG1			1.65	****
CD274			1.13	*
PSMB9	-1.09	*	-1.52	**

DEGs (gene name abbreviation)	Continuous Hypoxia, 8 Gy vs. Normoxia, 8 Gy		Transient Hypoxia, 8 Gy vs. Normoxia, 8 Gy	
	Log$_2$ fold change	Significance level	Log$_2$ fold change	Significance level
CSF2			1.30	****
PGK1			1.05	**

*: $p_{adj}<0.05$; **: $p_{adj}<0.01$; ***: $p_{adj}<0.001$; ****: $p_{adj}<0.0001$

EDN1, endothelin 1; BDNF Brain Derived Neurotrophic Factor, ABCA1, ATP binding cassette subfamily A member 1; TNFSF10, TNF superfamily member 10; PTHLH, parathyroid hormone like hormone; SLC6A6, solute carrier 6A6; ELF3, E72-like protein 3, OXTR, oxytocin receptor; PTGES, prostaglandin E synthase; MAP4K1, mitogen activated protein kinase kinase kinase kinase 1; CDK6, cyclin dependent kinase 6; VEGFC, vascular endothelial growth factor C; VIM, vimentin; IRF7, interferon regulatory factor 7; REV3L, REV3 like DNA directed polymerase zeta catalytic subunit; PTGS2, prostaglandin endoperoxide synthase 2; BMP2, bone morphogenetic protein 2; AHCTF1, AT-Hook Containing Transcription Factor 1 ; MYC, Myc proto-oncogene, BHLH transcription factor ; TNFAIP3, TNFα induced protein 3; UCP2, uncoupling protein 2; BLNK, B cell linker protein; IDO1, Indoleamine 2,3-Dioxygenase 1; EGFR, epidermal growth factor receptor; MYLK, myosin light chain kinase; MDK, midkine; APOD, Apolipoprotein D; THBS1, thrombospondin 1; CAV1, caveolin 1; CXCL1, C-X-C motif chemokine ligand 1; TERT, telomerase reverse transcriptase: FABP6, fatty acid binding protein 6; REL, c-Rel proto-oncogene; CR2, complement c3d receptor 2; MX1, MX dynamin like GTPase 1; UPP1, uridine phosphorylase 1; KITLG, c-Kit ligand; F3, factor 3; TREM1, triggering receptor expressed on myeloid cells 1; KCNK5, potassium two pore domain channel subfamily K member 5; KLF10, kruppel like factor 10; PSME2, proteasome activator subunit 2; NRG1, neuroregulin 1; CD274, CD274 molecule (PDL-1); PSMB9, Proteasome 20S subunit beta 9; CSF2, colony stimulating factor 2; PGK1, phosphoglycerate kinase 1.

3.7. NF-κB activation after radiation exposure in normoxia and hypoxia

NF-κB activation was studied in cells irradiated under hypoxia compared to those irradiated under normoxia. The intent was to evaluate the association between the differential regulation of NF-κB target genes (subchapter 3.6) and NF-κB pathway activation. Studies were done for using both A549 and H358 cells following X-rays exposure. Additionally, A549 cells were studied following carbon ions exposure as well.

The p65 nuclear localization was measured for each cell line in each oxygen protocol before and after irradiation and then normalized against the unirradiated normoxic control for that timepoint.

3.7.1. A549 cells after X-rays exposure at 20 %, 1 % and 0.1 % oxygen

Under normoxia, X-rays exposure resulted in increased p65 nuclear intensity 6 and 24 h after irradiation compared to the unirradiated control (Figure 1.1Figure 3.20 Upper Panel). In case of continuously hypoxic cells at 1 % O_2, p65 nuclear intensity showed a trend of rising earlier, 2 h post irradiation in comparison to its unirradiated control. The radiation-induced increase in p65 nuclear intensity under continuous hypoxia (1 % O_2) was also observed 6 h and 24 h after X-rays exposure.

However, the baseline p65 nuclear intensity at any time point was lower than that in the corresponding normoxic control.

Cells kept under continuous hypoxia at 0.1 % O_2 (Figure 3.20 Lower Panel) did not show any increase in p65 nuclear intensity following irradiation compared to their unirradiated controls. However, the baseline p65 nuclear intensity at any time point tended to be higher than that in the corresponding control.

So, it may be concluded that oxygen concentration of 1 % resulted in a trend toward earlier activation of the NF-κB pathway following X-rays exposure in A549 cells while the oxygen concentration of 0.1 % resulted in a constitutional increase in NF-κB pathway activation independent of irradiation.

3.7.2. A549 cells after X-rays exposure under normoxia, continuous hypoxia and transient hypoxia

In case of A549 cells maintained at 1 % O_2, reoxygenation of cells following X-rays exposure resulted in the same picture as continuous hypoxia with a trend toward earlier nuclear translocation resulting in higher nuclear intensity of p65 at 2 h compared to unirradiated control. p65 nuclear intensity increased also 6 h and 24 h following X-ray exposure (Figure 3.20 Upper Panel).

On the other hand, for cells maintained at 0.1 % O_2, reoxygenation dramatically decreased the constitutionally increased p65 nuclear intensity that was detected in case of continuous hypoxia (Figure 3.20 Lower Panel).
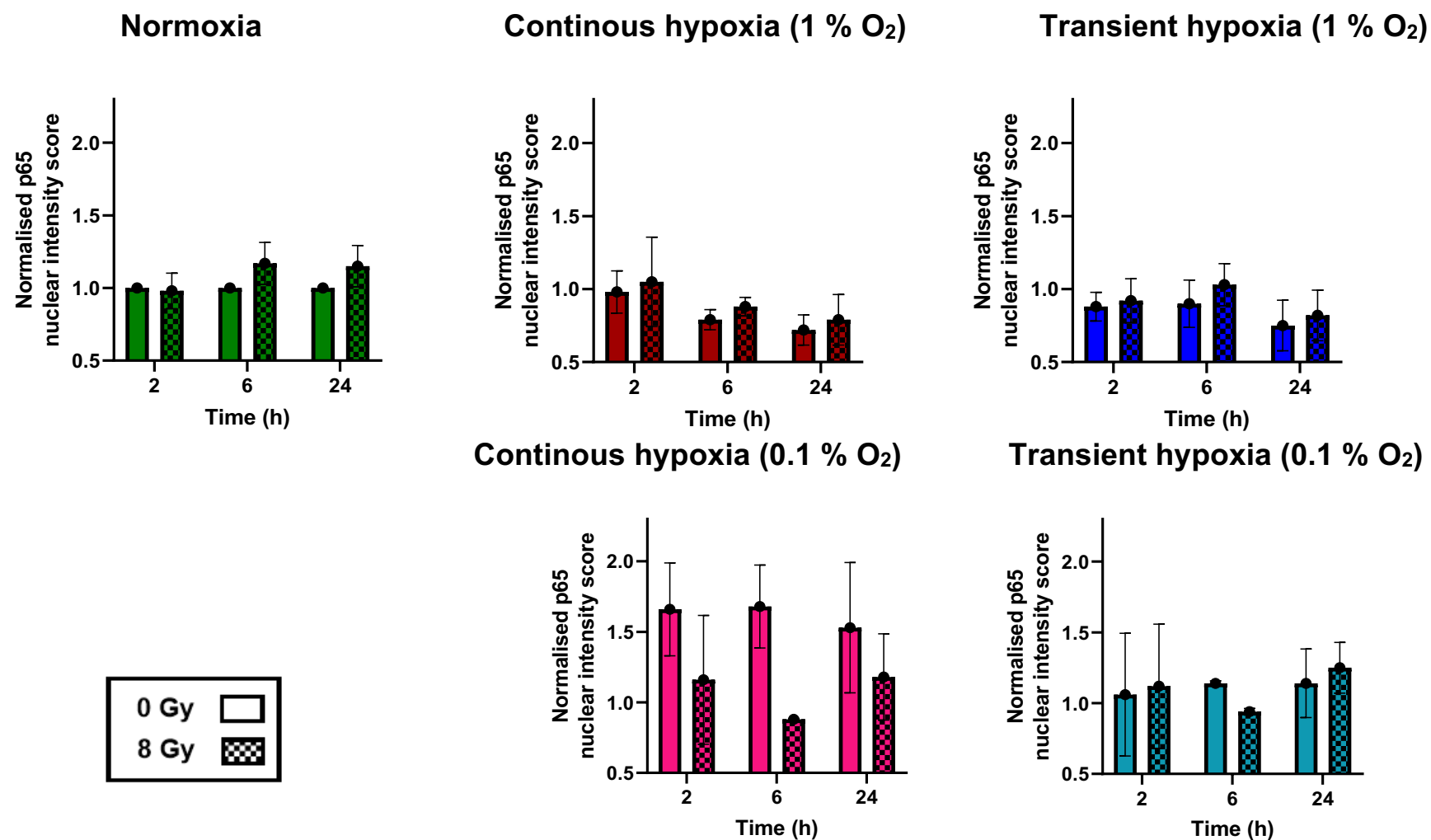
Figure 3.20   p65 translocation from cytoplasm to nucleus in A549 cells maintained at under different oxygen protocols after exposure to X-rays. Upper panel: normoxia (green), continuous hypoxia – 1 % O_2 (red) and transient hypoxia – 1 % O_2 (blue). Lower panel: continuous hypoxia – 0.1% O2 (pink) and transient hypoxia – 0.1 % O2 (cyan). The nuclear intensity score was normalized to the nuclear intensity score of unirradiated normoxic controls at corresponding time points following X-rays exposure. n = 3. Error bars represent SE.

3.7.3. A549 cells after carbon ion exposure under normoxia, continuous hypoxia and transient hypoxia

NF-κB pathway activation was analyzed in continuously and transiently hypoxic (1 % O_2) A549 cells in comparison to normoxic controls following carbon ion exposure to evaluate the effect of high-LET radiation (Figure 3.21).

Both continuously and transiently hypoxic A549 cells show an increase in p65 nuclear intensity 2 h after carbon ion exposure compared to their unirradiated controls. This early increase in p65 nuclear intensity did not occur in normoxic cells. Both normoxic and hypoxic cells show an increase in p65 nuclear intensity 6 and 24 h after irradiation. Furthermore, at 1 % O_2, A549 cells tend to have lower p65 nuclear intensity at baseline in the absence of irradiation compared to unirradiated normoxic controls for that time point.

In other words, hypoxic A549 cells show earlier activation of NF-κB pathway compared to normoxic controls following carbon ion exposure as it was the case following X-rays exposure.

3.7.1. H358 cells after X-rays exposure in normoxia, continuous hypoxia and transient hypoxia

NF-κB pathway activation was also evaluated in continuously and transiently hypoxic (1 % O_2) H358 cells in comparison to normoxic controls following X-rays exposure in order to determine possible differences or similarities in the response of A549 and H358 cells (Figure 3.22).

An increase in p65 nuclear intensity in response to X-rays exposure was detected in continuously hypoxic H358 cells at 2, 6 and 24 h after irradiation when compared to their unirradiated controls. Normoxic cells, on the other hand, only showed increase p65 nuclear intensity 6 h following X-rays exposure. As in A549 cells, p65 nuclear intensity was constitutionally lower in continuously hypoxic H358 cells compared to their normoxic counterparts.

In transiently hypoxic cells, p65 nuclear intensity did not increase following irradiation but constitutional p65 nuclear intensity in these cells appeared to be higher than that observed in continuously hypoxic cells at 2 and 24 h timepoints.

Normoxia

Continous hypoxia (1 % O₂)

Transient hypoxia (1 % O₂)
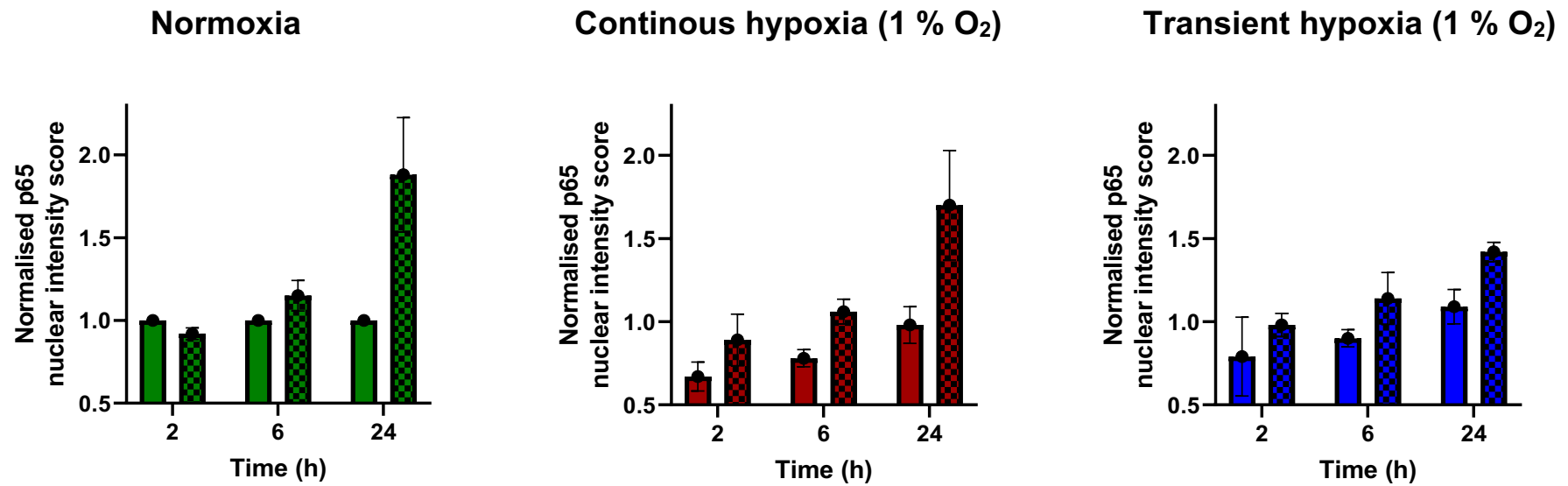
Figure 3.21   p65 translocation from cytoplasm to nucleus in A549 cells maintained at normoxia (green), continuous hypoxia – 1 % O₂ (red) and transient hypoxia – 1 % O₂ (blue) after exposure to carbon ions. The nuclear intensity scores were normalized to the nuclear intensity score of unirradiated normoxic controls at corresponding time points. n = 3. Error bars represent SE.

0 Gy

8 Gy
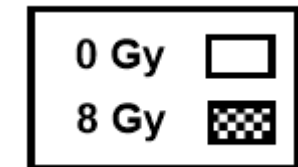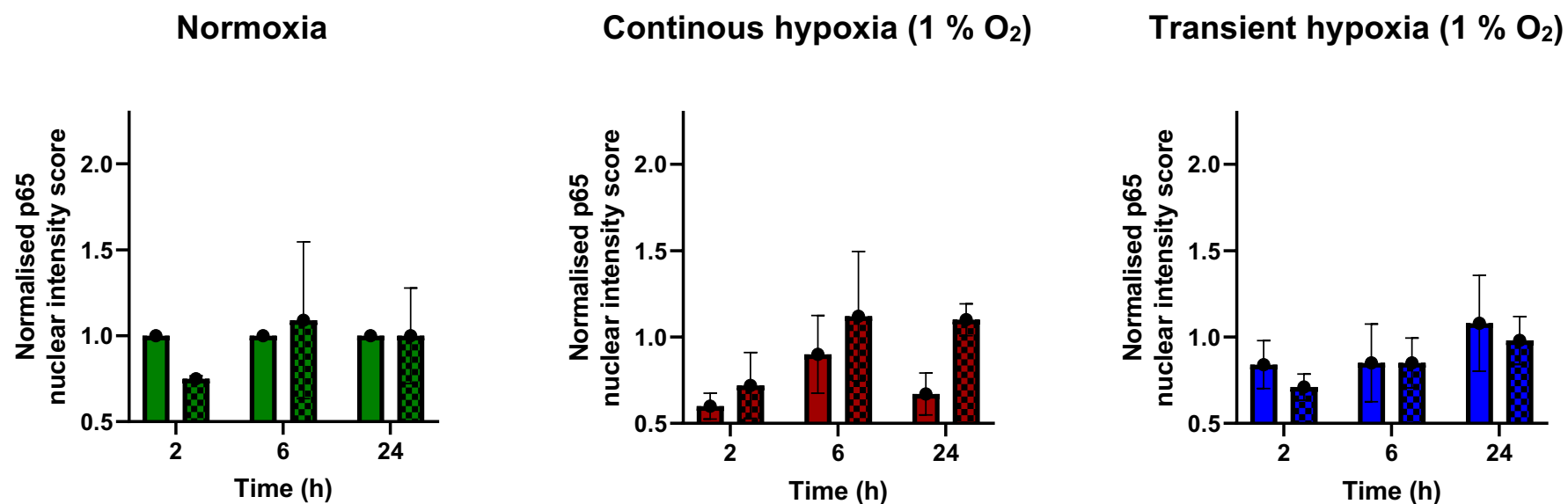
Figure 3.22   p65 translocation from cytoplasm to nucleus in H358 cells maintained at normoxia (green), continuous hypoxia – 1 % O_2 (red) and transient hypoxia – 1 % O_2 (blue) after exposure to X-rays. The nuclear intensity scores were normalized to the nuclear intensity score of unirradiated normoxic controls at corresponding time points. n = 3. Error bars represent SE.
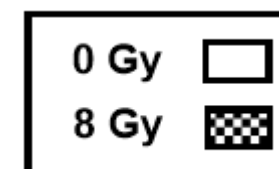
3.8. Secretion of NF-κB target cytokines after radiation exposure under normoxia and hypoxia

To determine if earlier activation of the NF-κB pathway in hypoxic cells translated into greater secretion of its target cytokines, IL-6 and IL-8 were selected because differential gene expression analysis showed that hypoxic A549 cells upregulated both IL-6 and IL-8 following irradiation compared to normoxic controls, while hypoxic H358 cells differentially upregulated only IL-8 in comparison to normoxic controls.

The IL-6 and IL-8 amounts measured in the supernatants of normoxic and hypoxic cells were normalized against the cell number in the respective cell culture dish to compensate for slower cell proliferation under hypoxia and after irradiation resulting in lower cell numbers. Therefore, the cytokine secretion was calculated as the amount in pg per one million cells. For the timepoint 6 h, the cumulative cytokine amount produced and secreted within 6 h after irradiation was quantified. For the 24 h timepoint, the amount accumulated in the supernatant over 24 h was quantified.

3.8.1. A549 cells following X-rays exposure at 20 %, 1 % and 0.1 % oxygen

For both timepoints, basal IL-6 secretion was increased in hypoxic A549 (1 % and 0.1 % O_2) cells compared to normoxic cells (Figure 3.23). Cells that were exposed to 8 Gy X-rays produced more IL-6 than unexposed controls and in this case, the lower the O_2 concentration, the higher was the IL-6 secretion in response to irradiation.

IL-8 secretion by A549 cells showed similar dependence on O_2 levels and X-rays exposure (Figure 3.23). These effects reach statistical significance 24 h after irradiation. X-rays-exposed cells produced more IL-8 than unexposed controls. In comparison to normoxic cells, continuously hypoxic cells maintained at 0.1 % O_2 had the highest secretion of IL-8, followed by continuously hypoxic cells maintained at 1 % O_2.

3.8.2. A549 cells following X-rays exposure in normoxia, continuous hypoxia and transient hypoxia

As shown in Figure 3.23, the presence (transient hypoxia) or absence (continuous hypoxia) of reoxygenation impacted overall IL-6 secretion. At the 24 h time point, continuously hypoxic cells at 1 % O_2 produced more IL-6 in the absence and presence of irradiation when compared to both normoxic and transiently hypoxic (1 % O_2) cells. Reoxygenation did not reduce IL-6 secretion significantly in transiently hypoxic cells initially kept at 0.1 % O_2 when compared with continuously hypoxic cells at 0.1 % O_2.

A similar trend was observed for IL-8 secretion by A549 cells where at the 24 h timepoint, continuously hypoxic cells at 1 % O_2 tended to produce more IL-8 in the absence or presence of irradiation in comparison to both normoxic and transiently hypoxic (1 % O_2) cells. Once again, as it was observed for IL-6, in cells initially at 0.1 % O_2, reoxygenation did not significantly reduce IL-8 secretion in transiently hypoxic cells kept initially at 0.1 % O_2 when compared with continuously hypoxic cells at 0.1 % O_2.

Lastly, the 24 h timepoint makes it clear that reoxygenation in case of transiently hypoxic cells initially kept at 1 % O_2, did not decrease IL-8 secretion as much as IL-6 secretion.

Overall, the cytokine results are indicative of a high probability of NF-κB activation in A549 cells secondary to X-ray exposure and also due to hypoxia.
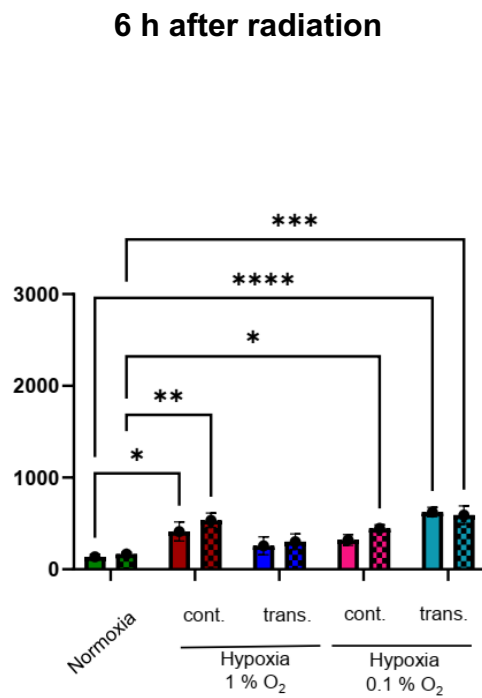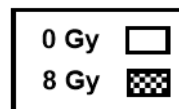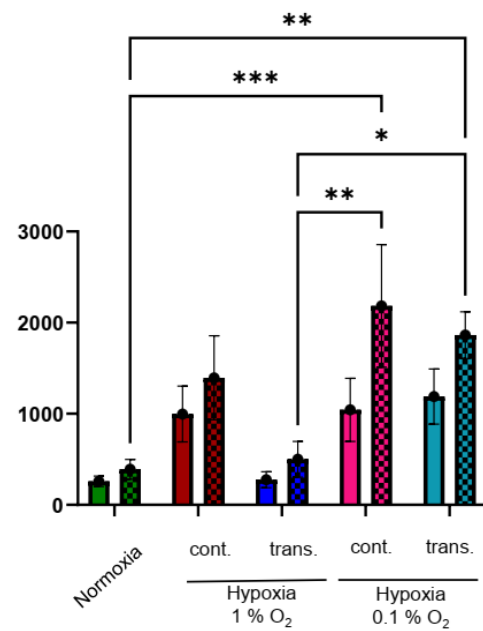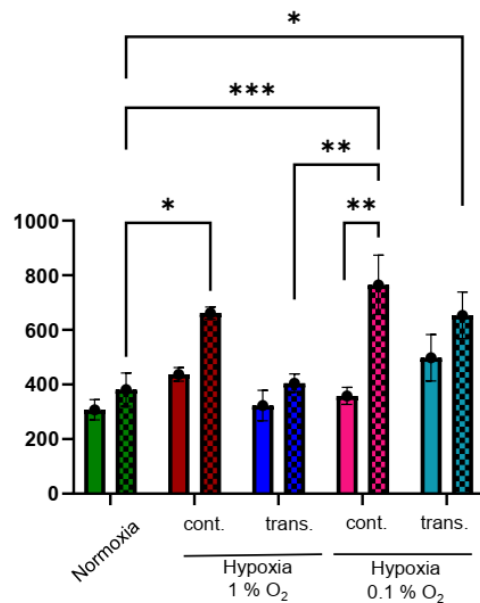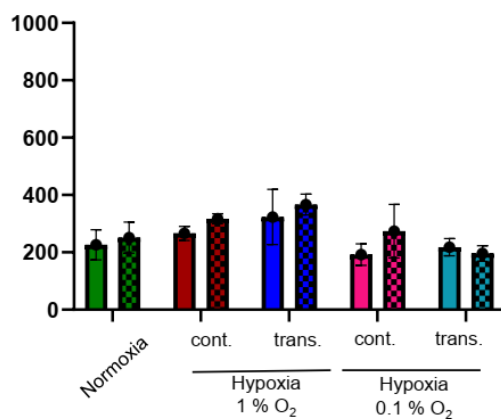
Figure 3.23   IL-6 (top) and IL-8 (bottom) secretion of A549 cells 6 h (left) and 24 h (right) after exposure to X-rays and incubation at 20 % (normoxia), 1 % or 0.1 % oxygen before and during (transient hypoxia) or before, during and after irradiation (continuous hypoxia). *: p<0.05; **: p<0.01; ***: p<0.001; ****: p<0.0001; n = 3. Error bars represent SE.

3.8.3. A549 cells following carbon ion exposure in normoxia, continuous hypoxia and transient hypoxia

Cytokine secretion of A549 cells after exposure to carbon ions (Figure 3.24) was quantified to determine whether the radiation quality (high-LET vs. low-LET) has an influence on IL-6 and IL-8 secretion under normoxia and hypoxia (1 % O_2).

As it was the case after irradiation with X-rays, IL-6 and IL-8 production were influenced by both, irradiation and O_2 levels. Carbon ion-exposed cells secreted more of these cytokines than their corresponding unirradiated controls. Cumulative IL-6 and IL-8 secretion 24 h following carbon ion exposure was greatest under continuous hypoxia yet reduction in IL-8 secretion following reoxygenation (in transiently hypoxic cells) was not as strong as for IL-6.

Furthermore, the cytokine release per one million A549 cells in the first 6 h was higher than that in the overall 24 h period for both normoxia and transient hypoxia leading to an overall lower IL-6 and IL-8 secretion after carbon ion exposure compared to X-rays exposure when normalized for cell count. Only the continuously hypoxic A549 seemed to be spared from this slowing down of cytokine secretion over time.

3.8.4. H358 cells following X-rays exposure in normoxia, continuous hypoxia and transient hypoxia

The effect of transient and continuous hypoxia on IL-6 and IL-8 secretion in comparison to normoxia, following X-rays exposure, was also studied using the H358 cells to assess possible similarities or differences to A549 cells.

While exposure of H358 cells to X-rays slightly increased their IL-6 production 24 h after irradiation, no stimulatory effect of hypoxia on cytokine release was observed (Figure 3.25).

In the absence of irradiation, basal IL-8 secretion tended to be higher in cells under continuous and transient hypoxia in comparison to those in normoxia. 24 h following irradiation, IL-8 secretion increased in both normoxic and continuously hypoxic cells although this increase was statistically significant only in case of normoxia. Transiently hypoxic H358 cells showed no increase in IL-8 secretion in response to X-rays exposure which can be correlated to them not showing an increase in p65 nuclear intensity following irradiation.

Overall, the IL-6 results are indicative of a high probability of NF-κB activation in H358 cells in response to X-rays exposure while the IL-8 results allude to the possibility of NF-κB activation secondary to both X-rays exposure and hypoxia.
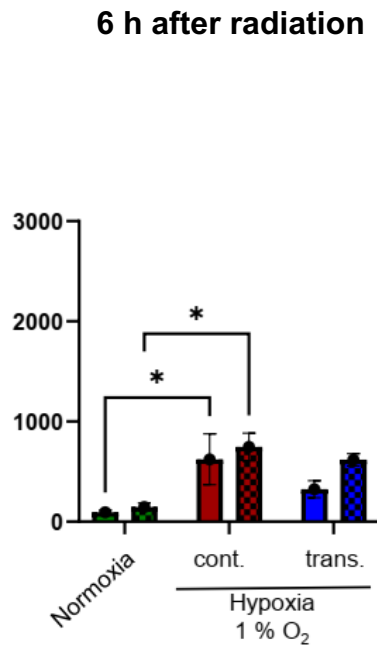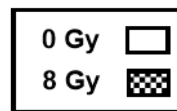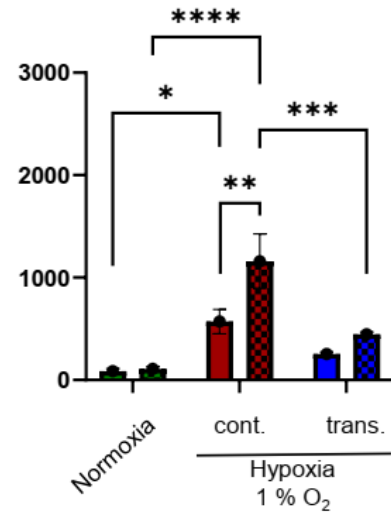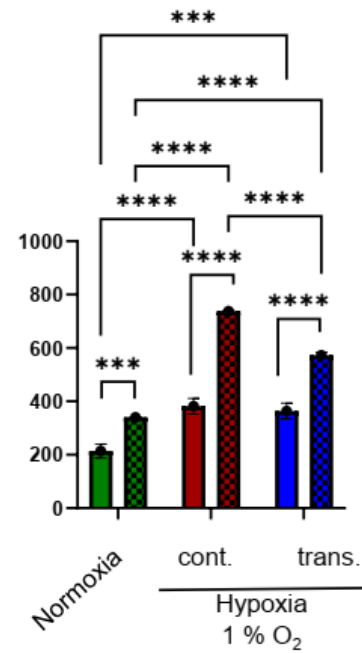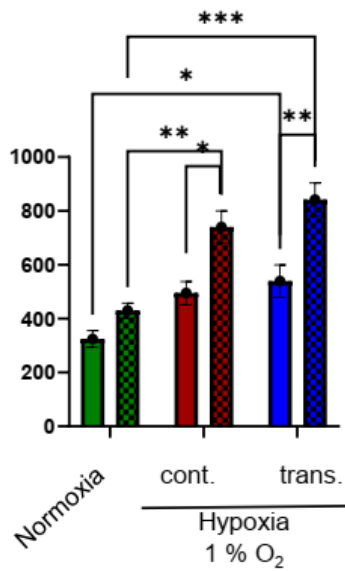
Figure 3.24   IL-6 (top) and IL-8 (bottom) secretion of A549 cells 6 h (left) and 24 h (right) after carbon ion exposure and incubation at 20 % (normoxia) or 1 % oxygen before and during (transient hypoxia) or before, during and after irradiation (continuous hypoxia). *: $p<0.05$; **: $p<0.01$; ***: $p<0.001$; ****: $p<0.0001$; n = 3. Error bars represent SE.
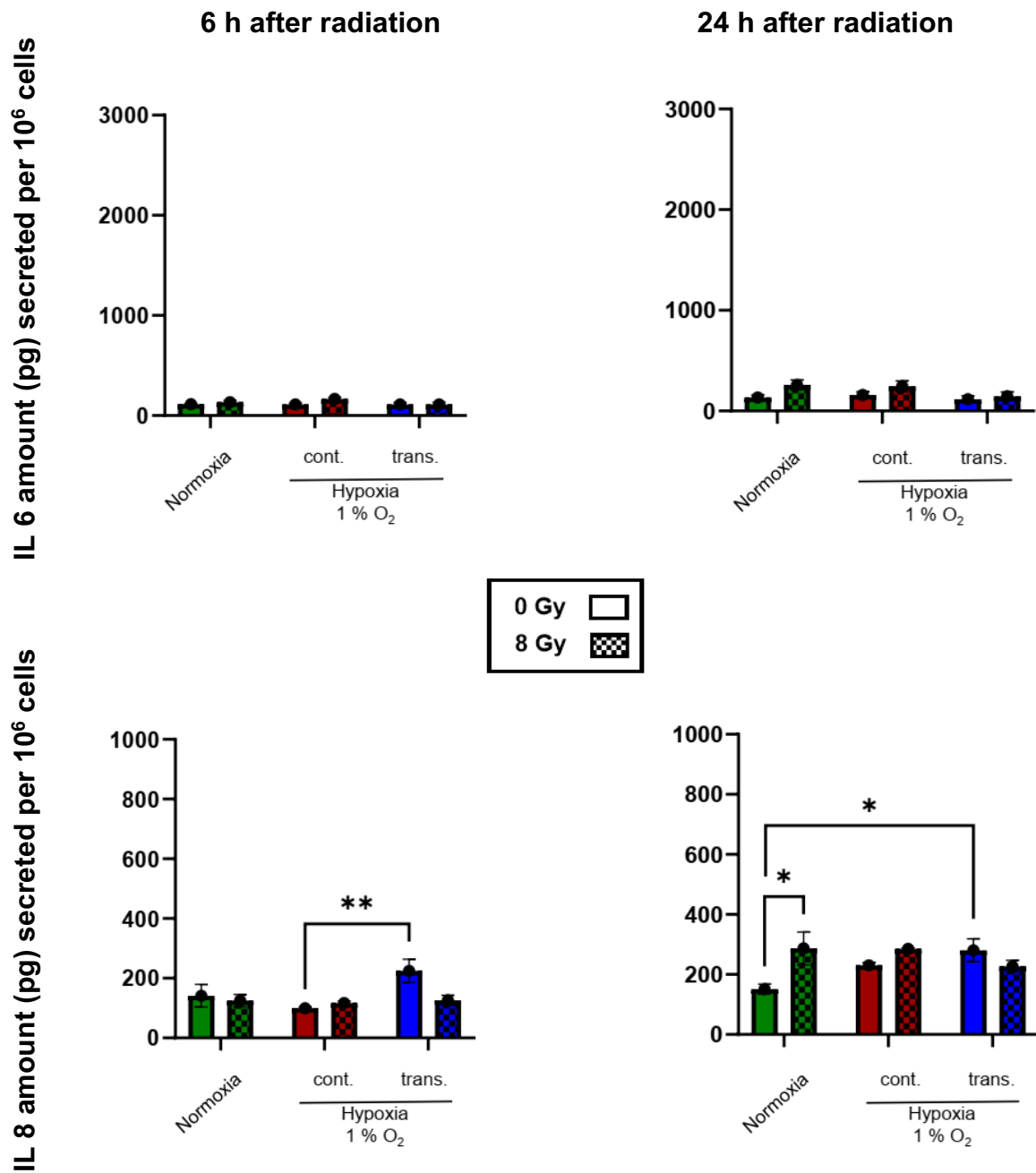
*Figure 3.25   IL-6 (top) and IL-8 (bottom) secretion of H358 cells 6 h (left) and 24 h (right) after X-rays exposure and incubation at 20 % (normoxia) or 1 % oxygen before and during (transient hypoxia) or before, during and after irradiation (continuous hypoxia). *: p<0.05; **: p<0.01; n = 3. Error bars represent SE.*

4. Discussion

This chapter aims to interpret results of this study in the context of existing literature and of the aims which were to characterize the influence of hypoxia and reoxygenation on resistance to low- and high-LET radiation, to evaluate the DDR under hypoxia and reoxygenation in the context of cell cycle progression, DSBR and activation of the pro-survival NF-κB pathway, and to correlate differential gene expression under hypoxia with these aspects of DDR (Figure 4.1).
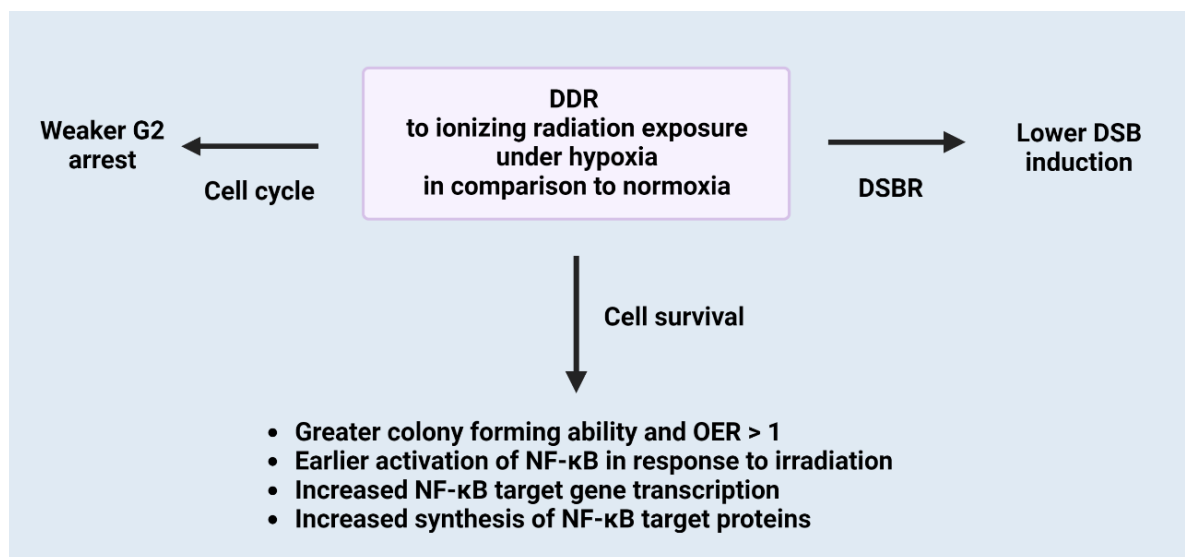
Figure 4.1   Schematic summarizing the DDR in A549 and H358 cells following exposure with low- and high-LET ionizing radiation.

DDR, DNA damage response; DSB, double strand break; DSBR, double strand break repair; G2, G2 phase of the cell cycle; OER, oxygen enhancement ratio. Created with Biorender.com.

4.1.   Hypoxia induces radioresistance in NSCLC cell lines

While it is textbook knowledge that tumor hypoxia induces radioresistance (50,58,77,78), there are also several reports in literature that tumor hypoxia may conversely confer radiosensitivity in tumor cells *in vitro* (79,80).

Therefore, as a first step in this work, it was imperative to establish the effect of X-irradiation in presence of 1 % and 0.1 % O_2 on cell survival in NSCLC cell lines *in vitro* through a standard functional assay like Puck's CFA assay. Both 1 % and 0.1 % O_2 concentrations are common occurrences in clinical tumors (24).

The D_0, which is the radiation dose that reduces the viable tumor cell population to 37 % (1 natural log kill) of the pre-irradiated cell number, was used as a measure of radioresistance. The higher the D_0, the greater is the radioresistance, and vice versa.

The oxygen enhancement ratio (OER) which is the ratio of the radiation dose needed to produce a biological effect at normal oxygen partial pressure (D_0 under normoxia) compared to that needed at reduced oxygen partial pressure (D_0 under hypoxia) was used as an additional index to objectively represent hypoxia-induced radioresistance.

Several conclusions can be drawn from CFA experiments carried out in this study.

4.1.1. The "oxygen effect" contributes to the observed radioresistance

The "oxygen effect" in radiobiology postulates that tumor hypoxia induces radioresistance in tumor cells as a result of reduced production of ROS decreasing "indirect" DNA damage, as well as reduced peroxidation of damaged DNA sites resulting in easier and faster repair (51). This is a physicochemical effect and depends on relative oxygenation at the time of irradiation. It is not impacted by hypoxia prior to or after irradiation.

The oxygen effect results in progressive increase in radioresistance in irradiated cells at O_2 partial pressures below 10 millimeters of mercury (mm Hg) (equal to 1.4 % O_2) compared to normoxia (Table 4.1). Under anoxia (0 mm Hg), the OER is around 3 in mammalian cells (51). This OER decreases to about 1.5 at an oxygen partial pressure of 3 mm Hg and reaches unity at an oxygen partial pressure of 10 mm Hg (51,81). 1 % O_2 is equal to 7.8 mm Hg while 0.1 % O_2 is equal to 0.78 mm Hg which are both in the radiobiological range where an oxygen effect may be observed.

To assess the *oxygen effect,* immediate plating (IP) CFAs comparing transiently hypoxic cells with normoxic controls were performed. The immediate seeding of irradiated cells for growth of colonies in IP experiments ruled out the impact of hypoxia-related DDR on repair and survival that occurs in case of late plating, while the subsequent reoxygenation of irradiated cells (transient hypoxia) eliminated the impact of continuous hypoxia on DDR following irradiation. In order to detect the impact of oxygen effect on cell survival, based solely on differences in radiochemistry, incubation time of cells should be minimized to as less as needed to bring intracellular O_2 concentration to 1 % and 0.1 % and the relatively long 48 h incubation time used in this work may influence the OER through non-radiochemical effects of hypoxia on DDR discussed later (82).

Radioresistance of A549 cells was higher at 1 % O_2 (D_0= 2.23 Gy; OER= 1.13) and 0.1 % O_2 (D_0= 2.09 Gy; OER= 1.05) compared to 20 % O_2 (D_0= 1.98 Gy) following X-rays exposure (Figure 3.5A; Table 3.2 & Table 3.3).

Table 4.1 O_2 partial pressures and oxygen effect in mammalian cells

O_2 partial pressures	Oxygen enhancement ratio (OER)	Reference
0 mm Hg (0 % O_2)	3	(51)
0.78 mmHg (0.1 % O_2)	1.05 ± 0.03	This work
3 mm Hg (0.4 % O_2)	1.5	(51,81)
7.8 mm Hg (1 % O_2)	1.13 ± 0.03	This work
10 mm Hg (1.4 % O_2)	1	(51,81)

The results were verified in the second NSCLC cell line, H358 (Figure 3.8A; Table 3.6 & Table 3.7), where cells incubated and exposed to X-rays under normoxia were slightly less radioresistant compared to H358 cells exposed to X-rays under 1 % O_2 (D_0= 2.36 Gy vs. 2.4 Gy respectively; OER= 1.02). The OER values though statistically significant are not noticeably higher than 1 and so the physicochemical effect of the lower molecular oxygen concentration resulting in lower initial damage does not appear particularly obvious in A549 and H358 cells.

When the oxygen effect is evaluated for high-LET carbon ions (Figure 3.7A; Table 3.4 & Table 3.5), the hypoxic A549 cells are in fact more radiosensitive than normoxic cells (D_0= 1.59 Gy

vs. 1.93 Gy respectively; OER= 0.83). This is mechanistically justifiable as high-LET radiation relies solely on "direct action" damage to DNA and is not dependent on ROS production for amplifying DNA damage through "indirect action" as is the case with X-rays (83).

4.1.2.   DDR contributes to observed radioresistance

Besides reduced initial DNA damage due to the *oxygen effect*, hypoxia is also known to impact cell repair, proliferation and pluripotency, thereby improving cell survival, through a multitude of cellular adaptations which confer an aggressive and treatment-resistant phenotype to the tumor cells during their hypoxic incubation. These hypoxia-induced phenotypic changes also influence the DDR to irradiation.

The experimental set up used to evaluate the role of the DDR in survival of NSCLC cells following prior hypoxic incubation were late plating (LP) CFAs comparing transiently hypoxic cells to normoxic controls. The seeding of cells after a delay of 24 h following irradiation in LP experiments screened out the cells that undergo early death and provided others time for repair and reconsolidation which is not the case in IP experiments, while the subsequent reoxygenation of irradiated cells (transient hypoxia) eliminated the impact of continuous hypoxia on DDR following irradiation. Nonetheless, IP experiments discussed earlier in section 4.1.1 may also be impacted in part by DDR modulation as part of the cellular response to hypoxia due to hypoxic incubation of 48 h.

Hypoxia-induced radioresistance in LP experiments was greater compared to IP experiments for both A549 and H358 cells. For A549 cells (Figure 3.5B; Table 3.2 & Table 3.3) exposed to 0.1 % O_2, D_0 increased from 2.09 Gy (OER= 1.05) to 2.87 Gy (OER= 1.64) while for those incubated at 1 % O_2 D_0 raised from 2.23 Gy (OER= 1.13) to 2.32 Gy (OER= 1.32) in IP vs. LP experiments using X-rays. In case of carbon ions (Figure 3.7B; Table 3.4 & Table 3.5), the D_0 augmented from 1.59 Gy (OER= 0.83) to 1.62 Gy (OER= 1.09) for A549 cells incubated at 1 % O_2 in IP vs. LP experiments. On the other hand, for normoxic cells, the D_0 decreased from 1.98 Gy to 1.75 Gy in IP vs. LP experiments in case of X-rays and from 1.93 Gy to 1.49 Gy in case of carbon ions. Finally, H358 cells (Figure 3.8B; Table 3.6 & Table 3.7) show the same trend where for cells incubated at 1 % O_2 the D_0 increased in IP vs. LP experiments from 2.40 Gy (OER= 1.02) to 2.73 Gy (OER= 1.08) which is higher than the increase in D_0 from 2.36 Gy to 2.54 Gy in cells incubated under normoxia.

Additionally, experiments with A549 cells incubated at 0.1 % O_2 show that radioresistance increases as severity of hypoxia increases, where cells at 1 % O_2 (D_0= 2.32 Gy; OER= 1.05) and 0.1 % O_2 (D_0= 2.87 Gy; OER= 1.64) are progressively more radioresistant than normoxic cells at 20 % O_2 (D_0= 1.75 Gy). Interestingly, in LP experiments with carbon ion exposure, hypoxic cells (D_0= 1.62 Gy, OER= 1.09) prove to be more radioresistant than normoxic cells (D_0= 1.49 Gy) as opposed to IP experiments where hypoxic cells were in fact more radiosensitive.

These results indicate that prior hypoxic incubation results in cellular adaptations in both NSCLC cell lines. These adaptations enable cells, when provided time through late plating, to modulate their DDR in a way which makes them more radioresistant to X-rays exposure. The DDR modulation also confers radioresistance against carbon ions as observed in A549 cell experiments.

According to literature, the observed hypoxia-induced radioresistance may be attributable to more effective DNA double strand break repair (DSBR) (78,82,84). In one of these studies, inhibition of DNA-PKc led to a 3.34 times reduction in surviving fraction of A549 cells after 4 Gy under hypoxia compared to 1.51 times reduction in the same under normoxia (78).

4.1.3. Hypoxia continuing after irradiation modulates DDR to confer both radioresistance and radiosensitivity

During radiotherapy, it is assumed that the tumor shrinks in response to a dose fraction and that reoxygenation of tumor cells occurs. However, this reoxygenation may be incomplete or delayed and hypoxia may persist after irradiation. Therefore, it was questioned whether tumor hypoxia continuing even after irradiation impacted the DDR and survival of NSCLC cells. To the best of my knowledge this question has not been addressed with clarity in existing literature.

The experimental setup for this purpose necessitated distinguishing between transiently and continuously hypoxic tumor cells, the former were kept hypoxic only until irradiation while the latter were kept hypoxic through the entire period of cell repair and colony growth. Both IP and LP experiments were performed.

Radioresistance in continuously hypoxic cells in LP CFAs (Figure 3.6B, Figure 3.7B & Figure 3.8B) largely mimicked results of LP CFAs in transiently hypoxic cells discussed in subchapter 4.1.2. Continuously hypoxic A549 cells were more radioresistant than normoxic cells with D_0 values of 2.16 Gy (OER= 1.23) compared to 1.75 Gy respectively in case of exposure to X-rays (Table 3.2 & Table 3.3). Also, H358 cells exposed to X-rays were more radioresistant under continuous hypoxia with a D_0 of 3.05 Gy (OER= 1.20) compared to 2.54 Gy for normoxic cells (Table 3.6 & Table 3.7). Similarly, after exposure of A549 cells to carbon ions, the D_0 of 2.27 Gy (OER= 1.52) for continuously hypoxic cells was higher compared to 1.49 Gy for normoxic cells (Table 3.4 & Table 3.5).

However, the findings of IP experiments were surprising: Even though cells maintained under continuous hypoxia were more radioresistant than those under normoxia in LP experiments, they were more radiosensitive than corresponding normoxic controls in IP experiments (Figure 3.6A, Figure 3.7A & Figure 3.8A). This was observed for A549 (D_0= 1.41 Gy vs. 1.98 Gy, OER= 0.71) and for H358 cells (D_0= 2.30 Gy vs. 2.36 Gy, OER= 0.97) exposed to X-rays (Table 3.2, Table 3.3, Table 3.6 & Table 3.7) as well as for A549 cells exposed to carbon ions (D_0= 1.61 Gy vs. 1.93 Gy, OER= 0.84) (Table 3.4 & Table 3.5).

Based on IP experiments, it appears that an overwhelming early effect of hypoxia continuing after irradiation *in vitro* is cell death. This effect gets masked in LP experiments where viable cells, having had ample time to repair, are seeded 24 h after irradiation. Since early cell death did not occur if cells are reoxygenated immediately after irradiation (transient hypoxia), it is concluded to be a direct consequence of continuous hypoxia on the DDR of cells.

The mechanistic explanation for exaggerated cell death under continuous hypoxia in case of IP may largely be contributed by activation of p53-mediated apoptosis following irradiation (79). However, in case of LP, the early pro-apoptotic DDR may be overtaken by later onset pro-survival DDR pathways. This explanation is supported by the observation that radiosensitivity of p53-null H358 cells is relatively less affected (D_0= 2.30 Gy vs. D_0= 2.36 Gy under hypoxia vs. normoxia) compared to p53-wt A549 cells (D_0= 1.41 Gy vs. 1.98 Gy under hypoxia vs. normoxia after X-rays exposure, and D_0= 1.61 Gy vs. 1.93 Gy under hypoxia vs. normoxia after carbon ion exposure) in IP experiments.

4.2. RBE of carbon ions is high regardless of oxygenation status

The relative biological effectiveness (RBE) is the ratio of the radiation dose of reference radiation to the radiation dose of test radiation required to produce the same biological effect. In this study, X-rays were the reference radiation while carbon ions were the test radiation. The RBE is thus used an index for quantifying the effectiveness of carbon ions in comparison to X-rays in killing A549 and H358 cells based on the D_0 values derived from the survival curves.

Based on the RBE values of carbon ions (Table 3.5), carbon ions are more effective than X-rays in killing A549 cells under normoxia as well as hypoxia (1 % O_2). Carbon ions are being used in increasing number of clinical trials because of their advantage of having a higher RBE compared to X-rays and physical advantages such as more precise dose targeting of the tumor and sparing of normal tissues (85). Clinical trials using carbon ions to treat NSCLC were started already in 1996 in Japan (86–91). Despite promising local tumor control and overall survival, due to high costs, charged particle therapy of lung cancer is still considered experimental (92).

The observation that RBE of carbon ions under hypoxia remains comparable to that under normoxia is encouraging from the therapy perspective and has been reported in literature recently in A549 cells at 1 % O_2, starting 16 h before irradiation with carbon ions in the spread-out Bragg peak (78). For comparison, in A549 cells, an RBE of 3 for carbon ions in the spread-out Bragg peak (LET 50-70 KeV/μm) was determined by Subtil et al. (2014) at GSI Helmholtzzentrum in Darmstadt, Germany (93).

For calculation of RBE of carbon ions, D_0 values were used that were calculated in a dose range from 0 to 4 Gy but not higher. This is because the carbon ions dose response curves show a sharp drop in dose gradient beyond 4 Gy regardless of oxygenation status. The normoxic survival curve up to a dose of 4 Gy is comparable to published data on A549 survival after carbon ion exposure in a similar LET range (94). Survival data for carbon ion doses above 4 Gy are scarce. Literature review suggests that this may be due to "overkill" or dose "wasting" which may be observed with high-LET radiation beyond a certain dose due to excess energy deposition beyond what is necessary to cause cell lethality (95).

4.3. Gene expression analysis following irradiation for profiling DDR in hypoxic cells

To light on potential molecular mechanisms explaining hypoxia-induced radioresistance observed in the NSCLC cell lines A549 and H358 *in vitro*, differential gene expression analysis was carried out for both cell lines following RNA extraction 4 h after irradiation under hypoxia (1 % O_2) vs. normoxia.

DDR following irradiation comprises three main components: cell cycle inhibition, DNA repair particularly DSB repair, and cell survival vs. cell death promoting signaling (52,96). Therefore, the analysis focused on differential expression of cell cycle genes, HR and NHEJ genes, and the target genes of the NF-κB pathway, a primary pro-survival and pro-inflammatory mammalian pathway, reported in literature to be activated following hypoxia and after irradiation.

4.3.1. Hypoxia minimally influences cell cycle transcriptional regulation in the absence of irradiation

A list of 129 genes relevant for cell cycle regulation was acquired based on KEGG signaling pathways database (97).

Differential gene expression in hypoxic A549 and H358 cells was evaluated following an incubation of 52 h under 1 % O_2 in comparison to corresponding normoxic controls in the absence of irradiation. In A549 cells, no cell cycle genes were differentially regulated in this comparison while in H358 cells a single gene, namely, CDKN1C was downregulated ($\log_2$ fold change = -1.42).

CDKN1C encodes a cyclin-dependent enzyme inhibitor that inhibits transitioning of cells from G1 to S phase through inhibition of Rb phosphorylation which maintains E2F suppression. Differential downregulation of CDKN1C following irradiation in hypoxic H358 cells may enhance G1/S transition (98).

The relevance of these findings will be discussed alongside results of cell cycle flow cytometric studies in later sections (4.4).

4.3.2. Irradiation under hypoxia regulates both cell cycle inhibitory and promoting genes

Cell cycle regulation in radiation-induced DDR gives irradiated cells time for DNA repair by inducing cell cycle arrests. Differential gene expression in both A549 and H358 cells was evaluated following irradiation under hypoxia compared to irradiation under normoxia.

Irradiation of hypoxic NSCLC cells *in vitro* resulted in regulation of various genes that work antagonistically to inhibit and promote the cell cycle. The overall predominant effect integrating these gene expression changed will be discussed in the context of the cell cycle flow cytometric studies in section 4.5.

4.3.2.1. Transcriptional regulation of cell cycle in A549 cells

In continuously hypoxic A549 cells, GADD45B was differentially upregulated following X-rays exposure but not following carbon ion exposure. E2F2 was differentially downregulated in hypoxic A549 cells following carbon ion exposure but not following X-rays exposure. Both GADD45B upregulation and E2F2 downregulation relative to normoxic cells may cause cell cycle inhibition under hypoxia.

GADD45B, $\log_2$ fold change = 1.20, besides its role in apoptosis, is long understood to

contribute to the G2/M arrest following DNA damage (99). More recently, knocking out GADD45B was shown to reduce radioresistance and tumor cell proliferation in an nasopharyngeal carcinoma cell line suggesting a link between GADD45B induction and enhanced radioresistance through MAPK pathway activation (100). Its differential upregulation following X-rays exposure in hypoxic cells may relatively inhibit G2/M transition.

E2F2, $\log_2$ fold change = -1.10, is a transcription activator whose expression is needed for cells to transition from G1 to S phase. Its overexpression may override the effects of growth inhibitory proteins, such as p16, p21, and p27 (101). Its differential downregulation in hypoxic A549 cells following carbon ions exposure may contribute to relative inhibition of cells transitioning from G1 to S phase.

4.3.2.2.   Transcriptional regulation of cell cycle in H358 cells

In continuously hypoxic H358 cells, STAG1, EP300 and RBL2 were upregulated along with downregulation of CDKN1C and GADD45G following X-rays exposure, in comparison to normoxic controls. The upregulation of STAG1 and EP300 along with downregulation of CDKN1C and GADD45G may promote cell cycle progression while upregulation of RBL2 may inhibit it.

STAG1, $\log_2$ fold change = 1.16, protein becomes part of the cohesion complex which is needed for sister chromatid cohesion during mitosis (102). Upregulation of STAG1 under hypoxia may facilitate mitosis and contribute toward cell proliferation and survival.

RBL2, $\log_2$ fold change = 1.18, protein complexes with the transcription repressor E2F4 and the complex causes inhibition of G1/S transition (103). Its differential upregulation in hypoxic H358 cells may enhance G1/S arrest.

EP300, $\log_2$ fold change = 1.15, codes for a histone acetyltransferase that acts as a cofactor for several transcription factors thereby resulting in transcription of several different genes. Its role in driving G1/S phase transition is well-documented in literature. EP300 inhibition causes cell accumulation in G1 phase through interference with GATA1 and MYC driven transcription (104). So, its differential upregulation in hypoxic H358 cells following X-rays exposure may enhance G1/S transition.

CDKN1C, $\log_2$ fold change = -1.92, downregulation following irradiation is amplified compared to its downregulation by hypoxia alone ($\log_2$ fold change = -1.92 vs. -1.42). Since its expression inhibits transitioning of cells from G1 to S phase, its downregulation following irradiation in hypoxic H358 cells may push cells from G1 to S phase (98).

GADD45G, $\log_2$ fold change = -1.52, like GADD45B, is understood to promote G2/M arrest through inhibition of CDK2/cyclin B1 (99). Its differential downregulation in hypoxic H358 cells following X-rays exposure may result in enhanced G2/M transition.

4.3.2.3.   Reoxygenation after irradiation alters transcriptional regulation of cell cycle

Reoxygenation following irradiation for a period of 4 h, results in normalizing differential gene expression back to that as under normoxia in case of A549 cells. However, reoxygenation of H358 cells following X-rays exposure for a period of 4 h, results in differential upregulation of MYC, TGFB2 and CDK6 and differential downregulation of E2F1 and E2F2. The only cell cycle-related gene that is downregulated in both continuous and transient hypoxia is GADD45G. The upregulation of TGFB2 alongside downregulation of E2F1 and E2F2 may inhibit the cell cycle while the upregulation of MYC and CDK6 alongside downregulation of GADD45G may promote cell cycle progression.

TGFB2, $\log_2$ fold change = 1.71, encoded protein transforming growth factor β2 has been known for decades to inhibit G1/S transition by preventing Rb phosphorylation. The phosphorylation of Rb dissociates it from E2F which can then act as a transcription factor for cyclins and CDKs needed for S phase entry (105). It has also been reported to cause G1 arrest through inhibition of cyclin E-CDK2 complex (106). Its differential upregulation in transiently hypoxic H358 cells reoxygenated following X-rays exposure may contribute to G1 arrest.

MYC, $\log_2$ fold change = 1.67, is known to induce the cell cycle progression by upregulating cyclins (A, B, D and E) and CDKs (1, 2, 4, 6), downregulating CDK inhibitors p15 (CDKN2B) and p21 (CDKN1A) and degrading the CDK inhibitor p27 (CDKN1B) (107,108). Its differential upregulation in irradiated, transiently hypoxic H358 cells following reoxygenation may cause cell cycle propagation, particularly G1/S transition.

CDK6, $\log_2$ fold change = 1.12, has often been reported as a redundant homolog of CDK4 but it has been found to be more commonly expressed in tumor cells compared to CDK4. It causes partial phosphorylation of Rb proteins which is then completed by cyclin E-CDK2 complex facilitating cell transition from G1 to S phase (109,110). Its differential upregulation in transiently hypoxic H358 cells reoxygenated following X-rays exposure may contribute to S phase entry.

E2F1, $\log_2$ fold change = -1.47, like **E2F2,** $\log_2$ fold change = -1.97, is a transcription activator whose expression is needed for cells to transition from G1 to S phase. Phosphorylation of Rb results in disinhibition of E2F1 to upregulate relevant cyclins and CDKs for S phase entry (101). Downregulation of E2F1 and E2F2 in irradiated, transiently hypoxic H358 cells following reoxygenation may inhibit G1/S transition.

GADD45G, $\log_2$ fold change = -1.31, was found to be downregulated following reoxygenation of irradiated H358 cells as was the case in continuously hypoxic H358 cells.

Irradiation of reoxygenated NSCLC cells *in vitro* resulted in regulation of various genes that work antagonistically to inhibit and promote the cell cycle. The overall predominant effect would only be visible in cell cycle flow cytometric studies discussed in sections 4.4 and 4.5.

4.3.3. Irradiation under hypoxia does not differentially regulate DSB repair genes

A list of 41 genes was compiled, identified as constituting Homologous repair (HR) and Non-homologous end joining (NHEJ) double strand break repair (DSBR) according to the KEGG signaling pathways database (111,112). Differential gene expression in both A549 and H358 cells was evaluated following irradiation under hypoxia compared to irradiation under normoxia.

None of the HR and NHEJ genes was differentially regulated in case of irradiation under hypoxia compared to irradiation under normoxia in A549 cells, neither for X-rays nor carbon ions exposure.

In H358 cells, **POLD2,** $\log_2$ fold change = -1.27, was downregulated. POLD2 stands for DNA Polymerase δ 2, Accessory Subunit. It has both polymerase and 3' to 5' exonuclease activity and is therefore involved in both DNA replication and repair. While the KEGG database places this enzyme in the HR pathway, it is mainly involved in long-patch base excision repair pathways and plays a role in managing DNA replication stress (113). Its role in influencing DSBR in response to irradiation with a fold change in this range is improbable but it may have an inhibitory effect on DNA replication.

Ionizing radiation can produce a spectrum of base lesions most commonly including 8-oxo-guanaine, thymine glycol, and formamidopyrimidines. It can also cause single strand breaks (SSBs). These SSBs have a unique signature in that the DNA breaks have 3′ phosphate or 3′-phosphoglycolate ends rather than 3′-OH ends. These lesions are generally effectively repaired and although they may increase mutagenicity if unrepaired but are not playing a significant role in cell death (114).

The reason to focus on DSBR only was that ionizing radiation is known to produce cytotoxicity mainly through unrepaired DSBs in nuclear DNA that result in inability of cells to replicate DNA effectively thereby stalling cell division (52,96,115).

DSBR begins immediately and can be completed within the first 24 h of initial damage, with most DSBR taking place within first 6 h, of which the first hour is the most important (48). While DSBR mainly comprises activation and recruitment of relevant nuclear proteins but transcription of DSBR proteins consumed and further needed picks up in tandem (114,116). In this context, analyzing DSBR differential gene expression 4 h after irradiation seems an appropriate time point for the purpose, but an additional earlier time point may have provided more information.

Not finding any DSBR genes differentially expressed 4 h following irradiation under hypoxia compared to that under normoxia implies that hypoxia-induced radioresistance may not be due to differential transcriptional upregulation of DSBR processes. However, this does not mean that there may not be qualitative differences in DSBR at different oxygen concentrations. For example, it has been reported in literature that DSBR is initiated earlier through faster ATM phosphorylation under hypoxia following X-rays irradiation (60).

Reoxygenation following irradiation did not result in changes in differential gene expression in the context of DSBR.

These findings will be discussed in correlation with the DSB induction and repair based on γH2Ax foci quantification in section 4.6.

4.3.4. Irradiation under hypoxia upregulates NF-κB target genes compared to irradiation under normoxia

Cell death vs. cell survival is the third component of the DDR to irradiation. A literature review revealed that the NF-κB cell signaling pathway is associated with modulating cellular responses to irradiation as well as to hypoxia with an overall effect of promoting cell survival in most cell types (31,62,117). NF-κB activation following a combined effect of irradiation and hypoxia has not been reported in literature to the best of my knowledge.

Several genes with κB promoter elements identified according to literature were upregulated under the combined effect of hypoxia (1 % O_2) and irradiation. The differentially expressed genes under hypoxia, 4 h following irradiation were evaluated using a standard list of NF-κB target genes from the Boston University gene resource database (118) and are categorized as described in the following subchapters and in Figure 4.2.
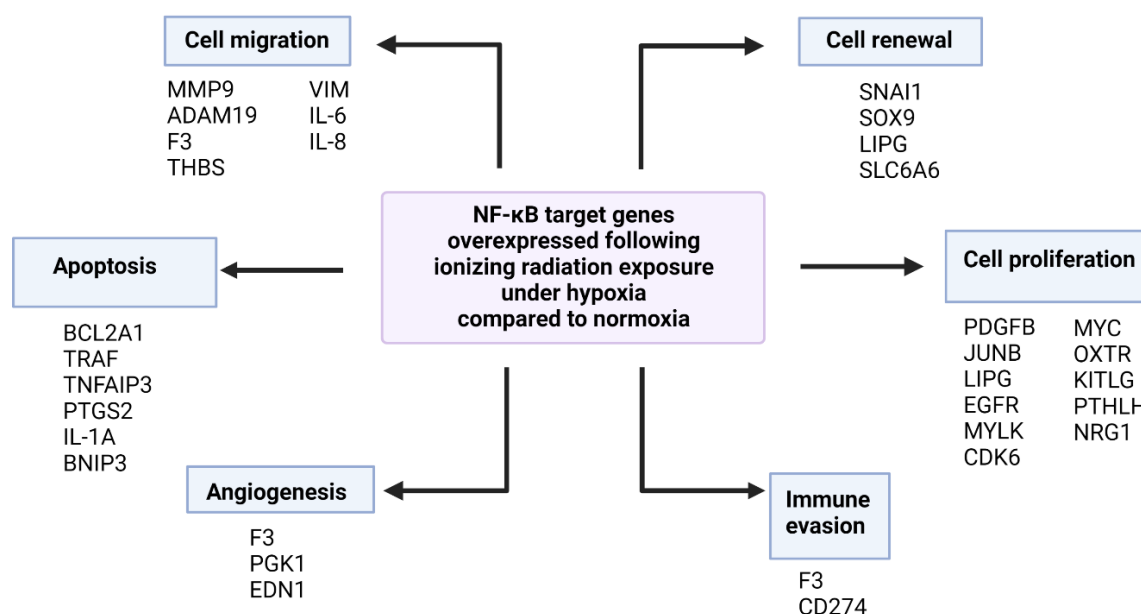
Figure 4.2   Various NF-κB target genes overexpressed in continuously and transiently hypoxic A549 and H358 cells following irradiation in comparison to irradiated normoxic controls. The genes are sorted according to primary functions that may contribute toward better cell survival outcomes.

MMP9, matrix metallopeptidase 9; ADAM19, A disintegrin and metalloproteinase 19; F3, factor 3; THBS, thrombospondin; VIM, vimentin; IL-6, interleukin 6; IL-8, interleukin 8; BCL2A1, B cell leukemia/lymphoma 2 related protein A1a; TRAF, TNF Receptor Associated Factor 1; TNFAIP3, TNFα Induced Protein 3; PTGS2, Prostaglandin-Endoperoxide Synthase 2; IL-1A, interleukin 1α; BNIP3, Bcl2 interacting protein; PGK1, Phosphoglycerate kinase 1; EDN1, endothelin 1; CD274; SNAI1, snail family transcriptional repressor 1; SOX9, SRY-Box Transcription Factor 9; LIPG, lipase G; SLC6A6, solute carrier family 6A6; PDGFB, platelet derived growth factor β; JUNB, transcription factor Jun-B; EGFR, epidermal growth factor receptor; MYLK, myosin light chain kinase; CDK6, cyclin dependent kinase; MYC, Myc proto-oncogene, BHLH transcription factor; OXTR, oxytocin receptor; KITLG, KIT ligand; PTHLH, parathyroid hormone like hormone; NRG1, neuroregulin 1. Created with Biorender.com.

4.3.4.1. Apoptosis-related target genes

The NF-κB pathway has a well-established anti-apoptotic role in most cell lines (119).

4 h following irradiation of (continuously) hypoxic A549 cells, two genes modulating apoptosis were upregulated in comparison to irradiated normoxic controls in case of both, X-rays and carbon ions exposure, namely IL1A (log_2 fold change = 3.52 after X-rays and 2.75 after carbon ions exposure) and BCL2A1 (log_2 fold change = 1.15 after X-rays and 1.52 after carbon ions exposure), the former being proapoptotic while the latter is antiapoptotic. Additionally, the proapoptotic BNIP3 (log_2 fold change = 1.10) was also upregulated following X-rays exposure while the antiapoptotic TRAF (log_2 fold change= 1.28) was upregulated following carbon ion exposure.

No apoptosis-modulating target genes were found to be upregulated in continuously hypoxic H358 cells following X-rays exposure.

Since there is upregulation of both pro-apoptotic and anti-apoptotic genes in A549 cells, it is hard to predict the overall effect of this gene upregulation. However, results from colony forming ability (CFA) assays indicate that this effect on cell survival under hypoxia is not vital because hypoxic cells were more radioresistant than normoxic counterparts.

Nonetheless, the strong upregulation of IL1A following irradiation in hypoxic A549 cells may explain the increased radiosensitivity of these cells in IP experiments while absence of apoptosis-related differential gene expression in hypoxic H358 cells may explain why the same was not detected in their case in IP CFA assays.

IL-1A, has been shown to propagate lung cancer by promoting angiogenesis and lymphangiogenesis in an M2-type macrophage-dependent manner (120). Additionally, and more importantly from the point of view of this research project, it has been reported to induce apoptosis both in normal and tumor cells (121,122). Its inhibition has been shown to suppress apoptosis in breast cancer cells (123).

4.3.4.2. Proliferation and survival-related target genes

Activation of the NF-κB pathway has been identified in a variety of tumors, such as breast and prostate cancers, and associated with tumor proliferation and disease aggressiveness (124,125).

A variety of NF-κB target genes regulating cell proliferation, migration, EMT and angiogenesis were found to be upregulated in hypoxic cells following irradiation and may contribute to hypoxia-induced radioresistance. However, the gene signature for each cell line was unique with little to no overlap.

Both X-rays and carbon ions exposure of A549 cells under (continuous) hypoxia (1 % O_2) resulted in upregulation of an overlapping set of genes namely F3, PDGFB, MMP9, ADAM19 and JUNB.

F3, log_2 fold change = 2.71 after X-rays and 2.06 after carbon ions exposure, also known as Tissue Factor, has been reported to be overexpressed in a variety of malignancies including lung cancer by a variety of mechanisms most commonly through MAPK and JUNB secondary to EGFR activation. F3 induces cell proliferation and angiogenesis via PAR2 activation as well as cell migration via p38 activation. Finally, F3 can support tumor cells to escape immune surveillance through recruitment of myeloid-derived suppressor cells (MDSCs) into the TME (126). F3 overexpression under hypoxia in A549 has been reported in literature previously (127).

PDGFB, $\log_2$ fold change = 1.78 after X-rays and 1.91 after carbon ions exposure, which is normally secreted by platelets and plays an essential role in the regulation of cell proliferation, cell migration and chemotaxis, can also be secreted by a variety of tumors including NSCLC and its inhibition has been shown to result in apoptosis of A549 cells (128). PDGFB has been reported to induce lymphatic metastasis of hypoxic breast cancer cells (129).

JUNB, $\log_2$ fold change = 1.40 after X-rays and 1.34 after carbon ions exposure, is a component of the transcription factor activator protein-1 (AP-1). It has been shown to promote breast cancer proliferation in an NF-κB-dependent manner and inhibition of NF-κB nuclear translocation inhibited AP-1 producing G1 cell cycle arrest (130). AP-1 has long been known to be activated in response to hypoxia (131).

MMP9 ($\log_2$ fold change = 1.62 after X-rays and 2.41 after carbon ions exposure) and **ADAM19** ($\log_2$ fold change = 1.62 after X-rays and 1.56 after carbon ions exposure) are metalloproteases that are important for ECM reorganization and cell migration which enhance cancer invasive and metastatic potential: A relevance to increased radioresistance observed in the *in vitro* experimental setup used in this study is unknown.

Genes that were exclusively regulated in response to X-rays exposure are PGK1 and GADD45B while genes exclusive to carbon ions exposure are SOX9, LIPG and SNAI1. Except for GADD45B (Growth arrest and DNA damage inducible Beta, $\log_2$ fold change = 1.20), all other genes promote cell proliferation, migration or survival.

PGK1, $\log_2$ fold change = 1.51, encodes a glycolytic enzyme that has been reported to have additional functions in angiogenesis, autophagy and DNA repair which are protective and proliferative for tumor cells. Greater expression of PGK1 by tumor cells results in tumor cell proliferation (132).

SNAI1, $\log_2$ fold change = 1.22, has been established as a major transcription factor for induction of EMT resulting in increased stemness and cell migration. Clinically, SNAI1 overexpression is associated with treatment resistance and decreased survival (133). Stabilization of SNAI1 in NSCLC has been shown to increase cell migration (134).

SOX9, $\log_2$ fold change = 1.47, results in cancer progression through maintenance of the cancer stem cell phenotype and by promoting cell survival and evasion of senescence (135). *SOX9* has been reported to be overexpressed in a large number of lung adenocarcinomas and its knockdown resulted in decreased tumor cell growth in concordance with p21 (CDKN1A) upregulation which is a cell cycle inhibitor (136).

LIPG, $\log_2$ fold change = 1.43, has been shown to be overexpressed in human basal-like triple-negative breast cancer (TNBC) and is understood to support cell proliferation, stemness and EMT features of TNBC independent of its function as a lipase (137).

Proliferation-related NF-κB target genes overexpressed under (continuous) hypoxia in H358 cells following X-rays exposure are AHCTF1, ABCA1, PTGS2, EGFR, MYLK and SLC6A6.

AHCTF1, $\log_2$ fold change = 1.80, encodes the nucleoporin ELYS which is involved in mitotic spindle assembly and nucleoporin assembly. Under-expression of AHCTF1 has been shown to shrink tumor burden in KRAS-driven hepatocellular carcinoma by inducing cell cycle arrest (138). It has also been shown to increase MYC transcript export rates from nucleus into the cytoplasm expediting their escape from nuclear degradation in colon cancer (139).

ABCA1, $\log_2$ fold change = 1.63, is a cholesterol efflux pump which has been shown to have tumor suppressor and antiproliferative effects in development and progression of chronic

myelomonocytic leukemia (CMML) (140).

PTGS2, $\log_2$ fold change = 1.59, has been shown to induce treatment resistance in NSCLC through up-regulation of the antiapoptotic BCL2 expression (141).

EGFR, $\log_2$ fold change = 1.53, is a well-established driver of tumorigenesis and tumor propagation mainly because of gene amplification and point mutations in NSCLC, breast cancer and glioblastoma multiforme but its transcriptional upregulation has also been reported. While its main effect is promoting tumor cell proliferation, previously unrecognized functions of EGFR are emerging continuously (142).

MYLK, $\log_2$ fold change = 1.50, has been shown to stimulate growth and metastasis in osteosarcoma cells through EGFR signaling pathway (143).

SLC6A6, $\log_2$ fold change = 1.11, encodes for a member of the family of sodium and chloride-ion-dependent transporters and transports taurine. Its overexpression has been shown to increase cell survival and chemoresistance in colorectal carcinoma cells by conferring cancer stem cell-like characteristics in them (144).

4.3.4.3. Inflammation-related target genes

Since NF-κB cell signaling is primarily a proinflammatory pathway, it is therefore unsurprising that following irradiation of hypoxic A549 cells, it upregulated transcription of several cytokines. However, only REL ($\log_2$ fold change = 1.11), an NF-κB family member, was upregulated in H358 cells under similar conditions.

The target cytokines are all chemo-attractants for leukocytes which can contribute to tumor cell survival by resulting in tumor-promoting inflammation and immune suppression. However, since the experimental design of this project did not take into consideration the influence by other cell types in the TME, the contribution of the immune cells in response to tumor-generated cytokines in promoting tumor survival and propagation is only very briefly discussed.

Of note is the **IL-8** target gene, $\log_2$ fold change = 1.38 after X-rays and 1.49 after carbon ions exposure, that was upregulated in hypoxic A549 cells following both X-rays and carbon ions exposure, because besides its role in recruiting immune cells, it also acts directly on tumor cells to induce EMT and thereby increasing their stemness, proliferation and migratory capacity. IL-8 is understood to be secreted by tumor cells passing through EMT. These cells may also enhance the expression of its receptors. Thus, IL-8 plays an important role in maintenance of the mesenchymal state by these tumor cells through autocrine signaling loops. IL-8 has been shown to stimulate a variety of EMT-related transcription factors including SNAI1, SNAI2 and Twist through a variety of cell signaling pathways including but not limited to PI3K/Akt and MAPK/Erk (145). IL-8 has been shown to be an indicator of cancer progression in human NSCLC (146).

Similarly, **IL-6**, $\log_2$ fold change = 1.13 after carbon ions exposure in hypoxic A549 cells, is noteworthy because it has a similar profile to IL-8 in case of NSCLC inducing EMT and promoting tumor aggressiveness and treatment resistance by acting on tumor cells. IL-6 is particularly interesting because not only is it a target gene of NF-κB but it can also activate NF-κB through a positive feedback loop (12).

Also, of note is **CD274**, also known as PDL1, which was slightly upregulated following carbon ion exposure ($\log_2$ fold change = 1.09) in A549 cells under continuous hypoxia. This along with some genes mentioned in preceding sections such as JUNB and IL-1A contribute through various mechanisms to increase immune escape which *in vivo* would be an important factor

contributing toward treatment resistance.

4.3.4.4.   Reoxygenation affects A549 and H358 cells in different ways

NSCLC cells were also reoxygenated following irradiation to reveal possible effects on gene expression in these transiently hypoxic cells relative to normoxic controls. The NSCLC cell lines A549 and H358 behaved very differently to reoxygenation following irradiation.

In case of transiently hypoxic A549 cells, reoxygenation following X-rays exposure led to a decrease in the number of upregulated NF-κB target genes 4 h after irradiation. The genes which were upregulated also had lower fold changes compared to those in continuously hypoxic cells, except for the antiapoptotic BCL2A1 (log_2 fold change = 1.15 under continuous hypoxia vs. 1.33 in transient hypoxia) for which the fold change was higher compared to normoxic controls following reoxygenation vs. continuous hypoxia. This may offer a mechanistic justification for the transiently hypoxic cells not showing the same radiosensitivity as continuously hypoxic cells in IP CFA assays.

In case of (transiently hypoxic) H358 cells, reoxygenation following X-rays exposure led to additional 20 NF-κB target genes being upregulated 4 h following irradiation.

Of these, three genes were upregulated in continuously hypoxic A549 cells following irradiation as well, namely, F3 (log_2 fold change = 1.53), IL-8 (log_2 fold change = 1.49) and CD274 (log_2 fold change = 1.13), and their tumor propagating functions have been discussed in sections 4.3.4.2 and 4.3.4.3.

Another five upregulated genes promote inflammation, namely, CXCL1, CXCL2, CSF2 and TNFAIP3, BLNK and TREM1. The protein products of these genes are acting on immune cells in TME leading to tumor promoting inflammation and immune evasion. Therefore, while they are important for tumor cell survival and proliferation *in vivo* but from the perspective of current study, they may not be playing any significant role in hypoxia-induced radioresistance observed in CFA assays.

Lastly, upregulation of APOD (log_2 fold change = 1.39) and KLF10 (log_2 fold change = 1.27) was shown previously to be correlated with decreased cell proliferation and better treatment outcomes (147–149) and, therefore, are not directly relevant to this discussion.

The significance of the remaining genes in enhancing tumor survival and radioresistance is discussed as follows:

EDN1, log_2 fold change = 2.29, encodes a vasoconstrictor peptide that has been shown to induce mitogenesis, apoptosis, angiogenesis, tumor invasion and metastasis (150).

THBS1, log_2 fold change = 2.25, encodes a secreted protein that has been shown to inhibit angiogenesis, promote tumor cell migration, regulate autophagy and senescence, and inhibit antitumor immunity by CD47-dependent regulation of innate and adaptive immune cells (151,152).

MYC, log_2 fold change = 1.67, is a proto-oncogene that has a role in cell cycle progression, apoptosis and differentiation. It is deregulated in >50 % of human cancers which is frequently associated with poor prognosis (153,154).

NRG, log_2 fold change = 1.65, is a ligand for HER3 and HER4 receptors and is involved in cell proliferation and migration in cancers, particularly pancreatic cancer (155).

VIM, log_2 fold change = 1.57, encodes a type III intermediate filament that is involved in cell adhesion and migration. When upregulated in solid tumors, it drives EMT and hence promotes

tumor aggressiveness and treatment resistance (156). It is used as a biomarker for the early detection of several cancers (157). Upregulation of Vimentin (VIM) in circulating NSCLC tumor cells was found to decrease the overall survival (3.2 vs. 7.1 months; p = 0.029) (158).

OXTR, $\log_2$ fold change = 1.50, has been found to be overexpressed in various malignant mesothelioma cell lines and is associated with poor treatment outcome while its knockdown resulted in increased tumor cell proliferation (159). OXTR has also been implicated in breast tumorigenesis via ERBB2 upregulation (160).

IL-8, $\log_2$ fold change = 1.49, though primarily related to inflammatory response by acting as a cytokine for immune cells in TME, is still mentioned separately here because as explained in subchapter 4.3.4.3, it can act in an autocrine fashion on tumor cells themselves to induce EMT and thereby increasing their stemness, proliferation and migratory capacity (145).

KITLG, $\log_2$ fold change = 1.44, also known as stem cell factor (SCF), is a ligand of the c-KIT tyrosine kinase receptor. Upregulation of KITLG has been demonstrated in several cancer types such as glioma, NSCLC, and colorectal cancer and has been shown to play an important role in regulating cell proliferation, migration and survival through the MAPK pathway (161).

PTHLH, $\log_2$ fold change = 1.22, is an autocrine/paracrine ligand that has been reported to act as a driver for EMT in Crohn's disease via activation of transcription factor RUNX2 (162). It has also been found to be upregulated in head and neck squamous cell carcinoma (HNSCC) where it stimulates tumor cell proliferation through the same RUNX2-dependent mechanism (163).

CDK6, $\log_2$ fold change = 1.12, plays a vital role in regulating G1 cell cycle progression through partial phosphorylation of Rb proteins which is then completed by CDK2-cyclin E complex. CDK6 has also been reported to have a transcriptional role in tumor angiogenesis. Up-regulation of CDK6 is associated with several cancer types (109).

Thus, while reoxygenation in irradiated A549 cells appears to revert cells toward gene expression signature under normoxia within 4 h, it results in upregulation of a new set of proliferation-related genes in the irradiated H358 cells.

Correlating this with CFA assay data, reversion of gene expression does not impact radioresistance in transiently hypoxic (reoxygenated) A549 cells in LP experiments but may provide a survival advantage in IP experiments due to BCL2A1. On the other hand, the differential gene regulation signature in transiently hypoxic (reoxygenated) H358 cells appears to be contributing in the relatively lower radioresistance compared to continuously hypoxic cells.

4.4. Hypoxia slows down cell cycle progression of NSCLC cells

Growth kinetics studies in the absence of irradiation revealed that the doubling times of A549 cells under O_2 concentrations of 1 % and 0.1 % in comparison to normoxia increased by about 32 % and 128 %, respectively, while the doubling times of H358 cells under O_2 concentrations of 1 % and 0.1 % in comparison to normoxia increased by about 57 % and 106 %, respectively (Table 3.1). While studies show that hypoxia can in some cases promote cell proliferation in fetal (164) and tumor cells (129,165), the effect of hypoxia in most cases is inhibitory on cellular proliferation (33).

The observed decline in proliferation rate in hypoxic A549 and H358 cells implies slowing down of the cell cycle. Possible explanations are discussed below.

4.4.1. By favoring G1 phase redistribution

Cells that had been kept in culture for 48 h in hypoxia were sampled at various time points over the next 24 to 48 h while maintaining hypoxia (continuous hypoxia). A549 cells were incubated in presence of 1 % and 0.1 % O_2. In H358 cells, the effects on distribution of cells in the different cell cycle phases of 1 % O_2 only were examined.

Cell cycle analysis showed that in hypoxic A549 cells a higher percentage of cells were in G1 and S phases compared to normoxic cells of which a higher percentage of cells were in G2 and this was true at both 1 % and 0.1 % O_2 (Figure 3.10). A higher percentage of hypoxic H358 cells was in G1 compared to normoxic cells but population differences to normoxic cells were inconspicuous in S phase; a higher percentage of normoxic H358 cells was in G2 (Figure 3.12).

This observed phase redistribution of cells toward G1 under hypoxia is already documented in literature and occurs through inhibition of G1/S phase transition via a variety of different transcriptional and post-translational mechanisms (166–168). This results in a higher proportion of quiescent cells, slowing down tumor proliferation.

When it comes to radiosensitivity, the general concept is that a higher proliferation rate results in greater cytotoxicity while a lower rate of proliferation may lead to treatment resistance. This concept was first introduced as a "Law" in 1906 by Bergonié and Tribondeau and holds ground as a good first approximation principle in radiation oncology even today (169).

So, G1 redistribution in NSCLC cell lines under hypoxia *in vitro*, resulting in reduced proliferation, may be a contributing factor toward observed radioresistance in CFA experiments. Furthermore, in radiobiology, cells in G1 phase are assumed to be more radioresistant than cells in late G2/M phases (48).

While searching for mechanistic explanations for the observed G1 redistribution under hypoxia, p53 stabilization under hypoxia leading to p21-induced activation of the G1/S checkpoint offers a common explanation. However, since G1 redistribution occurred not only in the p53-wt A549, but also in the p53-null H358, other mechanisms may be at work.

One such mechanism is the HIF-1 pathway which can decrease c-Myc expression counteracting its downregulating effect on p21 and p27 (33). HIF-1 can further inhibit c-Myc by interfering with its partner protein Myc-associated protein X (Max) (25). Lastly, HIF-1 can physically displace c-Myc from its binding sites on the DNA helix resulting in de-repression of p21 and p27 synthesis. Overexpression of these CDKIs due to c-Myc suppression inhibits CDK4, CDK6 and cyclin D inhibiting the cell cycle in G1 phase (33). Hypoxia also inhibits DNA replication by inhibiting the mini-chromosome maintenance (MCM) protein complex crucial for initiating DNA replication. This is understood to happen through inhibition of the MCM complex

after binding with HIF-1 and HIF-2 protein dimers secondary to their activation under hypoxia (25,33,170).

NF-κB pathway activation under hypoxia can also inhibit cell cycle progression in the G1 phase. This pathway may be activated by hypoxia either through ROS or via action of PHDs and FIH. Overexpression of its subunit p65 has been shown to arrest cells at G1/S-phase checkpoint. Additionally, it has been shown to increase p21 expression by activating the Formin-2 (FMN2) protein which is a component in the p14ARF tumor suppressor pathway (167).

However, it is important to note that differential gene expression analysis (section 4.3.1) revealed no cell cycle-related gene to be differentially expressed after 52 h of continuous hypoxia in comparison to normoxia except for CDKN1C downregulation in H358 cells. This downregulation seems to be in response to pre-existing cell cycle inhibition in G1 as its effect would be to push cells from G1 to S phase, and not a cause for it. While cross-sectional analysis of gene expression at a single timepoint may be insufficient to rule out transcriptional causes for G1 redistribution in hypoxic A549 and H358 cells as changes in transcription of cell cycle genes might be observed at an earlier time during hypoxic incubation, nonetheless, it does advocate looking for non-transcriptional explanations for it.

There can be several post-translational causes for inhibition of cell cycle at the G1/S checkpoint. A common mechanism would be stabilization of Rb-E2F complex through inhibition of its phosphorylation. Similarly, activation of CDKs also depends on their phosphorylation by CAK (cyclin-dependent kinase activating kinase) in addition to their binding with corresponding cyclins. CDK activity may also be regulated by inhibitory phosphorylation by Wee1 and by phosphatase activity CDC25 (168). The direct phosphorylation of E2F4 by IKKα and IKKβ resulting in its nuclear accumulation has been reported which stabilizes the Rb complex resulting in G1 arrest (167).

4.4.2.   By decoupling glycolysis and oxidative phosphorylation

Redistribution of hypoxic cells in the quiescent G1 phase may simply be due to metabolic adaptation secondary to diminished ATP production. This was explored by performing glucose consumption and lactate production assays (Figure 3.3).

Glucose uptake in A549 cells growing at 0.1 % O_2 and 1 % O_2 was found to be higher than those growing at 20 % O_2 after 48 h and 72 h of incubation. Similarly, glucose uptake was found to be equivalent or higher in H358 cells growing at 0.1 % or 1 % O_2 in comparison to those growing in normoxia after 48 h and 72 h of incubation. In other words, the observed decline in growth rate under hypoxia in this study was not associated with a relative decline in glucose uptake when uptake was normalized for cell number. On the other hand, the relative lactate excretion under hypoxia increased sharply as a function of cell number from 24 h onward for both A549 and H358 cells growing at 0.1 % O_2 and 1 % O_2 in comparison to those growing in normoxia.

This indicates shunting of glucose into the glycolytic pathway that is uncoupled with an equivalent increase in oxidative phosphorylation in hypoxic cells. Since glycolysis produces 18 times less ATP than oxidative phosphorylation, the overall impact would therefore still be that of nutrient deprivation explaining the observed decline in cell proliferation as a compensatory response to diminished ATP synthesis. Correlation between reduced proliferation rate and switch over from oxidative phosphorylation to glycolysis under hypoxia has been well documented in literature (171).

Also notable is that H358 having a slower proliferation rate than A549 also show lower glucose uptake and lactate excretion at any oxygen concentration thereby indicating a direct relationship between energy metabolism and cell proliferation rate (Figure 3.4).

Lastly, whether the A549 and H358 cells show aerobic glycolysis (Warburg effect) cannot be commented upon based on this study because no comparison was done with a relevant non-cancerous cell line as it was not deemed relevant to the stated aims of this study.

4.5.   Hypoxia alters effects of irradiation on cell cycle progression of NSCLC cells

Cell cycle inhibition is an important part of the DDR to ionizing radiation exposure. Of particular importance in cancer cells is the G2 arrest after irradiation by inhibition of phase transitioning at the G2/M checkpoint. This provides the irradiated cells time to repair DNA damage following irradiation before entering mitosis and segregating the duplicated chromatids.

Cell cycle arrest at the G2/M checkpoint gives valuable information about contribution of HR pathway in double strand break repair since in mammalian cells, HR is only possible in late S and G2 phases once DNA has already been replicated and the sister chromatid can be used as template for repair.

4.5.1.   Reduced G2 inhibition is accompanied with persistent G1 inhibition

After a single dose of 8 Gy X-rays, normoxic A549 cells responded by inhibition of G2/M transition (Figure 3.10) such that the maximum percentage of cells under G2 arrest was 62 % 12 h after irradiation (Table 3.8). Of H358 cells receiving the same dose, 69 % cells were under G2 arrest 18 h after irradiation (Figure 3.12; Table 3.9) which is surprising considering that the G2/M checkpoint is mainly under p53 control and H358 cells are p53 null.

Under a state of continuous hypoxia at 1 % O_2, the maximum percentage of A549 cells under G2 arrest is 33 % and that of H358 cells is 52 %. Under hypoxia, a smaller portion of cells under G2 arrest was matched by a higher proportion of cells pooled in G1 as was the case in the absence of radiation reported earlier under section 4.3.2. While G1 cell populations under normoxia dropped after irradiation to 30 % for A549 cells and to 15 % for H358 cells, under hypoxia they only dropped to 53% for A549 cells and to 29 % for H358 cells.

A G2 arrest following irradiation is normally induced by p53 stabilization which activates p21 which in turn blocks phosphorylation of CDK1 that then is unable to propel the cell cycle from G2 to M phase. However, since H358 cells are p53 null, other mechanisms must also be at play. One such mechanism involves CDC25C which normally dephosphorylates CDK1 allowing the CDK1-cyclin B to move cells through the G2/M checkpoint. However, irradiation may activate CHK1/2 which phosphorylate CDC25C initiating its binding to 14-3-3 proteins instead of CDK1, resulting in inhibition of CDK1-cyclin B and thus in G2 arrest (172).

So mechanistic explanations for diminished G2/M block under hypoxia may involve reduced phosphorylation downstream of p21 and of CDC25C. Furthermore, differential expression data for cell cycle-related genes revealed several genes being regulated under hypoxia in a way that might promote cell cycle progression and therefore, may also be responsible for the G2/M transitioning. Furthermore, chronic hypoxia (<0.1 % O_2) has been reported to downregulate cyclin B expression and CDK1 activity in G2 phase cells (173). Downregulation of cyclin B may not be apparent in our differential gene expression studies because G2 phase cells were not evaluated separately.

However, the diminished G2 population under hypoxia may not be because of diminished

G2/M blockade but rather due to a greater proportion of hypoxic cells continuing to stay in the quiescent G1 phase even after irradiation because of slower energy metabolism as explained in previous section.

4.5.2. Cell cycle response under hypoxia unimpacted by severity of hypoxia

The relative distribution of cells in different phases of the cell cycle, when grown and irradiated at 1 % O_2 vs. 0.1 % O_2, was statistically similar (Figure 3.10; Table 3.8). At both O_2 concentrations, both before and after irradiation, at any given time point, the proportion of cells in G1 is higher and that in G2 is lower than under normoxia; however, there is no clear indication that reducing O_2 concentration from 1 % to 0.1 % exaggerates the differences compared to normoxia in a concentration-dependent manner.

4.5.3. Cell cycle response under hypoxia unimpacted by reoxygenation

Reoxygenation, principally, should result in resumption of protein synthesis that might have been inhibited under hypoxia due to ATP depletion. This would include cell cycle-related regulatory proteins and enzymes as well, possibly resulting in changes in cell cycle progression following reoxygenation.

However, even after reoxygenation, irradiated cells continued to show a diminished G2 block and a persistent G1 block for up to 24 h following reoxygenation. This observation is true across the two cell lines (Figure 3.9 & Figure 3.12) and also for both high- (carbon ions; Figure 3.11) and low-LET (X-rays) ionizing radiation.

Comparing this observation to differential gene expression data for cell cycle genes in transiently hypoxic (reoxygenated) cells, it can be deduced that the normalization of transiently hypoxic A549 gene expression to that of normoxic counterparts, or the upregulation of cell cycle-promoting MYC in transiently hypoxic H358 cells, do not immediately impact cell cycle phase distribution pattern and take at least 24 h to return cells to normoxic behavior in terms of cell cycle progression.

Previous studies have shown that reoxygenation does not immediately result in cell cycle progression through G2/M checkpoint in the presence of functional p21 and p27 (174). Furthermore, reoxygenation has been reported to cause inhibitory phosphorylation of CDK2 and CDC25C both of which are involved in cell-cycle arrest at the G2/M checkpoint (175).

4.5.4. Cell cycle response under hypoxia unimpacted by LET

Using carbon ions (Figure 3.11; Table 3.8) to deliver an energy dose comparable to that used in experiments with X-rays in the A549 cells yields a similar response of a diminished G2 block under hypoxia (maximum G2 population of 38 % vs. 33 % in carbon ion vs. X-rays exposure) in the presence of a relative G1 block (minimum G1 population of 52 % vs. 53 % in carbon ion vs. X-rays exposure). However, the length of time that the cells remain in G2 arrest was increased following carbon ion exposure in comparison to X-rays exposure. This is consistent with literature where same energy doses of carbon ions produce a more persistent G2 block than X-rays in variety of cancer cell lines (176) including a NSCLC cell line (177).
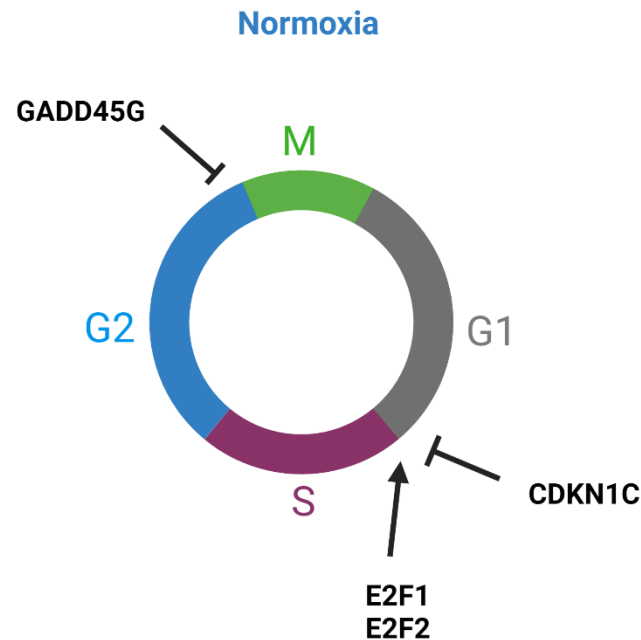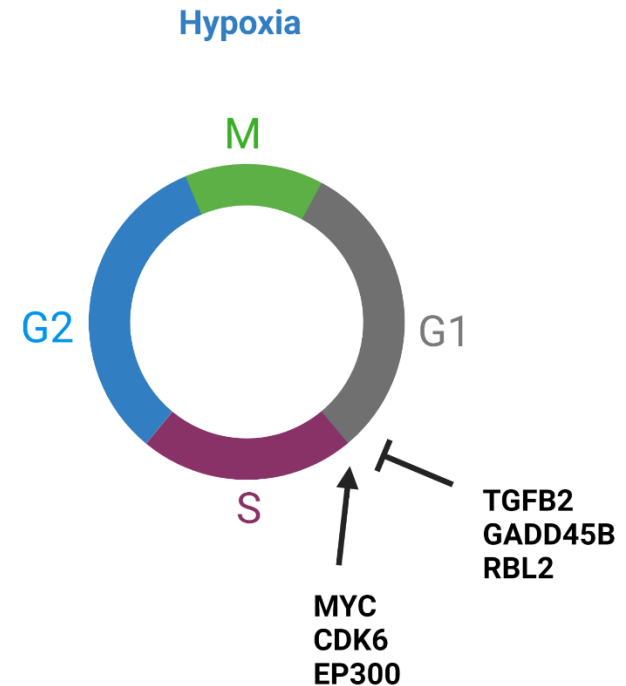
Figure 4.3   Differential regulation of cell cycle genes after irradiation under normoxia and hypoxia.

Following irradiation under normoxia, GADD45G was overexpressed compared to irradiation under hypoxia. GADD45G inhibits G2/M transition. CDKN1C, E2F1, and E2F2 were also overexpressed, the former inhibits G1/S transition while the latter two facilitate it (A).

Following irradiation under hypoxia, no cell cycle gene regulating the G2/M checkpoint was found to be overexpressed when compared to irradiation under normoxia. Several genes inhibiting and facilitating the G1/S checkpoint were overexpressed (B).

GADD45G & B, growth arrest and DNA damage inducible gene G & B; CDKN1C, cyclin dependent kinase inhibitor 1C; E2F1 & 2, E2F transcription factors 1 & 2; MYC, Myc proto-oncogene, BHLH transcription factor; CDK6, cyclin dependent kinase 6; EP300, E1A-associated protein p300; TGFB2, transforming growth factor β2; RBL2, RB transcriptional corepressor like 2; Created with Biorender.com.

148

4.5.5. Implication of cell cycle response for DNA repair and cell survival

An important implication of diminished G2 population under hypoxia is that hypoxic cells will have a lower likelihood of DSB repair via the HR pathway. This is because the HR pathway can only be activated once DNA has been replicated and a DNA template for repair is available in form of the newly synthesized sister chromatid. This is only the case in late S and G2 phases. Cells trapped in G2 phase following irradiation, therefore, have a higher chance of HR based DSB repair. On the other hand, cells trapped in G1 and early S phases cannot utilize higher fidelity HR and are dependent on lower fidelity NHEJ for DSB repair which over time may increase mutagenicity in tumor cells.

Furthermore, if the diminished G2 population following irradiation of hypoxic cells is simply due to a higher quiescent G1 population, cells being in radioresistant G1 phase may be contributing to the hypoxia-induced radioresistance that was detected in CFA assays.

4.6. Hypoxia decreases DNA double strand break formation following X-rays exposure of NSCLC cells

DNA damage repair is an important component of the DDR following irradiation. As explained earlier, the most important form of DNA repair following irradiation is DSBR. DNA DSB induction and repair can be experimentally monitored through γH2AX foci formation and resolution. However, these experiments cannot distinguish between the two pathways of homologous repair (HR) and nonhomologous end joining (NHEJ).

The radiation dose was 2 Gy for both X-rays and carbon ions and the higher dose of 8 Gy used in all other experiments was avoided. This was done to ensure reliable counting of DSBs which would have become unfeasible at higher doses because of the overlapping of γH2AX foci.

In both NSCLC cell lines (Table 3.11), A549 (30.0 vs. 24.9 foci, 1 h after exposure, Figure 3.14) and H358 (7.9 vs. 6.0 foci, 1 h after exposure; Figure 3.16), on average a lower number of DSBs was observed after irradiation under hypoxia (1 % O_2) compared to exposure under normoxia. The trend is lost for carbon ions exposure under hypoxia compared to normoxia (15.1 vs. 15.2 foci, 1 h after irradiation, Figure 3.15).

This is well in line with the physicochemical impact of the absence of molecular oxygen at the time of X-rays exposure resulting in decreased ROS formation and ROS-induced DNA damage which translates into fewer DSBs formation. However, progressive acquisition of a radioresistant phenotype due to chronic hypoxia (48 h incubation) prior to irradiation may also contribute to the reduced number of DSBs induced by irradiation under hypoxia. On the other hand, carbon ions being high-LET radiation mostly induce "direct damage" to DNA and which is not affected by presence of molecular oxygen for DSB formation. That DSB induction following carbon ions exposure is relatively unaffected by hypoxia in comparison to X-rays exposure has also been reported recently (60).

The difference in DSB formation between the two cell lines for the same dose is not surprising. Different cell lines have different radiosensitivity (178) and based on the CFA experiments, the D_0 values for H358 compared to A549 already helped to establish that H358 is a more radioresistant cell line.

The average DSB formation after irradiation with carbon ions appears lower compared to that following same energy dose of X-rays. This is also not surprising because high-LET radiation produces less wide-spread ionization events compared to X-rays for the same dose (60) but due to the dense energy deposition along the particle tracks, the nature of lesions is more

complex (cluster lesions) which makes them more difficult to repair. This is apparent in the form of faster DSB resolution following X-rays resulting in steeper curves compared to carbon ion exposure.

Finally, it is important to note that the observed decline in number of DSBs under hypoxia 1 h after irradiation may be in part due to less DSB formation and in part due to faster repair under hypoxia in the first hour. Indeed, DSBR starts almost immediately after ionizing radiation-induced DNA damage (48); nonetheless, and an initial timepoint of 1 h is still suitable to measure DSB induction as γH2AX foci resolution slightly lags behind actual DSBR (179).

Literature review articles suggest that hypoxia suppresses HR by inhibiting expression of Rad51 and BRCA1 but may promote NHEJ by increasing expression of DNA-PKcs (22,81). However, no such transcriptional regulation was observed in A549 and H358 cells in the differential gene expression analysis 4 h after irradiation which did not show any DSBR genes to be upregulated under hypoxia.

This, however, does not rule out more effective DSBR under hypoxia in the first hour after irradiation due to post-translational modifications following irradiation, for example, faster phosphorylation of ATM under hypoxia secondary to DNA damage (60). In fact, chronic hypoxia has also been shown to phosphorylate ATM even in the absence of irradiation (180).

4.6.1.   Decline in DNA DSB formation is proportional to oxygen concentration

In A549 cells maintained and irradiated at 20 %, 1 % and 0.1 % O_2, an average number of DSBs 1 h after X-rays exposure of 30.0, 24.9 and 19.2 foci per cell nucleus was counted (Table 3.11; Figure 3.13) indicating a progressively lower formation of DSBs as the oxygen concentration decreases.

This is well in line with the physicochemical impact of the absence of molecular oxygen at the time of irradiation resulting in decreased ROS formation and ROS-induced DNA damage which translates into fewer DSB formation. However, progressive acquisition of a radioresistant phenotype due to chronic hypoxia (48 h incubation) prior to irradiation in an oxygen concentration-dependent manner may also contribute to the reduced number of radiation-induced DSBs at 1 % and 0.1 % O_2.

4.6.2.   Hypoxia does not induce spontaneous DNA DSBs

Following DSBs over time, in the absence of radiation, under both normoxia and hypoxia, reveals no significant difference indicating that hypoxia does not spontaneously cause DSBs above those under normoxia for both concentrations – 1 % O_2 (in A549 and H358 cells; Figure 3.14 & Figure 3.16) or 0.1 % O_2 (in A549 cells; Figure 3.13). The observation that hypoxia does not lead to additional DSBs by itself in the absence of irradiation has been reported in literature already (22,180).

4.6.3.   Reoxygenation alters DNA DSB induction

Reoxygenation following extreme hypoxia (0.1 % O_2, Figure 3.13) resulted in a greater number of DNA DSBs, 1 h after X-rays exposure, in A549 cells (26.2 foci/nucleus under transient hypoxia vs. 19.2 foci/nucleus under continuous hypoxia; Table 3.11). However, the effect of reoxygenation in cells maintained and irradiated at 1 % O_2 (Figure 3.14 & Figure 3.16) is the opposite, that is, the average number of DNA DSBs 1 h after exposure was found to be lower (21.8 foci/nucleus in A549 and 4.9 foci/nucleus in H358) than those cells maintained continuously under hypoxia (24.9 foci/nucleus in A549 and 6.0 foci/nucleus in H358).

The mechanistic explanation for this is unclear. Reoxygenation results in ROS production

which can ionize DNA and cell organelles directly but are also known to activate a number of cells signaling pathways such as NF-κB, HIF-1α and EGFR pathways (26,181). The two different O_2 concentrations may influence activation of these pathways differentially impacting DSB induction and repair in different manners following reoxygenation. Additionally, following reoxygenation after severe hypoxic conditions (< 0.1 % O_2 for < 8 h), the stalled DNA replication forks can restart (180), something which is not reported for higher oxygen concentrations like 1 % O_2.

4.6.4. LET impacts repair kinetics independent of oxygenation status

Although residual DSBs 24 h after irradiation were comparable to unirradiated controls for both X-rays and carbon ion exposure at a dose of 2 Gy regardless of oxygenation status, DNA DSBs took longer to resolve following carbon ion exposure compared to X-rays exposure under both normoxia and hypoxia (Figure 3.15) based on a flatter curve gradient. The observation that DSBs persist longer following carbon ion exposure compared to X-rays exposure was already reported for human pancreatic cancer stem-like cells (59) and is attributed to more complex DSBs and cluster lesions induced by high-LET radiation.

Interestingly, the initial γH2AX foci number is lower (15.1 $\pm$ 1.0) after exposure to carbon ions when compared to X-rays (30.0 $\pm$ 2.9, under normoxia) at the same energy dose of 2 Gy. The average number of carbon ion hits that was expected for an average cell nucleus size of 118.8 $\pm$ 52.5 μm^2 was 21 (Table 2.11). Confluence of foci induced by separate carbon ion hits and damage clusters without double strand breaks could explain the lower than expected (15 vs. 21) foci number.

4.7. Irradiation causes earlier onset of NF-κB activation under hypoxia in NSCLC cells

In order to determine if differential expression of NF-κB target genes under hypoxia was linked to activation of NF-κB, meaning its liberation from IκB and translocation into the nucleus, nuclear localization the NF-κB subunit p65 following irradiation under hypoxia was compared to that under normoxia.

The transcription factor NF-κB encompasses a variety of homo- and heterodimers of NF-κB subunits (see section 1.2.1.2) (182). However, the nuclear translocation of cytosolic p65 within the NF-κB dimer (usually p65/p50) after its detachment from inhibitory IκB is a common way for the activation of NF-κB signaling in response to stimuli like DAMPs, ROS, hypoxia, ionizing radiation, DNA damage, cytokines etc. and has been carried out regularly to assess NF-κB activation (119,183–185). Nuclear translocation of activated p65 begins within minutes following an appropriate stimulus but it may persist for several hours to days depending upon the stimulus (186).

Measurement of the nuclear intensity of fluorescent p65 antibody in normoxic and hypoxic cells after irradiation was carried out and normalized against corresponding normoxic, unirradiated controls.

It was revealed that cells kept under continuous 1 % O_2 start showing an increase in p65 nuclear intensity as early as 2 h after irradiation compared to their unirradiated controls (1.05 vs. 0.98) and this increase builds up at 6 h and 24 h time points following radiation (Figure 3.20). Normoxic cells, on the other hand, tend to show an increase in p65 nuclear intensity at earliest 6 and 24 h after irradiation.

This earlier increase in p65 nuclear intensity, at the 2 h post-exposure time point, is interpreted as earlier onset of p65 nuclear translocation which in turn marks the earlier activation of the NF-κB pathway in hypoxic cells. It may explain the relatively great number of NF-κB target genes that were upregulated early (4 h) after irradiation.

While the rise in p65 nuclear intensity in A549 cells, 2 h following X-ray exposure, is minimal, the rise is much more conspicuous in A549 cells compared to their unirradiated controls (0.89 vs. 0.67) 2 h after carbon ion exposure (Figure 3.21) and also in H358 cells compared to their unirradiated controls (0.69 vs. 0.59) 2 h after X-rays exposure (Figure 3.22).

Since NF-κB activation studies under the combined effects of irradiation and hypoxia are not reported in literature to the best of my knowledge, so direct comparison of these results with other studies is not possible.

4.7.1. Reoxygenation affects radiation-induced NF-κB activation differently in A549 and H358 cells

Reoxygenation of previously hypoxic cells is accompanied by ROS production, resumption of protein synthesis and activation of secondary cell signaling which may have variable effects on NF-κB activation following irradiation.

While reoxygenation of A549 cells (Figure 3.20) previously maintained at 1 % O_2 did not change the trend of earlier NF-κB activation 2 h post irradiation, the same in case of H358 cells (Figure 3.22) resulted in lower p65 nuclear intensity in irradiated cells compared to unirradiated controls 2 h post irradiation (0.88 vs. 0.92 in A549 and 0.88 vs. 0.74 in H358). No increase in p65 nuclear localization was observed 6 h and 24 h post-irradiation in reoxygenated H358 cells

compared to corresponding unirradiated controls either.

One mechanistic explanation could be that ROS production resulting from reoxygenation results in NF-κB inactivation in H358 cells. Indeed, the relationship between ROS and NF-κB is complex and while the more common effect of ROS is NF-κB activation (26,39,117,185), nonetheless, ROS production resulting in NF-κB inactivation in some cell lines has also been reported (187). But if this were the case, p65 nuclear localization should have decreased in unirradiated controls as well relative to normoxia. However, what can be observed is that p65 nuclear intensity in unirradiated, reoxygenated H358 cells keeps increasing over time (0.88 at 2 h vs. 1.06 at 24 h) when compared to corresponding unirradiated, normoxic controls. It is, therefore, possible that the effect of irradiation on p65 nuclear localization in reoxygenated H358 cells may have been masked by the effect of reoxygenation alone in increasing p65 nuclear localization. Keeping into consideration the higher number of NF-κB target genes differentially upregulated under transient hypoxia (reoxygenation) in comparison to normoxic and continuously hypoxic cells, this seems likely.

Lastly, it is possible that one or more of the differentially upregulated target proteins in case of reoxygenation may be involved in downregulating NF-κB activation through negative feedback loops, as has been reported for many NF-κB target genes in literature (188).

Therefore, reoxygenation seems to influence H358 cells differently compared to A549 cells by progressively increasing basal NF-κB activation in an irradiation-independent manner.

4.7.2.   Extreme hypoxia (0.1 % O$_2$) increases basal NF-κB activation in an irradiation-independent manner

As opposed to p65 nuclear translocation at 1 % O$_2$, when A549 cells were maintained and exposed to X-rays in presence of only 0.1 % O$_2$, it was observed that irradiation of hypoxic cells led to a decrease in p65 nuclear intensity (Figure 3.20) compared to unirradiated controls. This could mean that at such low oxygen concentrations, irradiation results in NF-κB inactivation. However, this seems less likely as the p65 nuclear intensity in hypoxic, unirradiated cells is much higher than in corresponding normoxic, unirradiated controls. Additionally, the p65 nuclear intensity in irradiated, hypoxic cells is also higher than in irradiated, normoxic controls 2 h and 24 h after X-rays exposure. Therefore, it seems that such a low oxygen concentration (0.1 %) results in high basal NF-κB activation in an irradiation-independent manner which masks the effect of irradiation.

While hypoxia being an independent driver of NF-κB activation is well-established (39,55,189–191), comparison of its activation at different oxygen concentrations either exclusively or in conjunction with irradiation was not found during literature review.

4.7.3.   NF-κB activation is stronger following high-LET irradiation compared to low-LET irradiation

In A549 cells, p65 nuclear localization was greater in response to carbon ion exposure compared to X-rays exposure across both early (2 h and 6 h) as well as late (24 h) time points following irradiation, in the case of normoxic, continuously hypoxic as well as transiently hypoxic cells (Figure 3.20 & Figure 3.21). NF-κB activation has been previously compared for X-rays and high-LET radiation including energetic carbon and argon ions in human embryonic kidney (HEK/293) cells illustrating higher p65 nuclear localization in response to high-LET irradiation with a maximal NF-κB activation in the LET range of 91 to 272 KeV/μm (62,192,193).

4.8. Irradiation increases secretion of NF-κB target cytokines by NSCLC cells under hypoxia

To determine if earlier activation of NF-κB under hypoxia discussed in the previous section resulted in increased synthesis of two of its target proteins, IL-6 and IL-8 secretion was evaluated following irradiation. NF-κB is the primary transcription factor for both cytokines, IL-6 and IL-8 (194,195).

The RNA sequencing results showed that A549 cells are capable of differentially upregulating transcription of both interleukin genes, IL-6 and IL-8, under hypoxia following irradiation while hypoxic H358 were shown to differentially upregulate only IL-8 compared to normoxic cells following irradiation.

Besides their inflammatory roles, both, IL-6 and IL-8, are involved in cancer survival and proliferation. IL-6 has been shown to increase cancer "stemness" and pluripotency through upregulation of the pluripotency transcription factor OCT-4 in breast cancer cells (196). IL-6 has also been demonstrated to induce EMT, promote proliferation and inhibit apoptosis in prostate carcinoma (197). It is particularly important in promoting osseous metastases (198). IL-8 promotes tumor angiogenesis, increases endothelial and cancer cell proliferation, as well as potentiates migration of endothelial and cancer cells (199). In xenografts of A549 cells, anti-IL-8 antibodies were shown to reduce tumor growth (200).

The concentration of these cytokines in cell culture supernatants was quantified by ELISA, 6 h and 24 h following irradiation, both under hypoxia and normoxia, and then normalized for the cell count (1×10^6 cells) to consider possible reductions in cell number induced by hypoxia or/and radiation exposure.

Following X-rays exposure under continuous hypoxia of 1 % O_2 concentration, both A549 (Figure 3.23) and H358 cells (Figure 3.24) secreted higher amounts of IL-8 compared to that under normoxia. Additionally, continuously hypoxic A549 cells also secreted more IL-6 compared to normoxic counterparts following X-rays exposure (Figure 3.23).

Finally, A549 cells also secreted higher amounts of IL-6 and IL-8 under continuous hypoxia following carbon ion exposure (Figure 3.25). The said increased secretion of target cytokines is consistent both at 6 h and 24 h after irradiation.

Besides being in line with RNA sequencing data, this is also consistent with the results of p65 translocation studies where earlier activation of NF-κB in hypoxic cells following irradiation may explain greater secretion of NF-κB target cytokines under said conditions (Figure 4.4).

Increased IL-6 expression in response to ionizing radiation exposure has been demonstrated in HeLa cells where destruction of the NF-κB promoter region in the IL-6 gene abolished basal and radiation-induced IL-6 expression (201). Increased IL-8 production in NSCLC cell lines (A549, H446 and PC-9) in response to X-rays has also been demonstrated recently where the p38/MAPK inhibitor SB203580 and the NF-κB inhibitor BAY11-7082 blocked radiation-induced IL-8 upregulation (202). Enhanced cytokine secretion including IL-6 and IL-8, in response to high-LET radiation has been well documented both in normal (203,204) and malignant cells (205). However, the effect of hypoxia on radiation-induced IL-6 or IL-8 secretion was not found in literature.
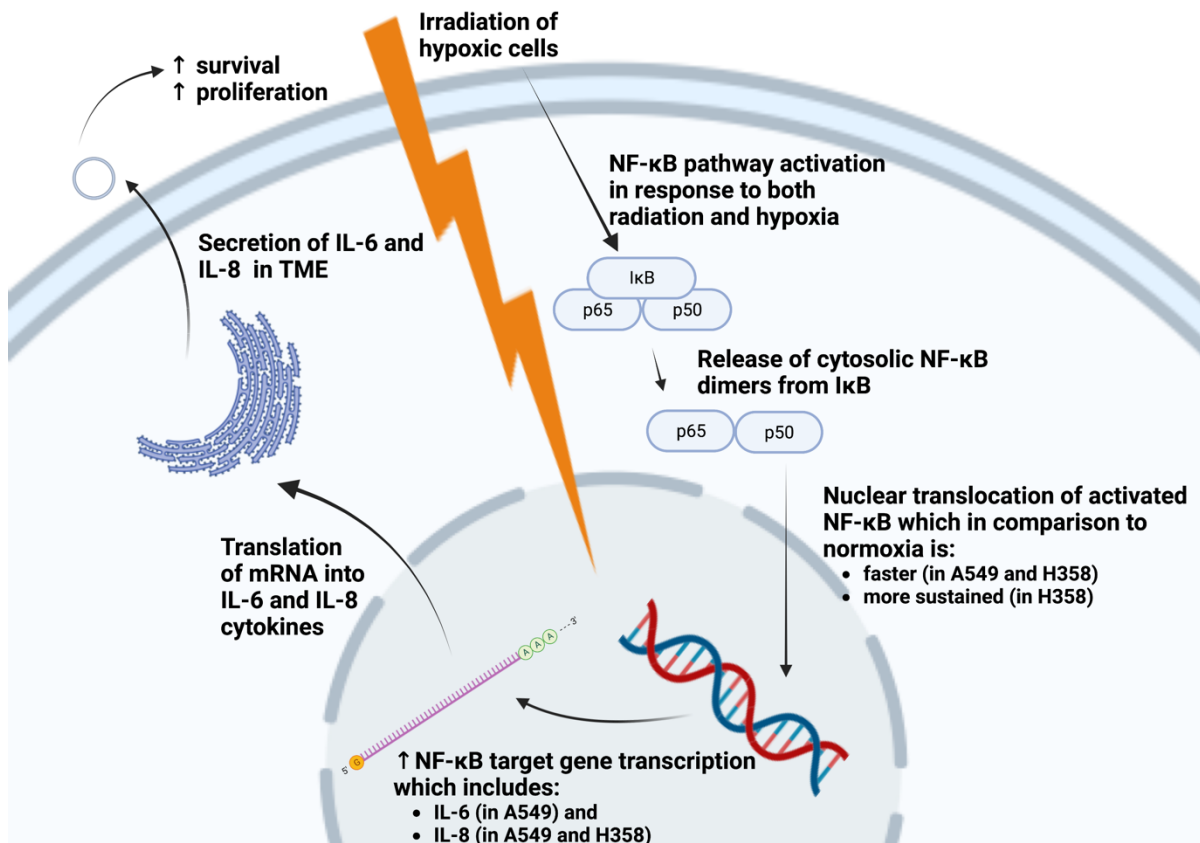
Figure 4.4   IL-6 and IL-8 secretion is found to be higher in A549 and that of IL-8 only in H358 cells under hypoxia compared to normoxia. Their secretion increases further under hypoxia following irradiation compared to irradiated normoxic controls. The increase in secretion under the combined effect of irradiation and hypoxia is associated with an earlier p65 nuclear translocation in cells irradiated under hypoxia. Differential gene expression analysis also shows overexpression of several NF-κB target genes including those for IL-6 and IL-8.

IκB, inhibitor of κB; TF, transcription factor; IL-6 & 8; interleukin 6 & 8; mRNA, messenger RNA; TME, tumor microenvironment. Created with Biorender.com.

4.8.1. Radiation-induced increase in secretion of NF-κB target proteins is proportional to oxygen concentration

The increase in both IL-6 and IL-8 secretion by continuously hypoxic A549 cells following X-rays exposure was inversely proportional to the oxygen concentration, that is, it was greater for 0.1 % O_2 compared to 1 % O_2 (Figure 3.23). This relationship was observed at both time points of investigation, 6 and 24 h after irradiation. The effect of severity of hypoxia on radiation-induced IL-6 or IL-8 secretion has not been described before to the best of my knowledge.

The increase in cytokine secretion in (continuously) hypoxic cells following irradiation in an O_2 concentration-dependent fashion remains consistent with results of p65 nuclear translocation studies discussed in section 4.7 whereby higher basal activity of NF-κB at 0.1 % O_2 may explain the higher amount of cytokine secretion in comparison to 1 % or 20 % O_2.

4.8.2.　NF-κB target proteins secretion also increases under influence of hypoxia alone

Even in the absence of irradiation, IL-6 and IL-8 secretion of (continuously) hypoxic cells maintained at 1 % O_2 increased in A549 cells when compared with normoxic controls (Figure 3.23). In H358 cells, only IL-8 secretion increased (Figure 3.24).

Hypoxia-induced cytokine release from tumor cells as well as from inflammatory and stromal cells in the tumor microenvironment has been demonstrated multiple times (206–210). The inflammatory response to hypoxia is mediated mainly by the NF-κB pathway (55,189). The role of HIF in IL-6 and IL-8 production has also been reported recently and appears dependent on cell type. HIF-1α decreases IL-6 and IL-8 production in human gingival epithelial cells (211) but increases it in osteoblasts (212). Hypoxia has also been reported to increase IL-6 (213) and IL-8 (214) secretion by human liver macrophages.

Higher cytokine secretion under the influence of hypoxia only does not appear readily consistent with results of p65 translocation studies carried out using 1% O_2 where hypoxic cells show a relatively lower basal p65 nuclear intensity in the absence of irradiation compared to unirradiated normoxic controls. This apparently reduced p65 intensity may be misleading considering that the hypoxic cells are exposed to 1 % O_2 starting 48 h prior to irradiation which could activate NF-κB at some point during this period. Once NF-κB translocates into the nucleus, it is quickly followed by IκB molecules that bind to them thereby inactivating them and transporting them back into the cytosol. Therefore, the lower p65 intensity signal in the nucleus does not necessarily mean that NF-κB activation has not already occurred during the protracted period of hypoxia and that NF-κB-induced transcription is not already underway manifesting as a higher amount of target protein synthesis.

4.8.3.　Reoxygenation alters secretion of NF-κB-dependent cytokines

In comparison to continuous hypoxia, reoxygenation (transient hypoxia) modulates both basal cytokine secretion as well as irradiation-induced cytokine production.

In case of transiently hypoxic A549 cells (1 % O_2), reoxygenation results in the loss of higher basal secretion of IL-6 and IL-8 that was observed under continuous hypoxia. Furthermore, cytokine secretion is largely comparable to that observed in normoxic controls (Figure 3.23).

After X-rays exposure, transiently hypoxic A549 cells (1 % O_2) do not show any noteworthy increase in IL-6 or IL-8 secretion in comparison to normoxic cells. This correlates well with the differential expression of NF-κB target genes which showed that as opposed to continuously hypoxic cells, a lower number of NF-κB target genes was upregulated in transiently hypoxic A549 cells (1 % O_2) in response to X-rays exposure compared to those irradiated under normoxia. Furthermore, IL-6 and IL-8 were not differentially upregulated as it was the case for continuously hypoxic cells.

This is not the case in H358 cells where transiently hypoxic (1 % O_2) cells produce higher basal amounts of IL-8 compared to not just normoxic cells but also to continuously hypoxic cells (Figure 3.24). This correlates well with p65 nuclear translocation studies where reoxygenation had resulted in progressively increasing basal p65 nuclear localization in comparison to normoxia and continuous hypoxia. Following X-rays exposure, reoxygenation does not lead to an increased secretion of IL-8 compared to corresponding unirradiated control. This also correlates with findings of nuclear translocation studies where X-rays exposure did not further

increase p65 nuclear intensity in reoxygenated cells. Nonetheless, differential gene expression analysis showed that as opposed to continuously hypoxic cells, in transiently hypoxic H358 cells (1 % O$_2$), a greater number of NF-κB target genes was upregulated following X-rays exposure compared to those irradiated under normoxia. Furthermore, differential upregulation of IL-8 became significant in reoxygenated cells following irradiation which was not the case in continuously hypoxic cells.

In conclusion, it appears that reoxygenation results in greater p65 nuclear translocation, higher NF-κB-mediated transcription of the IL-8 gene and greater IL-8 secretion by H358 cells. However, in A549 cells, reoxygenation reduces NF-κB-mediated transcription of IL-6 and IL-8 and decreases their secretion. No studies were found comparing effect of reoxygenation in the presence or absence of ionizing radiation on NF-κB target cytokines or even cytokines in general. However, enhanced nuclear accumulation of activated p65 has been reported in rat lung tissue *in vivo* following repeated hypoxic and reoxygenation cycles (56). Similarly, cyclic hypoxia has been associated with increased IL-6 production in human coronary artery smooth muscle cells (215).

4.9. Conclusion

Hypoxia-induced radioresistance was demonstrated by colony forming ability assays in both A549 (p53-wt) and H358 (p53-null) NSCLC cell lines. This radioresistance increases as oxygen concentration is reduced from 1 % to 0.1 % and is a result of not just the radiochemical effect of hypoxia in modulating radiation toxicity but heavily reliant on cellular adaptations to hypoxia and subsequent reoxygenation.

This radioresistance was observed in response to low-LET ionizing radiation. In response to high-LET radiation, this radioresistance appears only after exposure to high doses (6 and 8 Gy) and therefore, high-LET radiation may be more effective in eliminating hypoxic NSCLC cells.

Hypoxia-induced radioresistance in NSCLC is associated with redistribution of the cell population from the G2 into the G1 phase of the cell cycle and lower induction of DSBs.

Radioresistance in hypoxic NSCLC cells is also associated with earlier activation of the NF-κB pathway under hypoxia along with upregulation of proliferation-related NF-κB target genes as well greater synthesis of NF-κB-dependent cytokines. Thus, cytokine secretion may be used as a prognostic marker in NSCLC. Many upregulated NF-κB target genes are associated with EMT which is understood as a mechanism for developing tumor aggressiveness and metastasis.

Some chemotherapeutic drugs like taxanes and bortezomib have already been reported to inhibit this pathway which contributes to their efficacy in breast cancer and multiple myeloma respectively (216). Inhibition of the NF-κB pathway as a next step to see if it reduces hypoxia-induced radioresistance in NSCLC may provide useful insights into its therapeutically targeting.

5. References

1.   Cancer Statistics [Internet]. SEER. [cited 2022 Jul 25]. Available from: https://seer.cancer.gov/statistics/index.html

2.   Salem A, Asselin MC, Reymen B, Jackson A, Lambin P, West CML, et al. Targeting Hypoxia to Improve Non–Small Cell Lung Cancer Outcome. JNCI J Natl Cancer Inst. 2018 Jan 1;110(1):14–30.

3.   Park JY, Jang SH, Kim HI, Kim JH, Park S, Hwang YI, et al. Thyroid transcription factor-1 as a prognostic indicator for stage IV lung adenocarcinoma with and without EGFR-sensitizing mutations. BMC Cancer. 2019 Dec;19(1):574.

4.   Hanahan D, Weinberg RA. Hallmarks of Cancer: The Next Generation. Cell. 2011 Mar;144(5):646–74.

5.   de Bruin EC, McGranahan N, Mitter R, Salm M, Wedge DC, Yates L, et al. Spatial and temporal diversity in genomic instability processes defines lung cancer evolution. Science. 2014 Oct 10;346(6206):251–6.

6.   Ji W, Weng X, Xu D, Cai S, Lou H, Ding L. Non-small cell lung cancer cells with deficiencies in homologous recombination genes are sensitive to PARP inhibitors. Biochem Biophys Res Commun. 2020 Jan 29;522(1):121–6.

7.   Imielinski M, Berger AH, Hammerman PS, Hernandez B, Pugh TJ, Hodis E, et al. Mapping the Hallmarks of Lung Adenocarcinoma with Massively Parallel Sequencing. Cell. 2012 Sep 14;150(6):1107–20.

8.   Addeo A, Passaro A, Malapelle U, Banna GL, Subbiah V, Friedlaender A. Immunotherapy in non-small cell lung cancer harbouring driver mutations. Cancer Treat Rev. 2021 May 1;96:102-179.

9.   Non-small cell lung cancer clinical practice guidelines [Internet]. National comprehensive cancer network [cited 2022 Jul 20]. Available from: https://www.nccn.org/professionals/physician_gls/pdf/nscl.pdf

10.   Schuurbiers OCJ, Meijer TWH, Kaanders JHAM, Looijen-Salamon MG, de Geus-Oei LF, van der Drift MA, et al. Glucose Metabolism in NSCLC Is Histology-Specific and Diverges the Prognostic Potential of 18FDG-PET for Adenocarcinoma and Squamous Cell Carcinoma. J Thorac Oncol. 2014 Oct;9(10):1485–93.

11.   Liu Y, He C, Huang X. Metformin partially reverses the carboplatin-resistance in NSCLC by inhibiting glucose metabolism. Oncotarget. 2017 Sep 6;8(43):75206–16.

12.   Fong KM. Lung cancer * 9: Molecular biology of lung cancer: clinical implications. Thorax. 2003 Oct 1;58(10):892–900.

13.   Yuan A, Yu CJ, Kuo SH, Chen WJ, Lin FY, Luh KT, et al. Vascular endothelial growth factor 189 mRNA isoform expression specifically correlates with tumor angiogenesis, patient survival, and postoperative relapse in non-small-cell lung cancer. J Clin Oncol Off J Am Soc Clin Oncol. 2001 Jan 15;19(2):432–41.

14.   Esposito L, Conti D, Ailavajhala R, Khalil N, Giordano A. Lung Cancer: Are we up to the Challenge? Curr Genomics. 2010 Nov;11(7):513–8.

15.   Zhou J, Tang Z, Gao S, Li C, Feng Y, Zhou X. Tumor-Associated Macrophages: Recent

Insights and Therapies. Front Oncol. 2020 Feb;10:188.

16.   Bremnes RM, Al-Shibli K, Donnem T, Sirera R, Al-Saad S, Andersen S, et al. The Role of Tumor-Infiltrating Immune Cells and Chronic Inflammation at the Tumor Site on Cancer Development, Progression, and Prognosis: Emphasis on Non-small Cell Lung Cancer. J Thorac Oncol. 2011 Apr;6(4):824–33.

17.   Raskov H, Orhan A, Gaggar S, Gögenur I. Cancer-Associated Fibroblasts and Tumor-Associated Macrophages in Cancer and Cancer Immunotherapy. Front Oncol. 2021 May;11:668731.

18.   Seidel JA, Otsuka A, Kabashima K. Anti-PD-1 and Anti-CTLA-4 Therapies in Cancer: Mechanisms of Action, Efficacy, and Limitations. Front Oncol. 2018 Mar 28;8:86.

19.   Champiat S, Ileana E, Giaccone G, Besse B, Mountzios G, Eggermont A, et al. Incorporating Immune-Checkpoint Inhibitors into Systemic Therapy of NSCLC. J Thorac Oncol. 2014 Feb;9(2):144–53.

20.   Otsuki Y, Saya H, Arima Y. Prospects for new lung cancer treatments that target EMT signaling. Dev Dyn. 2018;247(3):462–72.

21.   Ortiz-Prado E, Dunn JF, Vasconez J, Castillo D, Viscor G. Partial pressure of oxygen in the human body: a general review. Am J Blood Res. 2019 Feb;9(1):1–14.

22.   Begg K, Tavassoli M. Inside the hypoxic tumour: reprogramming of the DDR and radioresistance. Cell Death Discov. 2020 Dec;6(1):77.

23.   Span PN, Bussink J. Biology of Hypoxia. Semin Nucl Med. 2015 Mar;45(2):101–9.

24.   Hockel M, Vaupel P. Tumor Hypoxia: Definitions and Current Clinical, Biologic, and Molecular Aspects. JNCI J Natl Cancer Inst. 2001 Feb;93(4):266–76.

25.   Wigerup C, Påhlman S, Bexell D. Therapeutic targeting of hypoxia and hypoxia-inducible factors in cancer. Pharmacol Ther. 2016 Aug;164:152-69.

26.   Michiels C, Tellier C, Feron O. Cycling hypoxia: A key feature of the tumor microenvironment. Biochim Biophys Acta BBA - Rev Cancer. 2016 Aug;1866(1):76–86.

27.   Al Tameemi W, Dale TP, Al-Jumaily RMK, Forsyth NR. Hypoxia-Modified Cancer Cell Metabolism. Front Cell Dev Biol. 2019 Jan;7:4.

28.   Wang GL, Jiang BH, Rue EA, Semenza GL. Hypoxia-inducible factor 1 is a basic-helix-loop-helix-PAS heterodimer regulated by cellular O2 tension. Proc Natl Acad Sci. 1995 Jun 6;92(12):5510–4.

29.   Eales KL, Hollinshead KER, Tennant DA. Hypoxia and metabolic adaptation of cancer cells. Oncogenesis. 2016 Jan;5(1):e190–e190.

30.   Sen R, Baltimore D. Inducibility of κ immunoglobulin enhancer-binding protein NF-κB by a posttranslational mechanism. Cell. 1986 Dec 26;47(6):921–8.

31.   Singh V, Gupta D, Arora R. NF-kB as a key player in regulation of cellular radiation responses and identification of radiation countermeasures. Discoveries (Craiova). 2015 Mar 31;3(1):e35.

32.   Hellweg CE. The Nuclear Factor κB pathway: A link to the immune system in the radiation response. Cancer Lett. 2015 Nov 28;368(2):275–89.

33.   Hubbi ME, Semenza GL. Regulation of cell proliferation by hypoxia-inducible factors.

Am J Physiol - Cell Physiol. 2015 Dec 15;309(12):C775–82.

34.   Li X, Liu X, Xu Y, Liu J, Xie M, Ni W, et al. KLF5 promotes hypoxia-induced survival and inhibits apoptosis in non-small cell lung cancer cells via HIF-1α. Int J Oncol. 2014 Oct 1;45(4):1507–14.

35.   Russo MA, Sansone L, Carnevale I, Limana F, Runci A, Polletta L, et al. One Special Question to Start with: Can HIF/NFkB be a Target in Inflammation? Endocr Metab Immune Disord Drug Targets. 2015;15(3):171-85.

36.   Pettersen EO, Ebbesen P, Gieling RG, Williams KJ, Dubois L, Lambin P, et al. Targeting tumour hypoxia to prevent cancer metastasis. From biology, biosensing and technology to drug development: the METOXIA consortium. J Enzyme Inhib Med Chem. 2015;30(5):689-721.

37.   Walsh JC, Lebedev A, Aten E, Madsen K, Marciano L, Kolb HC. The Clinical Importance of Assessing Tumor Hypoxia: Relationship of Tumor Hypoxia to Prognosis and Therapeutic Opportunities. Antioxid Redox Signal. 2014 Oct 1;21(10):1516–54.

38.   Joseph JP, Harishankar MK, Pillai AA, Devi A. Hypoxia induced EMT: A review on the mechanism of tumor progression and metastasis in OSCC. Oral Oncol. 2018 May;80:23-32.

39.   Kang HH, Kim IK, Lee H in, Joo H, Lim JU, Lee J, et al. Chronic intermittent hypoxia induces liver fibrosis in mice with diet-induced obesity via TLR4/MyD88/MAPK/NF-kB signaling pathways. Biochem Biophys Res Commun. 2017 Aug 19;490(2):349–55.

40.   Thomlinson RH, Gray LH. The Histological Structure of Some Human Lung Cancers and the Possible Implications for Radiotherapy. Br J Cancer. 1955 Dec;9(4):539–49.

41.   van Elmpt W, Zegers K, Reymen B, Even AJG, Dingemans AMC, Öllers M, et al. Multiparametric imaging of patient and tumour heterogeneity in non-small-cell lung cancer: quantification of tumour hypoxia, metabolism and perfusion. Eur J Nucl Med Mol Imaging. 2016 Feb;43(2):240–8.

42.   Ren W, Mi D, Yang K, Cao N, Tian J, Li Z, Ma B. The expression of hypoxia-inducible factor-1α and its clinical significance in lung cancer: a systematic review and meta-analysis. Swiss Med Wkly. 2013 Sep 6;143:w13855.

43.   Li C, Lu HJ, Na FF, Deng L, Xue JX, Wang JW, et al. Prognostic Role of Hypoxic Inducible Factor Expression in Non-small Cell Lung Cancer: A Meta-analysis. Asian Pac J Cancer Prev. 2013 Jun 30;14(6):3607–12.

44.   Yang SL, Ren QG, Wen L, Hu JL. Clinicopathological and prognostic significance of hypoxia-inducible factor-1 alpha in lung cancer: a systematic review with meta-analysis. J Huazhong Univ Sci Technolog Med Sci. 2016 Jun;36(3):321-327.

45.   Simpson JR, Bauer M, Perez CA, Wasserman TH, Emami B, Doggett RL, et al. Radiation therapy alone or combined with misonidazole in the treatment of locally advanced non-oat cell lung cancer: report of an RTOG prospective randomized trial. Int J Radiat Oncol Biol Phys. 1989 Jun;16(6):1483–91.

46.   Bernier J, Denekamp J, Rojas A, Trovò M, Horiot JC, Hamers H, et al. ARCON: Accelerated radiotherapy with carbogen and nicotinamide in non small cell lung cancer: A phase I/II study by the EORTC. Radiother Oncol. 1999 Aug 1;52(2):149–56.

47.   von Pawel J, von Roemeling R, Gatzemeier U, Boyer M, Elisson LO, Clark P, et al. Tirapazamine plus cisplatin versus cisplatin in advanced non-small-cell lung cancer: A report

of the international CATAPULT I study group. Cisplatin and Tirapazamine in Subjects with Advanced Previously Untreated Non-Small-Cell Lung Tumors. J Clin Oncol Off J Am Soc Clin Oncol. 2000 Mar;18(6):1351–9.

48.   Vens C, Koritzinsky M, Wouters BG. Irradiation-induced damage and the DNA damage response. In: Basic Clinical Radiobiology. 5th ed. Taylor & Francis; 2019. p. 9–22.

49.   Nickoloff JA, Sharma N, Taylor L. Clustered DNA Double-Strand Breaks: Biological Effects and Relevance to Cancer Radiotherapy. Genes. 2020 Jan;11(1):99.

50.   Moeller BJ, Richardson RA, Dewhirst MW. Hypoxia and radiotherapy: opportunities for improved outcomes in cancer treatment. Cancer Metastasis Rev. 2007 Jul 24;26(2):241–8.

51.   Horseman MR, Brown JM, The oxygen effect and therapeutic approaches to tumour hypoxia. In: Basic Clinical Radiobiology. 5th ed. Taylor & Francis; 2019. p. 188–205.

52.   Maier P, Hartmann L, Wenz F, Herskind C. Cellular Pathways in Response to Ionizing Radiation and Their Targetability for Tumor Radiosensitization. Int J Mol Sci. 2016 Jan 14;17(1):102.

53.   Elmore S. Apoptosis: A Review of Programmed Cell Death. Toxicol Pathol. 2007;35(4):495–516.

54.   Munshi A, Ramesh R. Mitogen-Activated Protein Kinases and Their Role in Radiation Response. Genes Cancer. 2013 Sep 1;4(9–10):401–8.

55.   Koong AC, Chen EY, Giaccia AJ. Hypoxia Causes the Activation of Nuclear Factor κB through the Phosphorylation of IκBα on Tyrosine Residues1. Cancer Res. 1994 Mar 1;54(6):1425–30.

56.   Gonchar O, Mankovska I, Gonchar O, Mankovska I. Hypoxia/Reoxygenation modulates Oxidative Stress Level and Antioxidative Potential in Lung Mitochondria: Possible participation of P53 and NF-KB Target Proteins. Arch Pulmonol Respir Care. 2017 May 19;3(1):035–43.

57.   El-Nachef L, Al-Choboq J, Restier-Verlet J, Granzotto A, Berthel E, Sonzogni L, et al. Human Radiosensitivity and Radiosusceptibility: What Are the Differences? Int J Mol Sci. 2021 Jul 2;22(13):7158.

58.   Kabakov AE, Yakimova AO. Hypoxia-Induced Cancer Cell Responses Driving Radioresistance of Hypoxic Tumors: Approaches to Targeting and Radiosensitizing. Cancers. 2021 Jan;13(5):1102.

59.   Oonishi K, Cui X, Hirakawa H, Fujimori A, Kamijo T, Yamada S, et al. Different effects of carbon ion beams and X-rays on clonogenic survival and DNA repair in human pancreatic cancer stem-like cells. Radiother Oncol. 2012 Nov;105(2):258-65.

60.   Wozny AS, Alphonse G, Cassard A, Malésys C, Louati S, Beuve M, et al. Impact of hypoxia on the double-strand break repair after photon and carbon ion irradiation of radioresistant HNSCC cells. Sci Rep. 2020 Dec 7;10(1):21357.

61.   Pouget JP, Mather SJ. General aspects of the cellular response to low- and high-LET radiation. Eur J Nucl Med. 2001 Apr;28(4):541–61.

62.   Chishti AA, Baumstark-Khan C, Koch K, Kolanus W, Feles S, Konda B, et al. Linear Energy Transfer Modulates Radiation-Induced NF-kappa B Activation and Expression of its Downstream Target Genes. Radiat Res. 2018 Jan;189(4):354–70.

63.   Boissonnat G, Fontbonne JM, Balanzat E, Boumard F, Carniol B, Cassimi A, et al. Characterization and performances of DOSION, a dosimetry equipment dedicated to radiobiology experiments taking place at GANIL. Nucl Instrum Methods Phys Res Sect Accel Spectrometers Detect Assoc Equip. 2017 Jun 1;856:1–6.

64.   Durantel F, Balanzat E, Cassimi A, Chevalier F, Ngono-Ravache Y, Madi T, et al. Dosimetry for radiobiology experiments at GANIL. Nucl Instrum Methods Phys Res Sect Accel Spectrometers Detect Assoc Equip. 2016 Apr;816:70–7.

65.   Wulf H, Kraft-Weyrather W, Miltenburger HG, Blakely EA, Tobias CA, Kraft G. Heavy-Ion Effects on Mammalian Cells: Inactivation Measurements with Different Cell Lines. Radiat Res. 1985 Nov 1;104(2s):S122–34.

66.   Korzyńska A, Zychowicz M. A method of estimation of the cell doubling time on basis of the cell culture monitoring data. Biocybern Biomed Eng. 2008;28(4):75–82.

67.   Glucose-GloTM Assay Technical Manual [Internet]. [cited 2022 Sep 1]. Available from: https://www.promega.de/resources/protocols/technical-manuals/101/glucose-glo-assay-protocol/

68.   Lactate Glo Assay Protocol [Internet]. [cited 2022 Sep 1]. Available from: https://www.promega.de/en/resources/protocols/technical-manuals/101/lactate-glo-assay-protocol/

69.   Puck TT, Marcus PI. Action of x-rays on mammalian cells. J Exp Med. 1956 May 1;103(5):653–66.

70.   Kiefer J. Target theory and survival curves. J Theor Biol. 1971 Feb;30(2):307–17.

71.   Suntharalingam N, Podgorsak EB, Hendry JH. Basic Radiobiology. In: Radiation Oncology Physics: A Handbook for Teachers and Students. Austria: International Atomic Energy Agency; 2005. p. 485–504.

72.   Babraham Bioinformatics - FastQC A Quality Control tool for High Throughput Sequence Data [Internet]. [cited 2022 Aug 31]. Available from: https://www.bioinformatics.babraham.ac.uk/projects/fastqc/

73.   de Sena Brandine G, Smith AD. Falco: high-speed FastQC emulation for quality control of sequencing data. F1000Research. 2021 Jan 27;8:1874.

74.   Bolger AM, Lohse M, Usadel B. Trimmomatic: a flexible trimmer for Illumina sequence data. Bioinforma Oxf Engl. 2014 Aug 1;30(15):2114–20.

75.   Dobin A, Davis CA, Schlesinger F, Drenkow J, Zaleski C, Jha S, et al. STAR: ultrafast universal RNA-seq aligner. Bioinformatics. 2013 Jan;29(1):15–21.

76.   Liao Y, Smyth GK, Shi W. The Subread aligner: fast, accurate and scalable read mapping by seed-and-vote. Nucleic Acids Res. 2013 May 1;41(10):e108.

77.   Kato Y, Yashiro M, Fuyuhiro Y, Kashiwagi S, Matsuoka J, Hirakawa T, et al. Effects of Acute and Chronic Hypoxia on the Radiosensitivity of Gastric and Esophageal Cancer Cells. Anticancer Res. 2011 Oct 1;31(10):3369–75.

78.   Klein C, Dokic I, Mairani A, Mein S, Brons S, Häring P, et al. Overcoming hypoxia-induced tumor radioresistance in non-small cell lung cancer by targeting DNA-dependent protein kinase in combination with carbon ion irradiation. Radiat Oncol. 2017 Dec 29;12(1):208.

79.   Leszczynska KB, Foskolou IP, Abraham AG, Anbalagan S, Tellier C, Haider S, et al.

Hypoxia-induced p53 modulates both apoptosis and radiosensitivity via AKT. J Clin Invest. 2015 Jun 1;125(6):2385–98.

80. Zölzer F, Streffer C. Increased radiosensitivity with chronic hypoxia in four human tumor cell lines. Int J Radiat Oncol. 2002 Nov;54(3):910–20.

81. Liu C, Lin Q, Yun Z. Cellular and Molecular Mechanisms Underlying Oxygen-Dependent Radiosensitivity. Radiat Res. 2015;183(5):487–96.

82. Hauth F, Toulany M, Zips D, Menegakis A. Cell-line dependent effects of hypoxia prior to irradiation in squamous cell carcinoma lines. Clin Transl Radiat Oncol. 2017 Aug 1;5:12–9.

83. Schlaff CD, Krauze A, Belard A, O'Connell JJ, Camphausen KA. Bringing the heavy: carbon ion therapy in the radiobiological and clinical context. Radiat Oncol. 2014 Mar 28;9(1):88.

84. Hirayama R, Furusawa Y, Fukawa T, Ando K. Repair Kinetics of DNA-DSB Induced by X-rays or Carbon Ions under Oxic and Hypoxic Conditions. J Radiat Res (Tokyo). 2005 Sep;46(3):325–32.

85. Weyrather WK, Kraft G. RBE of carbon ions: Experimental data and the strategy of RBE calculation for treatment planning. Radiother Oncol. 2004 Dec 1;73:S161–9.

86. Kadono K, Homma T, Kamahara K, Nakayama M, Satoh H, Sekizawa K, et al. Effect of heavy-ion radiotherapy on pulmonary function in stage I non-small cell lung cancer patients. Chest. 2002 Dec;122(6):1925–32.

87. Miyamoto T, Yamamoto N, Nishimura H, Tujii H, Yamaguchi Y. [Heavy ion therapy for non-small cell lung cancer]. Nihon Geka Gakkai Zasshi. 1999 Nov;100(11):729–34.

88. Bonnet RB, Bush D, Cheek GA, Slater JD, Panossian D, Franke C, et al. Effects of proton and combined proton/photon beam radiation on pulmonary function in patients with resectable but medically inoperable non-small cell lung cancer. Chest. 2001 Dec;120(6):1803–10.

89. Miyamoto T, Yamamoto N, Nishimura H, Koto M, Tsujii H, Mizoe J etsu, et al. Carbon ion radiotherapy for stage I non-small cell lung cancer. Radiother Oncol. 2003 Feb 1;66(2):127–40.

90. Iwata H, Murakami M, Demizu Y, Miyawaki D, Terashima K, Niwa Y, et al. High-dose proton therapy and carbon-ion therapy for stage I nonsmall cell lung cancer. Cancer. 2010 May 15;116(10):2476–85.

91. Yamamoto N, Miyamoto T, Nishimura H, Koto M, Tsujii H, Ohwada H, et al. Preoperative carbon ion radiotherapy for non-small cell lung cancer with chest wall invasion—pathological findings concerning tumor response and radiation induced lung injury in the resected organs. Lung Cancer. 2003 Oct 1;42(1):87–95.

92. Pijls-Johannesma M, Grutters JPC, Verhaegen F, Lambin P, De Ruysscher D. Do We Have Enough Evidence to Implement Particle Therapy as Standard Treatment in Lung Cancer? A Systematic Literature Review. The Oncologist. 2010 Jan;15(1):93–103.

93. Subtil FSB, Wilhelm J, Bill V, Westholt N, Rudolph S, Fischer J, et al. Carbon ion radiotherapy of human lung cancer attenuates HIF-1 signaling and acts with considerably enhanced therapeutic efficiency. FASEB J. 2014 Mar;28(3):1412–21.

94. Dai Y, Wei Q, Schwager C, Hanne J, Zhou C, Herfarth K, et al. Oncogene addiction

and radiation oncology: effect of radiotherapy with photons and carbon ions in ALK-EML4 translocated NSCLC. Radiat Oncol Lond Engl. 2018 Jan 5;13:1.

95.   Jones B, Hill MA. Physical characteristics at the turnover-points of relative biological effect (RBE) with linear energy transfer (LET). Phys Med Ampmathsemicolon Biol. 2019 Nov;64(22):225010.

96.   Sjostedt S, Bezak E. Non-targeted effects of ionising radiation and radiotherapy. Australas Phys Eng Sci Med. 2010 Sep;33(3):219–31.

97.   KEGG_CELL_CYCLE [Internet]. [cited 2022 Aug 5]. Available from: https://www.gsea-msigdb.org/gsea/msigdb/cards/KEGG_CELL_CYCLE

98.   Borges KS, Arboleda VA, Vilain E. Mutations in the PCNA-binding site of CDKN1C inhibit cell proliferation by impairing the entry into S phase. Cell Div. 2015 Mar 28;10(1):2.

99.   Vairapandi M, Balliet AG, Hoffman B, Liebermann DA. GADD45b and GADD45g are cdc2/cyclinB1 kinase inhibitors with a role in S and G2/M cell cycle checkpoints induced by genotoxic stress. J Cell Physiol. 2002 Sep;192(3):327–38.

100.   Ma Y, Huang D, Li X, Cheng W, Huang X, Feng H, et al. GADD45B induced the enhancing of cell viability and proliferation in radiotherapy and increased the radioresistance of HONE1 cells. Open Chem. 2021 Jan 1;19(1):1224–34.

101.   Chen L, Yu JH, Lu ZH, Zhang W. E2F2 induction in related to cell proliferation and poor prognosis in non-small cell lung carcinoma. Int J Clin Exp Pathol. 2015 Sep 1;8(9):10545–54.

102.   Arruda NL, Carico ZM, Justice M, Liu YF, Zhou J, Stefan HC, et al. Distinct and overlapping roles of STAG1 and STAG2 in cohesin localization and gene expression in embryonic stem cells. Epigenetics Chromatin. 2020 Dec;13(1):32.

103.   Zhu Y, Gu J, Li Y, Peng C, Shi M, Wang X, et al. MiR-17-5p enhances pancreatic cancer proliferation by altering cell cycle profiles via disruption of RBL2/E2F4-repressing complexes. Cancer Lett. 2018 Jan 1;412:59–68.

104.   Garcia-Carpizo V, Ruiz-Llorente S, Sarmentero J, Graña-Castro O, Pisano DG, Barrero MJ. CREBBP/EP300 bromodomains are critical to sustain the GATA1/MYC regulatory axis in proliferation. Epigenetics Chromatin. 2018 Jun 8;11(1):30.

105.   Hocevar BA, Howe PH. Mechanisms of TGF-beta-induced cell cycle arrest. Miner Electrolyte Metab. 1998;24(2–3):131–5.

106.   Schoecklmann HO, Rupprecht HD, Zauner I, Sterzel RB. TGF-beta1-induced cell cycle arrest in renal mesangial cells involves inhibition of cyclin E-cdk 2 activation and retinoblastoma protein phosphorylation. Kidney Int. 1997 Apr;51(4):1228–36.

107.   García-Gutiérrez L, Bretones G, Molina E, Arechaga I, Symonds C, Acosta JC, et al. Myc stimulates cell cycle progression through the activation of Cdk1 and phosphorylation of p27. Sci Rep. 2019 Dec 10;9(1):18693.

108.   García-Gutiérrez L, Delgado MD, León J. MYC Oncogene Contributions to Release of Cell Cycle Brakes. Genes. 2019 Mar 22;10(3):244.

109.   Tadesse S, Yu M, Kumarasiri M, Le BT, Wang S. Targeting CDK6 in cancer: State of the art and new insights. Cell Cycle. 2015 Aug 28;14(20):3220–30.

110.   Tigan AS, Bellutti F, Kollmann K, Tebb G, Sexl V. CDK6—a review of the past and a glimpse into the future: from cell-cycle control to transcriptional regulation. Oncogene. 2016

Jun;35(24):3083–91.

111. KEGG_HOMOLOGOUS_RECOMBINATION [Internet]. [cited 2022 Aug 5]. Available from: https://www.gsea-msigdb.org/gsea/msigdb/cards/KEGG_HOMOLOGOUS_RECOMBINATION

112. KEGG_NON_HOMOLOGOUS_END_JOINING [Internet]. [cited 2022 Aug 5]. Available from: https://www.gsea-msigdb.org/gsea/msigdb/cards/KEGG_NON_HOMOLOGOUS_END_JOINING.html

113. Fuchs J, Cheblal A, Gasser SM. Underappreciated Roles of DNA Polymerase δ in Replication Stress Survival. Trends Genet. 2021 May;37(5):476–87.

114. Chatterjee N, Walker GC. Mechanisms of DNA damage, repair, and mutagenesis. Environ Mol Mutagen. 2017;58(5):235–63.

115. Lomax ME, Folkes LK, O'Neill P. Biological Consequences of Radiation-induced DNA Damage: Relevance to Radiotherapy. Clin Oncol. 2013 Oct;25(10):578–85.

116. Essers J, Vermeulen W, Houtsmuller AB. DNA damage repair: anytime, anywhere? Curr Opin Cell Biol. 2006 Jun 1;18(3):240–6.

117. Tafani M, Pucci B, Russo A, Schito L, Pellegrini L, Perrone GA, Villanova L, Salvatori L, Ravenna L, Petrangeli E, Russo MA. Modulators of HIF1α and NFkB in Cancer Treatment: Is it a Rational Approach for Controlling Malignant Progression? Front Pharmacol. 2013 Feb 12;4:13.

118. NF-kB Target Genes » NF-kB Transcription Factors | Boston University [Internet]. [cited 2022 Aug 4]. Available from: https://www.bu.edu/nf-kb/gene-resources/target-genes/

119. Park MY, Jang HD, Lee SY, Lee KJ, Kim E. Fas-associated Factor-1 Inhibits Nuclear Factor-κB (NF-κB) Activity by Interfering with Nuclear Translocation of the RelA (p65) Subunit of NF-κB. J Biol Chem. 2004 Jan 23;279(4):2544–9.

120. Watari K, Shibata T, Kawahara A, Sata K ichi, Nabeshima H, Shinoda A, et al. Tumor-derived interleukin-1 promotes lymphangiogenesis and lymph node metastasis through M2-type macrophages. PloS One. 2014;9(6):e99568.

121. Xie K, Wang Y, Huang S, Xu L, Bielenberg D, Salas T, et al. Nitric oxide-mediated apoptosis of K-1735 melanoma cells is associated with downregulation of Bcl-2. Oncogene. 1997 Aug;15(7):771–9.

122. Guo C, Yang XG, Wang F, Ma XY. IL-1α induces apoptosis and inhibits the osteoblast differentiation of MC3T3-E1 cells through the JNK and p38 MAPK pathways. Int J Mol Med. 2016 Jul 1;38(1):319–27.

123. Perrott KM, Wiley CD, Desprez PY, Campisi J. Apigenin suppresses the senescence-associated secretory phenotype and paracrine effects on breast cancer cells. GeroScience. 2017 Apr 4;39(2):161–73.

124. Lessard L, Karakiewicz PI, Bellon-Gagnon P, Alam-Fahmy M, Ismail HA, Mes-Masson AM, et al. Nuclear Localization of Nuclear Factor-κB p65 in Primary Prostate Tumors Is Highly Predictive of Pelvic Lymph Node Metastases. Clin Cancer Res. 2006 Oct 4;12(19):5741–5.

125. Zhang YC, Huo FC, Wei LL, Gong CC, Pan YJ, Mou J, et al. PAK5-mediated phosphorylation and nuclear translocation of NF-κB-p65 promotes breast cancer cell proliferation in vitro and in vivo. J Exp Clin Cancer Res. 2017 Oct 17;36(1):146.

126.   Han X, Guo B, Li Y, Zhu B. Tissue factor in tumor microenvironment: a systematic review. J Hematol OncolJ Hematol Oncol. 2014 Aug 1;7:54.

127.   Eisenreich A, Zakrzewicz A, Huber K, Thierbach H, Pepke W, Goldin-Lang P, et al. Regulation of pro-angiogenic tissue factor expression in hypoxia-induced human lung cancer cells. Oncol Rep. 2013 Jul 1;30(1):462–70.

128.   Xi Y, Chen M, Liu X, Lu Z, Ding Y, Li D. CP-673451, a platelet-derived growth-factor receptor inhibitor, suppresses lung cancer cell proliferation and migration. OncoTargets Ther. 2014 Jul 3;7:1215–21.

129.   Liang G, Liu Z, Tan L, Su A, Jiang WG, Gong C. HIF1α-associated circDENND4C Promotes Proliferation of Breast Cancer Cells in Hypoxic Environment. Anticancer Res. 2017 Aug 1;37(8):4337–43.

130.   Xu L, Ning H, Gu L, Wang Q, Lu W, Peng H, et al. Tristetraprolin induces cell cycle arrest in breast tumor cells through targeting AP-1/c-Jun and NF-κB pathway. Oncotarget. 2015 Oct 19;6(39):41679–91.

131.   Fantozzi I, Zhang S, Platoshyn O, Remillard CV, Cowling RT, Yuan JXJ. Hypoxia increases AP-1 binding activity by enhancing capacitative Ca2+ entry in human pulmonary artery endothelial cells. Am J Physiol-Lung Cell Mol Physiol. 2003 Dec;285(6):L1233–45.

132.   He Y, Luo Y, Zhang D, Wang X, Zhang P, Li H, et al. PGK1-mediated cancer progression and drug resistance. Am J Cancer Res. 2019 Nov 1;9(11):2280–302.

133.   Suresh B, Lee J, Kim KS, Ramakrishna S. The Importance of Ubiquitination and Deubiquitination in Cellular Reprogramming. Stem Cells Int. 2016 Jan 6;2016:e6705927.

134.   Cai J, Li M, Wang X, Li L, Li Q, Hou Z, et al. USP37 Promotes Lung Cancer Cell Migration by Stabilizing Snail Protein via Deubiquitination. Front Genet. 2020 Jan 10;10:1324.

135.   Aldaz P, Otaegi-Ugartemendia M, Saenz-Antoñanzas A, Garcia-Puga M, Moreno-Valladares M, Flores JM, et al. SOX9 promotes tumor progression through the axis BMI1-p21CIP. Sci Rep. 2020 Jan 15;10(1):357.

136.   Jiang SS, Fang WT, Hou YH, Huang SF, Yen BL, Chang JL, et al. Upregulation of SOX9 in Lung Adenocarcinoma and Its Involvement in the Regulation of Cell Growth and Tumorigenicity. Clin Cancer Res. 2010 Aug 31;16(17):4363–73.

137.   Lo PK, Yao Y, Lee JS, Zhang Y, Huang W, Kane MA, Zhou Q. LIPG signaling promotes tumor initiation and metastasis of human basal-like triple-negative breast cancer. Elife. 2018 Jan 19;7:e31334.

138.   Morgan KJ, Doggett K, Geng FS, Whitehead L, Smith KA, Hogan BM, et al. Elys deficiency constrains Kras-driven tumour burden by amplifying oncogenic stress [Internet]. bioRxiv; 2021 Aug 4; 457580.

139.   Scholz BA, Sumida N, de Lima CDM, Chachoua I, Martino M, Tzelepis I, et al. WNT signaling and AHCTF1 promote oncogenic MYC expression through super-enhancer-mediated gene gating. Nat Genet. 2019 Dec;51(12):1723–31.

140.   Viaud M, Abdel-Wahab O, Gall J, Ivanov S, Guinamard R, Sore S, et al. ABCA1 Exerts Tumor-Suppressor Function in Myeloproliferative Neoplasms. Cell Rep. 2020 Mar;30(10):3397-3410.e5.

141.   Lin XM, Luo W, Wang H, Li RZ, Huang YS, Chen LK, Wu XP. The Role of

Prostaglandin-Endoperoxide Synthase-2 in Chemoresistance of Non-Small Cell Lung Cancer. Front Pharmacol. 2019 Aug 8;10:836.

142. Sigismund S, Avanzato D, Lanzetti L. Emerging functions of the EGFR in cancer. Mol Oncol. 2018 Jan;12(1):3–20.

143. Yang M, Zhang T, Zhang Y, Ma X, Han J, Zeng K, et al. MYLK4 promotes tumor progression through the activation of epidermal growth factor receptor signaling in osteosarcoma. J Exp Clin Cancer Res. 2021 May 12;40(1):166.

144. Yasunaga M, Matsumura Y. Role of SLC6A6 in promoting the survival and multidrug resistance of colorectal cancer. Sci Rep. 2014 Apr 30;4(1):4852.

145. Long X, Ye Y, Zhang L, Liu P, Yu W, Wei F, et al. IL-8, a novel messenger to cross-link inflammation and tumor EMT via autocrine and paracrine pathways (Review). Int J Oncol. 2016 Jan 1;48(1):5–12.

146. Millar HJ, Nemeth JA, McCabe FL, Pikounis B, Wickstrom E. Circulating Human Interleukin-8 as an Indicator of Cancer Progression in a Nude Rat Orthotopic Human Non–Small Cell Lung Carcinoma Model. Cancer Epidemiol Biomarkers Prev. 2008 Aug 14;17(8):2180–7.

147. Bajo-Grañeras R, Crespo-Sanjuan J, García-Centeno RM, Garrote-Adrados JA, Gutierrez G, García-Tejeiro M, et al. Expression and potential role of apolipoprotein D on the death-survival balance of human colorectal cancer cells under oxidative stress conditions. Int J Colorectal Dis. 2013 Jun;28(6):751–66.

148. Søiland H, Søreide K, Janssen EAM, Körner H, Baak JPA, Søreide JA. Emerging concepts of apolipoprotein D with possible implications for breast cancer. Cell Oncol Off J Int Soc Cell Oncol. 2007;29(3):195–209.

149. Memon A, Lee WK. KLF10 as a Tumor Suppressor Gene and Its TGF-β Signaling. Cancers. 2018 Jun;10(6):161.

150. Grant K, Loizidou M, Taylor I. Endothelin-1: a multifunctional molecule in cancer. Br J Cancer. 2003 Jan 27;88(2):163–6.

151. Isenberg JS, Roberts DD. THBS1 (thrombospondin-1). Atlas Genet Cytogenet Oncol Haematol. 2020;24(8):291–9.

152. Kaur S, Bronson SM, Pal-Nath D, Miller TW, Soto-Pantoja DR, Roberts DD. Functions of Thrombospondin-1 in the Tumor Microenvironment. Int J Mol Sci. 2021 Apr 27;22(9):4570.

153. Chen H, Liu H, Qing G. Targeting oncogenic Myc as a strategy for cancer treatment. Signal Transduct Target Ther. 2018 Feb 23;3(1):1–7.

154. Dang CV. MYC on the Path to Cancer. Cell. 2012 Mar 30;149(1):22–35.

155. Ogier C, Colombo PE, Bousquet C, Canterel-Thouennon L, Sicard P, Garambois V, et al. Targeting the NRG1/HER3 pathway in tumor cells and cancer-associated fibroblasts with an anti-neuregulin 1 antibody inhibits tumor growth in pre-clinical models of pancreatic cancer. Cancer Lett. 2018 Sep 28;432:227–36.

156. Wu S, Du Y, Beckford J, Alachkar H. Upregulation of the EMT marker vimentin is associated with poor clinical outcome in acute myeloid leukemia. J Transl Med. 2018 Jun 20;16(1):170.

157. Jung S, Yi L, Kim J, Jeong D, Oh T, Kim CH, et al. The Role of Vimentin as a Methylation

Biomarker for Early Diagnosis of Cervical Cancer. Mol Cells. 2011 May 31;31(5):405–11.

158. Katsarou SD, Messaritakis I, Voumvouraki A, Kakavogiannis S, Kotsakis A, Alkahtani S, et al. Detyrosinated α-Tubulin, Vimentin and PD-L1 in Circulating Tumor Cells (CTCs) Isolated from Non-Small Cell Lung Cancer (NSCLC) Patients. J Pers Med. 2022 Feb;12(2):154.

159. Kodama Y, Tanaka I, Sato T, Hori K, Gen S, Morise M, et al. Oxytocin receptor is a promising therapeutic target of malignant mesothelioma. Cancer Sci. 2021 Sep;112(9):3520–32.

160. Li D, San M, Zhang J, Yang A, Xie W, Chen Y, et al. Oxytocin receptor induces mammary tumorigenesis through prolactin/p-STAT5 pathway. Cell Death Dis. 2021 Jun;12(6):588.

161. Yang Z, Liu S, Wang Y, Chen Y, Zhang P, Liu Y, et al. High expression of KITLG is a new hallmark activating the MAPK pathway in type A and AB thymoma. Thorac Cancer. 2020;11(7):1944–54.

162. He S, Xue M, Liu C, Xie F, Bai L. Parathyroid Hormone–Like Hormone Induces Epithelial-to-Mesenchymal Transition of Intestinal Epithelial Cells by Activating the Runt-Related Transcription Factor 2. Am J Pathol. 2018 Jun 1;188(6):1374–88.

163. Chang WM, Lin YF, Su CY, Peng HY, Chang YC, Hsiao JR, et al. Parathyroid Hormone-Like Hormone is a Poor Prognosis Marker of Head and Neck Cancer and Promotes Cell Growth via RUNX2 Regulation. Sci Rep. 2017 Jan 25;7(1):41131.

164. Hu R, Wang Q, Jia Y, Zhang Y, Wu B, Tian S, et al. Hypoxia-induced DEC1 mediates trophoblast cell proliferation and migration via HIF1α signaling pathway. Tissue Cell. 2021 Dec;73:101616.

165. Gwak GY, Yoon JH, Kim KM, Lee HS, Chung JW, Gores GJ. Hypoxia stimulates proliferation of human hepatoma cells through the induction of hexokinase II expression. J Hepatol. 2005 Mar;42(3):358–64.

166. Gardner LB, Li Q, Park MS, Flanagan WM, Semenza GL, Dang CV. Hypoxia Inhibits G1/S Transition through Regulation of p27 Expression*. J Biol Chem. 2001 Mar 1;276(11):7919–26.

167. Druker J, Wilson JW, Child F, Shakir D, Fasanya T, Rocha S. Role of Hypoxia in the Control of the Cell Cycle. Int J Mol Sci. 2021 Jan;22(9):4874.

168. Ortmann B, Druker J, Rocha S. Cell cycle progression in response to oxygen levels. Cell Mol Life Sci. 2014;71(18):3569–82.

169. Vogin G, Foray N. The law of Bergonié and Tribondeau: A nice formula for a first approximation. Int J Radiat Biol. 2013 01;89(1):2–8.

170. Semenza GL. Hypoxia. Cross talk between oxygen sensing and the cell cycle machinery. Am J Physiol-Cell Physiol. 2011 Sep;301(3):C550–2.

171. Li Y, Zhao L, Li XF. Hypoxia and the Tumor Microenvironment. Technol Cancer Res Treat. 2021 Aug 5;20:15330338211036304.

172. Hakem R. DNA-damage repair; the good, the bad, and the ugly. EMBO J. 2008 Feb 20;27(4):589–605.

173. Hasvold G, Lund-Andersen C, Lando M, Patzke S, Hauge S, Suo Z, et al. Hypoxia-

induced alterations of G2 checkpoint regulators. Mol Oncol. 2016 May 1;10(5):764–73.

174.   Green SL, Freiberg RA, Giaccia AJ. p21Cip1 and p27Kip1Regulate Cell Cycle Reentry after Hypoxic Stress but Are Not Necessary for Hypoxia-Induced Arrest. Mol Cell Biol. 2001 Feb 15;21(4):1196–206.

175.   Kim BM, Choi JY, Kim YJ, Woo HD, Chung HW. Reoxygenation following hypoxia activates DNA-damage checkpoint signaling pathways that suppress cell-cycle progression in cultured human lymphocytes. FEBS Lett. 2007 Jun 26;581(16):3005–12.

176.   Suetens A, Konings K, Moreels M, Quintens R, Verslegers M, Soors E, et al. Higher Initial DNA Damage and Persistent Cell Cycle Arrest after Carbon Ion Irradiation Compared to X-irradiation in Prostate and Colon Cancer Cells. Front Oncol. 2016 Apr 13;6:87.

177.   Ma H, Takahashi A, Sejimo Y, Adachi A, Kubo N, Isono M, et al. Targeting of Carbon Ion-Induced G2 Checkpoint Activation in Lung Cancer Cells Using Wee-1 Inhibitor MK-1775. Radiat Res. 2015 Dec;184(6):660-9.

178.   El-Awady RA, Dikomey E, Dahm-Daphi J. Radiosensitivity of human tumour cells is correlated with the induction but not with the repair of DNA double-strand breaks. Br J Cancer. 2003 Aug;89(3):593–601.

179.   Kinner A, Wu W, Staudt C, Iliakis G. γ-H2AX in recognition and signaling of DNA double-strand breaks in the context of chromatin. Nucleic Acids Res. 2008 Oct;36(17):5678–94.

180.   Olcina MM, Grand RJ, Hammond EM. ATM activation in hypoxia - causes and consequences. Mol Cell Oncol. 2014 Jan 1;1(1):e29903.

181.   Marhuenda E, Campillo N, Gabasa M, Martínez-García MA, Campos-Rodríguez F, Gozal D, et al. Effects of Sustained and Intermittent Hypoxia on Human Lung Cancer Cells. 2019;61(4):5.

182.   McCool KW, Miyamoto S. DNA damage-dependent NF-κB activation: NEMO turns nuclear signaling inside out. Immunol Rev. 2012;246(1):311–26.

183.   Di Z, Herpers B, Fredriksson L, Yan K, Water B van de, Verbeek FJ, et al. Automated Analysis of NF-κB Nuclear Translocation Kinetics in High-Throughput Screening. PLOS ONE. 2012 Dec 27;7(12):e52337.

184.   Fuseler JW, Merrill DM, Rogers JA, Grisham MB, Wolf RE. Analysis and Quantitation of NF-κB Nuclear Translocation in Tumor Necrosis Factor Alpha (TNF-α) Activated Vascular Endothelial Cells. Microsc Microanal. 2006 Jun;12(3):269–76.

185.   Moreno R, Sobotzik JM, Schultz C, Schmitz ML. Specification of the NF-κB transcriptional response by p65 phosphorylation and TNF-induced nuclear translocation of IKKε. Nucleic Acids Res. 2010 Oct 1;38(18):6029–44.

186.   Nonaka M, Chen XH, Pierce JE, Leoni MJ, McIntosh TK, Wolf JA, et al. Prolonged activation of NF-kappaB following traumatic brain injury in rats. J Neurotrauma. 1999 Nov;16(11):1023-34.

187.   Chaudhary S, Raghuram GV, Mittra I. Is inflammation a direct response to dsDNA breaks? Mutat Res Mol Mech Mutagen. 2018 Mar 1;808:48–52.

188.   Kim D, Kolch W, Cho KH. Multiple roles of the NF-κB signaling pathway regulated by coupled negative feedback circuits. FASEB J. 2009;23(9):2796–802.

189.   Koong AC, Chen EY, Mivechi NF, Denko NC, Stambrook P, Giaccia AJ. Hypoxic Activation of Nuclear Factor-κB Is Mediated by a Ras and Raf Signaling Pathway and Does Not Involve MAP Kinase (ERK1 or ERK2)1. Cancer Res. 1994 Oct 1;54(20):5273–9.

190.   Patel H, Zaghloul N, Lin K, Liu SF, Miller EJ, Ahmed M. Hypoxia-induced activation of specific members of the NF-kB family and its relevance to pulmonary vascular remodeling. Int J Biochem Cell Biol. 2017 Nov 1;92:141–7.

191.   Nanduri J, Yuan G, Kumar GK, Semenza GL, Prabhakar NR. Transcriptional responses to intermittent hypoxia. Respir Physiol Neurobiol. 2008 Dec 10;164(1):277–81.

192.   Hellweg CE, Baumstark-Khan C, Schmitz C, Lau P, Meier MM, Testard I, et al. Carbon-Ion-Induced Activation of the NF-κB Pathway. Radiat Res. 2011 Jan 11;175(4):424–31.

193.   Hellweg CE, Baumstark-Khan C, Schmitz C, Lau P, Meier MM, Testard I, et al. Activation of the Nuclear Factor κB pathway by heavy ion beams of different linear energy transfer. Int J Radiat Biol. 2011 Sep 1;87(9):954–63.

194.   Hoffmann E, Dittrich-Breiholz O, Holtmann H, Kracht M. Multiple control of interleukin-8 gene expression. J Leukoc Biol. 2002;72(5):847–55.

195.   Brasier AR. The nuclear factor-κB–interleukin-6 signalling pathway mediating vascular inflammation. Cardiovasc Res. 2010 May 1;86(2):211–8.

196.   Kim SY, Kang JW, Song X, Kim BK, Yoo YD, Kwon YT, et al. Role of the IL-6-JAK1-STAT3-Oct-4 pathway in the conversion of non-stem cancer cells into cancer stem-like cells. Cell Signal. 2013 Apr 1;25(4):961–9.

197.   Nguyen DP, Li J, Tewari AK. Inflammation and prostate cancer: the role of interleukin 6 (IL-6). BJU Int. 2014;113(6):986–92.

198.   Tawara K, Oxford JT, Jorcyk CL. Clinical significance of interleukin (IL)-6 in cancer metastasis to bone: potential of anti-IL-6 therapies. Cancer Manag Res. 2011 May 18;3:177–89.

199.   Waugh DJJ, Wilson C. The Interleukin-8 Pathway in Cancer. Clin Cancer Res. 2008 Nov 3;14(21):6735–41.

200.   Yuan A, Chen JJW, Yao PL, Yang PC. The role of interleukin-8 in cancer cells and microenvironment interaction. Front Biosci J Virtual Libr. 2005 Jan 1;10:853–65.

201.   Beetz RUP T Oppel, W Kaffenberger, RA Rupec, M Meyer, D Van Beuningen, P Kind, G Messer, A. NF-κB and AP-1 are responsible for inducibility of the IL-6 promoter by ionizing radiation in HeLa cells. Int J Radiat Biol. 2000 Jan 1;76(11):1443–53.

202.   Song YH, Chai Q, Wang N la, Yang FF, Wang GH, Hu JY. X-rays induced IL-8 production in lung cancer cells via p38/MAPK and NF-κB pathway. Int J Radiat Biol. 2020 Nov 1;96(11):1374–81.

203.   Laurent C, Leduc A, Pottier I, Prévost V, Sichel F, Lefaix JL. Dramatic Increase in Oxidative Stress in Carbon-Irradiated Normal Human Skin Fibroblasts. PLOS ONE. 2013 Dec 23;8(12):e85158.

204.   Simoniello P, Wiedemann J, Zink J, Thoennes E, Stange M, Layer PG, et al. Exposure to Carbon Ions Triggers Proinflammatory Signals and Changes in Homeostasis and Epidermal Tissue Organization to a Similar Extent as Photons. Front Oncol. 2016 Jan 8;5:294.

205.   Zhou H, Yang P, Li H, Zhang L, Li J, Zhang T, et al. Carbon ion radiotherapy boosts

anti-tumour immune responses by inhibiting myeloid-derived suppressor cells in melanoma-bearing mice. Cell Death Discov. 2021 Nov 3;7(1):1–10.

206.   Larsen M, Tazzyman S, Lund EL, Junker N, Lewis CE, Kristjansen PEG, et al. Hypoxia-induced secretion of macrophage migration-inhibitory factor from MCF-7 breast cancer cells is regulated in a hypoxia-inducible factor-independent manner. Cancer Lett. 2008 Jul 8;265(2):239–49.

207.   O'Rourke RW, White AE, Metcalf MD, Olivas AS, Mitra P, Larison WG, et al. Hypoxia-induced inflammatory cytokine secretion in human adipose tissue stromovascular cells. Diabetologia. 2011 Jun 1;54(6):1480–90.

208.   Gulliksson M, Carvalho RFS, Ullerås E, Nilsson G. Mast Cell Survival and Mediator Secretion in Response to Hypoxia. PLOS ONE. 2010 Aug 23;5(8):e12360.

209.   Rattigan Y, Hsu JM, Mishra PJ, Glod J, Banerjee D. Interleukin 6 mediated recruitment of mesenchymal stem cells to the hypoxic tumor milieu. Exp Cell Res. 2010 Dec 10;316(20):3417–24.

210.   Yang M, Ma C, Liu S, Sun J, Shao Q, Gao W, et al. Hypoxia skews dendritic cells to a T helper type 2-stimulating phenotype and promotes tumour cell migration by dendritic cell-derived osteopontin. Immunology. 2009;128(1pt2):e237–49.

211.   Takedachi M, Iyama M, Sawada K, Mori K, Yamamoto S, Morimoto C, et al. Hypoxia-inducible factor-1α inhibits interleukin-6 and -8 production in gingival epithelial cells during hypoxia. J Periodontal Res. 2017;52(1):127–34.

212.   Niu X, Chen Y, Qi L, Liang G, Wang Y, Zhang L, et al. Hypoxia regulates angeogenic-osteogenic coupling process via up-regulating IL-6 and IL-8 in human osteoblastic cells through hypoxia-inducible factor-1α pathway. Cytokine. 2019 Jan 1;113:117–27.

213.   Gao RY, Wang M, Liu Q, Feng D, Wen Y, Xia Y, et al. Hypoxia-Inducible Factor-2α Reprograms Liver Macrophages to Protect Against Acute Liver Injury Through the Production of Interleukin-6. Hepatology. 2020;71(6):2105–17.

214.   Rydberg EK, Salomonsson L, Hultén LM, Norén K, Bondjers G, Wiklund O, et al. Hypoxia increases 25-hydroxycholesterol-induced interleukin-8 protein secretion in human macrophages. Atherosclerosis. 2003 Oct 1;170(2):245–52.

215.   Kyotani Y, Itaya-Hironaka A, Yamauchi A, Sakuramoto-Tsuchida S, Makino M, Takasawa S, et al. Intermittent hypoxia-induced epiregulin expression by IL-6 production in human coronary artery smooth muscle cells. FEBS Open Bio. 2018;8(5):868–76.

216.   Gaptulbarova KA, Tsyganov MM, Pevzner AM, Ibragimova MK, Litviakov NV. NF-kB as a potential prognostic marker and a candidate for targeted therapy of cancer. Exp Oncol. 2020 Dec;42(4):263–9.

6. Abbreviations

ABCA1	ATP Binding Cassette Subfamily A Member 1
ADAM19	A disintegrin and metalloprotease 19
AHCTF1	AT-Hook Containing Transcription Factor 1
ALK	Anaplastic lymphoma kinase
ALOX12	Arachidonate 12-Lipoxygenase, 12S Type
ANGPT1 & 2	Angiopoietin 1 & 2
APC	Antigen presenting cell
APOBEC	Apolipoprotein B mRNA editing enzyme, catalytic polypeptide-like
APOD	Apolipoprotein D
ATM	Ataxia telangiectasia mutant gene
ATP	Adenosine triphosphate
BAK (or Bak)	BCL2 antagonist/killer 1
BAX	BCL2 associated X apoptosis regulator
BCL2	BCL2 apoptosis regulator
BCL2A1	B cell leukemia/lymphoma 2 related protein A1a
BCL2L1 (or BCL-X)	BCL2-like 1
BCL2L2 (or Bcl-w),	BCL2 like 2
BDNF	Brain Derived Neurotrophic Factor
BER	Base excision repair
BLNK	B cell linker protein
BMP2	Bone morphogenetic protein 2
BNIP3	BCL2 Interacting Protein 3
BRAF	B-Raf proto-oncogene
BRCA1	Breast cancer 1 gene
BRCA2	Breast cancer 2 gene
Breg	Regulatory B cells
BUB1	BUB1 Mitotic Checkpoint Serine/Threonine Kinase
c-myc	MYC Proto-Oncogene, BHLH Transcription Factor
CA-IX	Carbonic anhydrase IX
CAFs	Cancer associated fibroblasts
CAV1	Caveolin 1
CBP	Creb-binding protein
CCL2	C-C motif chemokine ligand 2

CCL28	C-C motif chemokine ligand 28
CCR2	C-C motif chemokine receptor type 2
CCR5	C-C motif chemokine receptor type 5
CDC25	Cell division cycle 25A
CDK	Cyclin dependent kinase
CDK4	Cyclin dependent kinase 4
CDK6	Cyclin dependent kinase 6
CDKI	Cyclin dependent kinase inhibitor
CDKN1A	Cyclin dependent kinase inhibitor 1A
CDKN1C	Cyclin dependent kinase inhibitor 1C
CDKN2A	Cyclin dependent kinase inhibitor 2A
CHK1	Cell cycle checkpoint kinase 1
CHK2	Cell cycle checkpoint kinase 2
COX	Cytochrome-C oxidase
CR2	Complement c3d receptor 2
CSA	Cockayne syndrome protein A
CSB	Cockayne syndrome protein B
CSF2	Colony stimulating factor 2
CtIP	C-terminal binding protein interacting protein
CTLA4	Cytotoxic T-lymphocyte associated protein 4
CTLs	Cytotoxic T Lymphocytes
CXCL1	C-X-C motif chemokine ligand 1
CXCR4	CXC-motif receptor type 4
DAMPs	Damage associated molecular patterns
DAPI	4′,6-diamidino-2-phenylindole
DDR	DNA damage response
DISC	Death-inducing signaling complex
DMSO	Dimethyl sulfoxide
DSB	Double strand break
DSBR	Double strand break repair
E2F1	E2F transcription factor 1
E2F2	E2F transcription factor 2
ECM	Extracellular matrix
EDN1	Endothelin 1
EDTA	Ethylenediaminetetraacetic acid

EGF	Epidermal growth factor
EGFR	Epidermal growth factor recepto
ELF3	E74 like factor 2
EML4	Echinoderm microtubule-associated protein-like 4
ENO2	Enolase 2
EP300	E1A-associated protein p300
ERBB	Avian Erythroblastic Leukemia Viral Oncogene Homolog
ERBB1	Avian Erythroblastic Leukemia Viral Oncogene Homolog 1
ERBB2	Avian Erythroblastic Leukemia Viral Oncogene Homolog 2
ERK	Extracellular signal-regulated MAP kinase
F3	Factor III
FABP6	Fatty acid binding protein 6
FADD	Fas associated death domain protein
FAS or CD95	Fas cell surface death receptor
FASLG or CD178	Fas ligand
FBS	Fetal bovine serum
FDG	18F-fluorodeoxyglucose (FDG)
FHIT	Fragile histidine triad diadenosine triphosphatase
FIH	Factor inhibiting HIF
FUS or FUS1	FUS RNA binding protein
GADD45	Growth arrest and DNA damage inducible genes
GADD45B	Growth arrest and DNA damage inducible gene B
GADD45G	Growth arrest and DNA damage inducible gene G
GLUT1	Glucose transporter type 1 (or solute carrier family 2 member 1)
GNRH2	Gonadotropin releasing hormone 2
GPDH	Glyceraldehyde 3-phosphate dehydrogenase
GTP	Guanosine triphosphate
GTPase	Guanosine triphosphatase
H2AX	H2A histone family member X
H_2O_2	Hydrogen per oxide
HER2	Human epidermal growth factor receptor 2
HIF	Hypoxia inducible factor
HMGB1	High mobility group box 1 protein
HR	Homologous repair
HREs	Hypoxia response elements

IDO1	Indoleamine 2,3-Dioxygenase 1
IKK	IκB Kinase
IL1	Interleukin 1
IL-1A	Interleukin 1A
IL6	Interleukin 6
IL8	Interleukin 8
IRF7	Interferon regulatory factor 7
IRR	inflammatory reparative response
IκB	Inhibitor of Kappa B
JAK/STAT3	Janus kinase-signal transducer and activator of transcription 3
JUNB	Transcription factor Jun-B
KCNK5	Potassium two pore domain channel subfamily K member 5
KITLG	KIT ligand
KLF5	Krüppel-like factors 5
Kras	Kirsten Rat Sarcoma virus oncogene homolog
LDH	Lactate dehydrogenase
LET	Linear energy transfer
LIG4	DNA ligase 4
LIPG	Lipase G
LOH	Loss of heterozygosity
LOX	Lysyl hydroxylase
MAP	Mitogen activated protein
MAP4K	Mitogen activated protein kinase kinase kinase kinase 1
MAPK	Mitogen activated protein kinase
Max	Myc associated protein X
MCL1 (or Mcl-1)	MCL1 apoptosis regulator, BCL2 family member
MCM complex	Mini-chromosome maintenance complex
MDK	Midkine
MDM2	Mouse double minute 2 homolog proto-oncogene
MDSC	Myeloid-derived suppressor cells
MERLIN	Moesin-ezrin-radixin like
MET	Met proto-oncogene
MHC	Major histocompatibility complex
mm Hg	Millimeters of mercury
MMP9	Matrix metallopeptidase 9

MMR	Mismatch repair
MRE11	Meotic recombination 11 homolog 1
MRN complex	MRE11, RAD50 and NBS1 complex
MSH	MutS Homolog proteins
MX1	MX dynamin like GTPase 1
MYC	Myc proto-oncogene, BHLH transcription factor
MYLK	Myosin light chain kinase
NBS1	Nijmegen break syndrome 1
NEMO (or IκBγ)	NF-κB essential modulator
NER	Nucleotide excision repair
NF-κB	Nuclear factor κB
NF2	Moesin-ezrin-radixin like (MERLIN) tumor suppressor gene
NHEJ	Non-homologous end joining
NIK	NFκB inducing kinase
NK cells	Natural killer cells
NRG1	Neuroregulin 1
O_2	Oxygen
$O_2^{\bullet-1}$	super oxide anion
OER	Oxygen enhancement ratio
$OH^{\bullet}$	Hydroxyl radical
OS	Overall survival
OXTR	Oxytocin receptor
PARP	Poly-(ADP-ribose) polymerase
PBS	Phosphate buffered saline
PCNA	proliferating cell nuclear antigen
PD-1	Programmed cell death 1
PDGF-β (or PDGFB)	Platelet-derived growth factor-β
PDL1 (or CD274)	Programmed death ligand 1
PES	Polyethersulfone
PET	Positron emission tomography
PGK1	Phosphoglycerate kinase 1
PHD	Prolyl hydroxylase
PI	Propidium iodide
PI3K	Phosphatidylinositol 3-kinase

PIDD	P53 induced death domain containing protein
PKM2	Pyruvate kinase isozyme M2
PMMA	Poly methyl methacrylate
POLD2	DNA polymerase delta 2
PRKDC	Protein Kinase, DNA-Activated, Catalytic Subunit
PSMb9	Proteasome 20S subunit beta 9
PSME2	Proteasome activator subunit 2
PTAFR	Platelet activating factor receptor
PTGES	Prostaglandin E synthase
PTGS2	Prostaglandin-Endoperoxide Synthase 2
PTHLH	Parathyroid Hormone Like Hormone
PTPN11	Protein tyrosine phosphatase non-receptor type 11
PUMA	P53-upregulated modulator of apoptosis
RAD50	Rad50 homolog double strand break repair protein
RAD51	Rad51 recombinase
RASSF1A	Ras association domain family member 1
RB	Retinoblastoma gene
RBE	Relative biological effectiveness
RBL2	RB transcriptional corepressor like 2
REL	c-Rel proto-oncogene
RET	Ret proto-oncogene
REV3L	REV3 like DNA directed polymerase zeta catalytic subunit;
RIOK3	Right open reading frame kinase 3
RIP1	Receptor interacting protein 1
RNF168	Ring finger protein 168
RNF8	Ring finger protein 8
ROS	Reactive oxygen species
ROS1	UR2 sarcoma virus oncogene homolog 1
SDF-1	Stromal-derived factor-1
SDF-1α	Stromal-derived factor 1α
SEMA3B	Semaphorin 3B
SIPS	Stress-induced premature senescence
SLC2A	Solute carrier family 2A
SLC6A6	Solute carrier family 6A6
SNAI1 or snail	Snail family transcriptional repressor 1,

SNAI2 or Slug	Snail family transcriptional repressor 2
SOX9	SRY-Box Transcription Factor 9
SSB	Single strand break
SSBR	Single strand break repair
STAG1	Stromal antigen 1
SUMO1	Small ubiquitin like modifier 1
TAK1	TGF-β activated kinase 1
TAMs	Tumor associated macrophages
TBE	Tris-borate-EDTA
TCF3	Transcription factor 3
TCR	T cell receptor
TERT	Telomerase reverse transcriptase
TGF-α	Transforming growth factor alpha
TGFB2	Transforming growth factor beta 2
THBS1	Thrombospondin 1
TKI	Tyrosine kinase inhibitor
TME	Tumor microenvironment
TNF	Tumor necrosis factor
TNFAIP3	TNFα Induced Protein 3
TNFSF10	TNF superfamily member 10
TNFSF11 (or RANKL)	TNF superfamily member 11
TNFSF13B (or BAFF)	TNF superfamily member 13b
TP53	Tumor protein p53 gene
TP53BP1	Tumor protein p53 binding protein 1
TRAF	TNF Receptor Associated Factor 1
Treg	Regulatory T cell
TREM1	Triggering receptor expressed on myeloid cells 1
TSGs	Tumor suppressor genes
TSP-1	Thrombospondin 1
TTF-1	Thyroid transcription factor 1
Twist 1	Twist family basic helix loop helix (BHLH) transcription factor 1
Twist 2	Twist family basic helix loop helix (BHLH) transcription factor 2
UCP2	Uncoupling protein 2
Uimc1	Ubiquitin interaction motif containing protein 1

UPP1	Uridine phosphorylase 1
VEGFA	Vascular endothelial factor A
VEGFC	Vascular endothelial growth factor C
VEGFR	Vascular endothelial factor receptor
VHL	Von hippel lindau factor
VIM	Vimentin
XLF	XRCC4-like factor
XPC	Xeroderma pigmentosum complementation group C
XRCC1	X-ray repair cross complementing 1
XRCC4	X-ray repair, complementing defective, in Chinese hamster, 4
Z	Atomic number
Zeb 1	Zinc finger E-box binding homeobox 1
Zeb 2	Zinc finger E-box binding homeobox 2

7.   Acknowledgements

8. CV

PERSONAL   Hasan Nisar

Date of Birth	**March 23, 1985**
Nationality	**Pakistan**
Contact Address	**Department of Radiation Biology, Institute of Aerospace Medicine, German Aerospace Center (DLR), Linder Höhe, 51147, Cologne, Germany.**
Office Phone number	**+92 51111 174 327**
Cell Phone number	**+92 3454938666**
Email	**hasanisar@pieas.edu.pk, hasanisar@gmail.com**
Online Profile	**https://www.researchgate.net/profile/Hasan_Nisar**

EDUCATIONAL & PROFESSIONAL HISTORY

2018 Onward	**At present, pursuing PhD Tumor and Radiation Biology** University of Cologne, Cologne, Germany.
2011-2018	**Held University Teaching and Research Faculty Position for 7 years** Department of Medical Sciences, Pakistan Institute of Engineering and Applied Sciences, Islamabad, Pakistan.
2015-2016	**Worked as Clinical Oncology Practitioner for 6 months** As Radiation Oncologist at Institute of Nuclear Medicine and Oncology Lahore (INMOL), Pakistan.
2009-2011	**Completed 2 year MSc Radiation and Medical Oncology** From Pakistan Institute of Engineering & Applied Sciences (PIEAS), Islamabad, Pakistan.
2010-2011	**Completed Hospital Training in Clinical Oncology for 1 year** In Radiation and Medical Oncology at Nuclear Oncology and Radiotherapy Institute (NORI), Islamabad and Central Military Hospital (CMH), Rawalpindi.
2003-2009	**Completed Double Bachelors in Medicine and Surgery** From Rawalpindi Medical College, University of Health Sciences, Lahore, Pakistan.
2008-2009	**Worked as Clinical Resident for 1 year** In Internal Medicine at Federal Government Polyclinic, Islamabad for 6 months In Ophthalmology at Holy Family Hospital, Rawalpindi for 6 months.

ACADEMIC ACHIEVEMENTS

Publications (all peer-reviewed)

1. Chishti AA, Baumstark-Khan C, **Nisar H**, Hu Y, Konda B, Henschenmacher B, Spitta LF, Schmitz C, Feles S, Hellweg CE. The Use of ProteoTuner Technology to Study Nuclear Factor κB Activation by Heavy Ions. Int J Mol Sci. 2021 Dec 16;22(24):13530

2. Gul B, Ashraf S, Khan S, **Nisar H,** Ahmad I. Cell refractive index: Models, insights, applications and future perspectives. PDPT. 2021, 33: 102096.

3. Khan MA, Maken RN, **Nisar H**, Fatima I, Khan IU, Masood M, Shahid AB. The Role of Preoperative Carcinoembryonic Antigen in Recurrence of Resectable Colorectal Carcinoma. Acta Clin Croat. 2020, 59(2): 216-221.

4. Rehman SU, Farooq A, **Nisar H**, Fatima I, Masood M, Shahid A. To Study the Response of Locally Advanced Nasopharyngeal Cancer to Concurrent Chemo-radiotherapy. J Kuwait Med Assoc. 2020, 52(3):291-296.

5. Khan S, Farooq A, Masood M, Shahid AB, Khan IU, **Nisar H**, Fatima I. Smokeless tobacco use and risk of oral cavity cancer. Turk J Med Sci. 2020, 50: 291-297

6. Anjum W, Maken RN, **Nisar H**, Fatima I, Masood M, Shahid AB. Epidemiology and Treatment Outcomes of Sinonasal Tumors: A Single Institute's Experience in Pakistan. J Coll Physicians Surg Pak. 2019, 29(4):356-360.

7. Ahmad I, **Nisar H**. Dosimetry Perspectives in Radiation Synovectomy. Physica Medica. 2018, 47:64–72.

8. Sattar A, Masood M, **Nisar H**, Fatima I, Shahid A. Disease Characteristics and Treatment Outcome of Testicular Germ Cell Tumors Treated with Platinum−Based Regimens. JCPSP. 2018, 28(4):292−296.

9. Zamir A, Farooq A, **Nisar H**, Fatima I, UllahKhan I, Masood M, Shahid A. Studying the Efficacy of Escalated Dose Conformal Radiation Therapy in Prostate Carcinoma − Pakistan Experience. JCMA. 2017, 80(11):705–711.

10. Rehman A, Allaudin Z, **Nisar H**, Khan IU, Fatima I, Shami A, Masood M, Shahid A. Efficacy and Toxicity of Concurrent Chemoradiation in Inoperable Oral Carcinoma in Pakistani Population. JCPSP. 2017, 27(6):342–347.

11. Razaq T, **Nisar H**, Roohi S, Shehzad A, Ahmad I. Administration of 99mTc−DTPA in Combination with Doxorubicin Alters the Radiopharmaceutical Biodistribution in Rats. IRJNM. 2017, 25(2):122–128.

12. Ullah I, Ahmad I, **Nisar H**, Khan S, Ullah R, Rashid R, Mahmood H. Computer Assisted Optical Screening of Human Ovarian Cancer Using Raman Spectroscopy. PDPT.2016, 15:94–99.

13. Ahmad I, Rehman A, Khan J, Rafi M, Khurshid A, **Nisar H**, S.S.Z. Zaidi, Masroor Ikram. Effects of Varying Local Temperature on the Optical Properties of Cells In−vitro. PDPT. 2015, 12(3):459–465.

Fellowships, Projects and Awards
- Secured research project titled "P1206-H: Epithelial Mesenchymal Transformation (EMT) in Hypoxic Human Carcinoma Cells after Carbon Ion Exposure" at Ganil, Caen France in 2019.
- DAAD−HEC PhD Scholarship for Pakistani Students to pursue PhD in Germany in 2018.
- UICC International Research Fellowship for Cancer Technology Transfer (ICRETT) in 2017.
- Pakistan Atomic Energy Commission National Scholarship for Masters Studies in 2009.

Conferences
- Participated in DeGBS annual meeting September 27-29, 2021 in Germany.
- Participated in 45th Asia Pacific Advanced Networking (APAN 45) conference in Singapore in 2018 as focal person from my employing organization.
- PIEAS National Symposium on Nuclear Medicine and Oncology, October 2017.

CORE COMPETENCES

Standard methods and specialized techniques

- **Radiation and Tumor Biology**
  - Sound knowledge of didactic components like histopathology, genetics, radiation and medical physics.
  - Cell culture, cell growth curves and colony forming assays.
- **Radiotherapy**
  - Patient radiation dose prescription for solid tumors
  - Preparation of both 2D and 3D conformal treatment plans for malignant human solid tumors on Varian Treatment Planning Systems.
  - Side effect management and response assessment.
- **Chemotherapy**
  - Regimen selection and patient dose prescription for solid tumors
  - Chemotherapy drug preparation and administration
  - Side effect management and response assessment

Teaching

- **Taught 8 postgraduate courses** (5 in full and 3 in part) to medical doctors and medical physicists. List with details is attached as annexure.
- **Member of Board of Studies**, Department of Medical Sciences from 2014 to 2018.

- **Set annual entrance examination for MSc** Radiation and Medical Oncology on various occasions.
- **Set and marked year round examination** papers for courses I was teaching.

Research Supervision

- **Supervised of 17 Master Theses** pertaining to Oncology and Medical Physics. List with details is attached as annexure.
- **Reviewed Scientific Papers** and Research Projects for Pakistan Science Foundation and Pakistan Medical Council from 2016 to 2018.

Project Management

- **Served as Course Coordinator** from 2012 till 2017 **and as Research Project Coordinator** from 2017 to 2018 for MSc Radiation & Medical Oncology.
- **Co-designed course and program layout of MSc** Radiation and Medical Oncology.
- **PIEAS University Focal person for Tele–medical education** in collaboration with PERN, HEC, Pakistan from 2015 to 2018.
- **Member of PIEAS Public Relations** Division from 2017 to 2018.
- **Project Team Member of Quality Enhancement Cell** (QEC), PIEAS for MSc Radiation Medical Oncology from 2013 to 2018.

Workshops/ Seminars/ Online courses

- Participated in AMNZ Workshop titled "Technical English Writing" by Ann Wegner, on November 28 and 29, 2018.
- Participated in Bi-weekly On-line Course titled "Biostatistics for Biological and Health Sciences" by Prof. Dr. H. Anwar Ahmad in August to December, 2015.

Computer Programs

- Basic knowledge of Microsoft Office, SPSS v.15 and Endnote.

Languages

English	Reading, writing and speaking
Urdu	Reading, writing and speaking
German	A2 level

ACTIVITIES

Professional Memberships

- Licensed Medical Practitioner and Clinical Oncologist with Pakistan Medical and Dental Council (PMDC), Pakistan.
- Member, Pakistan Society of Clinical Oncology, Pakistan.
- Member Board of Studies, Department of Medical Sciences, Master Programs, PIEAS, Pakistan.
- Member of Association of UICC Fellows.

Volunteer activities

- Provided volunteer emergency medical services around university campus for students from 2011 till 2018.
- Created PIEAS graduated Clinical Oncologists Alumni network and used it to facilitate cancer patients around the country.

9. Appendix

Table 9.1   Cellular pathways and associated genes that were differentially regulated in continuous hypoxia in comparison to normoxia 4 h after X-ray exposure in A549 cells.

Cellular Pathway	DEGs (gene name abbreviation)	Continuous Hypoxia vs. Normoxia		Transient Hypoxia vs. Normoxia	
		Log$_2$ fold change	P$_{adj}$ value ($\alpha < 0.05$)	Log$_2$ fold change	P$_{adj}$ value ($\alpha < 0.05$)
Glycolysis/ Gluconeogenesis associated genes	ALDOC	3.35	****	2.91	****
	LDHA	1.47	****	1.18	****
	PGK1	1.51	****	1.17	****
Chemokine signaling pathway associated genes	CCL2	1.22	****	1.09	****
	GNG13	-1.12	**	-1.24	**
	GNG4	1.47	****	1.29	**
	DOCK2	1.45	****	1.35	****
HIF-1 signaling pathway associated genes	ALDOA	1.30	****		
	ANGPT1	-1.09	*		
	EGLN3	3.43	****		
	ENO2	1.11	****		
	HK2	1.74	****		
	IL6R	-1.04	****		
	PDK1	2.18	****		
	SERPINE1	1.94	****		
	SLC2A1	1.19	****		
	VEGFA	1.05	****		
Hippo signaling pathway associated genes	FRMD6	1.40	*		
	SOX2	-1.03	***		
	WNT5A	-1.18	*		
	WNT5B	2.49	****		
	WNT7A	2.32	**		
	BMP6	1.46	****		
	BMPR2	1.16	****		
	SERPINE1	1.94	****		
	TGFBR1	1.04	****		
PI3K-AKT signaling pathway associated genes	DDIT4	1.35	****		
	ANGPT1	-1.09	*		
	COL1A1	2.35	****		
	COL4A1	1.04	****		
	COL9A3	1.01	*		
	EFNA1	2.01	****		
	EFNA3	1.40	****		
	ITGA1	1.01	**		
	ITGA11	1.31	**		

Cellular Pathway	DEGs (gene name abbreviation)	Continuous Hypoxia vs. Normoxia		Transient Hypoxia vs. Normoxia	
		Log$_2$ fold change	P$_{adj}$ value ($\alpha < 0.05$)	Log$_2$ fold change	P$_{adj}$ value ($\alpha < 0.05$)
	IL6R	-1.04	****		
	LAMB3	1.02	****		
	LAMC2	1.43	**		
	PDGFB	1.78	****		
	SGK1	1.15	**		
	VEGFA	1.05	****		
ECM receptor interaction associated genes	COL1A1	2.35	****		
	COL4A1	1.04	****		
	COL9A3	1.01	*		
	ITGA1	1.01	**		
	ITGA11	1.31	**		
	LAMB3	1.02	****		
	LAMC2	1.43	**		
Focal adhesion associated genes	COL1A1	2.35	****		
	COL4A1	1.04	****		
	COL9A3	1.01	*		
	FLNC	1.10	**		
	ITGA1	1.01	**		
	ITGA11	1.31	**		
	LAMB3	1.02	****		
	LAMC2	1.43	**		
	PDGFB	1.78	****		
	VEGFA	1.05	****		
Genes associated with pathways in cancer	CXCL8 (IL8)	1.38	*		
	CEBPA	-1.15	***		
	RASGRP3	1.58	****		
	WNT5A	-1.18	*		
	WNT5B	2.49	****		
	WNT7A	2.32	**		
	AGTR1	1.34	*		
	COL4A1	1.04	****		
	EGLN3	3.43	****		
	GADD45B	1.20	****		
	IL6R	-1.04	****		
	LAMB3	1.02	****		
	LAMC2	1.43	**		
	PDGFB	1.78	****		
	RET	1.19	**		
	SLC2A1	1.19	****		

Cellular Pathway	DEGs (gene name abbreviation)	Continuous Hypoxia vs. Normoxia		Transient Hypoxia vs. Normoxia	
		Log$_2$ fold change	P$_{adj}$ value ($\alpha < 0.05$)	Log$_2$ fold change	P$_{adj}$ value ($\alpha < 0.05$)
	TGFBR1	1.04	****		
	VEGFA	1.05	****		
	RASGRP3	1.58	****		
	ANGPT1	-1.09	*		
	CACNA1B	3.99	****		
	CACNA1I	2.06	**		
MAPK signaling pathway associated genes	EFNA1	2.01	****		
	EFNA3	1.40	****		
	FLNC	1.10	**		
	GADD45B	1.20	****		
	PLA2G4B	-1.32	*		
	PDGFB	1.78	****		
	TGFBR1	1.04	****		
	VEGFA	1.05	****		
	POU5F1	1.65	****		
	SOX2	-1.03	***		
Genes associated with signaling pathways regulating pluripotency of stem cells	WNT5A	-1.18	*		
	WNT5B	2.49	****		
	WNT7A	2.32	**		
	BMPR2	1.16	****		
	INHBA	1.55	**		
	ETS2	1.11	****		
	RASGRP3	1.58	****		
	ANGPT1	-1.09	*		
	EFNA1	2.01	****		
RAS signaling pathway associated genes	EFNA3	1.40	****		
	KSR2	1.44	****		
	PLA2G4B	-1.32	*		
	PDGFB	1.78	****		
	VEGFA	1.05	****		
cGMP-PKG signaling pathway associated genes	CREB5			1.28	**
	RGS2			1.28	*
*: p<0.05; **: p<0.01; ***: p<0.001; ****: p<0.0001					

Table 9.2   Expression of genes that were differentially regulated in A549 cells under continuous hypoxia in comparison to normoxia 4 h after carbon ion exposure. The genes were assigned to cellular pathways by means of DAVID.

Cellular Pathway	DEGs (gene name abbreviation)	Continuous Hypoxia 8 Gy vs. 0 Gy	
		Log$_2$ fold change	P$_{adj}$ value (α < 0.05)
NF-κB signaling pathway	BCL2A1	1.52	**
	CXCL8 (IL8)	1.49	****
	TRAF1	1.28	****
	TNFRSF13C	-1.07	***
	CARD11	1.15	****
	LAT	-1.56	***
Cellular senescence	CXCL8 (IL8)	1.49	****
	ETS1	1.03	****
	IGFBP3	1.57	*
	IL1A	2.75	****
	IL6	1.13	****
	PIK3CD	1.10	****
	SERPINE1	1.83	****
Relaxin signaling pathway	GNG13	-1.17	**
	CREB3L1	1.13	****
	COL1A1	1.75	****
	MMP9	2.41	****
	PIK3CD	1.10	****
	VEGFA	1.07	****
	VEGFD	-1.36	*
TNF signaling pathway	JUNB	1.34	****
	TRAF1	1.28	****
	CREB3L1	1.13	****
	IL6	1.13	****
	MMP9	2.41	****
	PIK3CD	1.10	****
	VEGFD	-1.36	*
Focal adhesion	COL1A1	1.75	****
	ITGA2	1.60	****
	ITGB6	1.47	***
	LAMB3	1.12	****
	LAMC2	2.14	****
	MYLK2	-1.12	*
	PIK3CD	1.10	****
	PDGFB	1.91	****
TGF ß signaling pathway	BMP6	1.87	****
	BMPR2	1.24	****
	FST	1.03	****

Cellular Pathway	DEGs (gene name abbreviation)	Continuous Hypoxia 8 Gy vs. 0 Gy	
		Log$_2$ fold change	P$_{adj}$ value (α < 0.05)
	GDF6	1.20	*
	INHBA	1.52	**
	INHBB	-1.16	****
	ID4	-1.10	**
	TIMP3	1.37	*
	WNT5B	2.26	****
	WNT7A	3.76	****
	COL1A1	1.75	****
	ESR1	-1.27	**
Proteoglycans in cancer	HOXD10	1.36	****
	IGF2	1.07	**
	ITGA2	1.60	****
	MMP9	2.41	****
	PIK3CD	1.10	****
	VEGFA	1.07	****
	CXCL8	1.49	****
	TNFRSF13C	-1.07	***
	TNFSF9	-1.09	****
	BMP6	1.87	****
	BMPR2	1.24	****
	GDF15	-1.14	****
Cytokine-cytokine receptor interaction	GDF6	1.20	*
	INHBA	1.52	**
	INHBB	-1.16	****
	IL1A	2.75	****
	IL31RA	1.05	****
	IL6R	-1.19	****
	IL6	1.13	****
	IL7R	1.14	****
	ETS1	1.03	****
	GNG13	-1.17	**
	EFNA2	1.16	***
	EFNA3	1.41	****
	FGF1	1.85	***
Ras signaling pathway	IGF2	1.07	**
	KSR2	1.12	****
	LAT	-1.56	***
	PIK3CD	1.10	****
	PDGFB	1.91	****
	VEGFA	1.07	****
	VEGFD	-1.36	*

Cellular Pathway	DEGs (gene name abbreviation)	Continuous Hypoxia 8 Gy vs. 0 Gy	
		Log$_2$ fold change	P$_{adj}$ value ($\alpha < 0.05$)
HIF signaling pathway	ALDOC	1.44	***
	EGLN3	2.03	****
	HK2	1.87	****
	IL6R	-1.19	****
	IL6	1.13	****
	PIK3CD	1.10	****
	PDK1	1.58	****
	SERPINE1	1.83	****
	VEGFA	1.07	****
Signaling pathways regulating pluripotency of stem cells	SOX2	-1.66	****
	WNT5B	2.26	****
	WNT7A	3.76	****
	AXIN2	-1.19	**
	BMPR2	1.24	****
	INHBA	1.52	**
	INHBB	-1.16	****
	ID4	-1.10	**
	PIK3CD	1.10	****
ns: not significant; *: p<0.05; **: p<0.01; ***: p<0.001; ****: p<0.0001			

Table 9.3   Cellular pathways and expression of associated genes that were differentially regulated under both continuous and transient hypoxia in comparison to normoxia 4 h after X-rays exposure (8 Gy) in H358 cells.

Cellular Pathway	DEGs (gene name abbre-viation)	Continuous Hypoxia, 8 Gy, vs. Normoxia, 8 Gy		Transient Hypoxia, 8 Gy, vs. Normoxia, 8 Gy	
		Log_2 fold change	P_{adj} value ($\alpha < 0.05$)	Log_2 fold change	P_{adj} value ($\alpha < 0.05$)
Adherence junctions associated genes	FER	1.38	****	1.23	***
	IQGAP1	1.10	**	1.01	*
	EGFR	1.53	**	1.29	*
	PTPRB	1.28	**	1.13	***
Regulation of actin cytoskeleton	IQGAP1	1.10	**	1.01	*
	EGFR	1.53	**	1.29	*
	ITGA2	1.17	*	1.36	*
	ITGAV	1.40	*	1.30	*
	ITGB8	1.59	*	2.26	****
	MYLK	1.50	**	1.66	****
	SSH1	1.18	*	1.01	*
Oxidative phosphoryla-tion associated genes	ATP5MC1	-1.37	*	-1.33	*
	ATP6V0D1	-1.36	*	-1.20	*
	NDUFS7	-1.20	*	-1.21	*
	NDUFB9	-1.07	*	-1.17	*
	NDUFA4L2	2.24	*	3.53	****

*: $p<0.05$; **: $p<0.01$; ***: $p<0.001$; ****: $p<0.0001$; n = 4

Table 9.4   Cellular pathways and expression of associated genes that were differentially regulated under continuous hypoxia in comparison to normoxia 4 h after X-rays exposure (8 Gy) in H358 cells.

Cellular Pathway	DEGs (gene name abbreviation)	Continuous Hypoxia, 8 Gy, vs. Normoxia, 8 Gy	
		Log$_2$ fold change	P$_{adj}$ value (α < 0.05)
HIF-1 signaling pathway associated genes	PFKFB3	2.00	**
	EP300	1.15	**
	MKNK2	1.23	*
	EGLN1	1.27	*
	EGLN3	2.26	*
	EIF4EBP1	-1.44	*
	HK2	1.99	**
	PRKCA	1.02	***
	PDK1	1.65	**
	VEGFA	1.67	*
EGFR Tyrosine kinase inhibitor resistance associated genes	MET	1.16	**
	SHC3	1.02	*
	SOS1	1.07	**
	EIF4EBP1	-1.44	*
	NF1	1.29	****
	PRKCA	1.02	***
	TGFA	1.03	*
	VEGFA	1.67	*
MAPK signaling pathway associated genes	ELK4	1.27	**
	MKNK2	1.23	*
	MET	1.16	**
	SOS1	1.07	**
	TAOK1	1.26	****
	CACNA2D1	1.13	*
	FGF22	-1.54	*
	HSPB1	-1.85	*
	IL1RAP	1.39	*
	MAPK8IP2	-1.16	*
	NF1	1.29	****
	PRKCA	1.02	***
	TGFA	1.03	*
	TGFBR1	1.05	*
	VEGFA	1.67	*
Hippo signaling pathway - multiple species associated genes	MOB1B	1.20	**
	TEAD1	1.19	*
	DCHS2	1.25	*
	LATS1	1.32	*
ERBB signaling	CBL	1.23	*

Cellular Pathway	DEGs (gene name abbreviation)	Continuous Hypoxia, 8 Gy, vs. Normoxia, 8 Gy	
		Log$_2$ fold change	P$_{adj}$ value ($\alpha < 0.05$)
pathway associated genes	SHC3	1.02	*
	SOS1	1.07	**
	EIF4EBP1	-1.44	*
	PRKCA	1.02	***
	TGFA	1.03	*
RAS signaling pathway associated genes	GNB4	1.02	*
	MET	1.16	**
	REL	1.11	**
	RAPGEF5	1.42	**
	SHC3	1.02	*
	SOS1	1.07	**
	FGF22	-1.54	*
	NF1	1.29	****
	PRKCA	1.02	***
	TGFA	1.03	*
	VEGFA	1.67	*

*: p<0.05; **: p<0.01; ***: p<0.001; ****: p<0.0001

Table 9.5   Cellular pathways and expression of associated genes that were differentially regulated under transient hypoxia in comparison to normoxia 4 h after X-rays exposure (8 Gy) in H358 cells.

| Cellular Pathway | DEGs (gene name abbreviation) | Transient Hypoxia, 8 Gy, vs. Normoxia, 8 Gy | |
		Log$_2$ fold change	P$_{adj}$ value ($\alpha < 0.05$)
Hippo signaling pathway associated genes	FRMD6	1.39	***
	MYC	1.67	****
	WNT7A	1.13	****
	ITGB2	1.17	**
	LATS2	1.21	*
	PARD6A	-1.17	****
	PPP2R2C	1.36	**
	SERPINE1	1.35	****
	SNAI2	1.34	**
RAS signaling pathway associated genes	ETS1	1.18	**
	KITLG	1.44	**
	RASA2	1.16	*
	RASAL2	1.36	****
	BDNF	1.02	*
	EFNA3	-1.02	*
	FLT3LG	-2.11	*
	KSR2	-1.65	**
	NGF	1.51	**
	VEGFC	1.06	**
PI3K-AKT signaling pathway associated genes	KITLG	1.44	**
	MYC	1.67	****
	BDNF	1.02	*
	CREB3L1	1.45	****
	F2R	1.67	****
	COL9A3	-1.85	****
	CDK6	1.12	**
	EFNA3	-1.02	*
	FLT3LG	-2.11	*
	IRS1	1.24	**
	ITGB4	1.11	****
	NGF	1.51	**
	NOS3	-1.07	****
	PKN1	-1.52	*
	PPP2R5B	1.12	****
	PPP2R2C	1.36	**
	THBS1	2.25	***
	VEGFC	1.06	**

Cellular Pathway	DEGs (gene name abbreviation)	Transient Hypoxia, 8 Gy, vs. Normoxia, 8 Gy	
		Log$_2$ fold change	P$_{adj}$ value ($\alpha < 0.05$)
Cell adhesion molecule associated genes	CD22	-2.22	****
	CD274	1.13	*
	L1CAM	1.76	****
	CLDN1	1.67	****
	CLDN11	1.27	***
	CLDN3	-1.64	****
	ITGB2	1.17	**
	HLA-DMA	-1.08	*
	HLA-DQB1	1.80	****
	NTNG2	-1.95	***
Tight junction associated genes	AMOTL2	1.28	**
	CLDN1	1.67	****
	CLDN11	1.27	***
	CLDN3	-1.64	****
	PARD6A	-1.17	****
	PRKAB2	1.06	**
	PPP2R2C	1.36	**
	TJP1	1.08	*
	TJP3	-1.58	****
NF-κB signaling pathway associated genes	BLNK	1.29	***
	CXCL1	1.12	***
	CXCL2	1.60	****
	CXCL8	1.49	***
	CD14	-1.66	**
	TNFAIP3	1.86	****
	TNFSF14	-2.05	*
	IL1R1	1.30	*
TNF signaling pathway associated genes	CXCL1	1.12	***
	CXCL2	1.60	****
	TNFAIP3	1.86	****
	CREB3L1	1.45	****
	CSF2	1.30	****
	EDN1	2.29	****
	VEGFC	1.06	**
Cytokine-cytokine receptor interaction associated genes	CXCL1	1.12	***
	CXCL2	1.60	****
	CXCL8	1.49	***
	TNFSF10	-1.97	****
	TNFSF14	-2.05	*
	CSF2RA	-1.09	**
	CSF2	1.30	****
	GDF11	-1.02	**

Cellular Pathway	DEGs (gene name abbreviation)	Transient Hypoxia, 8 Gy, vs. Normoxia, 8 Gy	
		Log$_2$ fold change	P$_{adj}$ value (α < 0.05)
	GDF15	-1.95	****
	IL1R1	1.30	*
	IL20RA	-2.26	*
	IL22RA1	-1.07	***
	NGF	1.51	**

*: p<0.05; **: p<0.01; ***: p<0.001; ****: p<0.0001

10. Erklärung

Ich versichere, dass ich die von mir vorgelegte Dissertation selbstständig angefertigt, die benutzten Quellen und Hilfsmittel vollständig angegeben und die Stellen der Arbeit - einschließlich Tabellen, Karten und Abbildungen -, die anderen Werken im Wortlaut oder dem Sinn nach entnommen sind, in jedem Einzelfall als Entlehnung kenntlich gemacht habe; dass diese Dissertation noch keiner anderen Fakultät oder Universität zur Prüfung vorgelegen hat; dass sie - abgesehen von unten angegebenen Teilpublikationen - noch nicht veröffentlicht worden ist sowie, dass ich eine solche Veröffentlichung vor Abschluss des Promotionsverfahrens nicht vornehmen werde. Die Bestimmungen dieser Promotionsordnung sind mir bekannt. Die von mir vorgelegte Dissertation ist von Professor Dr. med. Jens Jordan betreut worden.

Übersicht der Publikationen (bei Bedarf Seite anfügen):
NIL

Ich versichere, dass ich alle Angaben wahrheitsgemäß nach bestem Wissen und Gewissen gemacht habe und verpflichte mich, jedmögliche, die obigen Angaben betreffenden Veränderungen, dem Promotionsausschuss unverzüglich mitzuteilen.

19.04.2023
Datum

Unterschrift